



## 216715 NEWCOM<sup>++</sup>

### DR9.3

#### *Final report of the JRRM and ASM activities*

**Contractual Date of Delivery to the CEC:** *T0+36*

**Actual Date of Delivery to the CEC:** *T0+36*

**Editor(s):** Jordi Pérez-Romero (UPC)

**Participating institutions:** CNIT, CNRS, IST-TUL, PUT, UPC.

**Contributors:** António Serrador (IST-TUL), Luisa Caeiro (IST-TUL), Luís M. Correia (IST-TUL), Marco Moretti (CNIT), Emanuel Bezerra (UPC), Pawel Sroka (PUT), Hanna Bogucka (PUT), Miguel López-Benítez (UPC), Anna Umbert (UPC), Ferran Casadevall (UPC), Wassim Jouini (CNRS), Jacques Palicot (CNRS), Christophe Moy (CNRS), Adrian Kliks (PUT), Merouane Debbah (CNRS)

**Internal Reviewer(s):** Sergio Benedetto (ISMB)

**Workpackage number:** *WPR9*

**Nature:** *R*

**Total Effort Spent:** *15 PM*

**Dissemination Level:** *Public*

**Version:** *1*

#### **Abstract:**

This deliverable provides the final report with the summary of the activities carried out in NEWCOM<sup>++</sup> WPR9, with a particular focus on those obtained during the last year. They address on the one hand RRM and JRRM strategies in heterogeneous scenarios and, on the other hand, spectrum management and opportunistic spectrum access to achieve an efficient spectrum usage. Main outcomes of the workpackage as well as integration indicators are also summarised.

#### **Keyword list:**

Radio Resource Management (RRM), Joint Radio Resource Management (JRRM), Advanced Spectrum Management (ASM), Game Theory, OFDMA, Cognitive Radio Networks, Opportunistic Spectrum Access.



## TABLE OF CONTENTS

<b><u>LIST OF FIGURES .....</u></b>	<b><u>5</u></b>
<b><u>LIST OF TABLES .....</u></b>	<b><u>7</u></b>
<b><u>LIST OF ACRONYMS.....</u></b>	<b><u>8</u></b>
<b><u>1 INTRODUCTION.....</u></b>	<b><u>11</u></b>
1.1 OBJECTIVES.....	11
1.2 DOCUMENT STRUCTURE .....	11
<b><u>2 RRM AND JRRM ALGORITHMS.....</u></b>	<b><u>13</u></b>
2.1 INTRODUCTION.....	13
2.2 JRRM STRATEGIES AND ALGORITHMS .....	14
2.2.1 HETEROGENEOUS NETWORKS VHO MODEL .....	14
2.2.2 JRRM THEORETICAL PARAMETERS' VARIATION .....	14
2.3 COOPERATIVE RADIO RESOURCE MANAGEMENT IN MULTI VIRTUAL NETWORKS .....	16
2.3.1 SIMULATION SCENARIOS.....	20
2.3.2 SIMULATION RESULTS.....	21
2.4 ENERGY EFFICIENCY AWARENESS ON RADIO RESOURCE MANAGEMENT .....	25
2.4.1 METRICS AND COST FUNCTION TO RRM .....	25
2.5 SPECTRUM ALLOCATION FOR OFDMA NETWORKS .....	27
2.5.1 RADIO RESOURCE ALLOCATION IN A SINGLE-CELLULAR SCENARIO .....	27
2.5.2 RADIO RESOURCE ALLOCATION IN A MULTI-CELLULAR SCENARIO .....	38
2.6 GAME THEORY FOR OPTIMIZATION OF RRM.....	53
2.6.1 CRYSTALLIZED RATE REGIONS FOR MIMO TRANSMISSION .....	53
2.7 CONCLUSIONS .....	73
<b><u>3 ADVANCED SPECTRUM MANAGEMENT .....</u></b>	<b><u>76</u></b>
3.1 INTRODUCTION.....	76
3.2 MEASUREMENTS OF SPECTRUM AVAILABILITY.....	76
3.2.1 INTRODUCTION .....	76
3.2.2 MODELLING SPATIAL SPECTRUM OCCUPANCY .....	77
3.2.3 SPECTRUM SENSING STUDIES .....	89
3.3 DYNAMIC SPECTRUM ACCESS IN COGNITIVE RADIO NETWORKS.....	98
3.3.1 JOINT LEARNING DETECTION FRAMEWORK.....	98

3.3.2	OPPORTUNISTIC SPECTRUM ACCESS WITH SENSING ERRORS: EVALUATION OF UPPER CONFIDENCE BOUND ALGORITHMS PERFORMANCES .....	105
3.4	CONCLUSIONS .....	114
<b>4</b>	<b>CONCLUSIONS .....</b>	<b>116</b>
4.1	OVERVIEW OF MOST SIGNIFICANT OUTCOMES.....	116
4.2	INTEGRATION ACTIVITIES .....	117
	<b><u>REFERENCES.....</u></b>	<b><u>120</u></b>

## LIST OF FIGURES

Figure 2.1 – Different RAT clusters (reference scenario).....	14
Figure 2.2 – JRRM policies impact on LBN blocking.....	16
Figure 2.3 – JRRM policies impact on LBN delay.....	16
Figure 2.4 – Inter-VNet RRM and Intra-VNet RRM.....	17
Figure 2.5 – Physical cluster.....	20
Figure 2.6 – Simulation scenarios for different VNets composition.....	21
Figure 2.7 – Out of Contract for scenarios 1 and 2.....	22
Figure 2.8 – Service Level for scenarios 1 and 2.....	22
Figure 2.9 – Service Level for scenarios 1 and 3.....	23
Figure 2.10 – Service Level for scenarios 2 and 4.....	23
Figure 2.11 – Maximum Rate capacity without compensation.....	24
Figure 2.12 – VNet data rate for scenario 4 with VRRC.....	24
Figure 2.13 – Number of adaptations per type.....	25
Figure 2.14 – Network, users' power and information parameters map.....	26
Figure 2.15 – Impact on fairness of the sub-carrier re-assignment and power re-allocation of the FSRM-P policy.....	30
Figure 2.16 – Algorithm 1: Sub-carrier assignment of FSRM-P policy.....	31
Figure 2.17 – Algorithm 2: Power allocation of FSRM-P policy.....	32
Figure 2.18 – Cell fairness index as function of the number of users.....	35
Figure 2.19 – Total cell throughput as function of the number of users.....	35
Figure 2.20 – User satisfaction as function of the number of users.....	36
Figure 2.21 – Measured spectral efficiency $\eta m$ vs. duration of allocation phase $Ns$ .....	43
Figure 2.22 – Mean power per cell $Pm$ vs. duration of allocation phase $Ns$ .....	43
Figure 2.23 – Measured spectral efficiency $\eta m$ vs. target spectral efficiency $\eta$ (resource allocation and load control algorithm, no scheduler, same rate for all users).....	45
Figure 2.24 – Mean power per cell $Pm$ vs. measured spectral efficiency $\eta m$ (resource allocation and load control algorithm, no scheduler, same rate for all users).....	45
Figure 2.25 – Considered cell layout and observation area.....	49
Figure 2.26 – MIMO interference channel: general 2-cell 2-user model (a) and the details representation of the considered 2 $\times$ 2 case (b).....	54
Figure 2.27 – Achievable rate region for the MIMO interference channel - averaged over 2000 channel realizations.....	57
Figure 2.28 – Achievable rate region for the MIMO interference channel - one particular channel realization (user two observes strong interference).....	58
Figure 2.29 – Achievable rate region for the MIMO interference channel - the transmit power of the first user is twice higher than the transmit power of the second user.....	59
Figure 2.30 – Achievable rate region for the precoded MIMO interference channel.....	60
Figure 2.31 – Achievable rate region for the OFDM interference channel - results averaged over 2000 channel realizations.....	60
Figure 2.32 – Achievable rate region for the OFDM interference channel - one particular channel realization, maximum transmit power of the first user is two times higher than the maximum transmit power of the second user.....	61
Figure 2.33 – Regret-matching learning algorithm.....	67
Figure 2.34 – Crystallized rate regions in the interference limited case with marked learned point.....	68
Figure 2.35 – Crystallized rate regions in the noise limited case with marked learned point.....	68
Figure 2.36 – The convergence of the rate-matching algorithms - user 1.....	69
Figure 2.37 – The convergence of the rate-matching algorithms - user 2.....	69
Figure 2.38 – SVD-MIMO rate region - channel case 1.....	70
Figure 2.39 – SVD-MIMO rate region - channel case 2.....	70
Figure 2.40 – Achieved average rate versus codebook size.....	73
Figure 3.1 – Aerial view of UPC's Campus Nord in urban Barcelona, Spain.....	79

Figure 3.2 – Set of additional measurement locations within UPC’s Campus Nord in urban Barcelona, Spain.....	79
Figure 3.3 – Cross-correlation vs. distance for DCS.....	81
Figure 3.4 – Covariance vs. distance for DCS.....	81
Figure 3.5 – Normalised covariance vs. distance for DCS.....	82
Figure 3.6 – Semivariance vs. distance for DCS.....	82
Figure 3.7 – Cross-correlation vs. distance for UMTS.....	83
Figure 3.8 – Covariance vs. distance for UMTS.....	83
Figure 3.9 – Normalised covariance vs. distance for UMTS.....	84
Figure 3.10 – Semivariance vs. distance for UMTS.....	84
Figure 3.11 – Cross-correlation vs. SNR difference for DCS.....	86
Figure 3.12 – Covariance vs. SNR difference for DCS.....	86
Figure 3.13 – Normalised covariance vs. SNR difference for DCS.....	87
Figure 3.14 – Cross-correlation vs. SNR difference for UMTS.....	87
Figure 3.15 – Covariance vs. SNR difference for UMTS.....	88
Figure 3.16 – Normalised covariance vs. SNR difference for UMTS.....	88
Figure 3.17 – Semivariance vs. SNR difference for UMTS.....	89
Figure 3.18 – General scheme of the measurement platform.....	91
Figure 3.19 – Average power spectrum (averaged over more than 4800 2048-point FFTs) for some of the captured signals. Dashed lines represent the filter’s cut-off frequencies.....	93
Figure 3.20 – Probability of detection versus SNR: (a) $\alpha = 0$ dB ( $P_{fa} \leq 0.01$ ), (b) $\alpha = 0$ dB ( $P_{fa} \leq 0.10$ ). .....	94
Figure 3.21 – Probability of detection versus SNR: (a) $\alpha = 1$ dB ( $P_{fa} \leq 0.10$ ), (b) $\alpha = 2$ dB ( $P_{fa} \leq 0.10$ ). .....	94
Figure 3.22 – Moving-averaged normalised power received for some captured signals (moving-averaging window of 100 samples).....	96
Figure 3.23 – Probability of detection versus sample length.....	97
Figure 3.24 – Learning results tested on the channel 08A of the DAB-T standard. The curves compare the empirical ratio statistic to both the theoretical ratio distribution and Fisher-Snedecor distribution.....	104
Figure 3.25 – Learning results tested on the channel 10A of the DAB-T standard. The curves compare the empirical ratio statistic to both the theoretical ratio distribution and Fisher-Snedecor distribution.....	104
Figure 3.26 – Learning results tested on the channel 11B of the DAB-T standard. The curves compare the empirical ratio statistic to both the theoretical ratio distribution and Fisher-Snedecor distribution.....	105
Figure 3.27 – Representation of a CA observing and accessing an RF environment.....	108
Figure 3.28 – Percentage of time the $UCB_1$ -based CA selects the optimal channel under various sensing errors frameworks (over 10 available channels).....	113
Figure 3.29 – $UCB_1$ algorithm and Opportunistic Spectrum Access problem with sensing errors: regret simulation results.....	113

## LIST OF TABLES

Table 2.1 – JRRM traffic distribution variation scenarios. ....	15
Table 2.2 – JRRM VHOs strategies scenarios. ....	15
Table 2.3 – Service penetration per VNet. ....	21
Table 2.4 – Simulation scenarios. ....	21
Table 2.5 – Network data and power efficiency for different systems and services. ....	27
Table 2.6 – Simulation parameters. ....	33
Table 2.7 – Simulation parameters. ....	50
Table 2.8 – Performance comparison of selected algorithms with 200 users distributed in observation area – Max Rate optimization. ....	51
Table 2.9 – Performance comparison of selected algorithms with 400 users distributed in observation area – Max Rate optimization. ....	52
Table 2.10 – Performance comparison of selected algorithms with 200 users distributed in observation area – Proportional Fair optimization. ....	52
Table 2.11 – Performance comparison of selected algorithms with 400 users distributed in observation area – Proportional Fair optimization. ....	53
Table 2.12 – Achieved rates for channel definition (2.67). ....	72
Table 2.13 – Achieved rates for channel definition (2.68). ....	72
Table 3.1 – Channels measured in this study: Analogical/digital tv, Terrestrial Trunked Radio (TETRA), Terrestrial Digital Audio Broadcasting (DAB-T), Extended Global System for Mobile communications 900 downlink (E-GSM 900 DL), Digital Cellular System 1800 downlink (DCS 1800 DL) and Universal Mobile Telecommunications System Frequency-Division Duplex downlink (UMTS FDD DL). ....	92

**LIST OF ACRONYMS**

3G	3 <sup>rd</sup> Generation
ADC	Analogical to Digital Conversor
AMC	Adaptive Modulation and Coding
ASM	Advanced Spectrum Management
ATF	Adaptive Throughput-Based Fairness
AWGN	Additive White Gaussian Noise
BB	Base Band
BE	Best Effort
BS	Base Station
CA	Cognitive Agent
CDMA	Code Division Multiple Access
CFI	Cell Fairness Index
CoMP	COordinated MultiPoint
CR	Cognitive Radio
CRRM	Common Radio Resource Management
CSI	Channel State Information
CVRRM	Cooperative VNet RRM
DAB-T	Terrestrial Digital Audio Broadcasting
DAC	Digital to Analogical Conversion
DCS	Digital Cellular System
DL	DownLink
DSA	Dynamic Spectrum Access
DSAN	Dynamic Spectrum Access Network
EE	Energy Efficiency
EM	Expectaion Maximization
EvD	Eigenvalue Decomposition
FDD	Frequency Division Duplex
FDMA	Frequency Division Multiple Access
FPGA	Field Programmable Gate Array
FSRM	Fairness-Based Sum Rate Maximization
FSRM-P	Fairness-Based Sum Rate Maximization with Proportional Rate Constraints
GMM	Gaussian Mixture Model
GSM	Global System for Mobile communications
HHO	Horizontal HandOver

Reference DR9.3



HOL	Head Of Line
ICIC	Inter-Cell Interference Coordination
IF	Intermediate Frequency
ILP	Integer Linear Programming
InP	Infrastructure Providers
IWF	Iterative Water-Filling
JRRM	Joint Radio Resource Management
LP	Linear Programming
LTE	Long Term Evolution
MAB	Multi Armed Bandit
MAI	Multiple Access Interference
ME	Mobile Equipment
MIMO	Multiple Input Multiple Output
ML	Maximum-Likelihood
MM	Moment Method
MMF	Max-Min Fairness
MMR	Max-Min Rate
MMSE	Minimum Mean Squared Error
MR	Max Rate
MRRM	Multi Radio Resource Management
MT	Mobile Terminal
NP-ED	Neyman-Pearson Energy Detector
NRT	Non Real Time
NSM	Network Simplex Method
OFDM	Orthogonal Frequency Division Multiplexing
OFDMA	Orthogonal Frequency Division Multiple Access
OSA	Opportunistic Spectrum Access
PF	Proportional Fairness
PRB	Physical Resource Block
PSC	Packet Scheduler
PSD	Power Spectral Density
PU	Primary User
PU <sup>2</sup> RC	Per-User Unitary Rate Control
RA	Resource Allocator
RAT	Radio Access Technology
RR	Round Robin
RRA	Radio Resource Allocation

Reference DR9.3

RRM	Radio Resource Management
RT	Real Time
SDR	Software Defined Radio
SINR	Signal-to-Interference-plus-Noise Ratio
SISO	Single Input Single Output
SNR	Signal to Noise Ratio
SRM	Sum Rate Maximization
SRM-P	Sum Rate Maximization with Proportional Rate Constraints
SU	Secondary User
SUS	Semiorthogonal User Selection
SVD	Singular Value Decomposition
TDMA	Time Division Multiple Access
TETRA	TERrestrial TRunked RAdio
TSD	Transmit Selection Diversity
TTI	Transmission Time Interval
UCB	Upper Confidence Bound
UL	UpLink
UMTS	Universal Mobile Telecommunication System
USB	Universal Serial Bus
USRP	Universal Software Radio Peripheral
VCG	Vickey-Clarke-Groves
VHO	Vertical HandOver
VLinks	Virtual Links
VNets	Virtual Networks
VNO	Virtual Network Operators
VNodes	Virtual Nodes
VNP	VNet Providers
VRRC	VNet Requirements Radio Resource Control
ZF	Zero Forcing

# 1 INTRODUCTION

## 1.1 Objectives

NEWCOM<sup>++</sup> WPR9 addresses the development and evaluation of advanced Radio Resource Management (RRM) and spectrum management techniques for wireless communications systems in heterogeneous scenarios. In such scenarios different radio access technologies co-exist, so by a joint use of the available resources significant gains and a more efficient use of the spectrum can be achieved. Moreover, the developed strategies may be improved by introduction of cognitive network functionalities to provide the ability to adapt to changing conditions.

Under this framework, the objective of this deliverable is to present the final report with the technical activities that have been carried out in the context of NEWCOM<sup>++</sup> WPR9, with a particular focus on the ones realised during the third year, although proper references to the prior activities and preceding deliverable are given in order to build a self-contained deliverable.

## 1.2 Document structure

This document is organised in accordance with the activities carried out in the different working groups (WG) of WPR9:

- Chapter 2 deals with RRM and JRRM algorithms at different levels, comprising the work of working groups WG1, WG2 and WG3 in the following subsections, after the introductory Section 2.1:
  - Section 2.2 focuses on the JRRM algorithms and their evaluation in heterogeneous networks, with the main focus on vertical handover (VHO) procedures
  - Section 2.3 addresses the Cooperative Radio Resource Management in Multi Virtual Networks, based on the network virtualisation concept where infrastructure is shared by virtual operators
  - Section 2.4 deals with the energy efficiency awareness in RRM
  - Section 2.5 deals with the spectrum allocation problem in a cellular OFDMA system, with the analysis both on single-cell and multi-cell level.
  - Section 2.6 addresses the application of game theory for optimization of the RRM in cognitive radio, focusing in particular on the definition of crystallized rate regions for MIMO transmission.
- Chapter 3 presents the outcomes of investigation within working groups WG4 and WG5 in the advanced spectrum management field. The results and proposed algorithms are given in two subsections following the introductory Section 3.1:
  - Section 3.2 describes the results of the measurement campaign to detect spectrum availability, with the aim to establish spatial and temporal usage patterns from primary users in different licensed bands, and also different spectrum sensing studies are presented.
  - Section 3.3 focuses on Dynamic Spectrum Access strategies for Cognitive Radio Networks, presenting on the one hand a joint learning detection framework, evaluated using the measurements of the campaign and on the other hand an opportunistic spectrum access mechanism with sensing errors..

Finally, in chapter 4 the main conclusions and the summary of integration activities within WPR9 are outlined.



## 2 RRM AND JRRM ALGORITHMS

### 2.1 Introduction

This chapter focuses on the work carried out inside WPR9 associated with the development and analysis of Radio Resource Management (RRM) strategies for heterogeneous wireless systems. Motivated by the clear trend towards the increase in the user demand for high bit rate data services including Internet accessibility everywhere and anytime, RRM functions targeting the most efficient use of the scarce radio resources in the different technologies have received increased attention. RRM strategies are responsible for taking decisions concerning the setting of different parameters influencing on the radio interface behaviour, including aspects such as the number of simultaneous users transmitting with their corresponding powers, transmission bit rates, the corresponding code sequences or sub-carriers assigned to them, the number of users that can be admitted in a given cell, etc.

Furthermore, the future wireless arena is expected to be heterogeneous in nature, with a multiplicity of cellular, local area, metropolitan area and personal area technologies coexisting in the same geographical region. Also different deployments will be envisaged, with macro, micro, pico and femtocell deployments will be coexisting as the means to achieve the desired large capacities. Network heterogeneity has been in fact regarded as a new challenge to offer services to the users thanks to coordinating the available Radio Access Technologies (RATs), which on the other hand exhibit some degree of complementarity. In this way, not only the user can be served through the RAT that fits better to the terminal capabilities and service requirements, but also a more efficient use of the available radio resources can be achieved. This calls for the introduction of new RRM algorithms operating from a common perspective that take into account the overall amount of resources available in the existing RATs, and therefore are referred to as Common RRM (CRRM), Joint RRM (JRRM) or Multi RRM (MRRM).

Under these considerations, one of the activities in this field in WPR9 that is presented in section 2.2 will address the JRRM strategies. In particular, the vertical handover (VHO) policies in a heterogeneous scenario with coexisting low and high bit rate networks in different configurations are studied, analysing the impact of traffic splitting policies in terms of different QoS indicators such as blocking probabilities or delay. Another concept that has recently received attention in the context of heterogeneous networks is the network virtualisation, in which different Virtual Network Operators share the network infrastructure. Such concept leads to the problem of how to perform an adequate RRM among the shared resources by the different operators. In that respect, section 2.3 will address the network virtualisation in heterogeneous environments where different RATs coexist.

Section 2.4 will then focus on the introduction of energy efficiency awareness concepts on JRRM targeting the optimisation of the energy efficiency of the wireless networks by ensuring a proper match between real user data and required communication overhead. Different metrics are introduced to measure the power efficiency to transmit a certain useful data volume depending on the required overhead, and evaluated in a heterogeneous scenario with UMTS R99 and R5 technologies.

Another trend in the wireless technology evolution has been the introduction in the new standards of more efficient technologies enabling the use of larger bit rates over a certain bandwidth. This is the case of the introduction of OFDMA and MIMO technologies in e.g. LTE or LTE Advanced standards. In such case, the need for efficient usage of the limited existing radio resources calls for the deployment of new strategies and revolutionary visions. Section 2.5 will in particular focus on the spectrum allocation in OFDMA networks, addressing first a single-cellular scenario and then the multi-cellular case, from the perspective of distributed schemes. The problem of Inter-Cell Interference Coordination (ICIC) in MIMO scenarios will also be considered within this section.

Finally, section 2.6 will focus on the game-theoretic approaches to enable an optimisation of RRM procedures. In particular, a MIMO channel is considered and the crystallized rate regions for MIMO

transmission are studied. Specific MIMO techniques are considered and the correlated equilibrium concept to the rate region problem is applied, proposing a new Vickrey-Clarke-Groves (VCG) auction utility formulation and the modified regret-matching learning algorithm.

## 2.2 JRRM Strategies and Algorithms

### 2.2.1 Heterogeneous Networks VHO Model

In heterogeneous networks it is not frequent to find simple analytical models in literature that are capable of extracting the main characteristics of a Vertical Handover (VHO) process and their impact into Quality of Service (QoS). For example in [1], [2], [3] and [4] relatively complex models are used to optimise and trigger VHOs, based on radio signal levels among others. However, a simple model that depends on geographical considerations is very useful to assess JRRM performance; in this way, based on simple considerations, the impact of several parameters at user and network levels on the JRRM QoS performance can be easily evaluated.

Using a Horizontal Handover (HHO) analytical model as starting point, where user's cell crossing probabilities, crossing rates, drops, blocking can be evaluated, [4], it is assumed that Radio Access Technology (RAT) types are grouped in clusters (see Figure 2.1) and can be modelled as a single cell (using cellular HHO characteristics). This approach enables the use of the previous model mechanism to extract some VHOs assumptions and theoretical results. This means that users' previous transitions between cells borders of a given RAN are now translated to transitions between RATs borders (cluster based). This model is based on the traffic generation and on the heterogeneous network overall capacity. Thus, the model starts defining the number of active users, including the use of multiple services. The following conditions are assumed: network stability, infinite population, uniform users' distribution in the area, Poisson and exponential distributions for service session arrival and duration processes, respectively. This proposed theoretical model was defined and proposed in the previous NEWCOM<sup>++</sup> deliverable DR9.2 [5], where a reference scenario is proposed and some sub-scenarios variation impact are analysed. Then, relevant JRRM parameters variations are highlighted in this deliverable as described in the following sub-sections.

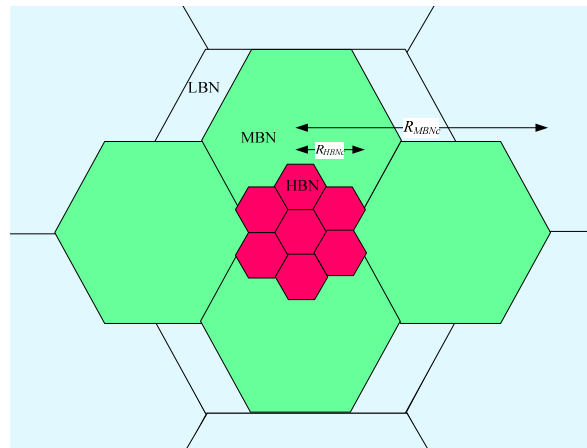


Figure 2.1 – Different RAT clusters (reference scenario).

### 2.2.2 JRRM Theoretical Parameters' Variation

In order to present some possible results produced by the previous mentioned model, the most relevant input and output parameters need to be decided. Since the focus of this activity is JRRM performance, then, the overall JRRM QoS and VHOs related parameters in the model should be the most explored ones. In particular, initial JRRM traffic distribution and VHO traffic percentage flow among RATs are the considered parameters to analyse the impact of their variation on the overall QoS.

The model includes two JRRM parameters,  $P_{Init,r}$  and  $P_{VHO}$ , which aim to simulate the initial traffic distribution into a given RAT  $r$ , which is a JRRM influence policy, and the VHO policy influence among RATs, respectively. Taking into account the first one, it is possible to setup some distribution percentages over the generated traffic delivered to the correspondent RAT, enabling the QoS evaluation in each RAT. Table 2.1 presents two scenario variations over the reference one, Low Bitrate Networks (LBNs)-Centric and High Bitrate Networks (HBNs)-Centric [6]. These variations are useful to understand the impact of traffic distribution in each RAT QoS. The LBN (one single BS in cluster), will be the RAT type that will have more difficulties to observe high levels of traffic since compared with other RATs it provides low capacity and high coverage. Therefore, LBN related traffic percentage distributed by the JRRM entity should be low, to keep LBN QoS indicators under control.

The second parameter  $P_{VHO}$  proposed by the model, is related to VHO traffic transfer among RATs. Similar to previous cases, in Table 2.2 it is presented some traffic transfer variations among LBN, MBN and HBNs. Again, these traffic scenario variations take the same name as in the previous case. Basically the idea is to transfer traffic from one RAT to another; however, these transfer percentages have a physical limit, which is related to geographical superposition among RAT clusters. The VHO transfer rule, if negative, means that traffic flow will be the opposite with respect to the one symbolised by the arrow.

Table 2.1 – JRRM traffic distribution variation scenarios.

RAT	JRRM traffic distribution [%]		
	LBN – Centric	Ref.	HBN – Centric
LBN	10	7	4
MBN	60	45	35
HBN	30	48	61

Table 2.2 – JRRM VHOs strategies scenarios.

VHO traffic transfer rule	JRRM VHOs [%]		
	LBN - Centric	Ref.	HBN – Centric
LBN→MBN	-10	0	10
MBN→HBN	-5	0	5

This sub-section presents the JRRM theoretical parameters' variation results. These are presented observing simultaneously two dimensions, one dimension is the initial traffic and the second is the VHO policy percentage distribution variation/trend. These variations are performed according to Table 2.1 and Table 2.2 parameters, expecting to have significant and different impacts on RATs' QoS indicators. These results are presented and discussed below.

In Figure 2.2, it is possible to observe the LBN blocking probability variation. The worst case, from the LBN view perspective, is when initial traffic distribution and VHO policy push traffic to LBNs (LBN-Centric) in both axels, leading LBN blocking probability to about 13%. It is also possible to observe that initial traffic distribution has more influence when compared with the VHO variation policy. This is because the VHO percentage has less freedom on amplitude range. The best case is when initial distribution tends to HBN-Centric, in this situation LBN initial traffic percentage will move from 10 to 4% of the total generated traffic. Though this seems a small variation, with 4% LBN will handle less than 50% previous case (LBN-Centric), leading the LBN blocking probability to be less than 1%.

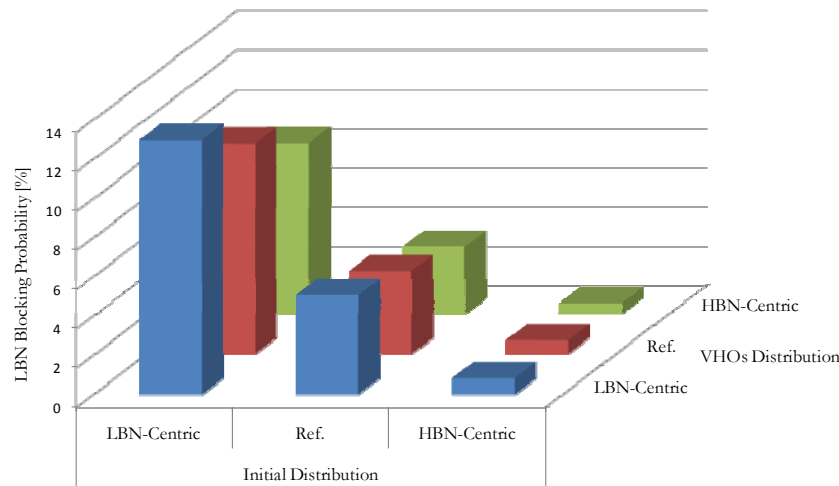


Figure 2.2 – JRRM policies impact on LBN blocking.

Another QoS indicator is delay. Figure 2.3 presents results for LBNs and here, similar to  $P_B$ , delay presents a parallel trend. However, note that delay values for LBN are only “acceptable” when HBN-Centric case is plotted, this means that offered traffic to LBN should be less in order to reach the delay values set by services’ constraints.

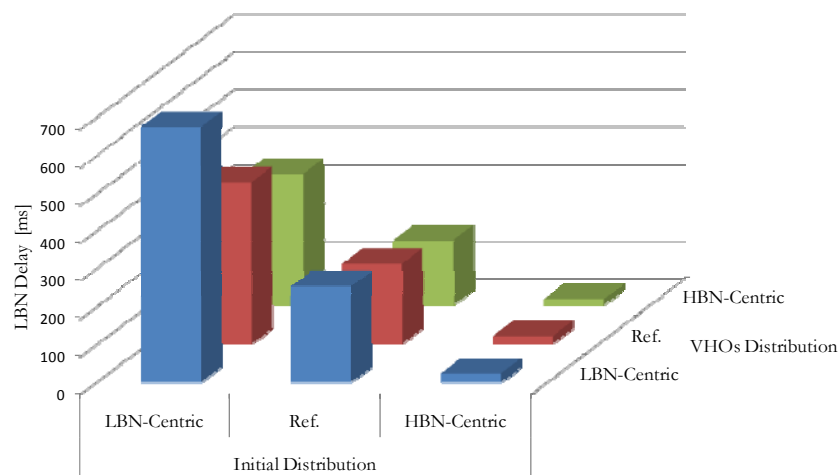


Figure 2.3 – JRRM policies impact on LBN delay.

## 2.3 Cooperative Radio Resource Management in Multi Virtual Networks

In future virtual networks environments [7], [8], in which heterogeneous networks coexist and new business roles and models are expected. Virtual Networks (VNets) cooperation for RRM is one of the most relevant issues, in order to achieve an efficient integration of different wireless technologies and the maintenance of QoS requirements.

The network virtualisation concept is based on network infrastructure sharing by different Virtual Network Operators (VNOs). Thus, RRM in VNets could be seen as a problem of wireless network sharing for multi-operator networks, which is already studied for the introduction of Mobile Virtual Networks Operators in 3<sup>rd</sup> Generation (3G) systems. Several RRM strategies for 3G multi-operator networks have been proposed in the literature, since there is a critical need for radio resource control among the multiple operators [9], [10], [11]. However, a considerable difference exists, since in that case operators are forced to use similar network functions, as defined by 3G specifications. Instead, in network virtualisation the existence of different types of functions and communication protocols for



each VNet is a fundamental issue. Additionally, the scope of those works is limited to one wireless access technology, and cannot benefit from possible trunking gains obtained by the cooperation among different RATs.

VNets pose some new challenges in the scope of cooperative RRM [12]. New stakeholders are expected in the market, like Infrastructure Providers (InP), VNet Providers (VNP) and VNOs. Since new relations and independencies must be considered, the interaction among these new stakeholders must be taken into account by cooperative RRM policies. Furthermore, the allocation of physical resources to different VNets introduces new constraints that should be considered to perform initial selection and handover decisions or radio resource allocation. At the RRM level, these constraints should also be taken in account, since the controlled radio resource unit pools are not static (from the operator view point). In fact, they are grouped according to the allocation of VNets, and may be reallocated to another VNet, or simply do not belong to any VNet.

According to VNets' environment characteristics, two different levels of RRM functions should be considered, Intra-VNet and Inter-VNet ones. The former allows managing how end-users of a VNet share the resources of that particular VNet; it is the VNO that can freely define what kind of RRM it uses within its VNet. The latter, from now on designated as Cooperative VNet RRM (CVRRM), is responsible for managing how physical resources are allocated to different VNets. CVRRM ensures that every VNet gets the amount of resources as negotiated in the VNet establishment phase. It should be stressed that it does not operate on the resources that are required by an individual end-user; instead, it considers the aggregated resource demands of different VNets, nevertheless, it can be triggered by individual demands that affect the aggregated ones. In a multi-access analogy, CVRRM, and also Intra-VNet RRM, are equivalent to the Multi-RRM [13] or Common RRM [14], with the difference of the operational context.

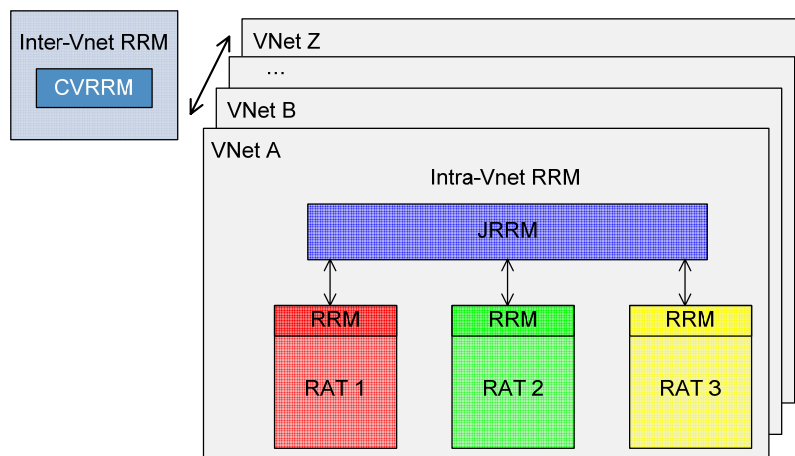


Figure 2.4 – Inter-VNet RRM and Intra-VNet RRM.

The CVRRM set of functionalities is devoted to the characteristics abstraction of heterogeneous wireless environments, from the virtualisation process, keeping the main cooperative RRM target, i.e., to optimise network resources usage and to provide the always best connectivity, while ensuring VNets QoS. The resources considered in the CVRRM context are the physical ones, nodes and links, and the virtual ones, Virtual Nodes (VNodes) and Virtual Links (VLinks). Radio resources, abstracted by channels, are also referred to in this scope.

CVRRM strategies are based on a global knowledge of physical resources, their allocation to virtual networks, the resources neighbour mapping, and fundamental VNets characteristics to which resources are allocated. The VNet “owners” agreements (Inter-VNPs, Inter-InPs and VNOs) are also important information that should be known. Therefore, CVRRM can react not only to the changes in the amount of resources allocated to a VNet, but also to the end-user requests that affect the aggregated resources (VNodes/VLinks). Appropriate resources monitoring and evaluation can determine changes in the resource allocation in order to maintain or optimise VNet requirements. This evaluation is performed

by a cost function that allows a unified comparison among all the resources, according to a given management policy, derived from [15].

Based on cooperative RRM concerns, namely, initial RAT access selection, vertical handover, and resources scheduling/allocation, three CVRRM main functions were identified:

- VNet Requirements Radio Resource Control (VRRC) – that manages physical resources allocation to different VNets, in order to ensure the amount of resources negotiated at the VNet establishment; it takes the possible changes in capacity/availability of radio resources that affect VNet requirements into account, e.g., data rate, delay, jitter, packet loss, and error rates.
- Initial VNet selection – allowing transparency to end-users in the process of VNet attachment and optimising VNets utilisation.
- VNet Handover support – in order to guarantee the always best connectivity, even when the VNet coverage is impossible, therefore, allowing handover between different VNets.

In order to establish a network model, some assumptions are taken: uniform coverage by all the wireless systems under analysis, and the inexistence of a specific requirement from the VNO related to the wireless technology in use. It is considered that VNOs do not care about the specific wireless technology being use, as long as the contractual requirements are ensured. Moreover, it is assumed that end-user nodes are mobile and multi-homed, i.e., capable of supporting different radio interfaces, so that it can connect to any available network.

Concerning the wireless access technologies involved, one considers Time Division/Frequency Division Multiple Access (TD/FDMA), Code Division Multiple Access (CDMA), Orthogonal Frequency Division Multiplexing (OFDM), and Orthogonal Frequency Division Multiple Access (OFDMA), as they cover most of the current wireless systems (GSM, UMTS, WiFi, and LTE), which from now on are considered as examples of such access technologies. Although, radio channel multiple access definition for each wireless technology is different, a level of abstraction is added, enabling a common approach to manage all radio resources. It is considered that each wireless link is generically composed of channels, which varies in number and capacity according to the wireless technology involved. However, the characteristics of each technology are taken into account, in order to emphasise the specific factors that influence channel capacity. The main feature considered here is the channel data rate.

VNets are classified according to their contractual requirements.

CVRRM functions will interact with a Monitoring Entity (ME) (e.g., the In-Network Management resource monitoring in the context of the 4WARD project [16]), which provides real time measurements, like available resources quantity and quality, neighbouring resources and failure detection. Furthermore, it is assumed that a ME instance exists in the physical node, providing global resource monitoring information, and in each virtual node, collecting its own monitoring information. The monitoring of the whole VNet is done through the association of several MEs instantiated in each of its VNodes, constituting an aggregated system. It is assumed that the ME, mainly the real time monitoring part, monitors the wireless medium and the node, therefore, providing the cost function inputs to computation, in order to allow the comparison among resources, and among VNets.

The strategies used in particular by VRRC are related to the contractual VNet requirements, and are reflected by key performance indicators weights in the cost function computation for resource evaluation.

The VRRC algorithm uses monitoring information, to compare the actual capacity with the contractual one, then, deciding on radio resources (re)allocation to a given VNet. The selection of additional radio resources is made in two steps:

- According to the radio resources availability into the same physical link. A VNet borrowing margin, similar to the one defined in [9], is associated to the VNet type and is adapted according to VNet usage. As an example, in a VNet with best effort requirements, channels

may be transferred (borrowed) to perform the total amount of data rate required by a VNet with stringent requirements, if no other channels are available. The opposite is only possible if the VNet with stringent is running on low usage.

- Based on the cost of neighbour resources, which reflects the resources availability according to an implemented strategy.

The scanning time of this decision process is adapted dynamically depending on resources utilisation, variability of the radio interface, and VNets characteristics. VRRC may also decide on the migration or adaptation of the amount of resources allocated to the VNets, in order to optimise radio resource usage, e.g., when the virtual resource runs on low usage over a long period of time.

In order to evaluate the VRRC performance, a set of output parameters was identified as follows: VNO satisfaction level, out of contract ratio and VLink utilisation. They are key indicators that allow a proper validation of the proposed model, by accessing critical issues related with the virtualisation process, such as virtual links with QoS guarantees. It is worthwhile to note that VNOs are indirectly the “users” from VRRC viewpoint.

The VNO satisfaction level,  $S_{VNO}$ , represents the VNO requests to use the remaining capacity, according to the contract established with the VNP, and this capacity is not available:

$$S_{VNO} = 1 - \left( \frac{R_{VL}^{in}}{R_{VL}^{act}} - 1 \right) \quad (2.1)$$

where  $R_{VL}^{in}$  is the data rate offered to the VLink and  $R_{VL}^{act}$  is the actual VLink data rate.

This equation is only applied when the data rate offered to the VLink is above the actual, and below the minimum contracted; otherwise, the value of  $S_{VNO}$  is zero.  $S_{VNO}$  accounts for the effective decrease in the amount of contracted resources perceived by the VNO. The analysis of this parameter should be made at VLink and VNet levels. Indirectly, it allows evaluating the network capability to react to radio/channel impairments that reduce the availability of the virtual resources. It can be used to monitor the virtual links, in order to detect contract violations.

The out of contract ratio is defined as the period of time, over the total sampling one, for which VNet contracted capacity is not available. It is a global metric, independent of the service level experienced by the VNO, since in low VNet usage, capacity reduction may not be perceived, due to enough remaining capacity to satisfy the VNO requests.

$$r_t^{nav} = \frac{R_{VL}^{min} - \left[ (N_{ch}^T - N_{ch}^o) \cdot R_{ch}^{max} + R_{VL}^{in} \right]}{R_{VL}^{min}} \quad (2.2)$$

where,  $N_{ch}^T$  is the total number of channels,  $R_{ch}^{max}$  is the maximum channel data rate in a cluster of resources, and  $N_{ch}^o$  is the number of occupied channels in the cluster,

$$N_{ch}^o = \frac{R_{VL}^{in}}{R_{ch}^{act}} \quad (2.3)$$

where  $R_{ch}^{act}$  is the actual channel data rate.

The out of contract ratio can be computed for a VLink and a VNet. The objective of this metric is the evaluation of network reaction to radio/channel impairments that reduces the availability of the virtual resources under VNet contracted requirements. The scanning time adaptation to fast or slow variability of the medium is another target to achieve.

VLink utilisation is defined as the ratio of the number of occupied channels over the total number of allocated channels:

$$\eta_{VL}^o = \frac{N_{ch}^o}{N_{ch}^{VL}} \quad (2.4)$$

where  $N_{ch}^{VL}$  is the number of VLink allocated channels.

This global metric should be applied to the individual VLinks in order to evaluate the possibility to introduce some balancing mechanisms to optimise physical link utilisation.

### 2.3.1 Simulation Scenarios

A set of scenarios was identified for simulations. The basic unit is a cluster with a total coverage area of 1km radius, composed by 1 TDMA, 7 CDMA, 10 OFDMA and 20 OFDM PhyBSs, distributed as illustrated by Figure 2.5. Over this physical infrastructure, 3 VNet were instantiated, 2 of them serving all the area and one just providing service in the central area (around 600m radius), Figure 2.5. The VNet composition varies according to the scenario, their service area being always the same.

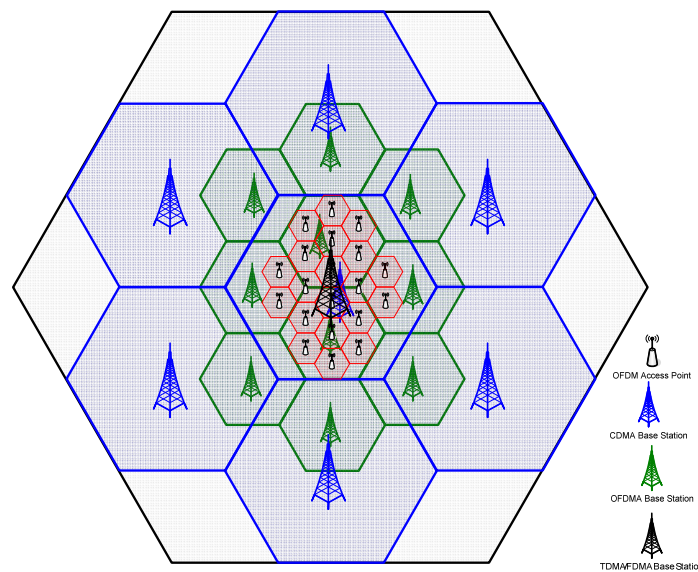


Figure 2.5 – Physical cluster.

Concerning the VNet type in terms of QoS guarantees, it is considered that VNet A and C, are guaranteed (GRT), providing services with stringent requirements and VNet B is best effort (BE), providing other services, see Table 2.3.

Network conditions that can cause reduction in the capacity of virtual resources have been forced by setting a high percentage of active end-users and periodically changing their SINR.

In order to analyse potential benefits of introducing the VRRC mechanism, the virtualisation percentage of the physical resources has been established in 90%. The requested capacity per VNet was defined by considering the total capacity of the cluster and the typical services' data rates provided by VNet.

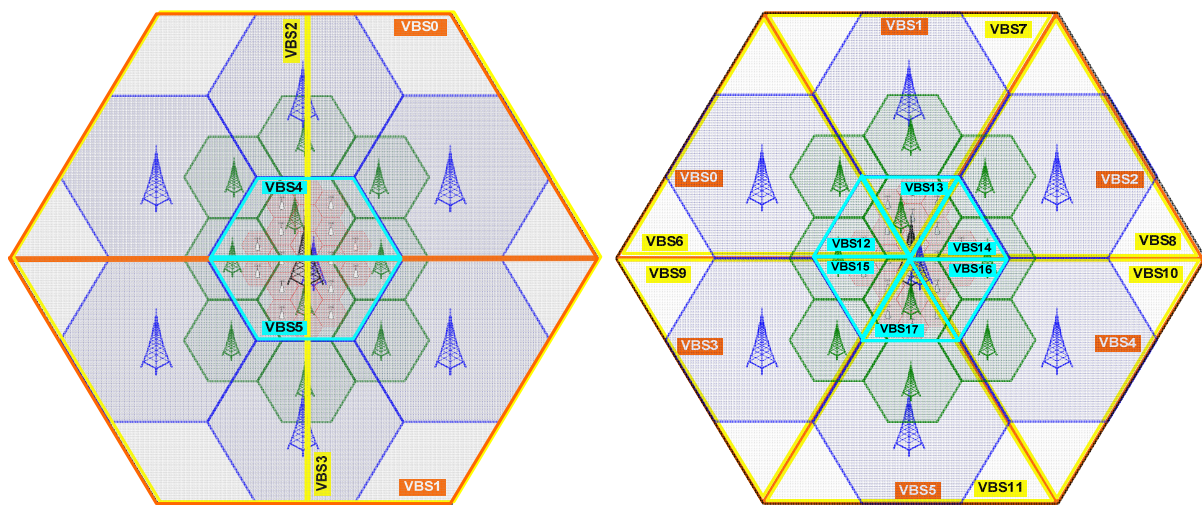
Important aspects covered in this study are the effects caused by changing the quantity of VBSs composing the VNet within the cluster, and the way VBSs are instantiated in the PhyBSs under different VBS requirements. Two different VBS instantiation strategies were considered for the VRRC algorithm assessment. The minPhyBS uses the minimum number of PhyBSs in the VBS coverage area, taking the RAT priority list for the set of services provided by the VNet into account. The MaxPhyBS uses all the PhyBSs under the VBS coverage area to perform the VBS requested capacity. Table 2-4 summarizes the simulated scenarios, which are illustrated in Figure 2.6.

Table 2.3 – Service penetration per VNet.

Services	Service penetration [%]		
	VNet A	VNet B	VNet C
VoIP	100		
Video Streaming			60
Tele-working/ Interactive gaming			40
FTP		2	
P2P		56	
Web		29	
Chat		8	
Email		5	

Table 2-4 – Simulation scenarios.

	Scenario 1	Scenario 2	Scenario 3	Scenario 4
Number of VBSs	6	6	2	2
Instantiation strategy	minPhyBS	MaxPhyBS	minPhyBS	MaxPhyBS



(a) Scenarios 1 and 3.

(b) Scenarios 2 and 4.

Figure 2.6 – Simulation scenarios for different VNets composition.

### 2.3.2 Simulation Results

In this section main results and analysis for Scenarios 1 and 2 are presented. Simulations have been performed for 60 minutes network time. The sampling period for network monitoring was 0.1s.

Results for BE VNet were not presented, since it is assumed that for this kind of VNets no compensation is applied. Instead the available capacity in the BE resources can be used by guaranteed VNets, according to a predefined borrowing margin.

When radio resources are allocated without any compensation mechanism, VNets are operating with out of contract values exceeding 0.8, meaning that data rate capacity provided by InP is below the minimum contracted at least 80% of the time, Figure 2.7. This is due to impairments of the wireless medium. It is also observed that when VRRC is introduced it partially compensates the reduction of

capacity by more radio channels allocation to the VBSs individually and indirectly for the VNet as VBSs aggregation. Note that VNet C, even with the introduction of VRRC, does not reach the minimum Out of Contract value. This is mainly because the services provided by VNet C, which are more demanding in terms of data rate need to use more channels per end-user, therefore increasing the difficulty for compensating the degradation in capacity.

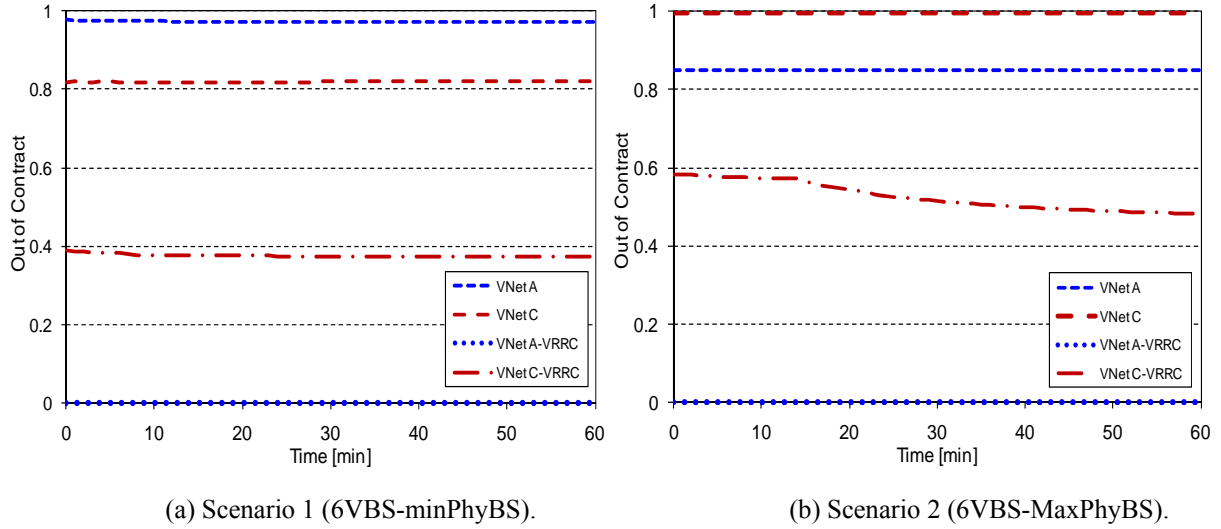


Figure 2.7 – Out of Contract for scenarios 1 and 2.

Results for Service Level, Figure 2.8, show that when radio resources are allocated without any compensation mechanism the VNets are always below its maximum Service Level (with values below 0.5), meaning that VNOs are trying to use the contracted rate but the InP is not providing at least the minimum agreed, due to degradation in the wireless medium or end-users mobility.

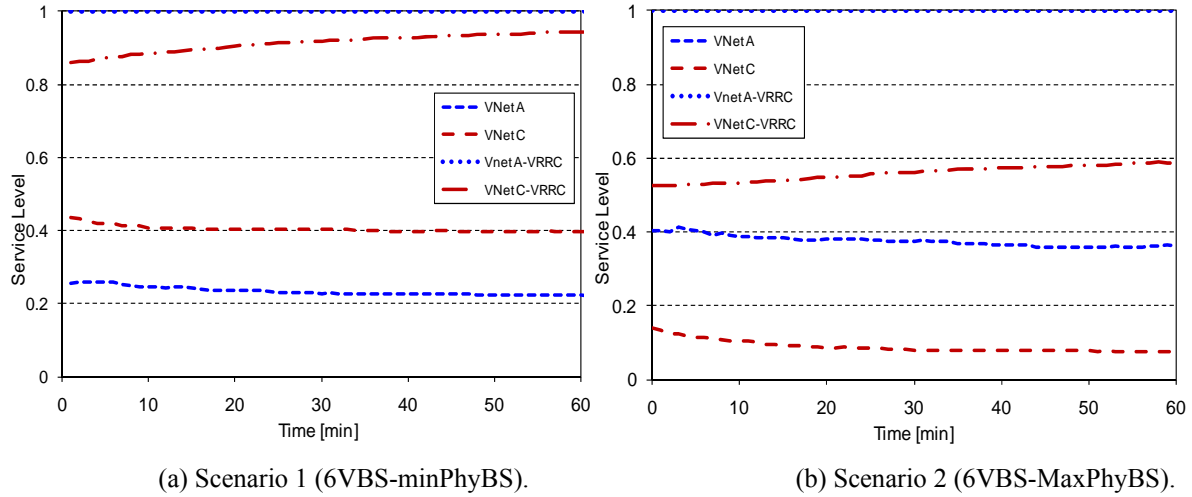


Figure 2.8 – Service Level for scenarios 1 and 2.

From Figure 2.8, it is also observed that the introduction of VRRC allows to partially compensating the reduction of capacity. As referred for Out of Contract, VNet C does not reach the maximum level of service even with VRRC introduction.

In order to analyse the impact of VBSs quantity in the VNets composition, Figure 2.9 depicts Service Level results for scenarios 1 and 3, and Figure 2.10 for scenarios 2 and 4. In the first set of graphs, Figure 2.9, the VBS instantiation strategy is the minPhyBS, and in the second set, Figure 2.10, is the MaxPhyBS. The analysis is just made for VNet C since VNet A Service Level is in both cases totally compensated by VRRC.

From Figure 2.9, it can be seen that for VNet C without compensation the minimum Service Level is 0.40 for 6 VBSs and 0.24 for 2 VBSs. With VRRC, the maximum Service Level obtained for VNet C Reference DR9.3

is 0.94, for scenario 1, which is lower than the obtained for scenario 3, 0.58. Therefore, scenario with higher number of VBSs achieves better Service Level with or without VRRC.

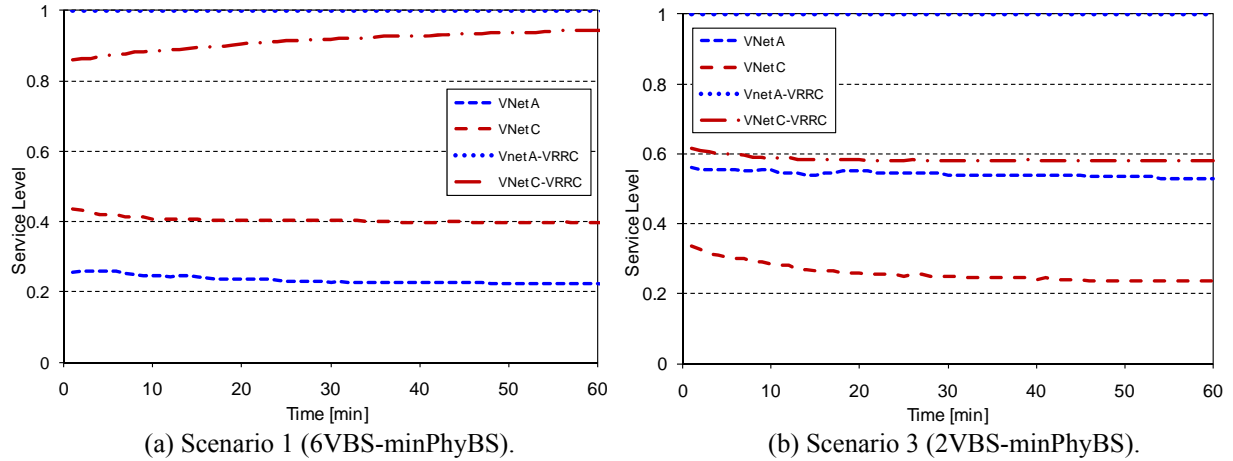


Figure 2.9 – Service Level for scenarios 1 and 3.

Figure 2.10 shows that for VNet C without compensation the minimum Service Level is 0.08 for scenario 2, and 0.6 for scenario 4. With VRRC, the maximum Service Level obtained for VNet C is 0.59, for scenario 2, which is lower than the obtained for scenario 4, 0.94. Therefore, instead of MaxPhyBS strategy for VBS instantiation, for minPhyBS strategy the scenario with lower quantity of VBSs achieves better Service Level with or without VRRC. It can then be concluded that VNet performance depends not only on the quantity of VBS defined for its implementation, but also on the strategies used to instantiate the VBS in the physical infrastructure.

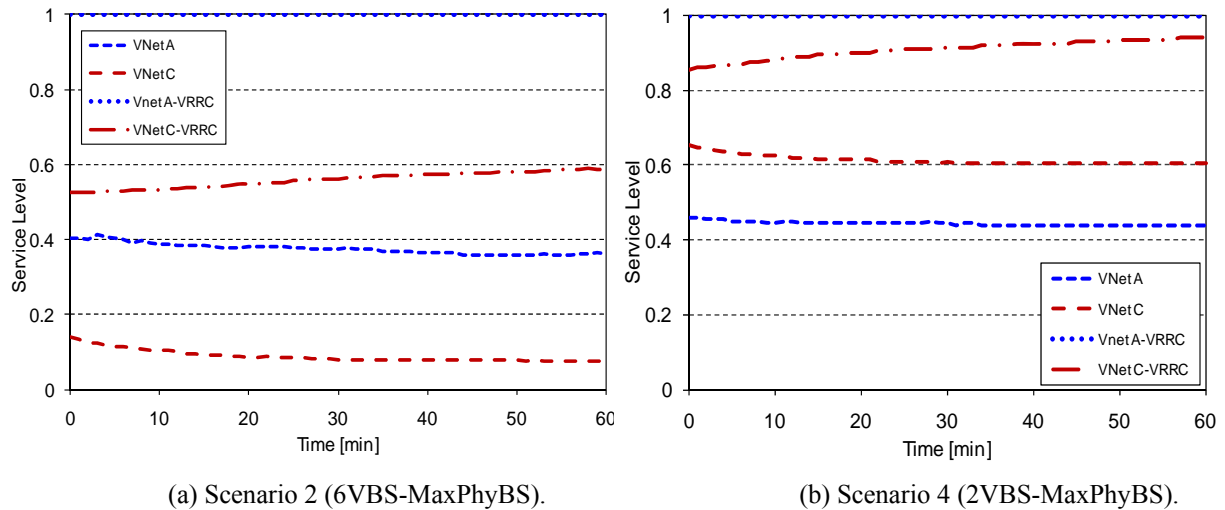


Figure 2.10 – Service Level for scenarios 2 and 4.

Figure 2.11 and Figure 2.12 present the VNets maximum data rate capacity and the required and minimum data rate contracted for scenario 4. It can be seen that before the introduction of VRRC the VNets are always operating below the minimum data rate. The introduction of VRRC algorithm allocates some unused resources in the cluster to compensate the reductions in capacity of radio channels, allowing VNet A to operate above its minimum data rate. However, the quantity of available resources in the cluster to reach the minimum data rate for VNet C is not enough. It must be stressed that the minimum rate value for this simulation is 65% and 70% of the required for VNets A and C, respectively. It was verified that if these values are increased to 70% and 75%, VNet C operates also above its minimum data rate as well as VNet A.



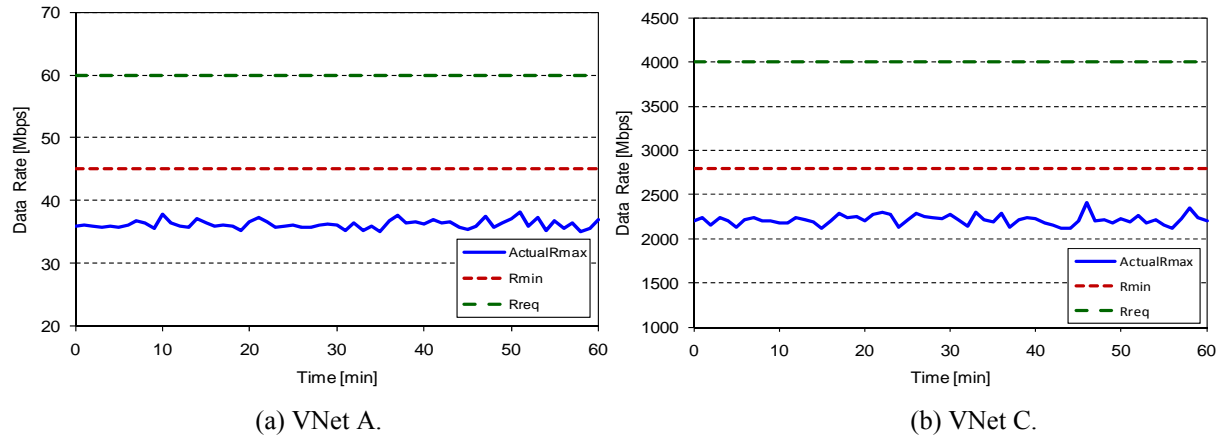


Figure 2.11 – Maximum Rate capacity without compensation.

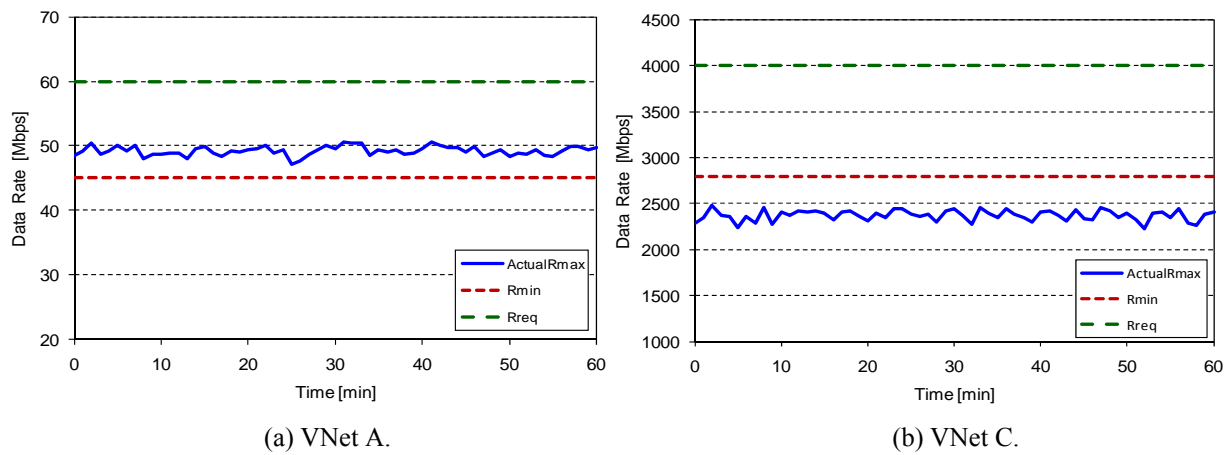


Figure 2.12 – VNet data rate for scenario 4 with VRRC.

Concerning the number of channel adaptations, three types are considered in the VRRC algorithm. The use of channels not yet virtualized in the same PhyBS in which the reduction is detected is a first type of adaptation. A second one makes use of channels borrowed from a VBS allowing for it and with available channels. Lastly, the use of available channels virtualized or borrowed from a neighbour PhyBS is also considered. It is important to refer that the PhyBS for running the VRRC algorithm is selected among all the PhyBSs in which the VBS is instantiated and according to the minimum utilization criterion.

Figure 2.13 illustrates the use of these three mechanisms for scenario 2, VNet with 6 VBSs and MaxPhyBS strategy. For VNet A the compensations are performed mainly using the channels non virtualized in the same PhyBS. For VNet C the BE VNet in the same PhyBS (using the borrowing margin) and the neighbour PhyBS are providing channels to perform the minimum VBSs' data rate.



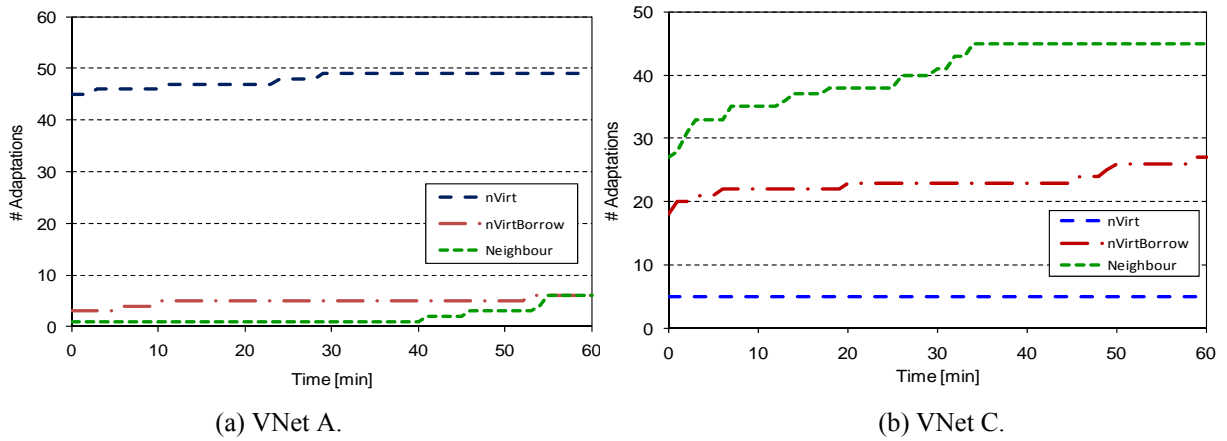


Figure 2.13 – Number of adaptations per type.

According to simulation results, the introduction of VRRC allows supporting the minimum bandwidth requirement in a wireless cluster, composed by several physical base stations from different RATs, providing service over a given coverage area. VRRC takes advantage of the set of shared resources available in the entire common cluster optimising their utilization in order to maintain the contracted capacity. In fact, since some radio resources are not used by the VNets instantiated in the cluster, VRRC reallocates them to guaranteed VNets, operating under data rate capacity reduction.

It must be stressed that although VRRC algorithm may give some support to guaranteed VNets, if the difference between the required and minimum data rate increases, the compensation could be insufficient. This is more critical when the services provided by VNets are more data rate demanding, since the performance degradation affects more channels simultaneously.

Concerning the number of VBSs composing the VNet and the used strategies for its instantiation, in the physical infrastructure, observing results one may conclude that VNet performance depends not only on the quantity of VBSs defined for its implementation, but also on the strategies used to instantiate the VBS in the physical infrastructure.

## 2.4 Energy Efficiency Awareness on Radio Resource Management

### 2.4.1 Metrics and Cost Function to RRM

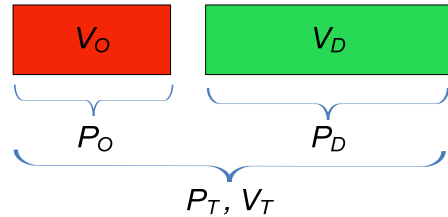
In general, when user data is transmitted, additional network signalling is attached. In some cases, even in an “empty” network, radio beacons transporting network information must be continuously transmitting useful data to standby mobile terminals. Moreover, user’s data includes other information, such as, radio channel formatting and coding overhead, high network layers protocol additional information, and retransmission of information when radio channel falls down. Therefore, in the end, the relation between real user data and overhead is relevant when discussing Energy Efficiency (EE) and the relation between transmitted bit and power.

One can divide the previous concepts into the following parameters, Figure 2.14:

1. The information volume related to overhead and signalling (includes network and users signalling data) issues, as well as retransmissions,  $V_O$  [bit];
2. The information volume only related to real user data generated by the application,  $V_D$  [bit];
3. The total information volume  $V_T$ , required to transmit a user data is defined by:

$$V_{T[\text{bit}]} = V_{O[\text{bit}]} + V_{D[\text{bit}]} \quad (2.5)$$

4. The power required to transmit the overhead information (includes network and users signalling data) defined as  $P_{O[w]}$ ;
5. The power required to transmit the user information defined as  $P_{D[w]}$ ;
6. The total power  $P_{T[w]}$ , defined by:

$$P_{T[w]} = P_{O[w]} + P_{D[w]} \quad (2.6)$$


The diagram illustrates the mapping of power and information parameters. It shows two main components: a red box labeled  $V_O$  and a green box labeled  $V_D$ . Below the red box is a bracket labeled  $P_O$ , and below the green box is a bracket labeled  $P_D$ . A larger bracket below both  $P_O$  and  $P_D$  is labeled  $P_T, V_T$ , indicating the total power and total information volume.

Figure 2.14 – Network, users' power and information parameters map.

The system or network data efficiency,  $\eta_{DT}$ , is defined by:

$$\eta_{DT} = \frac{V_{D[\text{bit}]}}{V_{T[\text{bit}]}} \quad (2.7)$$

establishing a relation between useful user data volume,  $V_D$ , and the overall required info to transmit user data.

The system or network power efficiency,  $\eta_{PT}$ , is defined by:

$$\eta_{PT} = \frac{P_{D[w]}}{P_{T[w]}} \quad (2.8)$$

establishing a relation between the power required to transmit useful user data volume,  $(P_D, V_D)$ , and the overall power required to transmit signalling and user data  $(P_T, V_T)$ . Additionally, further relations can be established, being assumed as an energy cost to the network. The total power cost required to transmit  $V_D$ ,  $C_U$  is as follows:

$$C_{U[w/\text{bit}]} = \frac{P_{T[w]}}{V_{D[\text{bit}]}} \quad (2.9)$$

Using a system level simulator [17], these metrics were implemented. Taking as a first approach a single cell scenario for each RAT, one can extract average results for network data efficiency, for power efficiency metrics and for the total power cost. First results are presented by Table 2.5, where data and power efficiency for R99 and R5 are compared. One may conclude that data efficiency is very similar in both RATs, the reason is that this metric is quite service dependent, and services are very similar in both RATs. Observing the power efficiency metric, one may conclude that R5 is more efficient since this RAT is capable to transmit more information with less power; the only exception is WWW due to protocols overhead. Observing  $C_U$ , one may conclude that R5 is much more cost efficient when compared with R99. These results are obtained for a long period of time to check if they converge to stable and comparable values. However, they can be taken at very short time scales; therefore time scale for these metrics depends only on RRM needs.

Table 2.5 – Network data and power efficiency for different systems and services.

Systems	Metrics	Voice	Video	Streaming	WWW
UMTS R99	$\eta_{DT}$	0.49	0.49	0.49	0.32
	$\eta_{PT}$	0.82	0.46	0.66	0.68
	$C_U$	9.68	1.34	5.15	25.32
UMTS R5	$\eta_{DT}$	0.5	0.49	0.49	0.33
	$\eta_{PT}$	0.94	0.69	0.74	0.64
	$C_U$	0.17	0.25	0.22	0.61

The Energy Efficiency (EE) gain is obtained after running simulations over the micro-urban multi-RAT scenario, by evaluating the RF power savings. The EE gain is generated by multi-RAT management algorithms. These algorithms are driven by the previous cost function which monitors each base station  $C_U$ . If a mobile terminal is not attached to the most EE base station then a vertical handover is triggered from low EE base stations to high ones.

First results for voice and WWW services present EE gains at RF level of 13 and 29% respectively. These gains are achieved by users that are moved (vertical handover) from UMTS R99 to R5.

## 2.5 Spectrum Allocation for OFDMA Networks

### 2.5.1 Radio resource allocation in a single-cellular scenario

#### 2.5.1.1 Introduction

This section is an extension of the work presented in [5]. The objective of the present work is to study the trade-off between resource efficiency and user fairness when opportunistic Radio Resource Allocation (RRA) strategies are used in an Orthogonal Frequency Division Multiple Access (OFDMA) system. In [5], three Radio Resource Allocation (RRA) approaches were studied:

- 1) Rate adaptive sub-carrier assignment and power allocation using optimization based on instantaneous data rates for Non-Real Time (NRT) services;
- 2) Multi-carrier Packet Scheduling (PSC) using utility functions based on average data rates for NRT services;
- 3) Multi-carrier PSC using utility functions based on delay for Real Time (RT) services.

A separate performance evaluation for each of the RRA approaches was presented in [5]. In the present work, we extend the first approach with the evaluation of a different algorithm found in the technical literature [27] and proposal of a novel algorithm, which was originally described in [28] and is able to guarantee several degrees of fairness according to the network operator's interests. Another contribution of the present work is the joint performance evaluation of the first and second approaches, which was not carried out in [5]. Finally, we update the mathematical formulation of the third

approach with a more accurate mathematical definition of the Head-Of-Line (HOL) delay needed for the correct design of the proposed RRA framework suitable for RT services.

### 2.5.1.2 Rate Adaptive Sub-carrier Assignment and Power Allocation Based on Combinatorial Optimization for NRT Services

In this section, we present a study on RRA combinatorial optimization based on the rate adaptive approach aiming at maximizing the overall rate with a power constraint [18], [19], [27], [28].

Three rate adaptive RRA optimization problems were evaluated in [5]:

- Sum Rate Maximization (SRM) [18];
- Max-Min Rate (MMR) [19];
- Sum Rate Maximization with Proportional Rate Constraints (SRM-P) [20].

In the following, the SRM-P problem is revised, and a new proposed problem called Fairness-Based Sum Rate Maximization with Proportional Rate Constraints (FSRM-P) is described.

#### 2.5.1.2.1 Sum Rate Maximization with Proportional Rate Constraints

Trying to balance the trade-off between capacity and fairness, reference [20] formulated a new optimization problem, which we call Sum Rate Maximization with Proportional Rate Constraints (SRM-P). The objective function is the sum capacity, but proportional fairness is assured by imposing a set of nonlinear constraints into the optimization problem, as indicated below:

$$\max_{\rho_{j,k}, p_{j,k}} \sum_{j=1}^M \sum_{k=1}^K \rho_{j,k} \cdot \log_2 (1 + \Gamma \cdot p_{j,k} \cdot \gamma_{j,k}), \quad (2.10)$$

$$s.t. \quad \sum_{j=1}^M \sum_{k=1}^K p_{j,k} \leq P_{total}, \quad (2.11)$$

$$p_{j,k} \geq 0, \quad \forall j, k, \quad (2.12)$$

$$\rho_{j,k} \in \{0, 1\}, \quad \forall j, k, \quad (2.13)$$

$$\sum_{j=1}^M \rho_{j,k} = 1, \quad \forall k, \quad (2.14)$$

$$R_i : R_j = \lambda_i : \lambda_j, \quad \forall i, j \in \{1 \dots M\}, i \neq j, \quad (2.15)$$

where  $K$  is the total number of sub-carriers and  $M$  is the number of MTs;  $p_{j,k}$  is the power and  $\gamma_{j,k}$  is the CNR of the  $k$ -th sub-carrier assigned to the  $j$ -th MT, respectively;  $\Gamma$  is the SNR gap;  $P_{total}$  is Base Station (BS) total transmit power; and  $\rho_{j,k}$  is the connection indicator, whose value 0 or 1 indicates whether sub-carrier  $k$  is assigned to MT  $j$  or not.; and  $\lambda_j$  is the proportional rate requirement of the  $j$ -th MT. On one hand, constraints (2.11) and (2.12) state that the sub-carriers' powers must be non-negative and the sum of powers among all sub-carriers must be lower or equal to the BS total transmit power. On the other hand, constraints (2.13) and (2.14) say that each sub-carrier must be assigned to only one user at any instant of time. Constraint (2.15) states that the user rates must follow the proportional rate requirements for each channel realization, which ensures the rates of different users to be proportional in any time scale of interest.

This problem was originally solved by [20], and that was the solution chosen in the performance evaluation conducted in [5]. However, the algorithm proposed in [20] involves solving nonlinear equations, which requires computationally expensive iterative operations, and thus it is not suitable for a cost-effective real-time implementation. Reference [27] extends the work in [20] by developing a sub-carrier assignment scheme that makes the power allocation problem linear while achieving approximate rate proportionality. This sub-carrier assignment scheme is explained in the following.

This greedy algorithm starts determining the number of sub-carriers  $N_j$  to be initially assigned to each user. This initial step is based on the reasonable assumption that the proportion of sub-carriers assigned to each user is approximately the same as their eventual rates after power allocation, and thus would roughly satisfy the proportional rate constraints. The next step assigns to each user the unallocated sub-carrier that has the maximum gain for that user. Next a greedy policy is applied, where the user that needs a sub-carrier most, i.e. the one that has the lowest proportional rate  $R_j / \lambda_j$  can choose the best sub-carrier for it. Once the user gets his required  $N_j$  sub-carriers, he can no longer be assigned any other sub-carriers in this step. The last step assigns the remaining  $N_{res}$  sub-carriers to the best users for them, where each user can get at most one unassigned sub-carrier. This is done in order to prevent the user with the best gains to get the rest of the sub-carriers. This policy balances achieving proportional fairness while increasing overall capacity.

After the sub-carrier assignment described above, the optimization problem (2.10) is simplified into maximization over continuous variables  $p_{j,k}$ , which can be solved optimally. The resulting power allocation problem is reduced to a solution of simultaneous linear equations, which can be optimally found with much less computational complexity. The power allocation is performed in two steps: power allocation among users and power allocation across sub-carriers per user. The first step solves the set of simultaneous linear equations and assigns the total power  $P_j$  for each user in order to maximize the capacity while enforcing the rate proportionality. The second step performs waterfilling and assigns the powers  $p_{j,k}$  for each user's sub-carriers subject to his total power constraint  $P_j$ .

#### 2.5.1.2.2 Fairness-Based Sum Rate Maximization with Proportional Rate Constraints

The rate adaptive RRA policies described above and also in [5], namely SRM, MMR and SRM-P, show static performances in the efficiency-fairness plane. SRM is one extreme, providing maximum efficiency in the resource usage. MMR is the other extreme in which maximum user fairness is achieved. Finally, SRM-P is a trade-off between those two. In the case of equal proportional rates constraints, SRM-P should present a performance similar to MMR, but with lower fairness and higher system capacity due to the use of a sophisticated power allocation that tries to maximize capacity. In this section we propose a novel RRA policy that includes fairness as a new degree of freedom in the optimization problem. Using this fairness/rate adaptive policy, the network operator can achieve different fairness levels in the system and can define in which operation point in the efficiency-fairness plane it wants the network to be.

The Fairness-Based Sum Rate Maximization with Proportional Rate Constraints (FSRM-P) optimization problem, which was originally proposed in [28], is a modification of the original SRM-P problem (2.10)-(2.15) in such a way that now fairness has to be taken into account in the optimization constraints. The new fairness constraint is given below:

$$\Phi_{cell} = \Phi_{cell}^{target}, \quad (2.16)$$

where  $\Phi_{cell}$  is the instantaneous Cell Fairness Index (CFI) and  $\Phi_{cell}^{target}$  is the desired target value. The CFI is defined as [26][28][29]:

$$\Phi_{cell}[n] = \frac{\left( \sum_{j=1}^M \phi_j[n] \right)^2}{M \cdot \sum_{j=1}^M (\phi_j[n])^2}, \quad (2.17)$$

where  $M$  is the number of MTs in the cell and  $\phi_j$  is the User Fairness Index (UFI) of the  $j$ -th MT given below:

$$\phi_j = R_j[n], \quad (2.18)$$

where  $R_j[n]$  is the instantaneous data rate of the  $j$ -th MT. Notice that  $1/M \leq \Phi_{cell} \leq 1$ . A perfect fair allocation is achieved when  $\Phi_{cell} = 1$ , which means that the rates allocated to all MTs are equal (all UFIs are equal). The worst allocation occurs when  $\Phi_{cell} = 1/M$ , which means that all resources were allocated to only one MT.

The fairness constraint (2.16) is used to replace the proportional rate constraints given by (2.15). This is done because the constraints (2.15) and (2.16) are incompatible. If the proportional rate constraints are met exactly, we have  $\Phi_{cell} = 1$  according to (2.17) and (2.18). The FSRM-P problem has to deal with a scenario where the proportional rate constraints have to be partially destroyed in order to decrease fairness and allow the network operator to have a controllable trade-off between resource efficiency and user fairness. However, the violation of the rate proportionalities in favour of fairness decrease has to be done in a way such that system capacity is maximized, as required by the objective function (2.10).

A two-step sub-optimum solution for the FSRM-P problem is proposed by algorithms 1 and 2 (see Figure 2.16 and Figure 2.17). An overview of the functioning of the FSRM-P policy is illustrated in Figure 2.15. Firstly, the final solution must be approached with a good start point, which we choose to be the SRM-P sub-carrier assignment. This initial solution is simple and takes into consideration the objective function and all optimization constraints, except the fairness constraint (2.15). After this initial resource allocation, we have  $\Phi_{cell} = \Phi_{SRM-P}$ , which is a value close to one. In the following, the fairness decrease is done by the FSRM-P sub-carrier re-assignment procedure (lines 9-27 of Algorithm 1) and power re-allocation procedure (Algorithm 2). The reasoning behind the fairness decrease is to take a little money (resource) from the poor (user with minimum proportional rate) and give it to whom can make the best use of it. In this way, we can decrease fairness destroying the least the rate proportionalities and maximize system capacity.

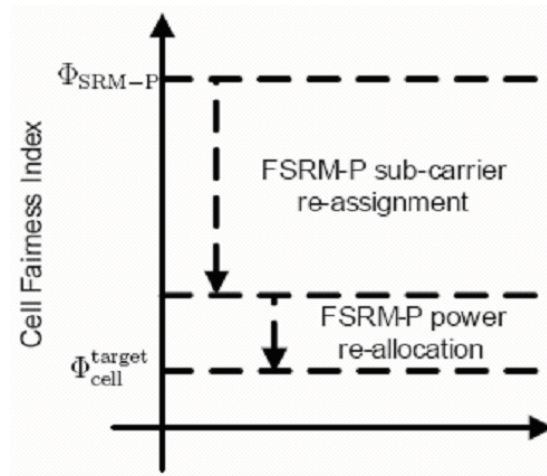


Figure 2.15 – Impact on fairness of the sub-carrier re-assignment and power re-allocation of the FSRM-P policy.

According to lines 9-27 of Algorithm 1, the fairness in the system can be decreased by removing the worst sub-carrier of the worst user (minimum proportional rate) and give it to the user with the highest channel quality to that sub-carrier. This process is repeated until the CFI roughly meets the target CFI. In this process of re-assigning sub-carriers following a policy of maximum resource efficiency, each sub-carrier can be possibly re-assigned only once. However, it may happen that the user with minimum proportional rate is the best owner of one or few sub-carriers, i.e. these sub-carriers have the highest channel gains to this user. In this particular case, these sub-carriers are not re-assigned. If a user ends up with no sub-carriers or with only his best sub-carriers, he does not participate on the sub-carrier re-assignment process any more.

The FSRM-P power re-allocation procedure depicted in Algorithm 2 follows a similar approach. Slices of power  $\Delta p$  are moved between sub-carriers of different users in order to decrease fairness until the target CFI is reached with an arbitrarily small error tolerance. In summary, the algorithm works as follows. The user with minimum proportional rate is selected. Possible rate decrements due to the removal of power  $\Delta p$  are calculated for all his sub-carriers. The sub-carrier that shows the lowest rate decrement is the one to lose that slice of power. For all the other sub-carriers of the other users, possible rate increments due to the addition of power  $\Delta p$  are calculated, and the one that presents the highest rate increment will receive that amount of power. The process is repeated until the target CFI is met with sufficient accuracy.

**Algorithm 1: Sub-carrier assignment of FSRM-P policy.**

```

Initialization
1:  $\mathcal{M} \leftarrow \{1, 2, 3, \dots, M\}$  // Users set
2:  $\mathcal{K} \leftarrow \{1, 2, 3, \dots, K\}$  // Sub-carriers set
3: for all  $j \in \mathcal{M}$  and  $k \in \mathcal{K}$  do
4:    $\rho_{j,k} \leftarrow 0$  // Reset connection matrix
5:    $\mathcal{K}_j \leftarrow \emptyset$  // Reset user sub-carriers subset
6:    $\mathcal{S} \leftarrow \emptyset$  // Reset blocked sub-carriers subset
7: end for

Initial sub-carrier assignment
8: Apply sub-carrier assignment of SRM-P policy

Sub-carrier re-assignment to decrease fairness
9: Calculate  $\Phi_{\text{cell}}$ 
10: while  $\Phi_{\text{cell}} > \Phi_{\text{cell}}^{\text{target}}$  do
11:    $j^* \leftarrow \arg \min_j \{R_j / \lambda_j\}, \forall j \in \mathcal{M}$  // Find available user with minimum proportional rate
12:    $k^* \leftarrow \arg \min_k \{\gamma_{j^*,k}\}, \forall k \in \mathcal{K}_{j^*} \text{ and } \forall k \notin \mathcal{S}$  // Find available sub-carrier assigned to user  $j^*$ 
    with minimum channel quality
13:    $j^{**} \leftarrow \arg \max_j \{\gamma_{j,k^*}\}, \forall j \in \mathcal{M}$  // Find available user with maximum channel quality on
    sub-carrier  $k^*$ 
14:   if  $j^{**} \neq j^*$  then
15:      $\rho_{j^*,k^*} \leftarrow 0$  // Remove the connection for user  $j^*$ 
16:      $\mathcal{K}_{j^*} \leftarrow \mathcal{K}_{j^*} - \{k^*\}$  // Update sub-carrier subset of user  $j^*$ 
17:      $R_{j^*} \leftarrow R_{j^*} - r_{j^*,k^*}$  // Update rate of user  $j^*$ 
18:      $\rho_{j^{**},k^*} \leftarrow 1$  // Set the connection for user  $j^{**}$ 
19:      $\mathcal{K}_{j^{**}} \leftarrow \mathcal{K}_{j^{**}} + \{k^*\}$  // Update sub-carrier subset of user  $j^{**}$ 
20:      $R_{j^{**}} \leftarrow R_{j^{**}} + r_{j^{**},k^*}$  // Update rate of user  $j^{**}$ 
21:   end if
22:    $\mathcal{S} \leftarrow \mathcal{S} + \{k^*\}$  // Update set of blocked sub-carriers
23:   if  $(\mathcal{K}_{j^*} \cap \mathcal{S} == \mathcal{K}_{j^*})$  or  $(\mathcal{K}_{j^*} == \emptyset)$  then // If user  $j^*$  does not have sub-carriers or if they
    are all blocked
24:      $\mathcal{M} \leftarrow \mathcal{M} - \{j^*\}$  // Remove user  $j^*$  from the set of available users
25:   end if
26:   Re-calculate  $\Phi_{\text{cell}}$ 
27: end while

```

Figure 2.16 – Algorithm 1: Sub-carrier assignment of FSRM-P policy.

**Algorithm 2: Power allocation of FSRM-P policy.**

**Initialization**

- 1:  $\mathcal{M} \leftarrow \{1, 2, 3, \dots, M\}$  // Users set
- 2:  $\mathcal{K} \leftarrow \{1, 2, 3, \dots, K\}$  // Sub-carriers set
- 3:  $\mathcal{U} \leftarrow \emptyset$  // Reset blocked users subset
- 4: Initialize  $\epsilon$  // Error tolerance of fairness index
- 5: Initialize  $\Delta p$  // Power step
- 6: **for all**  $j \in \mathcal{M}$  and  $k \in \mathcal{K}_j$  **do**
- 7:    $p_{j,k} \leftarrow P_{\text{total}}/K$  // Sub-carriers' powers are initialized with equal values
- 8: **end for**

**Power re-allocation to decrease fairness**  
 // After sub-carrier assignment is determined, power re-allocation is performed

- 9: Calculate  $\Phi_{\text{cell}}$
- 10: **while**  $|\Phi_{\text{cell}} - \Phi_{\text{cell}}^{\text{target}}| > \epsilon$  **do**
- 11:    $\mathcal{U} \leftarrow \arg_j \{R_j == 0\}$  // Update blocked users subset
- 12:    $j^* \leftarrow \arg \min_j \{R_j/\lambda_j\}, \forall j \in \mathcal{M} \text{ and } \forall j \notin \mathcal{U}$  // Find available user with minimum proportional rate
- 13:   **for all**  $k \in \mathcal{K}_{j^*}$  **do**
- 14:      $\Delta r_k^{\text{dec}} \leftarrow \frac{B}{K} \cdot \log_2(1 + p_{j^*,k} \cdot \gamma_{j^*,k}) - \frac{B}{K} \cdot \log_2(1 + (p_{j^*,k} - \Delta p) \cdot \gamma_{j^*,k})$
- 15:   **end for**
- 16:    $k^* \leftarrow \arg \min_k \{\Delta r_k^{\text{dec}}\}, \forall k \in \mathcal{K}_{j^*}$  // Find sub-carrier assigned to user  $j^*$  with minimum rate decrement
- 17:   **for all**  $j \neq j^*$  and  $k \in \mathcal{K}_j$  **do**
- 18:      $\Delta r_k^{\text{inc}} \leftarrow \frac{B}{K} \cdot \log_2(1 + (p_{j,k} + \Delta p) \cdot \gamma_{j,k}) - \frac{B}{K} \cdot \log_2(1 + p_{j,k} \cdot \gamma_{j,k})$
- 19:   **end for**
- 20:    $k^{**} \leftarrow \arg \max_k \{\Delta r_k^{\text{inc}}\}, \forall k \neq k^*$  // Find sub-carrier with maximum rate increment
- 21:    $j^{**} \leftarrow \arg_j \{\rho_{j,k^{**}} == 1\}, \forall j \in \mathcal{M}$  // Find user who has been assigned sub-carrier  $k^{**}$
- 22:    $p_{j^*,k^*} \leftarrow p_{j^*,k^*} - \Delta p$  // Power transfer (decrement)
- 23:    $\hat{R}_{j^*} \leftarrow R_{j^*} - \Delta r_{k^*}^{\text{dec}}$  // Update rate of user  $j^*$
- 24:    $p_{j^{**},k^{**}} \leftarrow p_{j^{**},k^{**}} + \Delta p$  // Power transfer (increment)
- 25:    $\hat{R}_{j^{**}} \leftarrow R_{j^{**}} + \Delta r_{k^{**}}^{\text{inc}}$  // Update rate of user  $j^{**}$
- 26:   Re-calculate  $\Phi_{\text{cell}}$
- 27: **end while**

Figure 2.17 – Algorithm 2: Power allocation of FSRM-P policy.

### 2.5.1.3 Joint Performance Evaluation of Fairness/Rate Adaptive RRA and Utility-Based PSC for NRT Services

The present work extends the performance evaluation depicted in [5], since it presents a joint comparison of fairness/rate adaptive RRA algorithms based on instantaneous data rates and utility-based packet scheduling based on average data rates for NRT services. The following algorithms will be evaluated:

- Fairness/rate adaptive RRA
  - Sum Rate Maximization (SRM) [5][18]
  - Max-Min Rate (MMR) [5][19]
  - Sum Rate Maximization with Proportional Rate Constraints (SRM-P) [27]
  - Fairness-Based Sum Rate Maximization with Proportional Rate Constraints (FSRM-P) [28]
- Utility-based PSC



- Max-Rate (MR) [5][21]
- Max-Min Fairness (MMF) [5][31]
- Proportional Fairness (PF) [5][23]
- Adaptive Throughput-Based Fairness (ATF) [24][29][30]

The main simulation parameters are shown in Table 2.6.

Table 2.6 – Simulation parameters

Parameter	Value
Number of cells	1
Maximum BS transmission power	1 W
Cell radius	500 m
MT speed	static
Carrier frequency	2 GHz
Number of sub-carriers	192
Sub-carrier bandwidth	15 kHz
Path loss	$L = 128.1 + 37.6 \log_{10} d$ (see section 2.3.1.1 of [5])
Log-normal shadowing standard dev.	8 dB
Small-scale fading	Typical Urban (TU) [22]
AWGN power per sub-carrier	-123.24 dBm
BER requirement	10 <sup>-6</sup>
Link adaptation	see section 2.3.1.1 of [5]
Transmission Time Interval (TTI)	0.5 ms
Traffic model	Full buffer
Throughput filtering time constant	50 (see [5])
ATF minimum exponent value	0
ATF maximum exponent value	1
ATF control time window	0.5 ms
ATF step size	0.1
ATF filtering constant	0.1
ATF CFI target	0.5
FSRM-P CFI target	0.8
Satisfaction requirement	640 kbps

The metrics used for evaluation and comparison of the investigated resource allocation algorithms were:

- Total cell throughput (resource allocation efficiency factor);

- Cell fairness index according to (2.17). It was assumed that the user fairness index  $\phi_j$  used in (2.17) was given by (2.18) for the case of fairness/rate adaptive RRA algorithms based on instantaneous data rate, or  $\phi_j = T_j$  (throughput) for the case of utility-based PSC algorithm based on average data rate;
- User satisfaction (percentage of satisfied users in the cell). A user is considered satisfied if:
  - The instantaneous data rate  $R_j$  is equal or higher than 640 kbps for the case of fairness/rate adaptive RRA algorithms; or
  - The achieved throughput at the end of his session is equal or higher than 640 kbps for the case of utility-based PSC algorithms.

The results presented in this section are obtained for all fairness/rate adaptive RRA algorithms presented averaged over 10000 snapshots (each with a simulation time span of 0.5 ms), and all utility-based PSC algorithms averaged over 10 snapshots (each with a simulation time span of 30s). The difference in the duration of the simulations is due to the fact that the utility-based optimization is based on average data rates and so it requires a larger time window. For the rate adaptive SRM-P algorithm (see section 2.5.1.2), the proportional rate requirements are set equal to one for all users, i.e.  $\lambda_j = 1$  ( $j = 1, \dots, M$ ). In case of the utility-based packet scheduling analysis, the power distribution over all sub-carriers was uniform with no power adaptation.

Figure 2.18 shows the mean cell fairness index calculated using (2.17) for different cell loads and various RRA algorithms. In this case the rate adaptive MMR and utility-based MMF algorithms outperform all the others. As expected, the SRM resource allocation and the MR PSC algorithms, which are designed to use the resources in the most efficient way, are the ones that present the lowest fairness indexes. The SRM-P resource allocation and the PF PSC algorithms achieve a static trade-off between resource efficiency and user fairness. The latter presents a more visible trade-off since the former shows a performance very close to the MMR resource allocation algorithm. Regarding the ATF and FSRM-P algorithms, we run simulations with two different target CFIs, 0.5 and 0.8, respectively. It can be observed that ATF and FSRM-P are successful to achieve its main objective, which is to guarantee a strict fairness distribution among the MTs. In the case of ATF this is achieved due to the feedback control loop that dynamically adapts the parameter  $\beta$  of the ATF priority function (see [5] for more details). On the other hand, in the case of FSRM-P, the fairness adaptation is done by the sub-carrier re-assignment and power re-allocation procedures depicted in Algorithms 1 and 2, respectively (see section 2.5.1.2). The advantage of the ATF and FSRM-P algorithms in comparison with the others is that they can be designed to provide any required fairness distribution, while the other strategies are static and do not have the freedom to adapt them and guarantee a specific performance result.

Figure 2.19 shows the total cell throughput for the different algorithms. As expected, the SRM resource allocation and the MR PSC algorithms are able to maximize the resource efficiency, while MMR and MMF present the lowest cell throughput. Since SRM-P and PF are trade-offs between SRM/MR and MMR/MMF, their performance lied between those extremes. Looking at Figure 2.18, one can expect that depending on the value of the ATF and FSRM-P target fairness index, their respective resource efficiencies would be somewhere in the middle between the performances of MMF/MMR, PF/SRM-P and MR/SRM. This can be observed in Figure 2.19. On one hand, since the ATF target fairness index is set to 0.5, ATF works as a hybrid scheduling policy between PF and MR. On the other hand, the FSRM-P performance in terms of total cell throughput lies between MMR and SRM-P since its target fairness index is set to 0.8. Notice that the throughput values presented by the MR PSC algorithm are lower than those observed with the rate adaptive SRM resource allocation. This was due to the fact that the simulations carried out for the PSC investigation did not consider power adaptation.

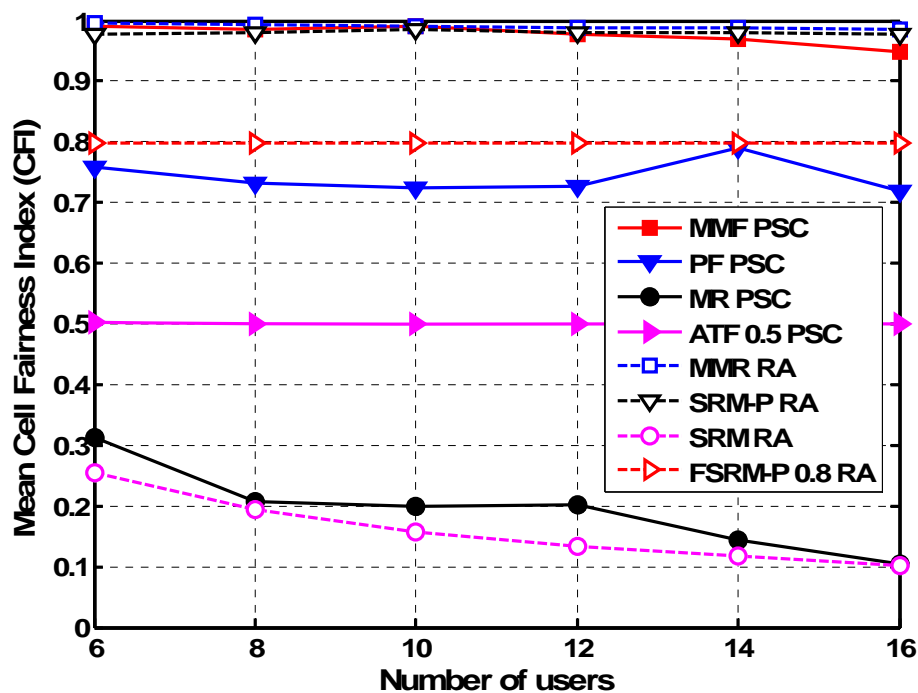


Figure 2.18 – Cell fairness index as function of the number of users.

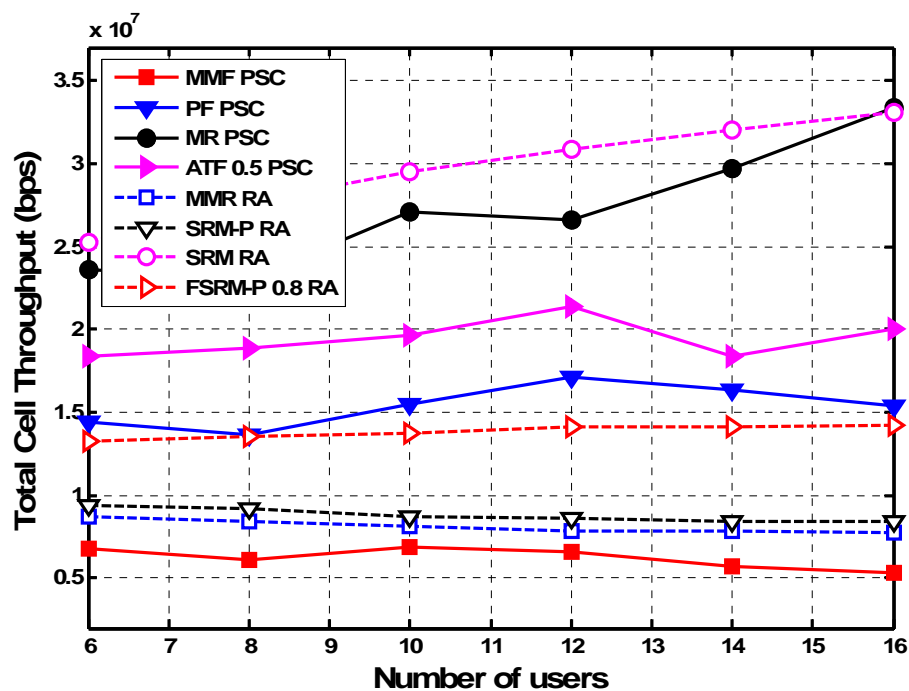


Figure 2.19 – Total cell throughput as function of the number of users.

The user satisfaction as a function of the number of users is depicted in Figure 2.20. It is interesting to see that the algorithms that achieve a trade-off between resource efficiency and user fairness, namely SRM-P, PF, ATF, and FSRM-P are the ones that present the highest user satisfaction. This indicates that it is not advantageous in terms of user satisfaction to use RRA algorithms that are located in the extremes of the efficiency-fairness plane (maximization of system capacity or maximization of user fairness). In general terms, the algorithms that maximize capacity achieve low and almost constant user satisfaction because they always give priority to few users with best channel conditions. On the

other hand, the algorithms that privilege user fairness present higher satisfaction for low system load but the performance decreases very fast when the number of users increases.

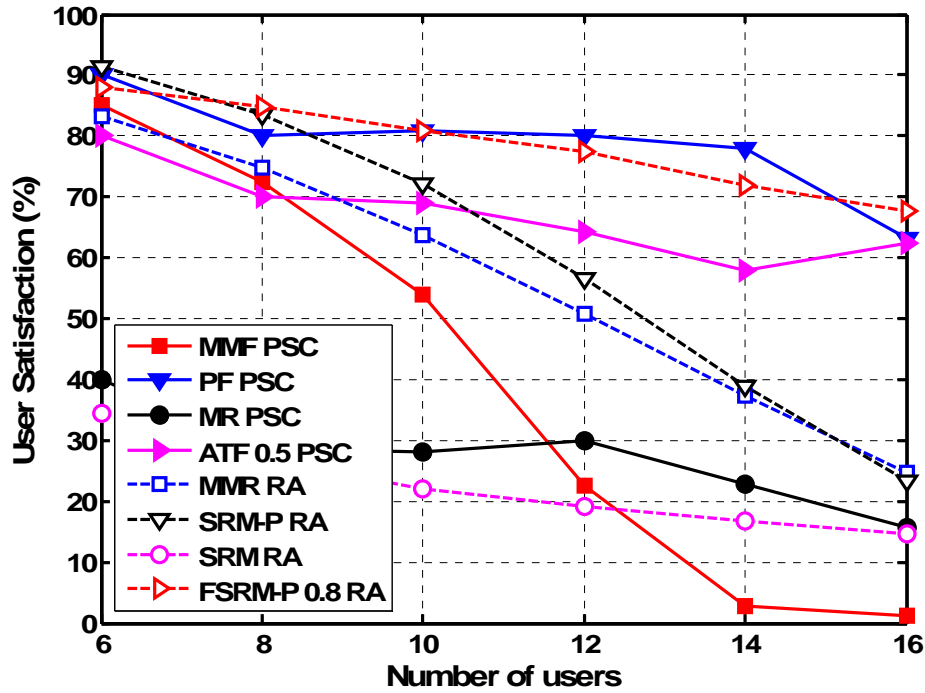


Figure 2.20 – User satisfaction as function of the number of users.

One last issue that should be taken into account is complexity. In general, the rate adaptive RRA strategies considered in this work, which are comprised of sub-carrier assignment and power allocation algorithms and are based on instantaneous data rate, present higher computational complexity than their counterparts that use utility-based PSC algorithms and are based on average data rates. Using less computational resources, the utility-based PSC algorithms show approximately the same performance in terms of fairness and system capacity compared with their rate adaptive counterparts and also good performance in terms of user satisfaction. Furthermore, both the adaptive utility-based ATF and the fairness/rate adaptive FSRM-P algorithms provide the flexibility to work in any operation point in the efficiency-fairness plane, but the former has the advantage of presenting less algorithmic complexity.

#### 2.5.1.4 Packet Scheduling Based on Utility Theory for RT Services

This section is an update of the correspondent section in [5]. The proposed RRA framework suitable for RT services is developed based on a more accurate definition of the HOL delay.

The considered optimization problem is the maximization of the total utility with respect to the delay of the Head-of-Line (HOL) packet, which can approximately be calculated by

$$d_j^{hol}[n+1] = d_j^{hol}[n] + \frac{N_j^{hol}[n] - R_j[n] \cdot t_{tti}}{T_j[n-1]}, \quad (2.19)$$

where  $N_j^{hol}[n]$  is the current number of bits in the HOL packet,  $t_{tti}$  is the duration of the TTI in seconds,  $T_j[n-1]$  is the average data rate (throughput) up to the previous scheduling period and  $R_j[n]$  is the instantaneous achievable transmission rate. If the  $j$ -th user has not been served by any

sub-carrier in the  $n$ -th TTI,  $R_j[n]$  is equal to zero and the HOL delay is incremented. This delay increment is calculated assuming that the remaining bits of the HOL packet will be transmitted using a rate equal to the throughput experienced so far by the MT. For sake of simplicity of the HOL delay, we assumed that the packets' arrival time is equal to the TTI duration. It is well known that in real networks, the packet arrival time depends on the type of application. For example, for the VoIP service the arrival time is equal to the voice frame duration, i.e. each VoIP packet arrives in the user buffer every 20 ms. However, this assumption does not invalidate the mathematical and conceptual RRA framework considered in this work, and make the optimization model much more tractable. Taking this into account, one can see in (2.19) that if the instantaneous transmission rate is such that all remaining bits of the HOL packet are transmitted in the current TTI, the HOL delay remains constant because the previous packet in the buffer will be the HOL packet now. Finally, the HOL delay is decremented when the instantaneous achievable transmission rate is high enough to transmit the remaining bits of the HOL packet and some bits of the preceding packets in the queue.

The mathematical formulation of this new optimization problem is presented below:

$$\max_{p_{j,k}, K_j} \sum_{j=1}^M U_j(d_j^{hol}[n]) \quad (2.20)$$

$$s.t. \quad \sum_{j=1}^M \sum_{k=1}^K p_{j,k} \leq P_{total}, \quad (2.21)$$

$$p_{j,k} \geq 0, \quad \forall j, k \quad (2.22)$$

$$\bigcup_{j \in \{1 \dots M\}} K_j \subseteq K \quad (2.23)$$

$$K_i \cap K_j = \emptyset, \quad \forall i, j \in \{1 \dots M\}, i \neq j \quad (2.24)$$

where  $K_j$  is the subset of sub-carriers assigned to the  $j$ -th MT,  $K$  is the set of all sub-carriers in the system,  $M$  is the set of all MTs in the system,  $p_{j,k}$  is the power of the  $k$ -th sub-carrier assigned to the  $j$ -th MT,  $P_{total}$  is total transmit power of the cell, and  $U_j(d_j^{hol}[n])$  is a concave and decreasing utility function based on the HOL delay  $d_j^{hol}[n]$  of the  $j$ -th MT. On one hand, constraints (2.21) and (2.22) state that the sub-carriers' powers must be non-negative and the sum of powers among all sub-carriers must be lower or equal to the BS total transmit power. On the other hand, constraints (2.23) and (2.24) say that there is a limited number of sub-carriers and that each one of them must be assigned to only one user at any instant of time.

Taking (2.19) into account, we can see that the derivative of  $U_j(d_j^{hol}[n])$  with respect to  $R_j$  can be expressed as

$$\frac{\partial U_j}{\partial R_j} = \frac{\partial U_j}{\partial d_j^{hol}} \cdot \frac{\partial d_j^{hol}}{\partial R_j} = \frac{\partial U_j}{\partial d_j^{hol}} \cdot \left( -\frac{t_{tti}}{T_j[n-1]} \right). \quad (2.25)$$

Since the TTI duration is sufficiently small, we can use the Lagrange theorem of the mean, which says that [25][21]

$$\begin{aligned}
& \sum_{j=1}^M U_j(d_j^{hol}[n+1]) - \sum_{j=1}^M U_j(d_j^{hol}[n]) \\
& \approx \sum_{j=1}^M \frac{\partial U_j}{\partial r_j} \Big|_{R_j=R_j[n-1]} \cdot (R_j[n] - R_j[n-1]) \\
& = \sum_{j=1}^M -\frac{\partial U_j}{\partial d_j^{hol}} \Big|_{d_j^{hol}=d_j^{hol}[n]} \cdot \frac{t_{tti}}{T_j[n-1]} \cdot (R_j[n] - R_j[n-1]) \\
& = \sum_{j=1}^M \left| \frac{\partial U_j}{\partial d_j^{hol}} \right| \Big|_{d_j^{hol}=d_j^{hol}[n]} \cdot \frac{t_{tti}}{T_j[n-1]} \cdot (R_j[n] - R_j[n-1]).
\end{aligned} \tag{2.26}$$

Considering that  $R_j[n-1]$  is known and fixed in the  $n$ -th TTI, the optimization objective function can be further simplified and expressed as

$$\max_{p_{j,k}, K_j} \sum_{j=1}^M \frac{|U'_j(d_j^{hol}[n])|}{T_j[n-1]} \cdot R_j[n], \tag{2.27}$$

where  $U'_j(d_j^{hol}[n]) = \frac{\partial U_j(d_j^{hol})}{\partial d_j^{hol}} \Big|_{d_j^{hol}=d_j^{hol}[n]}$  is the marginal utility of the  $j$ -th MT with respect to his current HOL delay, and  $d_j^{hol}[n]$  can be obtained from the recursive equation (2.19).

Therefore, the sub-carrier assignment problem employs the following reasoning: the MT  $j^*$  is chosen to transmit on the  $k$ -th sub-carrier in TTI  $n$  if it satisfies the condition given by:

$$j^* = \arg \max_j \left\{ |U'_j(d_j^{hol}[n])| \cdot \frac{c_{j,k}[n]}{T_j[n-1]} \right\}, \quad \forall j, \tag{2.28}$$

where  $U'_j(\cdot)$  is the marginal utility of the  $j$ -th MT,  $T_j[n-1]$  is the throughput of the  $j$ -th MT up to TTI  $n-1$ , and  $c_{j,k}[n]$  denotes the instantaneous achievable transmission efficiency of the  $j$ -th MT on the  $k$ -th sub-carrier.

One can notice that the sub-carrier assignment policy described in (2.28), which was achieved based on a more accurate mathematical definition of the HOL delay given by (2.19), is the same of the one used in [5]. That means that the RRA framework suitable for RT services presented in [5] remains valid.

## 2.5.2 Radio resource allocation in a multi-cellular scenario

This section is made-up by two subsections: a comparison of the performance of some distributed schemes in a SISO setting with ideal channel state information at the BS and a study on the impact of feedback in a coordinated scheduling in a MIMO scenario.

### 2.5.2.1 Distributed schemes

#### 2.5.2.1.1 Problem formulation

We consider a cellular system composed of  $N_{cells}$  cells that share the whole available spectrum, i.e., the frequency reuse is equal to one. In each cell  $i$  there is a base station and  $K(i)$  mobile users. The BS schedules the users and assigns them a subset of the radio channels. The modulation technique is multi-carrier and the multiple access scheme is OFDMA, so that within each cell the system

bandwidth is partitioned into orthogonal subcarriers and each user is assigned a different subset of subcarriers. To perform resource allocation, the BS needs to know channel gains and interference levels on all subcarriers for all users in the cell. To reduce allocation complexity, we group sets of adjacent subcarriers into subchannels. As long as the bandwidth spanned by a subchannel is smaller than the radio channel coherence bandwidth, the channel spectrum can be approximated as flat in the subchannel. Thus, we can assume that the choice of performing resource allocation on subchannels rather than on subcarriers causes almost no loss in diversity: power remains constant and coding is done across the tones in each subchannel. These assumptions closely mirror what is being done in existing OFDMA systems. In particular, in WiMAX [32] each time frame is subdivided into zones, each of which corresponds to a different operation mode. One of them is the band adaptive modulation and coding (band AMC) zone, in which contiguous subcarriers and OFDM symbols are grouped together into one basic allocation unit, called a subchannel. Similarly, in the UTRAN Long Term Evolution (LTE) system [33] the subcarriers in each Transmission Time Interval (TTI) are grouped into equal sized physical resource blocks (PRBs); each block is allocated to a single user, and a user can be scheduled on multiple PRBs.

Our goal is to minimize the overall power transmitted in each cell subject to a rate constraint per user: each BS  $i$  needs to assign to each served user  $k$  a set of orthogonal channels  $S_k^{(i)}$  and distribute power in such a way that all rate requirements  $R_k^{(i)}$  ( $k = 1, \dots, K(i)$ ) are met. By indicating with  $P_n^{(i)}$  the power transmitted on subchannel  $n$  in cell  $i$ , and using the Shannon capacity as a measure of the transmitted rate, the allocation problem can be formulated as a set of  $N_{cells}$  optimization problems. In cell  $i$  the problem is stated as:

$$\begin{aligned}
 & \min \sum_{k=1}^{K(i)} \sum_{n \in S_k^{(i)}} P_n^{(i)} \\
 & \quad s.t. \\
 & \sum_{n \in S_k^{(i)}} B \log_2(1 + \gamma_{k,n}^{(i)}) \geq R_k^{(i)} \quad k = 1, \dots, K(i) \\
 & S_j^{(i)} \cap S_k^{(i)} = \emptyset \quad \forall j \neq k \\
 & \bigcup_{k=1}^{K(i)} S_k^{(i)} \subseteq \{1, \dots, N\}
 \end{aligned} \tag{2.29}$$

where  $B$  is the bandwidth of each subchannel. The first set of constraints in (2.29) defines the rate requirements for the users. The received signal-to-interference-plus-noise ratio (SINR) for user  $k$  on subchannel  $n$  in cell  $i$ ,  $\gamma_{k,n}^{(i)}$  is computed as

$$\gamma_{k,n}^{(i)} = \frac{P_n^{(i)} |H_{k,n}^{(i)}|^2}{BN_0 + I_{k,n}^{(i)}} \tag{2.30}$$

where  $H_{k,n}^{(i)}$  is the channel gain between user  $k$  and the BS  $i$  on the  $n$ -th link, and  $N_0$  is the power spectral density of the zero-mean thermal noise. The MAI  $I_{k,n}^{(i)}$  affecting user  $k$  in the cell  $i$  on the  $n$ -th channel, is given by

$$I_{k,n}^{(i)} = \sum_{\substack{j=1 \\ j \neq i}}^{N_{cells}} P_n^{(j)} |H_{k,n}^{(j)}|^2 \tag{2.31}$$

The second set of constraints in (2.29) imposes that resource assignment is orthogonal within a cell. The solution of the  $N_{cells}$  optimization problems is not trivial. Even in the single-cell case, i.e.  $N_{cells} = 1$ , the problem is not convex and can be solved either by relaxing the exclusivity constraints on subchannel allocation [34] or, if the duality gap is zero, by finding the solution of the Lagrangian dual problem [35]. In both cases, finding the allocation is a computationally demanding strategy. Moreover, in our case, due to the interference, the allocation in one cell perturbs the allocations in all other cells

Reference DR9.3

and the effect of MAI is such that, given the user rate constraints, an allocation solution that meets all the requirement may not exist. Assuming lack of any centralized control, the presence of strong interference leads to the implementation of iterative strategies. For example, the iterative water-filling (IWF) algorithm was introduced to solve the problem of power allocation in presence of interference. In [36] each user repeatedly measures the received interference from all other users and accordingly selects its own power allocation by applying a waterfilling strategy on its channels, treating the interference as noise, until all users find a stable power allocation. This process results in a fully distributed and autonomous algorithm. In our case, in analogy with the IWF approach, each cell independently solves problem (2.29) on the base of the interference it measures and iteratively updates its allocation with the goal of satisfying all its rate requirements. Unfortunately, unlike in [36], the convergence of this approach is not guaranteed. Thus, the problem of convergence is addressed by progressively reducing the traffic load of the cells which can not find a stable allocation and fairness is established by implementing a layered architecture [37], where radio resource management and traffic policies are dealt with by separate and interacting algorithms a resource allocator (RA) and a packet scheduler (PSC).

#### 2.5.2.1.2 Radio resource allocation based on linear programming

The scheduler works on a frame-by-frame basis: at the beginning of a new frame, the scheduler dictates to the allocator the new set of rate requirements for all active users. We assume that the propagation channel is constant during the allocation process. Due to the MAI, the resource allocator may require a certain number of iterations to find an allocation closely matching the user rate requirements. The practical choice of the number of iterations of the allocation phase is a crucial issue since it has an impact on throughput, required overhead, and transmit power.

We reformulate channel assignment (2.29) as a linear programming (LP) problem and adopt a single transmission format (meaning error correction code and modulation) for all users [38]. Such a choice allows a great simplification of the allocation problem and, as shown in the Results section, has only a minor impact on allocation performance since most of the channel diversity is exploited by dynamically assigning channels to users [39]. The consequence of adopting just one transmission format is that the request of a given rate  $R^{(i)}(k)$  directly translates into the request of a certain number of subchannels  $r^{(i)}(k)$  ( $k = 1, \dots, K(i)$ ).

A given transmission format corresponds to a certain spectral efficiency  $\eta = \log_2[1 + \gamma(\eta)]$ , where  $\gamma(\eta)$ , the target SINR to achieve the spectral efficiency  $\eta$ , is  $\gamma(\eta) = 2^\eta - 1$ . Assuming perfect channel estimation, user  $k$  allocated in cell  $i$  on subchannel  $n$  transmits with rate  $R = B\eta$  if its measured SINR is  $\gamma_{k,n}^{(i)} > \gamma(\eta)$  and with rate  $R = 0$  otherwise. Thus, the power necessary to user  $k$  in cell  $i$  to transmit on subchannel  $n$  with spectral efficiency  $\eta$  is computed from (2.30) as  $P_{k,n}^{(i)}(\eta) = \gamma(\eta)(BN_0 + I_{k,n}^{(i)})/|H_{k,n}^{(i)}|^2$ .

Note that  $I_{k,n}^{(i)}$  is the MAI as measured in the previous iteration of the allocation phase. Under these hypotheses, once the transmission format is set, each subchannel has a certain fixed cost for each user and the allocation problem consists in finding the channel assignment that minimizes the sum of the costs in each cell. Thus, introducing the binary allocation variable  $b_{k,n}^{(i)}$ , which is 1 if subchannel  $n$  is assigned to user  $k$  in cell  $i$  and 0 otherwise, given a certain  $\eta$ , the resource allocation problem in cell  $i$  is formulated as follows:



$$\begin{aligned}
& \min_{\mathbf{b}^{(i)}} \sum_{n=1}^N \sum_{k=1}^{K^{(i)}} P_{k,n}^{(i)}(\eta) b_{k,n}^{(i)} \\
& \quad \text{s.t.} \\
& \sum_{n=1}^N b_{k,n}^{(i)} \leq r^{(i)}(k) \quad k = 1, \dots, K^{(i)} \\
& \sum_{k=1}^{K^{(i)}} b_{k,n}^{(i)} \leq 1 \quad n = 1, \dots, N \\
& \sum_{k=1}^{K^{(i)}} \sum_{n=1}^N b_{k,n}^{(i)} = C_{req}^{(i)} \\
& b_{k,n}^{(i)} \in \{0, 1\} \quad n = 1, \dots, N \quad k = 1, \dots, K^{(i)}
\end{aligned} \tag{2.32}$$

After allocation, the total rate assigned to user  $k$  in cell  $i$  is

$$R^{(i)}(k) = \sum_{n=1}^N b_{k,n}^{(i)} B\eta \tag{2.33}$$

1. The first set of constraints in (2.32) formulates the rate requirements per user. Following a different strategy with respect to (2.29), where user rate constraints impose that each user should achieve at least a certain rate, this set of constraints imposes that each user gets at most a certain number of resources. This constraint enforces the PSC policy: with the goal of guaranteeing long-term fairness,  $r^{(i)}(k)$  will be large for those users that have received a small share of resources and small or even zero for those users that have already received a large amount of radio resources. Without the limits imposed by these constraints, the RA would naturally assign all the resources to the users with the best channels only. Moreover, by setting a soft constraint, such as the maximal amount of resources, the PSC gives the RA enough freedom to exploit the diversity of the system.
2. The second set of constraints in (2.32) implements orthogonal access within the cell, i.e., one subchannel can be assigned to only one user per cell. It mirrors constraints (2.29).
3. The third constraint indicates the total amount of resources to assign in the cell and prevents the allocator from choosing the solution where all variable allocations are set to 0. Initially, it is  $C_{req}^{(i)} = N$  in every cell; then if, due to the MAI, the system is not able to converge to a steady allocation,  $C_{req}^{(i)}$  is progressively reduced until convergence.

The allocation variable is integer and can only assume the values 0 and 1; hence, we are dealing with an integer linear programming (ILP) problem. ILP problems are in many practical situations NP-hard. Nevertheless, it is possible to prove that, because of the total *unimodularity* property of the constraint matrix, the LP problem obtained from (2.32) by removing the integrality condition has still an integral optimal solution. As a consequence, LP methods can thus be used to solve the problem; in particular, the problem can be modelled as a network flow [40] and it can therefore be solved with very fast algorithms [41]. Among these, the network simplex method (NSM) is the most efficient solver for min-cost-max-flow network problems and runs in polynomial time [42].

The iterative implementation of resource allocation brings up two major problems: the allocation complexity and the overhead exchanged to update the resource costs. While the efficient formulation of the problem is intended to address the former issue, the latter needs to be discussed in detail. For each iteration of the allocation phase the RA needs updated knowledge of the interference power on each sub-channel for each user in the cell. Thus, with the objective to reduce the amount of signalling overhead, we assume that adjacent BSs are interconnected by high-capacity links, such as the X2 interface [43], supported in LTE. Under this hypothesis, the allocation phase conforms to the following iterative procedure

1) *Initialization*. Each user estimates the gains of the channels with its serving BS and all neighbouring base stations and signals this information to its BS. On the base of this information, each BS virtually

performs allocation solving the LP problem (2.32) and signals through the high-capacity links to the other BSs the power values that intends to use on each channel;

2) *Iteration*. At the beginning of a new iteration, each BS is able to compute for all its served users the interference and hence the power cost for each subcarrier. Having updated the costs, the BSs newly solve the allocation problem (2.32) and signal to all neighbouring BSs the new power vector until convergence.

3) *Power control*. After a fixed number  $N_s$  of iterations, those subchannels on which the target SINR value has not yet been reached are switched off; channel assignment is frozen, while power control is allowed to evolve for the next  $N_{pow}$  slots.

Before the power control phase, the only information that is actually exchanged in the air between users and BS is the vector of estimated channel gains at initialization. In practical scenarios, the overhead can be further reduced by signalling only the gains relative to the most interfering BS. All other information is exchanged among BSs through the high speed link. In this case the overhead amounts to signalling the vector of power values that a BS intends to transmit for each iteration. Although the BSs do exchange information, the allocation procedure remains distributed in the sense that each BS takes its allocation decisions autonomously from the others. At the end of the allocation phase each BS broadcasts the resource assignment for each user and the actual data transmission takes place. Moreover, since most of the signalling is exchanged through the connections between the BSs, the allocation phase of a new frame can be performed simultaneously with the end of the transmission phase of the preceding frame, so that at the beginning of a new frame the allocation is already set.

By allowing each cell to reduce its load when allocation convergence is not achievable, rather than performing a hard partitioning of the radio resources as in conventional systems, our proposed architecture implements a *soft partitioning*. Where possible, all cells in the system transmit over the same bandwidth, otherwise they use only a subset of the available radio channels. The cardinality of the subset is set by *ad-hoc* algorithms while the actual channel assignment is performed by the RA. In order to carry out a fully distributed strategy, each cell manages decides to reduce its load autonomously.

The goal of the PSC is to enforce long-term fairness so that the users in the cell achieve throughputs proportional to weights assigned to them. We adopt a credits-based packet scheduling algorithm, loosely based on CBFQ [44], but expressly designed for the OFDMA radio interface. The PSC schedules data blocks by taking account of the credits and weights of each user: the credits increase when the user is not scheduled to transmit, while they decrease when a transmission resource (subchannel) is assigned to it

#### 2.5.2.1.3 Numerical results

The system is a multi-cell OFDMA with  $N_{cells}=7$  hexagonal cells of radius  $R=500$  m. Each BS transmits over a downlink bandwidth  $W=5$  MHz so the sampling time is  $T_c=200$  ns. The path loss is proportional to the distance between the BS and the MS; the path loss exponent is  $\alpha=4$ . The overall bandwidth is divided into  $N=16$  subchannels shared by all the cells in the system. The propagation channel is static and frequency-selective Rayleigh fading with an exponentially decaying power delay profile. The channel delay spread is  $\sigma_\tau = 1$   $\mu$ s and the channel coherence bandwidth is assumed to be larger than the bandwidth spanned by each sub-band. Moreover, we consider a population of data users with very limited mobility so that the channel coherence time can be assumed to be very long. The number of active users at one time is  $K(i)=K$  ( $i=1, \dots, N_{cells}$ ), with  $K=8$  and, in the simulations where we take into account the scheduler, we set  $Creq=N$ . We assume that all BSs transmit with the same value of spectral efficiency  $\eta$ . The scheduler is designed to aim at achieving the same average throughput for all users in a cell. The results shown in the following have been obtained by averaging on 100 channel realizations; each simulation has a duration of 50 frames.

The main performance indicators are  $P_m$ , the mean overall transmitted power per cell and  $\eta_m$ , the measured spectral efficiency averaged over all subchannels and over all cells;  $\eta_m$  is computed as  $\eta_m = \eta E\{C_{req}(\eta)\} / N$  where  $C_{req}(\eta)$  is the cell load for a certain value of the target spectral efficiency  $\eta$ . If the cell load is never reduced for a given value of  $\eta$  then it is  $\eta_m = \eta$ .

### 2.5.2.1.3.1 Number of iterations

The number of iterations of the allocation phase  $N_s$  is the number of the iterations required to find a stable allocation. If  $N_s$  is too small, the allocation may not have enough time to converge and an excessive number of sub-channels may have to be switched off. However, increasing  $N_s$  leads to more overhead. In practice, relatively small values of  $N_s$  are sufficient to achieve a high spectral efficiency in the transmission phase.

Figure 2.21 and Figure 2.22 illustrate how our DLA performs as a function of  $N_s$  for various value of  $\eta$ . For intermediate values of the load ( $\eta = 2$  bit/s/Hz) a few iterations are sufficient to find a stable allocation with no need of reducing the cell load at all. As the cell load grows ( $\eta = 3$  bit/s/Hz), the DLA needs a larger number of iterations to find a feasible allocation but the system still performs very little load reduction. Further increases of the load ( $\eta = 4$  bit/s/Hz) require a much larger number of iterations and impose substantial load reductions.

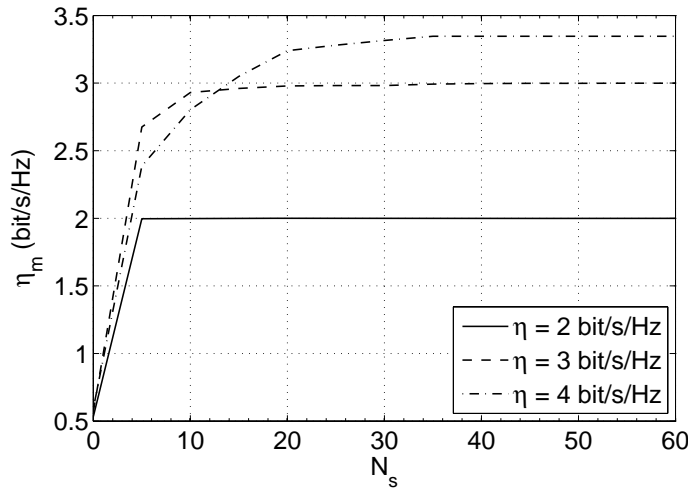


Figure 2.21 –Measured spectral efficiency  $\eta_m$  vs. duration of allocation phase  $N_s$

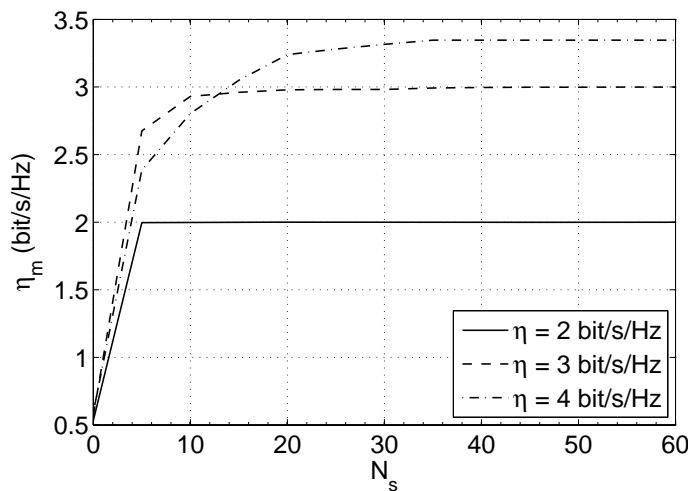


Figure 2.22 –Mean power per cell  $P_m$  vs. duration of allocation phase  $N_s$

It is worth comparing the performance for  $\eta=3$  and  $\eta=4$  bit/s/Hz after 10 iterations: the system measures approximately the same mean spectral efficiency but for  $\eta=4$  consumes almost twice as much power. In the following we set  $N_s=5$  for  $\eta \leq 2$ ,  $N_s = 10$  for  $2 < \eta \leq 3$  and  $N_s=20$  for  $3 < \eta \leq 4$  bit/s/Hz.

### 2.5.2.1.3.2 Algorithm performance

Figure 2.23 and Figure 2.24 compare the performance of the LPRA with other RA schemes encountered in the literature. To lay a common ground for comparison, since some of the schemes analyzed do not integrate easily in our layered architecture, the results are obtained simulating only one frame. In this case, we impose the same rate requirements to all users in the system and we do not take into account the PSC. As a consequence, in case of load reduction, any fairness issue is neglected.

The multi-assign (MARA) scheme [45] is an iterative heuristic based on a LP approach. Starting from the formulation (2.32), the MARA algorithm deals with interference by solving a centralized power control problem on each subchannel. Given a certain allocation, at each iteration the algorithm dissuades the users from using the subchannels where they cannot achieve their target SINR by artificially increasing the cost of those specific subchannels. To enforce convergence, the rate constraints for those users that are unable to find a stable allocation are progressively reduced. The RA scheme proposed by Pischella and Belfiore (PBRA) in [46] is an iterative algorithm made up of several steps:

- 1) Determine for each user and each subchannel a maximum SINR value so that the convergence of distributed power control is guaranteed;
- 2) Allocate subchannels to the users according to a heuristic that aims at power minimization under target data rate requirements;
- 3) Solve a convex optimization problem that sets a SINR target for each user respecting the constraints defined in step 1) and meeting the user rate constraints;
- 4) Perform distributed power control to meet the SINR targets of step 3).

Users for which it is not possible to meet the rate constraints in step 3) are simply switched off.

In case the BS does not possess any knowledge of channel and interference, resource allocation is static and performed randomly. To reduce the detrimental effect of MAI, we adopt a FFR partitioning of the available bandwidth as in [47]. Users close to the BS use the whole bandwidth in all the cells; the boundary area, instead, is partitioned into three sectors, each of which is associated to a different set of subchannels. By these means, the inter-cell interference can be greatly reduced. After FFR allocation (FFRA), the BS performs  $N_{pow}$  power control iterations and those subchannels which have not achieved their target SINR at the end of this phase are switched off.

We also compare the system performance with a dynamic FFR scheme as in [48]. We consider two approaches, denoted as FFR-A and FFR-B. In FFR-A, users close to the BS use the same bandwidth in all the cells, while users in the boundary area are separate on orthogonal bands. FFR-B, instead, allows partial overlapping between users in the center of the cell and users near to the border. Based on these frequency partitioning schemes, an interference graph where the nodes are represented by the MSs and the edges are the interference between two MSs is realized. Then, according to the topology of the network and the adopted frequency planning, resource allocation is performed by assigning different subchannels to the nodes connected by an edge. Once all possible channels assignment are performed, each BS performs  $N_{pow}$  iterations of power control and those subchannels which have not achieved their target SINR at the end of this phase are switched off.

Figure 2.23 plots  $\eta_m$  as a function of  $\eta$  for the different allocators. As expected, both the FFR schemes perform poorly since the most of the resources in each cell are not allocated due to the interference management scheme. Moreover, as the load of the cells increases, the FFR-A scheme exhibits lower performance than the FFR-B approach. For  $\eta > 2$  bit/s/Hz, the PBRA algorithm achieves a stable allocation by significantly reducing the load, while both LPRA and MARA schemes require a much more limited reduction in throughput. For  $\eta > 3$  bit/s/Hz, the centralized heuristic MARA is only slightly better than our solution.

Reference DR9.3

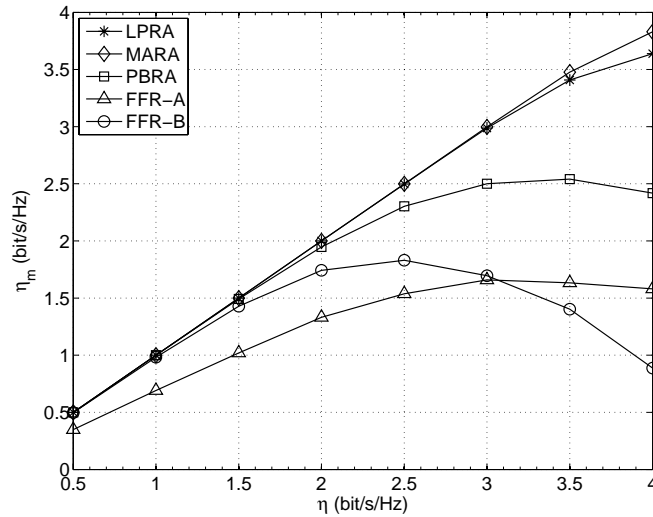


Figure 2.23 – Measured spectral efficiency  $\eta_m$  vs. target spectral efficiency  $\eta$  (resource allocation and load control algorithm, no scheduler, same rate for all users)

Figure 2.24 plots the mean power per cell  $P_m$  as a function of the sum rate. The FFRA and PBRA algorithms use somewhat less power at a high  $\eta$ , but only because they have reduced their load much more. The comparison between the LPRA and the MARA schemes is interesting because it reveals that the slight advantage of MARA in terms of throughput for large values of  $\eta$  is achieved at the cost of much higher values of transmitted power.

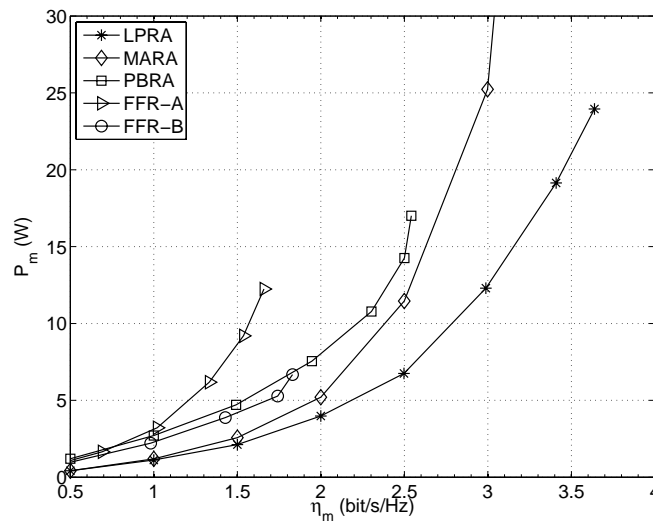


Figure 2.24 – Mean power per cell  $P_m$  vs. measured spectral efficiency  $\eta_m$  (resource allocation and load control algorithm, no scheduler, same rate for all users)

#### 2.5.2.1.4 Conclusions

We have studied the problem of resource allocation and power adaptation in the downlink of a multicell multicarrier system, with a frequency reuse distance equal to one. Allowing full frequency reuse can potentially bring about large gains in terms of spectral efficiency. However, inter-cell interference can adversely affect system performance. We introduced a loss cross layered architecture that integrates a packet scheduler with an adaptive resource allocator, designed to deal with multiple access interference; the two modules are coupled by a simple interface. The PSC takes care of the traffic policies and the RA tackles spectral efficiency. In this way the RA algorithm can strive for selfish spectral efficiency, while long term fairness is guaranteed by the PSC according to any desired policy (max-min fairness, weighted output fairness, proportional fairness, etc.). Each cell performs its resource management in a distributed way without any central controller. Simulation results show that

the proposed architecture is able to guarantee both high spectral efficiency and throughput fairness among flows.

### 2.5.2.2 Coordinated scheduling in a MIMO scenario

#### 2.5.2.2.1 Overview

Future cellular networks will need to provide high data rate services for a large number of users, which requires a high spectral efficiency over the entire cell area. One major challenge in providing ubiquitous broadband wireless access in cellular networks is to mitigate detrimental effects of cellular interference. Over the years, several different methods have been studied in order to mitigate ICI. Interference averaging techniques aim at average the interference over all users, thereby reducing the interference experienced by some users. Interference avoidance techniques on the other hand, aim at explicitly coordinate and avoid interference, e.g. by setting restrictions on how the radio resources are used. An example of this is ICIC, which is available in the 3GPP LTE standard [49].

Recently, even tighter interference coordination has gained significant interest under the name CoMP transmission and reception. CoMP refers to a system where the transmission and/or reception at multiple, geographically separated antenna sites is dynamically coordinated in order to improve system performance [50].

Coordinated multi-point transmission in the DL implies dynamic coordination among multiple geographically separated transmission points, and can be categorized as follows [51]:

- *Coordinated scheduling and/or beamforming schemes*- the data to a single UE is instantaneously transmitted from one of the transmission points in the coordination set (the set of points/cells that are coordinated), and that scheduling decisions and/or generated beams are coordinated in order to control the created interference. The main advantages of these schemes are that the requirements on the coordination links and on the backhaul are much reduced. Typically only information on scheduling decisions and/or generated beams (and information needed for their generation) need to be exchanged
- *Joint processing/transmission schemes* are - the data to a single UE is simultaneously transmitted from multiple transmission points in the CoMP set, to improve the received signal quality and/or cancel actively interference for other UEs. This category of schemes put higher requirements on the coordination links and the backhaul since the user data need to be made available at the multiple coordinated transmission points. The amount of data to be exchanged over the coordination links is also larger, e.g. channel knowledge.

Different coordination architectures can be considered depending on the organization and location of the coordinating entity: Two main schemes are distinguished, namely [52]:

- Distributed approach – the coordination is performed by direct communication between the coordinated nodes and only information necessary for coordination is exchanged (e.g. scheduling decisions and channel information). The scheduling and beamforming process is performed independently by each of the nodes.
- Centralized approach - a central coordinating node is responsible for coordination of scheduling and/or beamforming process and exchange of information. This scheme requires presence of an additional logical central entity. Moreover the amount of signalling information in this case is significantly larger than in the distributed case, thus making this approach more academic than practical.

Although different time scales are possible for the coordination in all the CoMP architectures, the most efficient schemes require the information needed for scheduling to be available at each coordinated BSs, which calls for very low-latency (on the order of the millisecond) information exchanges between coordinated nodes, or between the UE and all the coordinated nodes.

In any case, whatever the chosen architecture, studies have been performed on how the distributions of users in a given ideal cellular layout could improve the performances with respect to an uncoordinated case. As the number of users and nodes increase, the signaling overhead required for the inter-base information exchange and the amount of feedback needed from the users also increase. Therefore, cooperation should be restrained to a limited number of nodes. Therefore, the desired approach is to divide the network into clusters of cooperative cells. Cluster selection is obviously a key to

Reference DR9.3

cooperation algorithms performance. Basically cluster of cells for CoMP transmission can be formed in one of the proposed fashions [53]:

- UE-centric clustering - each UE chooses a small number of cells that are most suitable for cooperative transmission. The case of UE-centric coordination is challenging since the clusters are chosen in a dynamic way and may overlap.
- Static (network-centric) clustering - clusters are defined statically for all UEs of a given serving cell based on the neighborhood and trying to combine those cells with strongest mutual interference. In this case the performance for the UEs at the cluster boundaries can be compromised, as the interference problem is moved from cell-level to the cluster-level.
- Hybrid clustering - a set of clusters can be pre-defined for a given serving cell and the selection of the best cluster is assisted by the UE through feedback information.

In the next generation wireless networks usually sectorization is employed with the cell divided into a specific number of sectors. Therefore, two different coordination schemes are possible depending on the cluster formulation:

- Intra-site coordination (multisector coordination) with the coordinated BSs co-located in space.
- Inter-site coordination (multisite coordination) where the coordinated BSs are spatially distributed.

From the backhauling point of view the preferable scheme is the intra-site coordination, as the requirements on the physical media for transmission of signalling information is lower, as the coordinated nodes are co-located. On the other hand, the inter-site coordination can yield higher gains, as higher spatial diversity can be achieved.

#### 2.5.2.2.2 Limited feedback case

A common approach in the literature when evaluating the performance of resource allocation algorithms is to assume a perfect channel knowledge at each of the nodes. However, such assumption is not practical as in real communication systems only limited feedback of CSI is possible. Thus, two main types of feedback can be identified [51]:

- the explicit feedback involves reporting the raw channel as observed by the receiver (together with interference information), without assuming any transmission or receiver processing. Examples of explicit feedback include reporting the channel impulse response, or the channel covariance matrix, what results in large signalling overhead.
- the implicit feedback involves reporting channel-related characteristics assuming hypotheses on a particular transmission and/or reception processing; one typical example of implicit feedback is the CQI/PMI/RI feedback.

In addition, the UE transmission of UL sounding reference signal (SRS) can be usable for CSI estimation at multiple cells (coordination sites), in particular via the exploitation of the channel reciprocity property (both for FDD and TDD). However, the desirable approach is to employ the implicit feedback techniques, based on a pre-defined codebook of vector quantizers. Such approach is considered e.g. In PU<sup>2</sup>RC [54] scheme or LTE [49] feedback scheme. Different codebook generation methods have been proposed, which can be either static (LTE, PU<sup>2</sup>RC) or dynamic (random beamforming [55], LBG vector quantization [56]), with the periodic generation of vector quantizers based on stored CSI.

#### 2.5.2.2.3 Proposed centralised approach

The utility theory can be employed to derive the optimization criterion for the final resource allocation scheme. In a multi-cell scenario, the optimization objective is to maximize the aggregate utility of users in the entire network, where each user has its utility function of average throughput. Then, given the power allocation profile, the optimization problem is:

$$\max \sum_{i=1}^K U_i(\bar{r}_i[t]), \quad (2.34)$$

where  $U_i(x)$  is the utility function of user  $i$ , and  $\bar{r}_i[t]$  is the average throughput of user  $i$  at slot  $t$ , which can be expressed by using exponentially low pass filter as:

$$\bar{r}_i[t] = \left(1 - \frac{1}{T_c}\right) \bar{r}_i[t-1] + \frac{1}{T_c} r_i[t], \quad (2.35)$$

where  $T_c$  is the low-pass filter window length.  $r_i[t]$  is the instantaneous throughput of user  $i$  at slot  $t$ , which can be expressed as:

$$r_i[t] = \sum_{l \in F_i} c_{il} x_{il}, \quad (2.36)$$

with the maximum reliable transmission capability on subcarrier  $l$  denoted as  $c_{il}$ ,  $F_c$  representing the set of subcarriers, and  $x_{il}$  indicating whether subcarrier  $l$  is allocated to user  $i$ , with  $x_{il} \in \{0,1\}$ . The value of transmission capability  $c_{il}$  depends on the value of the signal to interference and noise ratio (SINR) in the subcarrier  $l$ , which is evaluated using equation:

$$\frac{S}{N+I} = \frac{P_{il} g_{il}}{N_0 + \sum_{\substack{j \in K^* \\ j \neq i}} P_{jl} g_{il} + \sum_{k \in K_{int}} P_{kl} g_{kl}}, \quad (2.37)$$

where  $P_{il}$  is the transmit power of user  $i$  on the subcarrier  $l$ ,  $N_0$  is the noise power,  $g_{il}$  is the channel gain between user  $i$  and its serving base station ( $K^*$ ) in the subcarrier  $l$ , and  $g_{kl}$  denotes the channel gain between the user  $i$  and the interfering base station, which belongs to the interfering BS set ( $K_{int}$ ). The channel gains  $g_{il}$  and  $g_{kl}$  depend on the respective channel coefficients, as well as on the beamforming and combining coefficients of BSs and user  $i$  respectively. Thus, to derive the optimal solution, the central resource allocation entity or the coordinated nodes should have the knowledge of the radio propagation condition between each user equipment and all the cell transmit antennas, including pathloss, shadow fading, and multipath fading characteristics. However, as this is practically hardly achievable, the required channel knowledge is limited only to the antennas within a coordination cluster.

An example of such approach, with aim to maximize the aggregate utility in the coordination cluster is considered in [57], where a suboptimal iterative coordinated resource allocation algorithm has been proposed, denoted as Coordinated MultiPoint scheduling (CoMP). Two optimization criteria have been considered: Max Rate (CoMP MR) and Proportional Fair (CoMP PF). However, the main disadvantage of such approach is that the proposed solution is centralized and requires presence of central coordinating entity in a cluster. Moreover, the coordinated scheduling technique does not consider beamforming coordination between the BSs which could provide further gain. Furthermore, a full channel information between each UE and each BS in the coordination cluster is assumed, which is not practical as it may result in significant signalling increase.

#### 2.5.2.2.4 Proposed distributed approach

To reduce the requirement on the backhaul in coordinated systems, a distributed approach is the preferable one. The coordination between all of the nodes can be performed only in form of exchange of CSI and scheduling decisions. Thus, we consider only the following cooperation between neighbouring nodes: each BS  $i$  signals the channel between the neighbouring BS  $j$  and the most affected set of users  $U_i$  served by BS  $i$  to BS  $j$ . To further limit the signalling information it is assumed that at most  $N_t$  channels can be reported, where  $N_t$  is the number of transmit antennas. Then, having received the information on the interfering channels from neighbouring BSs, each BS calculates the



correlation of the channels of each user  $k$  associated with this BS and the interfering channels for each PRB, according to the formula

$$\rho_k = \max_{l \in \bigcup_{j \neq i} U_j} \hat{\mathbf{h}}_{i,l} \cdot \hat{\mathbf{h}}_{i,k}^H, \quad \|\hat{\mathbf{h}}_{i,l}\| = 1 \forall l, l \quad (2.38)$$

where  $\hat{\mathbf{h}}_{i,l}$  is the effective normalized channel between BS  $i$  and user  $l$  in neighbouring BS.

Having obtained the correlation coefficients for every user, the BS selects a set of users  $U_i^*$  whose correlation factor is lower than the predefined threshold or whose the channel gain is higher than the gain of user experiencing interference in the neighbouring cell.

$$U_i^* = \{u_k, \rho_k < th \vee g_{i,k} > g_{j,l}\}, \quad (2.39)$$

where  $u_k$  denotes the user  $k$  associated with BS  $i$ ,  $g_{i,k}$  represents the channel gain between user  $u_k$  and BS  $i$  and  $g_{j,l}$  stands for the gain between user  $l$ , experiencing the highest channel correlation  $\rho_k$  with user  $u_k$ , and its BS  $j$ .

Finally, after performing the users pre-selection each BS allocates the available resources to users from  $U_i^*$  according to one of the well-known optimization criteria, such as the MR or PF.

#### 2.5.2.2.5 Simulation setup and performance evaluation

A multi-cell system model is considered in simulations, as shown in Figure 2.25, with the simulation assumptions summarized in Table 2.7. Coordination has been performed within static clusters comprising three neighbouring sectors. Perfect time and frequency synchronisation of the network is assumed. Link adaptation is assumed, where the modulation scheme is adaptively controlled based on the achieved SINR. The considered simulation scenario is the Urban Macro one specified for the IMT-A systems [58].

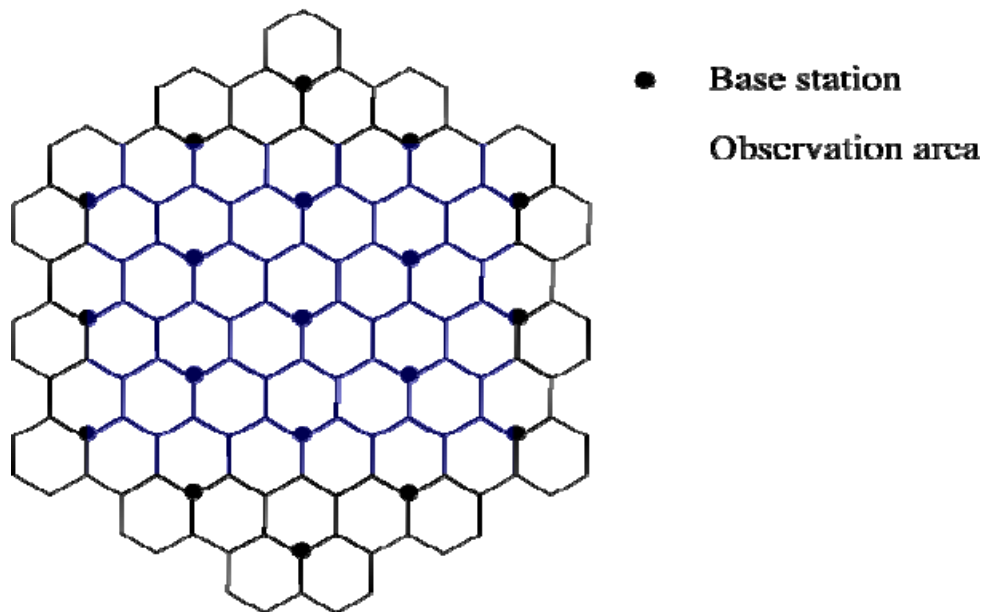


Figure 2.25 – Considered cell layout and observation area

Table 2.7 – Simulation parameters

Simulation parameter	Value
DL or UL	DL only
Number of sites	19
Number of BSs (sectors)	57
Sector angle	120°
Coordination cluster size	3 sectors
Clustering mode	Static
Number of users	200 or 400 (distributed uniformly in the rectangular observation area - blue in Figure 2.25)
PRB size (frequency $\times$ time)	12 $\times$ 7
Number of PRBs	100
Total Tx power	46 dBm
AMC schemes	11 schemes
MIMO	SDMA based on ZF precoding [59]
Number of Tx antennas	4
Number of Rx antennas	2
TTI	1 ms
Scenario	Urban Macro (UMa) [58]
CSI	Perfect/Quantized
Traffic model	Full buffer
Correlation threshold for the distributed resource allocation	0.4

Several resource allocation algorithms have been compared assuming different levels of coordination, specifically:

- no coordination: Round Robin (RR), Max Rate (MR), Semiorthogonal User Selection (SUS) [59] and Proportional Fair;
- static coordination (fractional frequency reuse mechanism [60]): Semiorthogonal User Selection (SUS (ffr)), Proportional Fair (PF (ffr));
- dynamic coordination in clusters comprising distributed BSs (inter-site coordination): COordinated MultiPoint Max Rate (CoMP MR), COordinated MultiPoint Proportional Fair (CoMP PF)

Reference DR9.3

- dynamic coordination in clusters comprising co-located BSs (intra-site coordination): COordinated MultiPoint Max Rate (CoMP MR), COordinated MultiPoint Proportional Fair (CoMP PF)
- dynamic coordination using the distributed approach: Distributed SUS, Distributed MR and Distributed PF.

The metrics of comparison were chosen as follows:

- average total cell rate, calculated as sum of average rates of all users in a cell;
- average cell-edge users' rate, where cell-edge users are the users whose distance to the BS is higher than 0.75 of the cell radius;
- Fairness factor, calculated using the formula (put a ref to the equation in Emanuel's part) for the entire network of 19 sites (network fairness) or calculated as average fairness achieved in a cell.

20 independent simulation runs have been performed for each of the considered cases, with the length of each run equal to 100 TTIs. The results are presented in two groups – separately for the optimization based on the Max Rate and Proportional Fair criterion.

Table 2.8 and Table 2.9 show the results obtained with the Max Rate optimization with 200 users and 400 users distributed uniformly in the observation area, respectively. One can notice that the dynamic coordination provides the highest average cell rate among all of the considered algorithms. The rate gain from coordination is around 55% with 200 users and over 100% with 400 users comparing to the original MR approach and up to 23% comparing to the SUS algorithm. Moreover, the gain in cell-edge users' rate is 40-50% with 200 users and up to 67% with 400 users when comparing with the MR, and up to 5% when comparing with the SUS. Furthermore, one can notice that slightly better performance is achieved with the intra-site coordination than in case of inter-site coordination, which is also more beneficial in terms of the required infrastructure, as the BSs are co-located.

Table 2.8 – Performance comparison of selected algorithms with 200 users distributed in observation area – Max Rate optimization

Scheduler	Cell rate [Mbps]	Cell-edge users' rate [Mbps]	Network fairness	Average cell fairness	Cell rate gain vs MR[%]	Cell-edge users' rate gain vs MR [%]	Rate gain vs SUS[%]	Cell-edge users' rate gain vs SUS [%]
RR	41.14	4.33	0.33	0.66	-26.16	-43.37	-46,97	-60,22
MR	55.71	7.64	0.33	0.62	-	-	-28,19	-29,75
SUS	77.58	10.88	0.36	0.57	39.25	42.35	-	-
SUS(ffr)	65.13	7.96	0.29	0.53	16.90	4.13	-16,05	-26,85
CoMP MR (inter-site)	89.28	11.42	0.36	0.55	60.26	49.47	15,09	5,00
CoMP MR (intra-site)	93.19	10.84	0.37	0.56	67.27	41.79	20,12	-0,40
Distributed SUS	69.18	9.51	0.33	0.55	24.17	24.51	-10.83	-12.53
Distributed MR	62.13	8.99	0.38	0.62	11.53	17.60	-19.91	-17.39

Table 2.9 – Performance comparison of selected algorithms with 400 users distributed in observation area – Max Rate optimization

Scheduler	Cell rate [Mbps]	Cell-edge users' rate [Mbps]	Network fairness	Average cell fairness	Cell rate gain vs MR[%]	Cell-edge users' rate gain vs MR [%]	Rate gain vs SUS[%]	Cell-edge users' rate gain vs SUS [%]
RR	43.71	2.71	0.31	0.54	-23.15	-34.07	-55.89	-61.48
MR	56.88	4.11	0.21	0.44	0.00	0.00	-42.60	-41.58
SUS	99.09	7.03	0.27	0.43	74.22	71.16	0.00	0.00
SUS(ffr)	88.18	5.09	0.22	0.40	55.04	23.84	-11.01	-27.65
CoMP MR (inter-site)	113.67	6.90	0.27	0.40	99.84	67.94	14.71	-1.88
CoMP MR (intra-site)	121.89	6.52	0.27	0.43	114.30	58.75	23.01	-7.25
Distributed SUS	90.72	6.23	0.25	0.39	59.50	51.66	-8.45	-11.39
Distributed MR	69.60	4.82	0.23	0.45	22.37	17.32	-29.76	-31.46

On the other hand, surprisingly high rate is achieved when using the SUS algorithm without any means of coordination. It clearly outperforms all non-coordinated schemes and the schemes based on static coordination (fractional frequency reuse). This is achieved thanks to the users selection scheme employed in this algorithm, which aims at maximization of the orthogonality of selected users' channels, thus indirectly reducing the inter-cell interference.

Although the proposed distributed approaches performs worse than the CoMP algorithm in terms of achieved rate, because of their simple coordination scheme, it provides a significant gain in cell rate (11-24% with 200 users and 20–60% with 400 users depending on the final allocation algorithm) and cell-edge users' rate (over 17% with 200 users and 17-50% with 400 users) compared to the original MR algorithm. On the other hand, the rate achieved using any of the distributed approaches is lower than in case of SUS algorithm, thus the use of such approach is rather not justified when considering the MR optimization.

Similar analysis have been performed for the PF optimization, with the results shown in Table 2.10 and Table 2.11 for 200 and 400 users distributed in the observation area, respectively. Clearly the best performer in terms of achieved cell rate is the CoMP PF approach, with the gain of up to 70% with 200 users and up to 180% with 400 users compared to the original PF algorithm. Moreover, the network fairness gain in this case is the highest, thanks to the clustering scheme, achieving over 90% with 200 users and up to 240% for 400 users vs the PF. On the other hand, the dynamic coordination scheme results in slight degradation of the average cell fairness, which is negligible compared with the gains from coordination.

Table 2.10 – Performance comparison of selected algorithms with 200 users distributed in observation area – Proportional Fair optimization

Scheduler	Cell rate [Mbps]	Cell-edge users' rate [Mbps]	Network fairness	Average cell fairness	Cell rate gain vs PF[%]	Cell-edge users' rate gain vs PF [%]	Fairness gain vs PF [%]	Cell-fairness gain vs PF [%]
PF	33.32	5.78	0.25	0.74	-	-	-	-
PF(ffr)	52.71	6.16	0.29	0.57	58.16	6.53	16.79	-22.83
CoMP PF (inter-site)	54.12	8.70	0.48	0.72	62.39	50.51	92.34	-3.61
CoMP_PF (intra-site)	57.20	9.23	0.46	0.74	71.66	59.64	83.78	-1.17
Distributed PF	47.84	7.70	0.44	0.72	43.56	33.16	76.13	-3.45

Table 2.11 – Performance comparison of selected algorithms with 400 users distributed in observation area – Proportional Fair optimization

Scheduler	Cell rate [Mbps]	Cell-edge users' rate [Mbps]	Network fairness	Average cell fairness	Cell rate gain vs PF[%]	Cell-edge users' rate gain vs PF [%]	Fairness gain vs PF[%]	Cell-fairness gain vs PF[%]
PF	20.77	2.27	0.13	0.71	-	-	-	-
PF(ffr)	56.22	3.61	0.23	0.49	170.65	59.21	79.26	-31.02
CoMP PF (inter-site)	57.75	5.24	0.43	0.66	177.99	130.98	240.70	-6.28
CoMP_PF (intra-site)	58.21	5.05	0.41	0.67	180.21	122.29	224.62	-5.13
Distributed PF	43.37	3.85	0.24	0.64	108.79	69.59	86.68	-9.27

The runner-up in terms of achieved rate when using the PF optimization is the PF algorithm with static coordination (fractional frequency reuse). However, one can notice that in this case the average cell fairness factor of resource allocation is much lower than in all other cases (20-30% lower), with the value of around 0.57 with 200 users and 0.49 with 400 users. Thus, the conclusion is that in case of static coordination the proportional fairness was not achieved.

Very interesting results have been obtained for the distributed approach. Although the rate gain (43% with 200 users and over 100% with 400 users) is lower than in case of CoMP PF and PF(ffr), the achieved cell-edge users' throughput is higher than in case of PF(ffr). Furthermore, the average cell fairness degradation is much lower than in case of PF(ffr) and similar to the values obtained for CoMP PF. Thus, taking into account the low requirement on infrastructure resources and signalling, the overall performance of this scheme is clearly better than when using the static coordination. It is debatable whether it is more beneficial to employ the CoMP PF scheme than the distributed scheme, as the CoMP requires significant additions in the network infrastructure (requires presence of the coordinating entity) and greatly increases the signalling in the network. Comparing the distributed scheme and the CoMP scheme the former could be more suited to be employed in existing wireless networks as it does not require any significant changes, simultaneously providing a significant increase in rate and network fairness.

Summarizing, the dynamic coordination approach provides significant gains in average cell rate, cell-edge users' rate and network fairness comparing to the non-coordinated scheduling schemes. However, the coordination when considering the MR optimization requires significant investments in infrastructure, as the distributed approach does not yield any gains. Slightly different situation is observed when using the PF optimization (which is actually the criterion considered in modern wireless networks, such as the LTE), where rate and network fairness gains can be achieved at low cost using the distributed approach.

Further improvements and higher gains can be achieved when considering coordination with dynamic clustering or user-centric clustering. In the static clustering scheme the actual problem of interference mitigation is moved from cell level to the cluster level, so the interference experienced on the cluster-edge will be much higher than on the cell-edge. This can be neglected when using a fully dynamic scheme, i.e. the dynamic clustering or user-centric clustering, however, these may put further additional requirements on the signalling or infrastructure.

## 2.6 Game Theory for Optimization of RRM

### 2.6.1 Crystallized rate regions for MIMO transmission

Game-theoretic techniques based on the utility maximization problem have received significant interest [61]-[64]. The game-theoretical solutions attempt to find equilibria, where each player of the

game adopts a strategy that they are unlikely to change. The best known and commonly used equilibrium is the Nash equilibrium [65]. However, the Nash equilibrium investigates only the individual payoff, and that may not be efficient from the system point of view. Better performance can be achieved using the correlated equilibrium [66], in which each user considers the others' behaviors to explore mutual benefits. In order to find the correlated equilibrium, one can formulate the linear programming problem and solve it using one of the known techniques, such as the Simplex algorithm [67]. However, in case of MIMO systems, the number of available game strategies is high, and the linear programming solution becomes very complex. Thus, a distributed solution can be applied, such as the regret-matching learning algorithm proposed in [62], to achieve the correlated equilibrium at lower computational cost. Moreover, the overall system performance may be further improved by an efficient mechanism design, which defines the game rules [68]. Thus, we examine the rate region for the MIMO interference channel based on the approach presented in [62], [69].

In our investigation we take into account specific MIMO techniques, such as transmit selection diversity, spatial waterfilling, SVD-MIMO, or codebook-based beamforming [70], [73]. We apply the correlated equilibrium concept to the rate region problem in the considered scenario, proposing a new Vickrey-Clarke-Groves (VCG) auction utility [65] formulation and the modified regret-matching learning algorithm. Furthermore, we demonstrate the application of the considered concept for the 2-user MIMO channel.

### 2.6.1.1 System Model for 2-User Interference MIMO Channel

We consider in our investigation the multicell uplink interference MIMO channel. Without loss of generality and for the sake of clarity, the channel model consists in the 2-user 2-cell scenario, in which each user (denoted as the Mobile Terminal (MT)) communicates with his own Base Station (BS) causing interference to the neighboring cell (see Figure 2.26(a)). Each MT is equipped with  $N_t$  (transmit) antennas, and each BS has  $N_r$  (receive) antennas. Moreover, user  $i$  can transmit data with maximum total power  $P_{i, \max}$ . Perfect channel knowledge in all MTs is assumed. In order to ease the analysis, we limit our derivation to the  $2 \times 2$  MIMO case (see Figure 2.26(b)), where both the transmitter and the receiver use only two antennas.

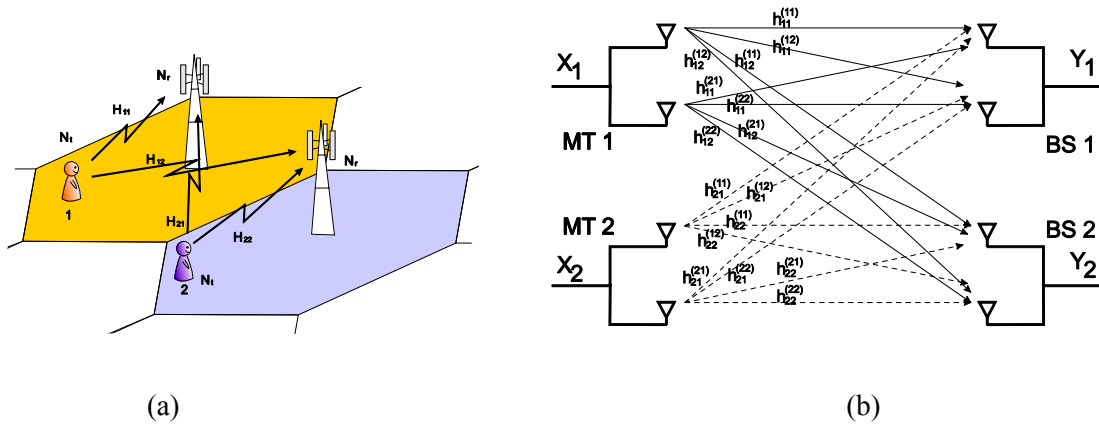


Figure 2.26 – MIMO interference channel: general 2-cell 2-user model (a) and the details representation of the considered  $2 \times 2$  case (b)

User  $i$  transmits the signal vector  $X_i \in \mathbb{C}^2$  through the multipath channel  $\mathbf{H} \in \mathbb{C}^{4 \times 4}$ , where

$$\mathbf{H} = \begin{pmatrix} \mathbf{H}_{11} & \mathbf{H}_{12} \\ \mathbf{H}_{21} & \mathbf{H}_{22} \end{pmatrix}, \quad \mathbf{H}_{ij} \in \mathbb{C}^{2 \times 2} \quad (2.40)$$

The channel matrix  $\mathbf{H}_{ij} = \{h_{k,l}^{(i,j)} \in \mathbb{C}, 1 \leq k, l \leq 2\}$  consists of the actual values of channel coefficients  $h_{k,l}^{(i,j)}$ , which define the channel between transmit antenna  $k$  at the  $i$ th MT and the receive antenna  $l$  at

the  $j$ th BS. In the considered 2-user  $2 \times 2$  MIMO case, only four channel matrices are defined, that is,  $\mathbf{H}_{11}$ ,  $\mathbf{H}_{22}$  (which describe channel between the first MT and first BS or second MT and second BS, respectively),  $\mathbf{H}_{12}$ , and  $\mathbf{H}_{21}$  (which describe the interference channel between first MT and second BS and between second MT and first BS, respectively). Additive White Gaussian Noise (AWGN) of zero mean and variance  $\sigma^2$  is added to the received signal. Receiver  $i$  observes the useful signal, denoted as  $Y_i$ , coming from the  $i$ th user. Moreover, in the interference scenario, receiver  $i$  (BS  $i$ ) receives also interfering signals from other users located at the neighboring cell  $Y_j$ ,  $j \neq i$ . One can find solid contribution on the interference channel capacity in the rich literature, for example, [74], [75], [76], [77]. When interference is treated as noise, the achievable rates for 2-user interference MIMO channel are defined as follows [76]:

$$\begin{aligned} \mathbf{R}_1(\mathbf{Q}_1, \mathbf{Q}_2) &= \log_2 \left( \det \left( \mathbf{I} + \mathbf{H}_{11} \mathbf{Q}_1 \mathbf{H}_{11}^* \cdot (\sigma^2 \mathbf{I} + \mathbf{H}_{21} \mathbf{Q}_2 \mathbf{H}_{21}^*)^{-1} \right) \right) \\ \mathbf{R}_2(\mathbf{Q}_1, \mathbf{Q}_2) &= \log_2 \left( \det \left( \mathbf{I} + \mathbf{H}_{22} \mathbf{Q}_2 \mathbf{H}_{22}^* \cdot (\sigma^2 \mathbf{I} + \mathbf{H}_{12} \mathbf{Q}_1 \mathbf{H}_{12}^*)^{-1} \right) \right) \end{aligned} \quad (2.41)$$

where  $R_1$  and  $R_2$  denote the rate of the first and second user, respectively,  $(\mathbf{A}^*)$  denotes transpose conjugate of matrix  $\mathbf{A}$ ,  $\det(\mathbf{A})$  is the determinant of matrix  $\mathbf{A}$ , and  $\mathbf{Q}_i$  is the  $i$ th user data covariance matrix, that is,  $E\{X_i X_i^*\} = \mathbf{Q}_i$  and  $\text{tr}(\mathbf{Q}_1) \leq P_{1, \max}$ ,  $\text{tr}(\mathbf{Q}_2) \leq P_{2, \max}$ . We define the rate region as  $\mathcal{R} = \cup \{\mathbf{R}_1(\mathbf{Q}_1, \mathbf{Q}_2), \mathbf{R}_2(\mathbf{Q}_1, \mathbf{Q}_2)\}$ . One can state that the formulas presented above allow us to calculate the rates that can be achieved by the users in the MIMO interference channel scenario in a particular case when no specific MIMO transmission technique is applied. Such approach can be interpreted as a so-called Transmit Selection Diversity (TSD) MIMO technique [70], where the BS can decide between one of the following strategies: to put all of the transmit power to one antenna ( $N_t$  strategies, where  $N_t$  is the number of antennas), to be silent (one strategy), or to equalize the power among all antennas (one strategy).

When the channel is known at the transmitter, the channel capacity can be optimized by means of some well known MIMO transmission techniques. Precisely, one can decide for example to linearize (diagonalize) the channel by the means of Eigenvalue Decomposition (EvD) or Singular Value Decomposition (SVD) [70], [71], [77], [78]. Such approach will be denoted hereafter as SVD-MIMO. Moreover, in order to avoid or minimize the interference between the neighboring users within one cell, BS can precode the transmit signal. In such a case, the sets of properly designed transmit and receive beamformers are used at the transmitter and receiver side, respectively. The precoders can be either calculated continuously based on the actual channel state information from all users or can be defined in advance (predefined) and stored in a form of a codebook, from which the optimal set of beamformers is selected for each user based on its channel condition. The later approach is proposed in the Long Term Evolution (LTE) standard where for the  $2 \times 2$  MIMO case a specific codebook is proposed [79]. Similar assumption is made for the so called Per-User Unitary Rate Control (PU<sup>2</sup>RC) MIMO systems, where the set of  $N$  beamformers is calculated [54], [72]. Since the process of finding the set of transmit and receive beamformers is usually time and energy consuming and require accurate Channel State Information (CSI), the optimal approaches (where the precoders are calculated based on the actual channel state) are replaced by the above-mentioned list of predefined beamformers stored in a form of a codebook. Since the number of precoders is limited, the performance of such approach could be worse than the optimal one, particularly in the interference channel scenario. Based on this observation, new techniques of generation of the set of  $N$  beamformers have been proposed. One of them is called random-beamforming [73], [80], since the set of precoders is obtained in a random manner. At every specified time instant, a new set of beamformers is randomly generated, from which the subset of precoders that optimize some predefined criteria is selected.

When the set of randomly generated beamformers is used, the set of receive beamformers has to be calculated at the receiver. Various criteria can be used, just to mention the most popular and academic ones: Zero-Forcing (ZF), Minimum Mean Squared Error (MMSE), or Maximum-Likelihood (ML) [70], [71]. In our simulation, we consider the combination of these methods, that is, ZF-MIMO, MMSE-MIMO, and ML-MIMO, with three different codebook generation methods-one of the size  $N$ ,  
Reference DR9.3

that is, generated randomly (denoted hereafter as RAN- $N$ ), one defined as proposed for LTE and one specified for PU<sup>2</sup>RC MIMO. In other words, the abbreviation ZF-MIMO-LTE describes the situation where the transmitter uses the LTE codebook and the set of receive beamformers is calculated using the ZF criterion. However, let us stress that (2.41) has to be modified when one of the precoding techniques (including SVD method, which is a particular case of precoding) is applied. Thus, the general equations for the achievable rate computation are defined as follows:

$$\begin{aligned} R_1(\mathbf{Q}_1, \mathbf{Q}_2) &= \log_2 \left( \det \left( \mathbf{I} + \mathbf{u}_1^* \mathbf{H}_{11} \mathbf{v}_1 \mathbf{Q}_1 \mathbf{v}_1^* \mathbf{H}_{11}^* \mathbf{u}_1 \cdot \left( \sigma^2 \mathbf{u}_1^* \mathbf{u}_1 + \mathbf{u}_1^* \mathbf{H}_{21} \mathbf{v}_2 \mathbf{Q}_2 \mathbf{v}_2^* \mathbf{H}_{21}^* \mathbf{u}_1 \right)^{-1} \right) \right) \\ R_2(\mathbf{Q}_1, \mathbf{Q}_2) &= \log_2 \left( \det \left( \mathbf{I} + \mathbf{u}_2^* \mathbf{H}_{22} \mathbf{v}_2 \mathbf{Q}_2 \mathbf{v}_2^* \mathbf{H}_{22}^* \mathbf{u}_2 \cdot \left( \sigma^2 \mathbf{u}_2^* \mathbf{u}_2 + \mathbf{u}_2^* \mathbf{H}_{12} \mathbf{v}_1 \mathbf{Q}_1 \mathbf{v}_1^* \mathbf{H}_{12}^* \mathbf{u}_2 \right)^{-1} \right) \right) \end{aligned} \quad (2.42)$$

where  $\mathbf{u}_i$  and  $\mathbf{v}_i$  denote the set of receive and transmit beamformers, respectively, obtained for the  $i$ th user. In a case of SVD-MIMO, the above-mentioned vectors are obtained by the means of singular value decomposition of the channel transfer matrix whereas for the other precoded MIMO systems, the set of receive coefficients is calculated as follows [77]:

- i. for Zero-Forcing receiver

$$\mathbf{u}_i = \left( \left( \mathbf{H}_{ii}^* \mathbf{H}_{ii} \right)^{-1} \cdot \mathbf{H}_{ii}^* \right)^* \quad (2.43)$$

- ii. for MMSE receiver

$$\mathbf{u}_i = \left( \left( \mathbf{H}_{ii}^* \mathbf{H}_{ii} + \sum_{j \neq i} \frac{P_j}{P_i} \mathbf{H}_{ji}^* \mathbf{H}_{ji} + \sigma^2 \mathbf{I} \right)^{-1} \cdot \mathbf{H}_{ii}^* \right)^* \quad (2.44)$$

- iii. for the ML receiver the elements of receive beamformers are equal to 1 (in other words, no receive beamforming is used).

The last Hermitian conjugate in (2.43) and in (2.44) is due to the assumed definition of the achievable user rates in (2.42). For comparison purposes, also the spatial waterfilling technique will be considered [81], where the transmit power is distributed among the antennas based on the waterfilling algorithm. The spatial waterfilling approach will be denoted hereafter as SWF-MIMO.

### 2.6.1.2 Achievable Rate Regions in a Case of TSD-MIMO Interference Channel

In [62], the achievable rate regions in the 2-user SISO scenario have been studied, where the authors have treated the interference as Gaussian noise. It has been stated that the rate region for the general  $n$ -user channel is found to be the convex hull of the union of  $n$  hyper-surfaces [61], which means that the rate regions entirely encloses a straight line that connects any two points which lie within the rate region bounds. In the 2-user case, the rate regions can be easily represented as the surface limited by the horizontal and vertical axes and the boundaries of the 2-dimensional hypersurface (straight lines). Let us stress that the same conclusions can be drawn for the MIMO case. We will then discuss various achievable rate regions for the interference MIMO channel. We will analyze the properties of the rate regions introduced below in three cases: when the results are averaged over 2000 channel realizations (Case A) and for specific channel realizations (Cases B and C).

The rate region for the general interference TSD-MIMO channel is depicted in Figure 2.27. The results have been obtained based on the assumption that both users transmit with the same uniform power  $P_{i,\max} = 1$  and the results have been averaged over 2000 channel realizations, for  $h_{k,l}^{(i,j)} \sim CN(0,1,0)$ . One can define three characteristic points on the border of the rate region, i.e. points A, B and C. Specifically, point A describes the situation, where the first user transmits with the maximum power and  $\mathbf{Q}_1$  is chosen such that  $\mathbf{Q}_1 = \arg \max_{\tilde{\mathbf{Q}}_1} R_1(\tilde{\mathbf{Q}}_1, \mathbf{Q}_2 = 0)$ . Point C can be defined in



the same way as point A, but with reference to the second user. Point B corresponds to the situation, where both users transmit with the maximum power and the distribution of the power among the antennas is optimal in the sum-rate sense, i.e.  $(\mathbf{Q}_1, \mathbf{Q}_2) = \arg \max_{\tilde{\mathbf{Q}}_1, \tilde{\mathbf{Q}}_2} (R_1(\tilde{\mathbf{Q}}_1, \tilde{\mathbf{Q}}_2) + R_2(\tilde{\mathbf{Q}}_1, \tilde{\mathbf{Q}}_2))$ . The first frontier line  $\Phi_{AB} = \Phi(\mathbf{Q}_{1,p}, \cdot, \cdot), p = P_{1,\max}$ , (where  $\mathbf{Q}_{i,p}$  denotes the covariance for which  $\text{tr}(\mathbf{Q}_i) = p$ ) is obtained when holding the total transmit power for the first user fixed and varying the total transmit power for the second user from zero to  $P_{2,\max}$ . Similarly, the second frontier line  $\Phi_{BC} = \Phi(\cdot, \mathbf{Q}_{2,p}), p = P_{2,\max}$  is characterized by holding the total transmit power of the second user fixed to  $P_{2,\max}$  and decreasing the total transmit power by the first user from  $P_{1,\max}$  to zero. One can observe that the achievable rate region for the two user  $2 \times 2$  MIMO case is not convex, thus the time-sharing approach seems to be right way for system capacity improvement. The potential time-sharing lines are also presented in the Figure 2.27.

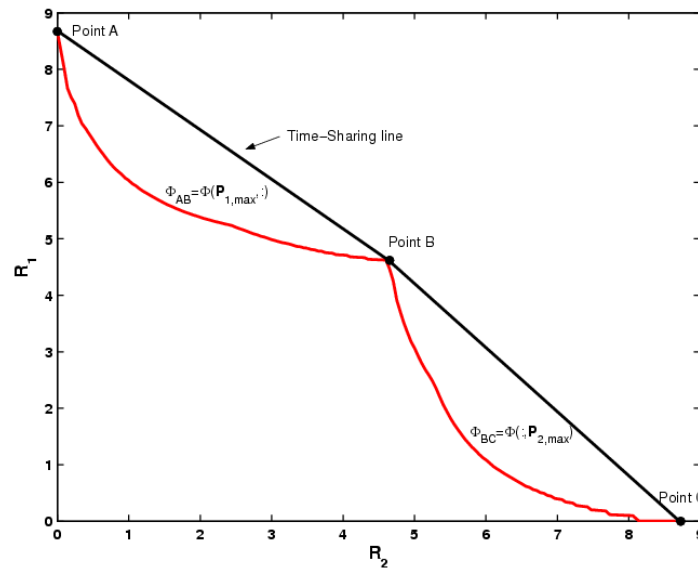


Figure 2.27 – Achievable rate region for the MIMO interference channel - averaged over 2000 channel realizations

Quite different conclusions can be drawn for a specific channel realization (i.e. the obtained rate regions are not averaged over many channel realizations), where the second user receives strong interference (see Figure 2.28). In such a case, new characteristic points can be indicated on the frontier lines of the achieved rate region. While the points A and C can be defined in the same way as in the previous case (i.e. when the results were averaged), two new points D and E appeared. All of the characteristic points define a combination of four possible situations. These are: a) user  $i$  balances all the power on the first antenna, b) user  $i$  balances all the power on the second antenna, c) user  $i$  divides the transmit power in an optimal way among both antennas, and d) user  $i$  does not transmit. When both users chose one of the four pre-defined strategies, one of the characteristic points (in our case points A, C, D, and E) on the frontier line of the rate regions can be reached. In Figure 2.28 the potential time-sharing lines are also plotted.

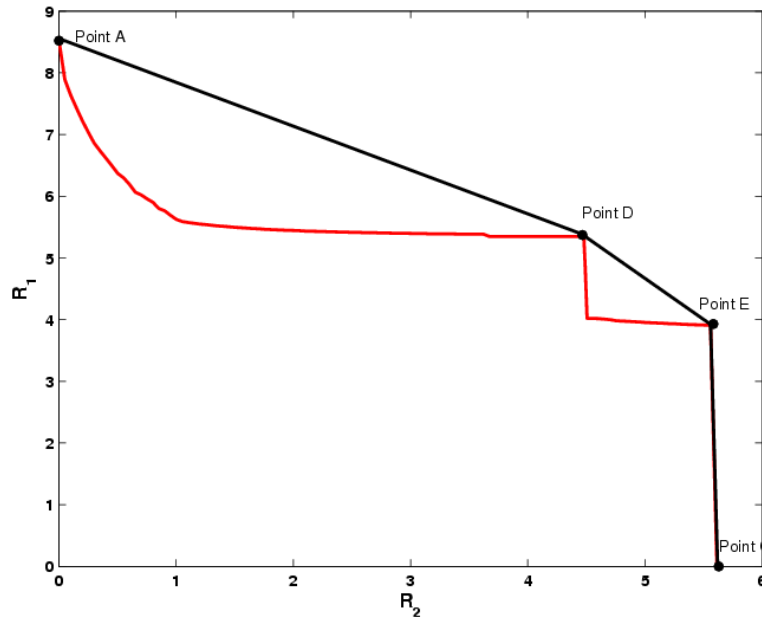


Figure 2.28 – Achievable rate region for the MIMO interference channel - one particular channel realization (user two observes strong interference)

In Figure 2.29 the results obtained for another fixed channel realization are presented, mainly a case is considered, where the first user transmits data with twice the maximum power (i.e.  $P_{1,\max} = 2 \cdot P_{2,\max}$ ) of user 2. One can observe that user 1 achieves significantly higher rates compared to user 2. For this situation, similar conclusions can be drawn as for the situation depicted in Figure 2.28, i.e. new characteristic points have occurred. Let us put the attention on the additional dashed curves which are enclosed inside the rate region, and usually start and finish in one of the characteristic points (depicted as small black-filled circles). These curves show the rate evolution achieved by both users when the users decide to choose one of the four predefined strategies. Let us define them explicitly: user  $i$  does not transmit any data (strategy  $\alpha_i^{(0)}$ ), puts all the transmit power to the antenna number 1 (strategy  $\alpha_i^{(1)}$ ) or 2 (strategy  $\alpha_i^{(2)}$ ) or distribute the total power equally between both antennas (strategy  $\alpha_i^{(3)}$ ). For example, the line with the plus marks denotes the following user behavior: starting from point  $A_1^*$ , when the first user transmits all the power on the first antenna and the second user is silent, the second user increases the transmit power on the second antenna from zero to  $P_{2,\max}$  achieving point  $A_2^*$ ; user 2 transmits with fixed power on the second antenna and the first user reduces the power from the  $P_{1,\max}$  to zero reaching point  $A_3^*$ . In other words, this line corresponds to the situation, when user 1 chooses strategy  $\alpha^{(1)}$ , and the user 2 selects strategy  $\alpha^{(2)}$ . The other lines below the frontiers show what rate will be achieved by both users when they decide to play one of the predefined strategies all the time. Let us notice that choosing the strategy  $\alpha^{(0)}$  by one of the user results in moving over the vertical or horizontal border of the achievable rate region, but it will be not considered in this investigation. It is worth mentioning that the frontier lines define the boundaries of the rate region that corresponds to choosing the best strategy in every particular situation by both users. In other words the frontier line is more or less similar to the rate achieved by both users when every time both of them select the best strategy for the actual value of transmit power, what can be approximated as switching between the dashed lines in order to maximize the instantaneous throughput.

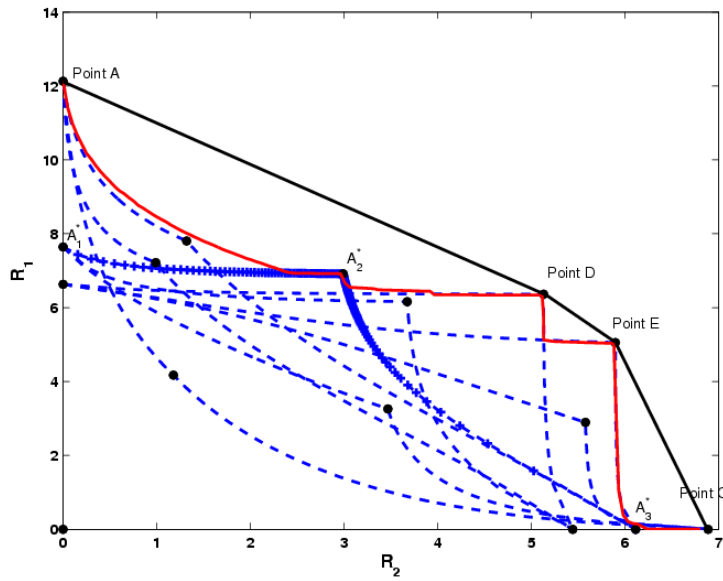


Figure 2.29 – Achievable rate region for the MIMO interference channel - the transmit power of the first user is twice higher than the transmit power of the second user

### 2.6.1.3 Achievable Rate Regions for the Precoded MIMO Systems

Similar analysis can be applied for the SVD-MIMO case. In such situation the BS can also select one of the four strategies defined in the previous subsection, however the precoder is computed in an (sub)-optimal way by the means of SVD based on the information on the channel transfer function. The channel transfer functions  $\mathbf{H}_{ij}$  that define the channel between user in the  $i$ -th cell and the  $j$ -th BS in a  $j$ -th cell, are assumed to be unknown by the neighboring BSs. An exemplary plot of the achievable rate region for 2000 channel realizations is presented in Figure 2.30. One can observe that the obtained rate region is concave thus the Time-Sharing approach seems to provide better results. As in a TSD-MIMO case the obtained results are characterized by a higher number of corner points (degrees of freedom) when compared to the SISO transmission. The transmitter can select one of the corner points in order to optimize some predefined criteria (like minimization of interference between users). The Spatial Water-Filling line is also shown in this Figure which matches the  $Q^{(3)} - Q^{(3)}$  line (i.e. the line, when both users choose the third strategy with equally distributed power among transmit antennas every time and control the transmit power to maximize the capacity). Let us stress the difference between the SWF-line and the SVD frontier line. The former is obtained as follows: user 1 transmit with the maximum allowed power  $P_{\max}$  using SWF technique and at the same time user 2 increases its power from 0 to  $P_{\max}$ . Next, the situation is reversed - the second user transmits with maximum allowed power and user 1 reduces the transmit power from  $P_{\max}$  to 0. In other words, the covariance matrix  $\mathbf{Q}_x$  is simply the identity matrix multiplied by the actual transmit power. Contrary to this case, the SVD frontier line represents the maximum possible rates that can be achieved by both users for every possible realization of the covariance matrix  $\mathbf{Q}_x$ , which trace is less or equal to the maximum transmit power, and when precoding based on SVD of the channel transfer function has been applied. The frontier line defines the maximum theoretic rates that can be achieved by both users. One can observe that although both lines start and end at the same points of the achievable rate region, the influence of interference is significantly higher in the SWF approach.

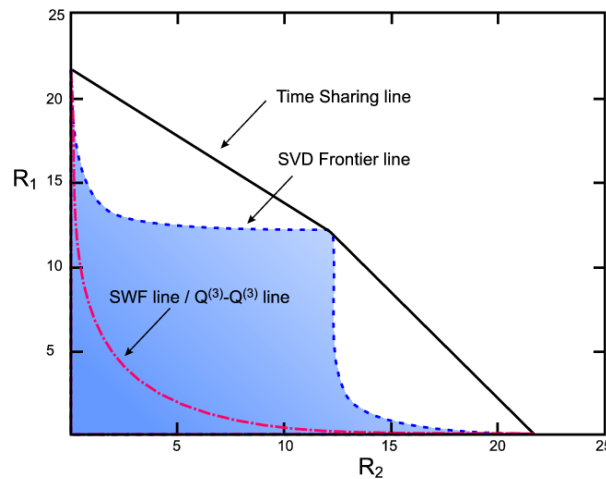


Figure 2.30 – Achievable rate region for the precoded MIMO interference channel

#### 2.6.1.4 Achievable Rate Regions for the OFDM Systems

The methodology proposed in the previous sections can be also applied in a case of OFDM transmission. In such a case the interferences will be observed only in a situation, when the neighboring users transmit data on the same subcarrier. Two achievable rate regions for OFDM transmission are presented below, i.e. in Figure 2.31 the rate region averaged over 2000 different channel realizations is shown and in Figure 2.32 the rate region achieved for one arbitrarily selected channel realization are presented (in particular, the channel between the first user and its BS was worse than the second user - channel attenuation was higher, and the maximum transmit power of the second user was twice higher than for the first one). In both figures the Time-Sharing lines are plotted. Moreover, the curves that show the rate region boundaries when the users play one specific strategy all the time are shown (represented as the dashed lines in the figure). The obtained results are similar to these achieved for the MIMO case. However, some significant differences can be found, like the difference in the achievable rates in general - the maximum achievable rates are lower in a OFDM case comparing to the MIMO scenario.

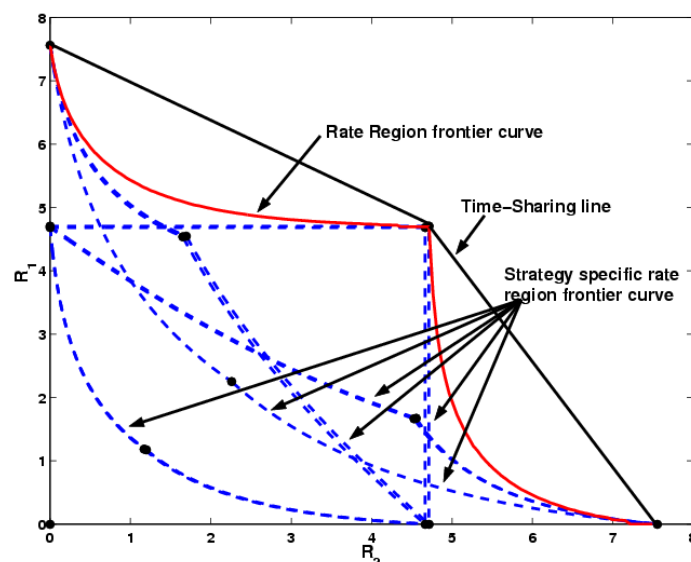


Figure 2.31 – Achievable rate region for the OFDM interference channel - results averaged over 2000 channel realizations

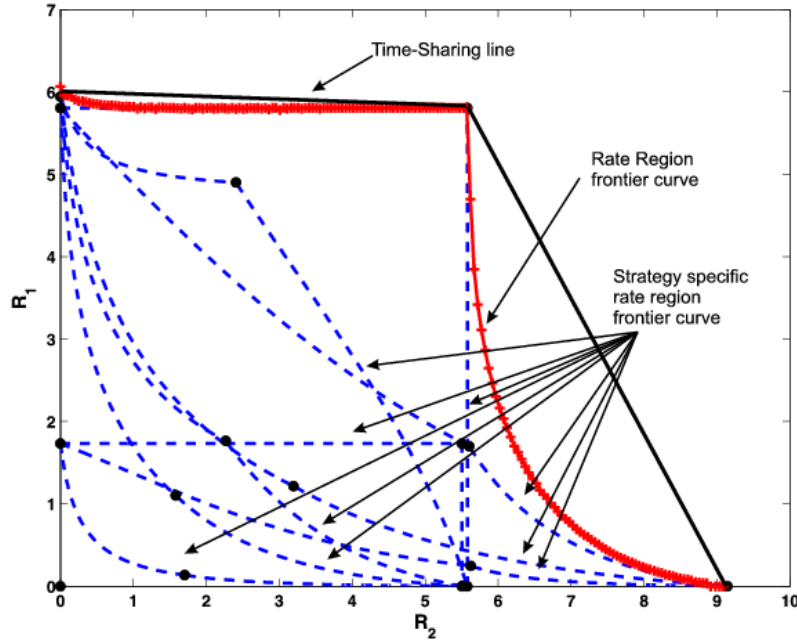


Figure 2.32 – Achievable rate region for the OFDM interference channel - one particular channel realization, maximum transmit power of the first user is two times higher than the maximum transmit power of the second user

#### 2.6.1.5 Crystallized Rate Regions and Time-Sharing

The idea of the Crystallized Rate Regions has been introduced in [62] and can be understood as an approximation of the achievable rate regions by the convex time-sharing hull, where the potential curves between characteristic points (e.g. A, B, and C in Figure 2.27) are replaced by the straight lines connecting these points.

One can observe from the results shown in Figure 2.29 that for the MIMO case the crystallized rate region for the 2-user scenario has much more characteristic points (i.e. the points, where both users transmit with the maximum power for selected strategy) than in the SISO case (see [62] for comparison). In order to create the convex hull, only such points can be selected, which lie on the frontier line. Moreover, the selection of all characteristic points that lie on border line could be non optimal, thus only a subset of these points should be chosen for the Time-Sharing approach (compare Figure 2.28 and Figure 2.29).

Let us denote each point in the rate region as  $\Phi(\mathbf{Q}_{1,p_1}, \mathbf{Q}_{2,p_2})$ , i.e.  $\text{tr}(\mathbf{Q}_{1,p_1}) = p_1$ ,  $0 \leq p_1 \leq P_{1,\max}$  and  $\text{tr}(\mathbf{Q}_{2,p_2}) = p_2$ ,  $0 \leq p_2 \leq P_{2,\max}$ . Point A in Figure 2.27 can be defined as  $\Phi(P_{1,\max}, 0)$ , i.e. user one transmits with the maximum total power and the second user is silent, point C, as  $\Phi(0, P_{2,\max})$ , i.e. the first user does not transmit any data and the second user transmits with the maximum total power, and point B is defined as  $\Phi(P_{1,\max}, P_{2,\max})$ , i.e. both users transmit with the maximum total power. One can observe that these points are corner (characteristic) points of the achievable rate region. In the 2-user  $2 \times 2$  TSD-MIMO channel there exist 15 points, which refer to any particular combination of the possible strategies. In general, for the  $n$ -user  $N_t \times N_r$  MIMO case, there exist  $(N_t + 2)^n - 1$  points, i.e. the  $i$ -th user can put all power to one antenna ( $N_i$  possibilities), divide the power equally among the antennas (one possibility) or be silent (one possibility). We do not take into account the case when all users are silent. In a SISO case,  $N_t = 1$  and the number of strategies is limited to two (i.e. the division of the power equally among all antennas denotes that all the power is transmitted through the antenna).

Following the approach proposed in [62] we state that instead of power control problem in finding the metrics  $\mathbf{P}_i$ , the problem becomes finding the appropriate time-sharing coefficients of the  $(N_t + 2)^n - 1$  corner points. For the 2-user  $2 \times 2$  TSD-MIMO case we will obtain 15 points, i.e.  $\Theta = [\theta_{k,l}]$  for  $0 \leq k, l \leq 3$ , which fulfill  $\sum_{k,l} \theta_{k,l} = 1$ . In our case, the time-sharing coefficients relate to the specific corner points, i.e. the coefficient  $\theta_{k,l}$  defines the point, where user 1 choose the strategy  $\alpha_1^{(k)}$  and user 2 selects the strategy  $\alpha_2^{(l)}$ . Consequently, (2.41) can be rewritten as in (2.45), where  $\mathbf{Q}_i^{(k)}$  denotes the  $i$ -th user covariance matrix while choosing the strategy  $\alpha_i^{(k)}$ . Let us stress that any solution point on the crystallized rate border line (frontier) will lie somewhere on the straight lines connecting any of the neighboring characteristic points.

$$\begin{aligned} \mathbf{R}_1(\Theta) &= \sum_{k,l} \theta_{k,l} \cdot \log_2 \left( \det \left( \mathbf{I} + \mathbf{H}_{11} \mathbf{Q}_1^{(k)} \mathbf{H}_{11}^* \cdot (\sigma^2 \mathbf{I} + \mathbf{H}_{21} \mathbf{Q}_2^{(l)} \mathbf{H}_{21}^*)^{-1} \right) \right) \\ \mathbf{R}_2(\Theta) &= \sum_{k,l} \theta_{k,l} \cdot \log_2 \left( \det \left( \mathbf{I} + \mathbf{H}_{22} \mathbf{Q}_2^{(l)} \mathbf{H}_{22}^* \cdot (\sigma^2 \mathbf{I} + \mathbf{H}_{12} \mathbf{Q}_1^{(k)} \mathbf{H}_{12}^*)^{-1} \right) \right) \end{aligned} \quad (2.45)$$

Similar conclusions can be drawn for the precoded MIMO systems, where (2.45), that defines the achievable rate in a time-sharing approach, has to be rewritten in order to include the transmit and receive beamformers set (see (2.46)).

$$\begin{aligned} R_1(\Theta) &= \sum_{k,l} \theta_{k,l} \cdot \log_2 \left( \det \left( \mathbf{I} + \mathbf{u}_1^* \mathbf{H}_{11} \mathbf{v}_1 \mathbf{Q}_1^{(k)} \mathbf{v}_1^* \mathbf{H}_{11}^* \mathbf{u}_1 \cdot (\sigma^2 \mathbf{u}_1^* \mathbf{u}_1 + \mathbf{u}_1^* \mathbf{H}_{21} \mathbf{v}_2 \mathbf{Q}_2^{(l)} \mathbf{v}_2^* \mathbf{H}_{21}^* \mathbf{u}_1)^{-1} \right) \right) \\ R_2(\Theta) &= \sum_{k,l} \theta_{k,l} \cdot \log_2 \left( \det \left( \mathbf{I} + \mathbf{u}_2^* \mathbf{H}_{22} \mathbf{v}_2 \mathbf{Q}_2^{(l)} \mathbf{v}_2^* \mathbf{H}_{22}^* \mathbf{u}_2 \cdot (\sigma^2 \mathbf{u}_2^* \mathbf{u}_2 + \mathbf{u}_2^* \mathbf{H}_{12} \mathbf{v}_1 \mathbf{Q}_1^{(k)} \mathbf{v}_1^* \mathbf{H}_{12}^* \mathbf{u}_2)^{-1} \right) \right) \end{aligned} \quad (2.46)$$

#### 2.6.1.6 Correlated Equilibrium for Crystallized Interference MIMO Channel

In general, each user plays one of  $N_s = N_c + 2$  strategies  $\alpha^{(k)}$ ,  $1 \leq k \leq N_c$ , where  $N_c$  is the number of antennas in case of TSD-MIMO and SVD-MIMO ( $N_c = N_t$ ), whereas for ZF/MMSE/ML-MIMO  $N_c$  denotes the codebook size ( $N_c = N$ ). As a result of playing one of the strategies, the  $i$ -th user will receive payoff, denoted hereafter  $U_i(\alpha_i^{(k)})$ . The aim of each user is to maximize its payoff with or without cooperation with the other users. Such a game leads to the well-known Nash equilibrium strategy  $\alpha_i^*$  [81] such that

$$U_i(\alpha_i^*, \mathbf{a}_{-i}) \geq U_i(\alpha_i, \mathbf{a}_{-i}), \forall i \in S \quad (2.47)$$

where  $\alpha_i$  represents the possible strategy of the  $i$ -th user, whereas  $\mathbf{a}_{-i}$  defines the set of strategies chosen by the other users, i.e.  $\mathbf{a}_{-i} = \{\alpha_j\}$ ,  $j \neq i$ , and  $S$  is the users set of the cardinality  $n$ . The idea behind the Nash equilibrium is to find the point of the achievable rate region (which is related to the selection of one of the available strategies), from which any user cannot increase its utility (increase the total payoff) without reducing other users' payoffs.

Moreover, in this context, the correlated equilibrium used in [62] instead of Nash equilibrium is defined as  $\alpha_i^*$  such that:

$$\sum_{\alpha_{-i} \in \Omega_{-i}} p(\alpha_i^*, \mathbf{a}_{-i}) [U_i(\alpha_i^*, \mathbf{a}_{-i}) - U_i(\alpha_i, \mathbf{a}_{-i})] \geq 0, \forall \alpha_i, \alpha_i^* \in \Omega_i, \forall i \in S \quad (2.48)$$

where  $p(\alpha_i^*, \mathbf{a}_{-i})$  is the probability of playing strategy  $\alpha_i^*$  in a case when other users select their own strategies  $\alpha_j$ ,  $j \neq i$ .  $\Omega_i$  and  $\Omega_{-i}$  denote the strategy space of user  $i$  and all the users other than  $i$ , respectively. The probability distribution  $p$  is a joint point mass function of the different combinations

of users strategies. As in [62], the inequality in correlated equilibrium definition means that when the recommendation to user  $i$  is to choose action  $\alpha_i^*$ , then choosing any other action instead of  $\alpha_i^*$  cannot result in higher expected payoff for this user. Note that the cardinality of the  $\Omega_{-i}$  is  $(N_c + 2)^{(n-1)}$ .

Let us stress out that the time-sharing coefficients  $\theta_{k,l}$  are the  $(N_c + 2)^{(n-1)}$  point masses that we want to compute. In such a case, the one-to-one mapping function between any time-sharing coefficient  $\theta_{k,l}$  and the corresponding point mass function  $p(\alpha_i^{(k)}, \alpha_j^{(l)})$  of the point  $\Phi(\alpha_i^{(k)}, \alpha_j^{(l)})$  can be defined as follows:

$$\theta_{k,l} = p(\alpha_i^{(k)}, \alpha_j^{(l)}) \quad (2.49)$$

where  $p(\alpha_i^{(k)}, \alpha_j^{(l)})$  is the probability of user  $i$  playing the  $k$ -th strategy and user  $j$  playing the  $l$ -th strategy.

### 2.6.1.7 The Mechanism Design

To resolve any conflicts between users, the Vickrey-Clarke-Groves (VCG) auction mechanism design is employed, which aims to maximize the utility  $U_i, \forall i$ , defined as:

$$U_i \stackrel{\Delta}{=} R_i - \zeta_i \quad (2.50)$$

where  $R_i$  is the rate of user  $i$  and the cost  $\zeta_i$  is evaluated as:

$$\zeta_i(\alpha) = \sum_{j \neq i} R_j(\alpha_{-i}) - \sum_{j \neq i} R_j(\alpha_i) \quad (2.51)$$

Hence, for the considered scenario with two users the payment costs for user 1 can be defined as:

$$\begin{aligned} \zeta_1(\alpha_1 = \mathbf{Q}_1^{(k)}, \alpha_2 = \mathbf{Q}_2^{(l)}) &= R_2(\alpha_1 = \mathbf{Q}_1^{(0)}, \alpha_2 = \mathbf{Q}_2^{(l)}) - R_2(\alpha_1 = \mathbf{Q}_1^{(k)}, \alpha_2 = \mathbf{Q}_2^{(l)}) = \\ &= \log_2 \left( \det(\mathbf{I} + \mathbf{H}_{22} \mathbf{Q}_2^{(l)} \mathbf{H}_{22}^* \cdot \sigma^{-2}) \right) - \log_2 \left( \det \left( \mathbf{I} + \mathbf{H}_{22} \mathbf{Q}_2^{(l)} \mathbf{H}_{22}^* \cdot (\sigma^2 \mathbf{I} + \mathbf{H}_{12} \mathbf{Q}_1^{(k)} \mathbf{H}_{12}^*)^{-1} \right) \right) \end{aligned} \quad (2.52)$$

where  $\mathbf{Q}_1^{(k)}$  and  $\mathbf{Q}_2^{(l)}$  are the covariance matrices corresponding to the strategies  $\alpha_1^{(k)}$  and  $\alpha_2^{(l)}$  selected by user 1 and user 2 respectively, what is denoted  $\alpha_i = \mathbf{Q}_i^{(k)}$ . The payment cost  $\zeta_2$  follows by symmetry. Thus, the VCG utilities can be calculated using (2.53):

$$\{U_1, U_2\} = \{U'_1(\mathbf{Q}_1^{(k)}, \mathbf{Q}_2^{(l)}), U'_2(\mathbf{Q}_1^{(k)}, \mathbf{Q}_2^{(l)})\} \quad (2.53)$$

where  $U'_1(\mathbf{Q}_1^{(k)}, \mathbf{Q}_2^{(l)})$ , and  $U'_2(\mathbf{Q}_1^{(k)}, \mathbf{Q}_2^{(l)})$  for the considered cases are defined as in (2.54), (2.59), and (2.61) respectively.

#### 2.6.1.7.1 TSD-MIMO case

In the investigated TSD-MIMO scenario no transmit and receive beamforming is applied, and the considered strategies represent the transmit antenna selection mechanism. Hence, the VCG utilities can be calculated as in (2.54). The first part of both formulas presents the achievable rate (payoff) of the  $i$ -th user if no auction theory is applied (no cost is paid by the user for starting playing). On the other hand last two parts express the price  $\zeta_i$  (defined as (2.51)) to be paid by the  $i$ -th user for playing the chosen strategy.

$$\begin{aligned}
U_1'(\mathbf{Q}_1^{(k)}, \mathbf{Q}_2^{(l)}) &= \log_2 \left( \det \left( \mathbf{I} + \mathbf{H}_{11} \mathbf{Q}_1^{(k)} \mathbf{H}_{11}^* \cdot (\sigma^2 \mathbf{I} + \mathbf{H}_{21} \mathbf{Q}_2^{(l)} \mathbf{H}_{21}^*)^{-1} \right) \right) - \\
&+ \log_2 \left( \det \left( \mathbf{I} + \mathbf{H}_{22} \mathbf{Q}_2^{(l)} \mathbf{H}_{22}^* \cdot \sigma^{-2} \right) \right) + \log_2 \left( \det \left( \mathbf{I} + \mathbf{H}_{22} \mathbf{Q}_2^{(l)} \mathbf{H}_{22}^* \cdot (\sigma^2 \mathbf{I} + \mathbf{H}_{12} \mathbf{Q}_1^{(k)} \mathbf{H}_{12}^*)^{-1} \right) \right) \\
U_2'(\mathbf{Q}_1^{(k)}, \mathbf{Q}_2^{(l)}) &= \log_2 \left( \det \left( \mathbf{I} + \mathbf{H}_{22} \mathbf{Q}_2^{(l)} \mathbf{H}_{22}^* \cdot (\sigma^2 \mathbf{I} + \mathbf{H}_{12} \mathbf{Q}_1^{(k)} \mathbf{H}_{12}^*)^{-1} \right) \right) - \\
&+ \log_2 \left( \det \left( \mathbf{I} + \mathbf{H}_{11} \mathbf{Q}_1^{(k)} \mathbf{H}_{11}^* \cdot \sigma^{-2} \right) \right) + \log_2 \left( \det \left( \mathbf{I} + \mathbf{H}_{11} \mathbf{Q}_1^{(k)} \mathbf{H}_{11}^* \cdot (\sigma^2 \mathbf{I} + \mathbf{H}_{21} \mathbf{Q}_2^{(l)} \mathbf{H}_{21}^*)^{-1} \right) \right)
\end{aligned} \tag{2.54}$$

Since the precoding vectors in case of TSD-MIMO correspond to the selection of one of the available transmit antennas (or the selection of both with equal power distribution), there are only four strategies are available to users, which correspond to the following covariance matrices:

$$\mathbf{Q}_i^{(0)} = \begin{pmatrix} 0 & 0 \\ 0 & 0 \end{pmatrix} \quad \mathbf{Q}_i^{(1)} = \begin{pmatrix} P_{i,\max} & 0 \\ 0 & 0 \end{pmatrix} \tag{2.55}$$

$$\mathbf{Q}_i^{(2)} = \begin{pmatrix} 0 & 0 \\ 0 & P_{i,\max} \end{pmatrix} \quad \mathbf{Q}_i^{(3)} = \begin{pmatrix} \frac{P_{i,\max}}{2} & 0 \\ 0 & \frac{P_{i,\max}}{2} \end{pmatrix} \tag{2.56}$$

When selecting the strategy corresponding to  $\mathbf{Q}_i^{(0)}$  user  $i$  decides to remain silent. On the contrary,  $\mathbf{Q}_i^{(1)}$  and  $\mathbf{Q}_i^{(2)}$  correspond to the situation when user  $i$  decides to transmit on antenna 1 or antenna 2, respectively. Finally,  $\mathbf{Q}_i^{(3)}$  is the covariance matrix representing the strategy when user  $i$  transmits on both antennas with equal power distribution.

#### 2.6.1.7.2 OFDM case

One may observe, that the proposed general mechanism design can be used to investigate the performance of OFDM transmission on the interference channel. This is the case when the channel matrices  $\mathbf{H}_{ij}, \forall \{i, j\}$  are diagonal, so the specific paths represent the orthogonal sub-carriers. Similarly to the previous subsection, first parts of the formulas present the achievable rate (payoff) of the  $i$ -th user if no auction theory is applied (no cost is paid by the user for starting playing). Next, last two parts defines the price  $\zeta_i$  (defined as (2.51)) to be paid by the  $i$ -th user for starting playing the chosen strategy. It is worth mentioning that since the above mentioned  $\mathbf{H} \mathbf{H}$  matrix is diagonal one can easily apply the eigenvalue decomposition (or singular value decomposition) to reduce the number of required operations. Hence, for the considered 2-user scenario the cost for user  $i$  can be evaluated as in (2.57) and (2.58) and the VCG utilities can be defined as in (2.59). For the sake of clarity, let us provide the interpretation of selected variables in the formulas below for the OFDM case:  $h_{k,k}^{(i,j)}$  is the channel coefficient that characterizes the channel on the  $k$ -th subcarriers between the  $i$ -th and the  $j$ -th user and  $q_{k,k}^{(i)}$  is the  $k$ -th diagonal element from the considered covariance matrix  $\mathbf{Q}^{(i)}$  of the  $i$ -th user.

$$\begin{aligned}
\zeta_1(\alpha_1 = \mathbf{Q}_1^{(k)}, \alpha_2 = \mathbf{Q}_2^{(l)}) &= R_2(\alpha_1 = \mathbf{Q}_1^{(0)}, \alpha_2 = \mathbf{Q}_2^{(l)}) - R_2(\alpha_1 = \mathbf{Q}_1^{(k)}, \alpha_2 = \mathbf{Q}_2^{(l)}) = \\
&= \log_2 \left( 1 + \frac{q_{11}^{(2)} |h_{11}^{(22)}|^2}{\sigma^2} \right) + \log_2 \left( 1 + \frac{q_{22}^{(2)} |h_{22}^{(22)}|^2}{\sigma^2} \right) - \\
&+ \log_2 \left( 1 + \frac{q_{11}^{(2)} |h_{11}^{(22)}|^2}{\sigma^2 + q_{11}^{(1)} |h_{11}^{(12)}|^2} \right) - \log_2 \left( 1 + \frac{q_{22}^{(2)} |h_{22}^{(22)}|^2}{\sigma^2 + q_{22}^{(1)} |h_{22}^{(12)}|^2} \right)
\end{aligned} \tag{2.57}$$



$$\begin{aligned} \zeta_2(\alpha_1 = \mathbf{Q}_1^{(k)}, \alpha_2 = \mathbf{Q}_2^{(l)}) &= R_1(\alpha_1 = \mathbf{Q}_1^{(k)}, \alpha_2 = \mathbf{Q}_2^{(0)}) - R_1(\alpha_1 = \mathbf{Q}_1^{(k)}, \alpha_2 = \mathbf{Q}_2^{(l)}) = \\ &= \log_2 \left( 1 + \frac{q_{11}^{(1)} |h_{11}^{(11)}|^2}{\sigma^2} \right) + \log_2 \left( 1 + \frac{q_{22}^{(1)} |h_{22}^{(11)}|^2}{\sigma^2} \right) - \end{aligned} \quad (2.58)$$

$$\begin{aligned} &+ \log_2 \left( 1 + \frac{q_{11}^{(1)} |h_{11}^{(11)}|^2}{\sigma^2 + q_{11}^{(2)} |h_{11}^{(21)}|^2} \right) - \log_2 \left( 1 + \frac{q_{22}^{(1)} |h_{22}^{(11)}|^2}{\sigma^2 + q_{22}^{(2)} |h_{22}^{(21)}|^2} \right) \\ U_1(\mathbf{Q}_1^{(k)}, \mathbf{Q}_2^{(l)}) &= \log_2 \left( 1 + \frac{q_{11}^{(1)} |h_{11}^{(11)}|^2}{\sigma^2 + q_{11}^{(2)} |h_{11}^{(21)}|^2} \right) + \log_2 \left( 1 + \frac{q_{22}^{(1)} |h_{22}^{(11)}|^2}{\sigma^2 + q_{22}^{(2)} |h_{22}^{(21)}|^2} \right) - \\ &+ \zeta_1(\alpha_1 = \mathbf{Q}_1^{(k)}, \alpha_2 = \mathbf{Q}_2^{(l)}) \end{aligned} \quad (2.59)$$

$$\begin{aligned} U_2(\mathbf{Q}_1^{(k)}, \mathbf{Q}_2^{(l)}) &= \log_2 \left( 1 + \frac{q_{11}^{(2)} |h_{11}^{(22)}|^2}{\sigma^2 + q_{11}^{(1)} |h_{11}^{(12)}|^2} \right) - \log_2 \left( 1 + \frac{q_{22}^{(2)} |h_{22}^{(22)}|^2}{\sigma^2 + q_{22}^{(1)} |h_{22}^{(12)}|^2} \right) - \\ &+ \zeta_2(\alpha_1 = \mathbf{Q}_1^{(k)}, \alpha_2 = \mathbf{Q}_2^{(l)}) \end{aligned}$$

#### 2.6.1.7.3 Precoded MIMO case

Obviously, the idea of correlated equilibrium and of application of the auction theorem described in the previous subsections, can be applied also for the precoded MIMO case. However, beside the straightforward modification of the formulas describing the payment cost (see (2.60)) and VCG utilities (see (2.61)) the set of possible strategies has to be interpreted in a different way. However, following the way provided in the previous subsections, one can interpret the formulas presented below in more detailed way. Thus, the first part of the formulas (2.61) presents the achievable rate (payoff) of the  $i$ -th user if no auction theory is applied (no cost is paid by the user for starting playing), whereas last two parts express the price  $\zeta_i$  (defined as (2.51)) to be paid by the  $i$ -th user for starting playing the chosen strategy.

$$\begin{aligned} \zeta_1(\alpha_1 = \mathbf{Q}_1^{(k)}, \alpha_2 = \mathbf{Q}_2^{(l)}) &= R_2(\alpha_1 = \mathbf{Q}_1^{(0)}, \alpha_2 = \mathbf{Q}_2^{(l)}) - R_2(\alpha_1 = \mathbf{Q}_1^{(k)}, \alpha_2 = \mathbf{Q}_2^{(l)}) = \\ &= \log_2 \left( \det(\mathbf{I} + \mathbf{u}_2^* \mathbf{H}_{22} \mathbf{v}_2 \mathbf{Q}_2^{(l)} \mathbf{v}_2^* \mathbf{H}_{22}^* \mathbf{u}_2 \cdot \sigma^{-2}) \right) - \\ &+ \log_2 \left( \det \left( \mathbf{I} + \mathbf{u}_2^* \mathbf{H}_{22} \mathbf{v}_2 \mathbf{Q}_2^{(l)} \mathbf{v}_2^* \mathbf{H}_{22}^* \mathbf{u}_2 \cdot \left( \sigma^2 \mathbf{u}_2^* \mathbf{u}_2 + \mathbf{u}_2^* \mathbf{H}_{12} \mathbf{v}_1 \mathbf{Q}_1^{(k)} \mathbf{v}_1^* \mathbf{H}_{12}^* \mathbf{u}_2 \right)^{-1} \right) \right) \\ \zeta_2(\alpha_1 = \mathbf{Q}_1^{(k)}, \alpha_2 = \mathbf{Q}_2^{(l)}) &= R_1(\alpha_1 = \mathbf{Q}_1^{(k)}, \alpha_2 = \mathbf{Q}_2^{(0)}) - R_1(\alpha_1 = \mathbf{Q}_1^{(k)}, \alpha_2 = \mathbf{Q}_2^{(l)}) = \\ &= \log_2 \left( \det(\mathbf{I} + \mathbf{u}_1^* \mathbf{H}_{11} \mathbf{v}_1 \mathbf{Q}_1^{(k)} \mathbf{v}_1^* \mathbf{H}_{11}^* \mathbf{u}_1 \cdot \sigma^{-2}) \right) - \\ &+ \log_2 \left( \det \left( \mathbf{I} + \mathbf{u}_1^* \mathbf{H}_{11} \mathbf{v}_1 \mathbf{Q}_1^{(k)} \mathbf{v}_1^* \mathbf{H}_{11}^* \mathbf{u}_1 \cdot \left( \sigma^2 \mathbf{u}_1^* \mathbf{u}_1 + \mathbf{u}_1^* \mathbf{H}_{21} \mathbf{v}_2 \mathbf{Q}_2^{(l)} \mathbf{v}_2^* \mathbf{H}_{21}^* \mathbf{u}_1 \right)^{-1} \right) \right) \end{aligned} \quad (2.60)$$

$$\begin{aligned}
U_1(\mathbf{Q}_1^{(k)}, \mathbf{Q}_2^{(l)}) &= \log_2 \left( \det \left( \mathbf{I} + \mathbf{u}_1^* \mathbf{H}_{11} \mathbf{v}_1 \mathbf{Q}_1^{(k)} \mathbf{v}_1^* \mathbf{H}_{11}^* \mathbf{u}_1 \cdot \left( \sigma^2 \mathbf{u}_1^* \mathbf{u}_1 + \mathbf{u}_1^* \mathbf{H}_{21} \mathbf{v}_2 \mathbf{Q}_2^{(l)} \mathbf{v}_2^* \mathbf{H}_{21}^* \mathbf{u}_1 \right)^{-1} \right) \right) - \\
&+ \log_2 \left( \det \left( \mathbf{I} + \mathbf{u}_2^* \mathbf{H}_{22} \mathbf{v}_2 \mathbf{Q}_2^{(l)} \mathbf{v}_2^* \mathbf{H}_{22}^* \mathbf{u}_2 \cdot \sigma^{-2} \right) \right) + \\
&+ \log_2 \left( \det \left( \mathbf{I} + \mathbf{u}_2^* \mathbf{H}_{22} \mathbf{v}_2 \mathbf{Q}_2^{(l)} \mathbf{v}_2^* \mathbf{H}_{22}^* \mathbf{u}_2 \cdot \left( \sigma^2 \mathbf{u}_2^* \mathbf{u}_2 + \mathbf{u}_2^* \mathbf{H}_{12} \mathbf{v}_1 \mathbf{Q}_1^{(k)} \mathbf{v}_1^* \mathbf{H}_{12}^* \mathbf{u}_2 \right)^{-1} \right) \right) \\
U_2(\mathbf{Q}_1^{(k)}, \mathbf{Q}_2^{(l)}) &= \log_2 \left( \det \left( \mathbf{I} + \mathbf{u}_2^* \mathbf{H}_{22} \mathbf{v}_2 \mathbf{Q}_2^{(l)} \mathbf{v}_2^* \mathbf{H}_{22}^* \mathbf{u}_2 \cdot \left( \sigma^2 \mathbf{u}_2^* \mathbf{u}_2 + \mathbf{u}_2^* \mathbf{H}_{12} \mathbf{v}_1 \mathbf{Q}_1^{(k)} \mathbf{v}_1^* \mathbf{H}_{12}^* \mathbf{u}_2 \right)^{-1} \right) \right) - \\
&+ \log_2 \left( \det \left( \mathbf{I} + \mathbf{u}_1^* \mathbf{H}_{11} \mathbf{v}_1 \mathbf{Q}_1^{(k)} \mathbf{v}_1^* \mathbf{H}_{11}^* \mathbf{u}_1 \cdot \sigma^{-2} \right) \right) + \\
&+ \log_2 \left( \det \left( \mathbf{I} + \mathbf{u}_1^* \mathbf{H}_{11} \mathbf{v}_1 \mathbf{Q}_1^{(k)} \mathbf{v}_1^* \mathbf{H}_{11}^* \mathbf{u}_1 \cdot \left( \sigma^2 \mathbf{u}_1^* \mathbf{u}_1 + \mathbf{u}_1^* \mathbf{H}_{21} \mathbf{v}_2 \mathbf{Q}_2^{(l)} \mathbf{v}_2^* \mathbf{H}_{21}^* \mathbf{u}_1 \right)^{-1} \right) \right)
\end{aligned} \tag{2.61}$$

In the previous cases (i.e. TSD-MIMO and OFDM) the selection of one of the predefined strategies means that the BS selects first, second or both antennas for transmission or is silent. In the SVD-MIMO case the selection of the covariance matrix  $\mathbf{Q}_i$  by the BS has an interpretation of choosing one of the calculated singular values (obtained as the result of singular value decomposition of the transfer channel matrix). Thus, for example by choosing the strategy corresponding to  $\mathbf{Q}_i^{(1)}$  means that we choose the first singular value and - in consequence - the transmit and receive precoding vector that correspond to this singular value. Moreover, selection of the third strategy corresponding to  $\mathbf{Q}_i^{(3)}$  has a meaning that no specific precoding has to be applied. Such situation can occur in a presence of high interference between adjacent cells. It has to be stressed that selection of the first strategy will be preferred since the precoding vectors that correspond to this particular singular value maximize the channel capacity. However, this statement can be no longer valid in a strong interference case. The obtained results show that in such situation the proposed algorithm converges to global optimum when the second or even third strategy is selected.

Different interpretation of the user strategies has to be defined for the ZF/MMSE/ML-MIMO transmission when the codebook of size  $N$  is used. In such a case the number of strategies has to be increased from 4 (as in TSD-MIMO case) to  $N+2$ , i.e. the player (BS) can choose to be silent (one strategy), not to use any specific beamformer (second strategy) or to use one of the predefined and stored in a codebook strategies (remaining  $N$  strategies).

#### 2.6.1.8 The Regret-Matching Algorithm

In [62] the regret-matching learning algorithm is proposed to learn in a distributive fashion how to achieve the correlated equilibrium set in solving the VCG auction. Since in [62] the interference channel with only one transmit and one receive antenna per user is considered, there are only two distinct binary actions  $\alpha_i^{(0)} = 0$  and  $\alpha_i^{(1)} = P_{\max}$  at every time  $t=T$ . However, in case of the considered MIMO interference channel with  $2 \times 2$  configuration there are more actions possible. Hence, the regret  $REG_i^T$  of user  $i$  at time  $T$  for playing action  $\alpha_i^{(k)}$  instead of other actions is

$$REG_i^T(\alpha_i^{(k)}, \mathbf{a}_i^{(-k)}) = \max \{ D_i^T(\alpha_i^{(k)}, \mathbf{a}_i^{(-k)}), 0 \} \tag{2.62}$$

where

$$D_i^T(\alpha_i^{(k)}, \mathbf{a}_i^{(-k)}) = \frac{1}{T} \sum_{j=1}^K \sum_{t \leq T, j \neq k} (U_i^t(\alpha_i^{(j)}, \mathbf{a}_{-i}) - U_i^t(\alpha_i^{(k)}, \mathbf{a}_{-i})) \tag{2.63}$$

where  $K$  is the cardinality of the set of all actions available to user  $i$ ,  $U_i^t(\alpha_i^{(j)}, \mathbf{a}_{-i})$  is the utility at time  $t$  and  $\mathbf{a}_{-i}$  is the vector specifying the other users actions.  $D_i^T(\alpha_i^{(k)}, \mathbf{a}_i^{(-k)})$  is the average payoff that user  $i$  would have obtained if it had played other action than  $\alpha_i^{(k)}$  every time in the past. Other definitions of

average payoff are possible, e.g. finding the maximum value of average payoffs of all strategies other than  $k$ .

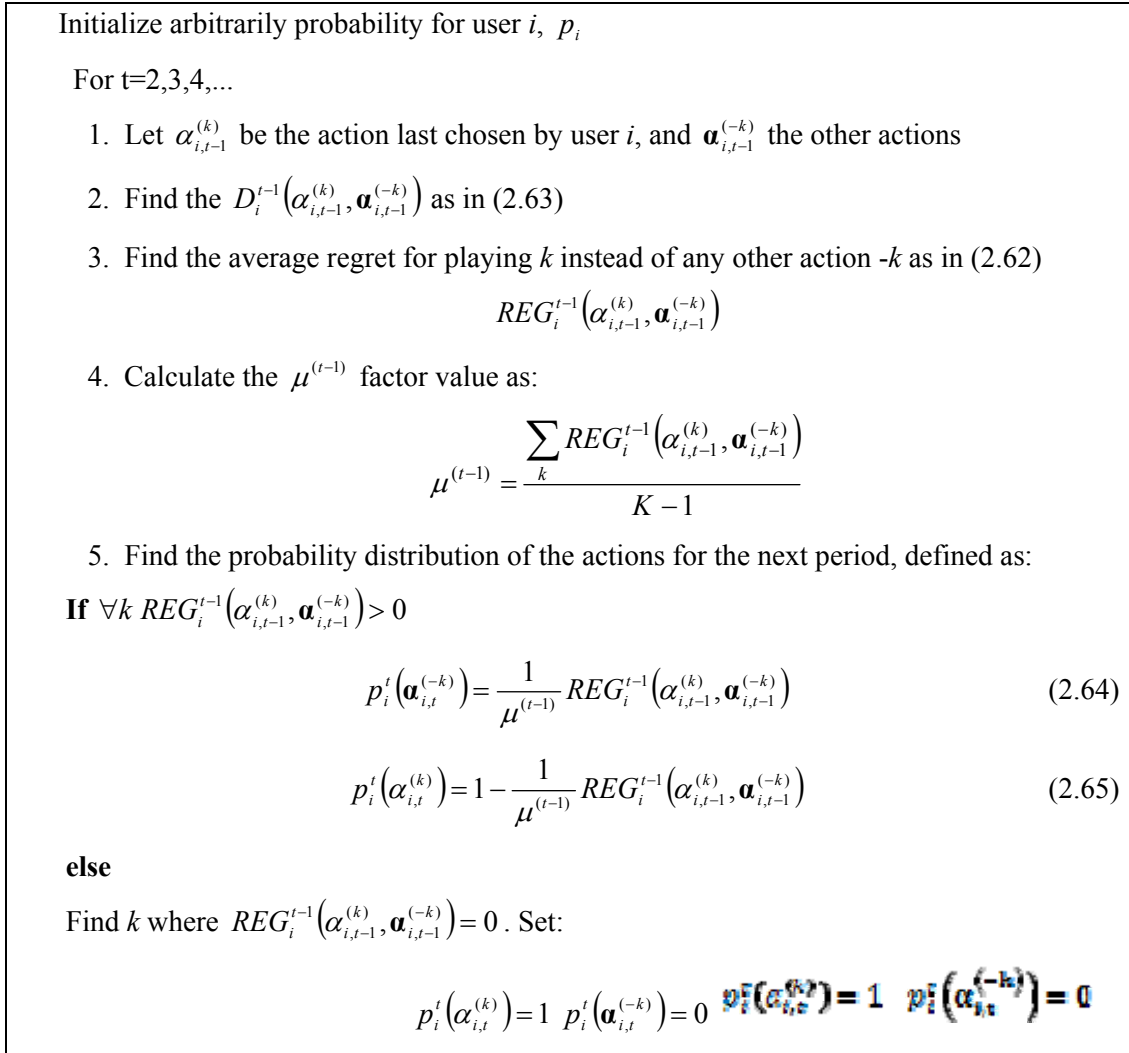


Figure 2.33 – Regret-matching learning algorithm

The details of the regret-matching learning algorithm are presented in Figure 2.33. According to the theorem presented in [68], if every user plays according to the proposed learning algorithm, then the found probability distribution should converge on the set of correlated equilibrium as  $T \rightarrow \infty$ .

### 2.6.1.9 Simulation Results

To validate the correctness of the proposed idea, the 2-user  $2 \times 2$  MIMO system has been simulated. In Figure 2.34 the crystallized rate region in the interference limited case has been shown, i.e. the case when strong interference between antennas exist. The channel matrices for this case have been set as:

$$\begin{aligned} \mathbf{H}_{11} &= \begin{pmatrix} 1 & 1 \\ 0.01 & 0.01 \end{pmatrix} & \mathbf{H}_{22} &= \begin{pmatrix} 0.01 & 0.01 \\ 1 & 1 \end{pmatrix} \\ \mathbf{H}_{12} &= \begin{pmatrix} 0.01 & 0.01 \\ 1 & 1 \end{pmatrix} & \mathbf{H}_{21} &= \begin{pmatrix} 1 & 1 \\ 0.01 & 0.01 \end{pmatrix} \end{aligned} \quad (2.66)$$

that implies that the first user observe strong interferences from the second user only on the second antenna while on the first antenna only the useful signal is received, and vice versa - the second users observes strong interference signal only on the first antenna. Such configuration explicitly leads toward choosing the strategy  $\alpha^{(1)}$  and  $\alpha^{(2)}$  by the first and second user, respectively, when the TSD-

MIMO is considered. This is shown in Figure 2.34, where the solid line corresponds to the frontier lines. One can observe that indeed - the learned solution is that the regret matching algorithms converges to the point  $(\alpha_1^{(1)}, \alpha_2^{(2)})$ . In other words, both users shall transmit with the maximum power all the times using the strategies  $\alpha_1^{(1)}$  and  $\alpha_2^{(2)}$ , respectively.

In this figure additional frontier lines of the possible rate regions when the users choose one (not optimal) of the possible strategies are presented, i.e. the dotted line represents the frontier line when both users choose the strategy  $\alpha_i^{(3)}$  all the time. This line corresponds to the interference limited SISO scenario in [62]. The dashed lines show the achievable rate regions boundaries, when one user plays the strategy  $\alpha^{(3)}$  all the time, while the other transmit the whole power through one antenna.

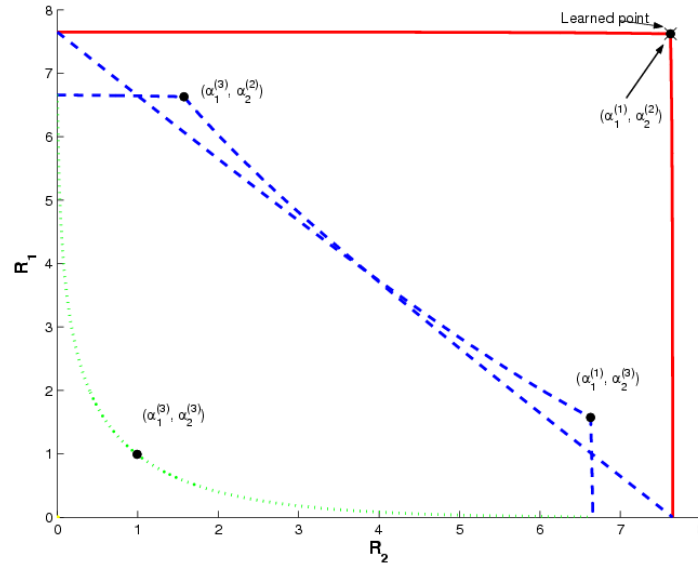


Figure 2.34 – Crystallized rate regions in the interference limited case with marked learned point

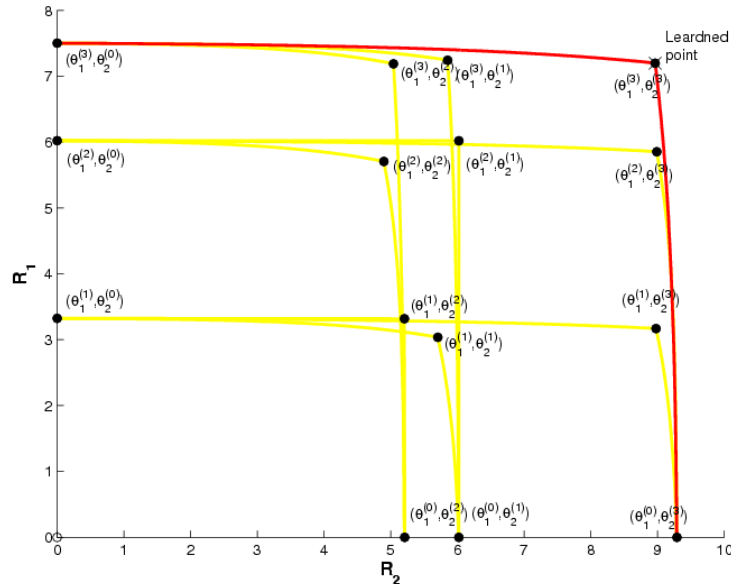


Figure 2.35 – Crystallized rate regions in the noise limited case with marked learned point

In Figure 2.35 the achievable rate region for the noise limited scenario is presented, i.e. both users observe the interferences coming from the neighboring cells, but the power of the interferences is significantly smaller than the power of the useful signal. In this figure all 15 characteristic points have been presented, as well as the achievable rate region boundaries (dotted lines) when both players select

one specific strategy and use them all the time. As expected, the learned point, i.e. the point at the Time-Sharing line that is indicated by the regret-matching algorithm, corresponds to selecting the strategy  $\alpha^{(3)}$  by both users all the time.

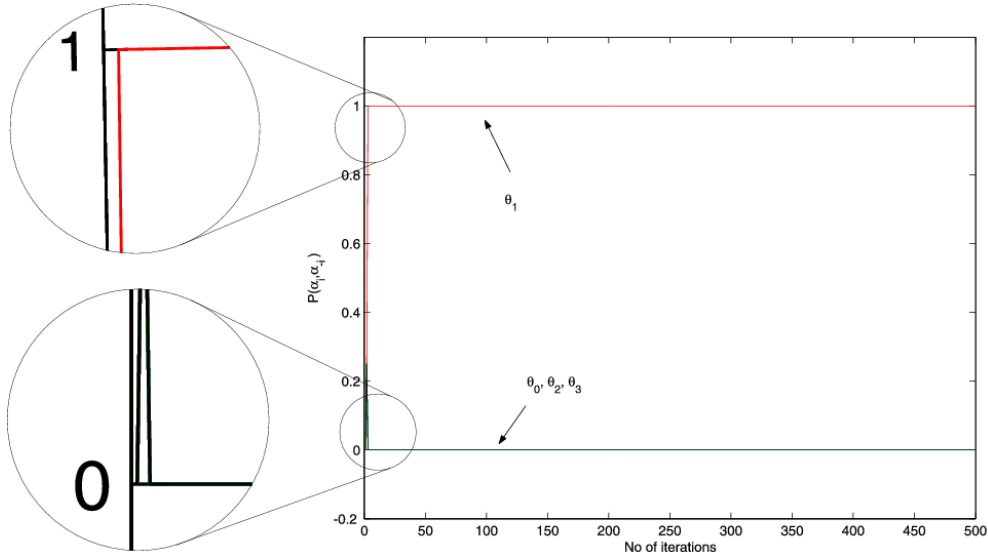


Figure 2.36 – The convergence of the rate-matching algorithms - user 1

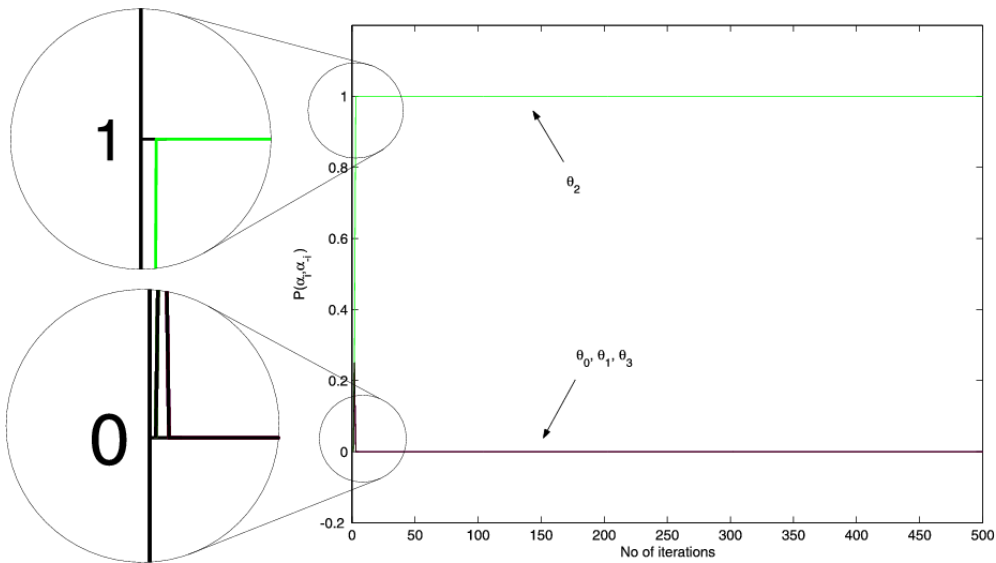


Figure 2.37 – The convergence of the rate-matching algorithms - user 2

Moreover, in Figure 2.36 and Figure 2.37 the convergence of the rate matching algorithm in terms of number of iterations in the interference limited TSD-MIMO scenario has been presented. The same channel matrices have been used as in (2.66). One can notice that the algorithm have found the optimal solution extremely fast. Indeed, after around 10 iterations the learned point fits ideally to the optimum solution and remains unchanged.

Similar conclusions can be drawn for the precoded MIMO case. The rate region obtained for the SVD-MIMO case for a particular channel realization is presented in Figure 2.38. The interpretation of any point in the SVD rate region is as follows - both Base Stations use Singular Value Decomposition in order to linearize the channel and the total transmit power is within the range  $<0, P_{max}>$ . Channel transfer matrices have been arbitrarily selected as follows:

$$\begin{aligned}
 \mathbf{H}_{11} &= \begin{pmatrix} 0.9 & 0.00099 \\ 0.00085 & 0.96 \end{pmatrix} & \mathbf{H}_{22} &= \begin{pmatrix} 0.96 & 0.000096 \\ 0.0000998 & 0.902 \end{pmatrix} \\
 \mathbf{H}_{12} &= \begin{pmatrix} 0.000094 & 0.00009 \\ 0.992 & 0.9992 \end{pmatrix} & \mathbf{H}_{21} &= \begin{pmatrix} 0.999 & 0.9904 \\ 0.0005 & 0.0001 \end{pmatrix}
 \end{aligned} \tag{2.67}$$

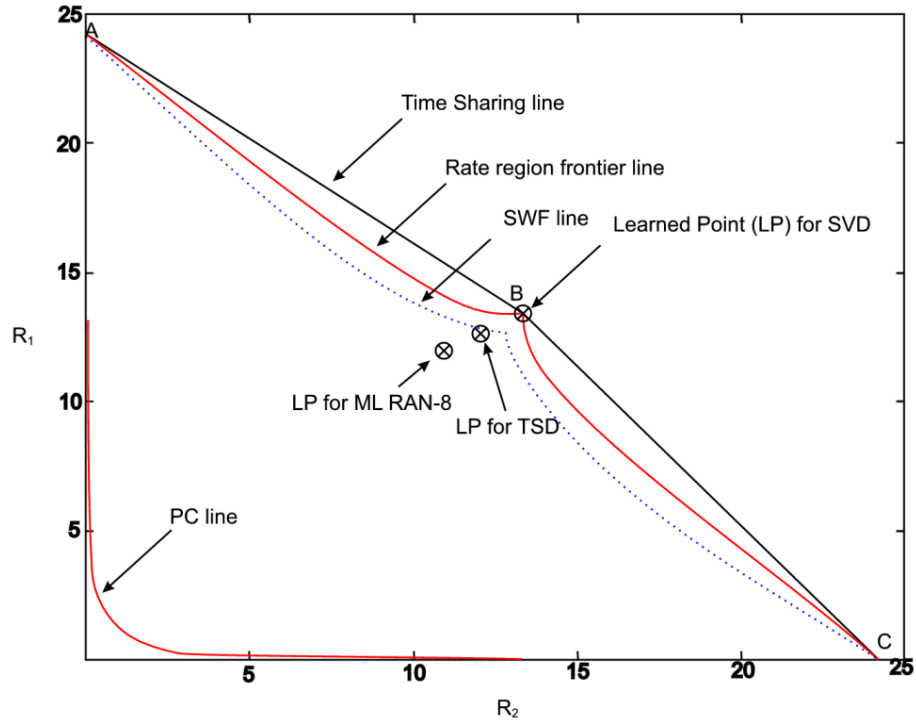


Figure 2.38 – SVD-MIMO rate region - channel case 1

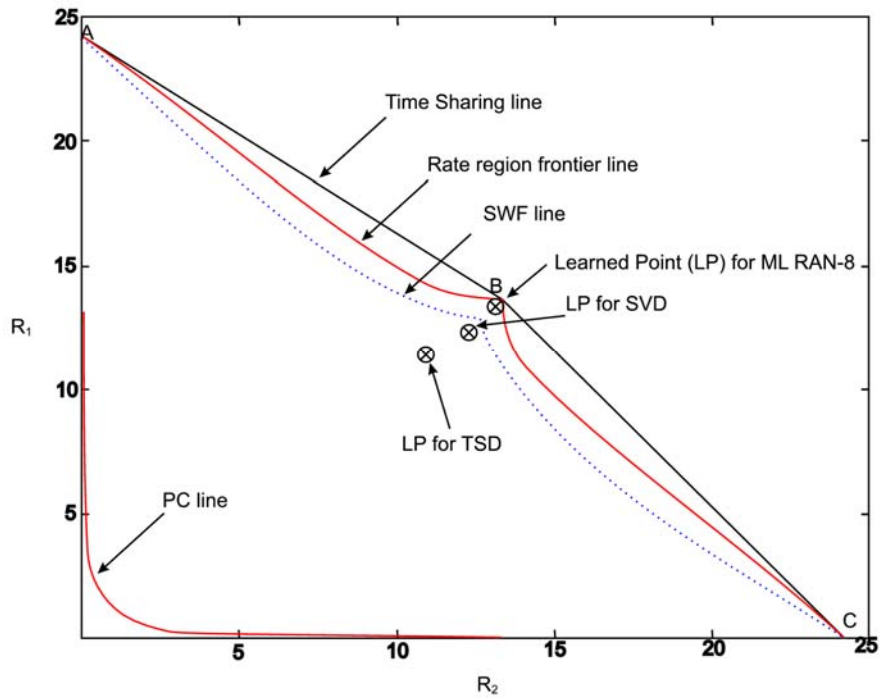


Figure 2.39 – SVD-MIMO rate region - channel case 2

This means that both users have good channel characteristic within their cells (no significant interference exist between the first transmit and second receive antenna as well as between second

Reference DR9.3

transmit and first receive antenna). However, first user causes strong interference on the second receive antenna of the second user, and the second users disturb significantly the signal received by the first user in his first antenna.

Analyzing the presented results one can observe that the obtained rate region is concave thus the Time-Sharing approach can provide better performance than continuous Power Control scheme (i.e. when both users transmit all the time and regulate the interference level by the means of the value of transmit power). The potential Time-Sharing Lines are presented in this figure. For the comparison purposes the line obtained for Spatial Water-Filling MIMO case has been plotted in Figure 2.38 (dotted line). The line has been derived in a following way: starting from point A (where user 2 does not transmit and user 1 uses the maximum power with the SWF technique), user 2 increase the total transmit power up to the maximum value; when both users transmit with the maximum total power point B is reached; finally user 1 decrease the transmit power from the maximum value to zero reaching the point C. Moreover the Power Control line has been presented - it is the case when both users selects wrong strategy achieving extremely low rates. In is worth mentioning that the Learned Points obtained for various MIMO techniques have been marked in the described figure. One can observe that for the optimal case (SVD technique) algorithm converges to the point B. Slightly worse results have been obtained for TSD-MIMO, where no specific precoding has been performed. The worse results, but still in the vicinity of the point B, are for the random beamforming technique when 8 various precoders have been stored in a codebook and Maximum Likelihood method is used at the receiver.

The same simulation have been carried out for other channel, when significant interference exist between all transmit and all receive antennas between  $i$ -th user and  $i$ -th BS. The channel transfer matrices have been selected as below:

$$\begin{aligned} \mathbf{H}_{11} &= \begin{pmatrix} 0.4 & 0.49 \\ 0.52 & 0.46 \end{pmatrix} & \mathbf{H}_{22} &= \begin{pmatrix} 0.45 & 0.49 \\ 0.47 & 0.45 \end{pmatrix} \\ \mathbf{H}_{12} &= \begin{pmatrix} 0.000094 & 0.00009 \\ 0.992 & 0.9992 \end{pmatrix} & \mathbf{H}_{21} &= \begin{pmatrix} 0.999 & 0.9904 \\ 0.0005 & 0.0001 \end{pmatrix} \end{aligned} \quad (2.68)$$

The obtained rate region, potential Time-Sharing lines, Spatial Water-Filling line and exemplary Power Control Line, as well as some Learned Points (for the same MIMO techniques as described in the previous case) have been presented in Figure 2.39. One can observe, that in such a case one of the Learned Points is close to the optimal one (Point B). However, this point is reached for random beamforming technique with Maximum-Likelihood method used at the receiver.

Specific rate values obtained for the considered MIMO implementations are given in Table 2.12 and Table 2.13 for channel definitions (2.67) and (2.68) respectively. The results obtained for all RAN-8 scenarios (i.e. ZF, MMSE and ML and when the codebook size is equal to 8) have been averaged over 1000 randomly generated codebooks. One can observe that for all cases, when the Regret Matching algorithm has been applied, the obtained rates are similar to each others and relatively close to the optimal solution. Only for the ZF/MMSE-MIMO cases when the random beamforming approach has been used the averaged results are significantly worse because of high dependency of algorithms efficiency on the actual set of transmit beamformers. If the randomly generated set of beamformers is well-defined (i.e. at least one precoder matches the actual channel conditions for the  $i$ -th user) the achieved rate is also close to the optimal point (see the maximum obtained values for one particular channel realization).

The efficiency of the random beamforming technique strongly depends on the number of precoders. However, the higher number of precoders the higher the complexity of the algorithm. Thus, in order to present the relation between the random beamforming technique efficiency and the codebook size the computer simulation have been carried out for the particular channel realization defined as above. The results, presented in Figure 2.40, have been obtained for 1000 various codebook realizations for each codebook size. One can observe that the obtained rate for both users increase logarithmically as the number of precoders increase.

Table 2.12 – Achieved rates for channel definition (2.67)

MIMO scheme	User 1	User2
TSD	13.17	12.77
SVD	13.17	13.28
ZF-RAN-8	5.12 (max. 12.24)	3.62 (max. 13.00)
MMSE-RAN-8	5.08 (max. 12.38)	3.64 (max. 13.13)
ML-RAN-8	12.51	11.81
ZF-LTE	12.87	12.98
MMSE-LTE	12.87	12.98
ML-LTE	12.90	13.00
ZF-PU <sup>2</sup> RC-8	12.87	12.98
MMSE-PU <sup>2</sup> RC-8	12.87	12.98
ML-PU <sup>2</sup> RC-8	12.90	13.00

Table 2.13 – Achieved rates for channel definition (2.68)

MIMO scheme	User 1	User2
TSD	11.40	11.23
SVD	12.23	12.11
ZF-RAN-8	4.25 (max. 11.25)	4.08 (max. 10.25)
MMSE-RAN-8	3.25 (max. 10.9)	4.07 (max. 11.05)
ML-RAN-8	12.08	11.95
ZF-LTE	12.13	11.96
MMSE-LTE	12.13	11.96
ML-LTE	12.89	12.93
ZF-PU <sup>2</sup> RC-8	12.13	11.96
MMSE-PU <sup>2</sup> RC-8	12.13	11.96
ML-PU <sup>2</sup> RC-8	12.89	12.93



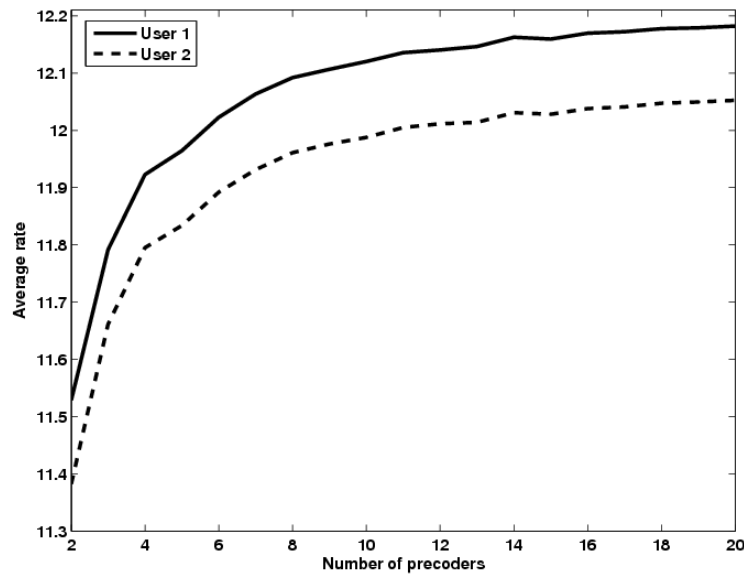


Figure 2.40 – Achieved average rate versus codebook size

## 2.7 Conclusions

This section has addressed the activities related to RRM and JRRM in heterogeneous networks within the context of WPR9. The following conclusions have been obtained:

- A new and simple model based on mobility, capable to combine multi-service traffic and heterogeneous networks capacity to evaluate VHOs and JRRM performance, is proposed and described. As output, this model has a set of VHO and JRRM performance metrics, these indicators being evaluated for different input scenarios variations. Computational results show that HBN is the RAT that produces more impact on JRRM, compared with other RATs, by handling/releasing more traffic, generating more signalling related with JRRM functionalities (i.e., triggering and managing VHOs).
- The CVRRM model aims to minimise the effect of QoS degradation inherent to radio interface, by evaluating globally the impact of heterogeneous network environment into the virtualisation approach. Simulation results have revealed that the introduction of VRRC allows supporting the minimum bandwidth requirement in a wireless cluster, composed by several physical base stations from different RATs, providing service over a given coverage area. VRRC takes advantage of the set of shared resources available in the entire common cluster optimising their utilization in order to maintain the contracted capacity. Although VRRC algorithm may give some support to guaranteed VNet, if the difference between the required and minimum data rate increases, the compensation could be insufficient, being this more critical for the more data rate demanding services. Concerning the number of VBSs composing the VNet and the used strategies for its instantiation, in the physical infrastructure, results indicate that VNet performance depends not only on the quantity of VBSs defined for its implementation, but also on the strategies used to instantiate the VBS in the physical infrastructure.
- This section has also addressed the energy efficiency awareness in RRM. To evaluate techniques and systems perform related with energy efficiency, new metrics were presented at radio interface, when energy consumption is an issue. This is clearly a future field to be explored at different levels such radio link, systems base band and networks. The first approach at JRRM level shows the potential energy gains that are possible to achieved at radio link. First results for voice and WWW services, presents energy efficiency gains at RF

level of 13 and 29% respectively. These gains are achieved by JRRM policies that moves users among RATs (using VHOs), in this case from UMTS R99 to R5.

- The problem of spectrum allocation for OFDMA networks focusing both on the single- and multi-cell scenarios has been studied. The research on single-cell scenarios has investigated several different algorithms elaborating trade-offs between different objective functions and quality-of-service indicators. The research on multi-cell scenarios has addressed both the problem of distributed resource allocation and coordinated resource allocation. From these studies the following conclusions can be extracted:
  - With respect to the single cell scenario, the joint comparison between Fairness/Rate Adaptive RRA and Utility-Based PSC for NRT Services have been studied aiming at investigating the trade-off between resource efficiency and fairness among users. Comparing the two approaches by means of simulation results, one can see clearly the direct relationship between Sum Rate Maximization (SRM) and Maximum Rate (MR) techniques, and also between Max-Min Rate (MMR) and Max-Min Fairness (MMF). Furthermore, possible trade-offs were presented, such as Sum Rate Maximization with Proportional Rate Constraints (SRM-P) and Fairness-Based Sum Rate Maximization with Proportional Rate Constraints (FSRM-P) in the case of rate adaptive RRA, and Proportional Fairness (AP) and Adaptive Throughput-Based Fairness (ATF) in the case of utility-based PSC. It is possible to achieve an efficient trade-off between resource efficiency and fairness using any of the two RRM approaches, and the algorithms that achieve this trade-off are the ones that present the highest user satisfaction. Furthermore, both the adaptive utility-based ATF and the fairness/rate adaptive FSRM-P algorithms provide the flexibility to work in any operation point in the efficiency-fairness plane. However, using less computational resources, utility-based PSC algorithms have the advantage of showing approximately the same performance in terms of fairness and system capacity compared with their rate adaptive counterparts and also good performance in terms of user satisfaction. Finally, an update of the mathematical formulation of a multi-carrier PSC using utility functions based on delay for RT services was presented. This update presents a more accurate mathematical definition of the HOL delay needed for the correct design of the proposed RRA framework suitable for RT services.
  - With respect to the Multi-cell scenario assuming a distributed resource allocation, the problem of resource allocation and power adaptation in the downlink of a multi-cell multi-carrier system has been investigated, with a frequency reuse distance equal to one. Allowing full frequency reuse can potentially bring about large gains in terms of spectral efficiency. However, multiple access interference (MAI) generated in adjacent cells that use the same radio resources adversely affects system performance. The effect of MAI is dealt by introducing a loose cross layered architecture that integrates a packet scheduler with an adaptive resource allocator. The resource allocation algorithm can strive for selfish spectral efficiency, while long term fairness is guaranteed by the packet scheduler according to any desired policy (max-min fairness, weighted output fairness, proportional fairness, etc.). Each cell performs its resource management in a distributed way without any central controller; an adaptive strategy can dynamically reduce the load of the cells in the system so that the iterative procedure always converges to a stable allocation, regardless of the interference. Simulation results show that the proposed architecture is able to guarantee both high spectral efficiency and throughput fairness among flows.
  - Also in a multi-cell scenario the idea of coordinated resource allocation has been proposed to minimize the impact of MAI on the system performance. Two algorithms, derived using the utility theory, have been considered, representing the distributed approach and the static clustering centralized approach, respectively. The proposed methods have been compared with other scheduling algorithms without any coordination or with fractional frequency reuse and significant gains in average cell

throughput, cell-edge throughput and fairness have been observed when applying the coordination. However, the performance improvement in terms of average cell throughput when comparing the coordinated algorithm with the SUS is around 20% at most and, taking into account the additional complexity of coordination, it is hard to decide upon whether the introduction of coordination is beneficial. Further extensive studies, including the realistic limited feedback scenario, are necessary to provide more information on the pros and cons of coordination.

- The concept of crystallized rate regions, introduced first in the context of finding the capacity of the SISO interference channel, has been applied to the MIMO and OFDM interference channels. The use of the correlated equilibrium instead of the well-known Nash equilibrium has been proposed and verified adequate for the considered 2-user MIMO/OFDM transmission scenario. Moreover, a new VCG auction utility function and the modified regret-matching algorithm have been derived for the generalized MIMO case. The correctness of application of the proposed crystallized rates region approach to the general MIMO and OFDM case has been verified in simulations of the 2-user 2-BS scenarios. Furthermore, obtained results show that the proposed regret-matching algorithm provides rapid convergence to the correlated equilibrium.

### 3 ADVANCED SPECTRUM MANAGEMENT

#### 3.1 Introduction

This chapter presents the activities that have been carried out inside WPR9 in the framework of Advanced Spectrum Management (ASM). They mainly contribute to one of the current research trends in the spectrum management which are the so-called Dynamic Spectrum Access Networks (DSANs), in which unlicensed radios, denoted as Secondary Users (SUs) are allowed to operate in licensed bands provided that no harmful interference is caused to the licensees, denoted as Primary Users (PU). One of the key enabling technologies for DSAN development is Cognitive Radio (CR), which has been claimed to be an adequate solution to the existing conflicts between spectrum demand growth and spectrum underutilization. This term Cognitive Radio, originally coined by J. Mitola III in [114], envisages a radio able to sense and be aware of its operational environment so that it can dynamically and autonomously adjust its radio operating parameters accordingly to adapt to the different situations.

Based on the above, this chapter is organised mainly in two main activities. The first one is devoted to perform a spectrum measurement campaign in order to identify primary user temporal and spatial usage patterns in specific environments for different ranges of frequencies. The outcome of this campaign can be an interesting input for the application and development of Dynamic Spectrum Access (DSA) to handle the access of secondary users to the available spectrum holes left by primary users. First results of the measurement campaign were presented in previous deliverable DR9.2 [5]. Section 3.2 will then present the new results, characterising the spatial correlation properties of spectrum occupancy measurements carried out in different positions. Also inside this section some spectrum sensing studies are presented, to determine whether a frequency band is actually being occupied by a primary signal or by noise. Measurements obtained with a Universal Software Radio Peripheral (USRP) and GNU Radio architecture are used to evaluate energy spectrum sensing based on real-world primary signals.

The second activity, presented in section 3.3, addresses the DSA problem from a both theoretical and empirical perspective making use of the previously explained measurements. In particular two elements are addressed in this section. The first one is a joint learning detection framework that makes use of a learning algorithm to alleviate the absence of information on the noise level present in the sensed samples. A second study addresses the opportunistic spectrum access to select the channel to be used by a secondary user based on the Multi-Armed Bandit paradigm considering a scenario with sensing errors.

#### 3.2 Measurements of Spectrum Availability

##### 3.2.1 Introduction

The measurement of real network activities constitutes an important step towards a realistic understanding of dynamic spectrum use and hence towards the practical deployment of the future Cognitive Radio (CR) technology. One important use of spectrum measurements is not only to convince regulatory bodies and policy makers on the necessity of new spectrum access policies but also to support them in taking actions to enhance the use of the currently underutilised spectral resources. Spectrum measurements are also useful in detecting which bands are subject to low utilisation levels, thus assessing and characterising the availability of unoccupied spectral resources in terms of frequency, time, and space. This information can be very helpful to the research community in order to identify the most suitable and interesting bands for the future deployment of the CR technology. Besides this, the empirical data captured in spectrum measurements can find many other interesting practical applications. One example is the evaluation and validation of existing and novel Dynamic Spectrum Access (DSA) techniques with real-world data. Another application is the development of realistic spectrum usage models based on empirical data, which could be interesting not only for theoretical analyses of DSA techniques but also for the development of innovative and accurate simulation tools. The measurement of real network activities therefore constitutes an

important step towards a realistic understanding of dynamic spectrum utilisation and hence towards the deployment of future CR networks.

Several measurement campaigns covering both wide frequency ranges [82]–[87] as well as some specific licensed bands [88]–[92] have been performed in diverse locations and scenarios in order to determine the degree to which allocated spectrum bands are occupied in real wireless communication systems. In the context of WPR9, a broadband spectrum measurement campaign has been carried out in the frequency range from 75 MHz to 7075 MHz in a urban environment in the city of Barcelona, Spain. The measurement setup as well as the methodological aspects considered in the measurement campaign were summarised in [5] and are exhaustively detailed in [93]. The spectrum occupancy results derived from this measurement campaign were presented in [94]–[99] and summarised in [5] as well. The measurement campaign quantified the spectrum occupancy of various allocated bands and analysed qualitatively the impact of considering various measurement locations and scenarios, including not only high points (as usually considered in previous works in the literature) but also indoor environments as well as outdoor locations at the ground level (in open areas and between buildings), on the spectral activity perceived by the nodes of a CR network. The variety of considered measurement scenarios provided a broad view and understanding of dynamic spectrum use under different realistic scenarios of practical interest. The impact of particular locations and scenarios was evaluated in a qualitatively manner, as discussed in [5]. Such study is extended here by analysing quantitatively the impact of considering various locations and scenarios on the perceived spectrum occupancy. This section explores various methods and procedures to analyse and characterise the impact of the user location on the spectrum perception. Such study serves as a good example of the potential applications that the empirical data captured in spectrum measurement campaigns can find in practice, while at the same time it illustrates various procedures for modelling spectrum occupancy.

### 3.2.2 *Modelling spatial spectrum occupancy*

The main objective of this section is to analyse the impact of a CR node's location on the perceived spectrum occupancy and explore various procedures to statistically characterise the spatial spectrum occupancy, which constitutes the basis for the realisation of spectrum occupancy models and, as such, an important point to assist the study and the development of CR. To this end, the captured empirical data were processed in order to compute various correlation parameters, which were further analysed with the aim of determining the correlation properties of spectrum occupancy.

The interest of analysing the spatial correlation of the perceived spectrum occupancy relies on its impact on the behaviour and performance of a network of CR nodes. In order to avoid harmful interference to licensed primary users, CR nodes must reliably detect the presence of primary signals. This function is referred to as *spectrum sensing* in the context of CR. It has been demonstrated that the performance of spectrum sensing can be improved by means of cooperation among CR nodes, thus leading to the so-called *cooperative spectrum sensing*, where the sensing information and/or results from various CR nodes are exchanged or gathered at a central entity and processed in order to reliably determine the presence/absence of a primary signal. Cooperative detection schemes enable the mitigation of the degrading effects of multi-path fading and shadowing. In the case of non-cooperative sensing, the sensitivity of a single secondary detector must be able to compensate not only for the path loss with respect to the primary transmitter but also for deep fades caused by other major sources of degradation such as multipath (fast) fading and shadow (slow) fading, which results in demanding sensitivity requirements for CR nodes that may be difficult to achieve in real hardware implementations [100]. These requirements, however, can be relaxed if secondary users cooperate among them by exchanging sensing information, which can help to mitigate the effects of multi-path fading and shadowing [101][102]. The degrading effects of multi-path fading can be overcome by means of cooperation because the multi-path fast fading process is correlated over distances in the order of the wavelength, which in practice means that fast fading at different radios is essentially uncorrelated. Thus, the presence of multiple radios can help to reduce the effects of severe multi-path fading at a single radio since they provide multiple independent realisations of related random variables. With multiple realisations, the probability that all users see a deep fading is lowered. As a result, the sensitivity requirements of individual CR nodes can be relaxed while at the same time the

probability of detection increases. On the other hand, shadowing can exhibit high correlation among different CR nodes if they are blocked by the same obstacle (e.g., building, mountain, etc.). In this case, cooperative gains in an environment where shadowing is correlated is limited by the cooperation footprint (i.e., the area in which users cooperate [102]) since the observation of nearby CR nodes is more likely to be correlated. In essence, a few independent users are more robust to primary signal misdetections than many correlated users [101][102]. Due to the necessity of cooperative spectrum sensing schemes in order to achieve the required sensitivity levels, and the importance of correlation among the spectral occupancy observations of cooperating CR nodes, the analysis and characterisation of the spectral occupancy's spatial correlation becomes an important and interesting topic, thus motivating the study performed in this section.

In order to analyse the spatial correlation of spectrum occupancy, the empirical data captured in the measurement campaign was employed. The measurement setup as well as the methodological aspects considered in the measurement campaign were summarised in [5] and are exhaustively detailed in [93]. The set of empirical data was extended by performing additional measurements at some complementary locations as illustrated in Figure 3.1 and Figure 3.2. As it can be appreciated in Figure 3.2, the set of additional measurement locations comprised a regular grid of 5×5 locations where each pair of consecutive points was 15 meters apart. Nevertheless, the geometry of the measurement site did not allow for the measurement of each point of such grid because two points (precisely the first and the last point of the fifth row) were not reachable by the measurement equipment. Instead, two other points placed at a much longer distance with respect to the step size were analysed in order to have a wider range of distances for the evaluation of spatial correlations. Differently from other spectrum measurement campaigns [103][104], in which two identical equipments were used simultaneously in order to determine the correlation between spectral occupation in different points, only one measurement equipment was available at the moment of performing the measurements. As a result, each point in Figure 3.2 was measured at a different time instant.

The spatial correlation study was conducted in the 1800–1880 MHz and 1880–2290 MHz band, which are mainly allocated to the Digital Cellular System (DCS) and Universal Mobile Telecommunications System (UMTS). There are several reasons that support our decision to analyse these spectrum bands. The main objective is to analyse spectrum occupancy and its correlation. In order to obtain reliable estimates of the spectral occupancy and its correlation, it is necessary to capture a sufficiently high number of primary signal samples. If channels with low occupancy levels were selected, most of the captured samples would correspond to noise, meaning that the measurement sessions would then need to be extended to long measurement periods in order to capture a high number of signal samples. By selecting channels with high occupancy levels, the measurement period required to capture a sufficiently high number of primary signal samples then reduces to feasible values. Although some parts of the selected bands remain unused, the channels being actually used in such bands are, in general, subject to high occupancy levels. According to this criterion, it would also be possible to select TV bands, since the channels employed in the TV bands are used virtually 100% of the time. However, in this case it is important to note that TV transmitters are normally intended to provide large coverage areas and, as a result, spectrum occupancy is expected to be correlated over large areas, meaning that the measured locations should be separated by longer distances in order to appreciate different correlation levels. Mobile communication systems, on the other hand, are intended for much lower coverage areas and, as result, a shorter separation among the measured points is required to observe correlation variations over space. By selecting mobile communication bands, it is possible to carry out the proposed correlation study within more practical geographical regions.

In order to analyse the spatial correlation of two measurement locations as a function of the distance between them, all possible combinations of pairs of locations having (approximately) the same distance in the considered grid were grouped. Such pairs were grouped using a binning procedure such that two pairs of measurement locations  $x_i$  and  $x_j$  are considered to belong to the same set if  $h-\Delta \leq \|x_i - x_j\| \leq h+\Delta$ , where  $h$  denotes the distance corresponding to the considered set,  $\|x_i - x_j\|$  is the actual distance between measurement locations  $x_i$  and  $x_j$ , and  $\Delta$  is an appropriate margin included in order to group points separated by a similar, but not exactly the same, distance. This procedure was configured in order to guarantee a significant number of elements in each vector of location pairs. Therefore, for



each set corresponding to a distance  $h$ , it is possible to create two vectors  $\mathbf{U}(h)$  and  $\mathbf{V}(h)$ , which contain the average Power Spectral Density (PSD), measured by the spectrum analyser, for all the pairs of locations associated to the length  $h$ .

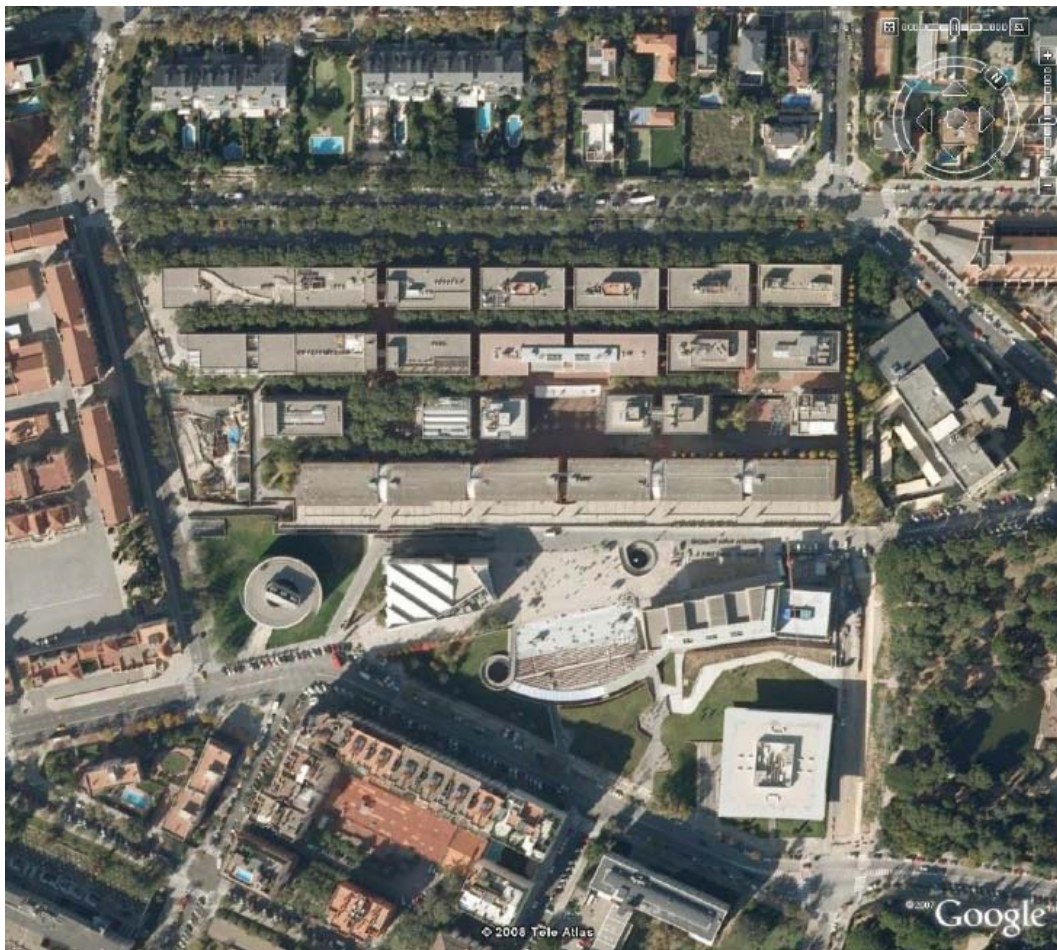


Figure 3.1 – Aerial view of UPC's Campus Nord in urban Barcelona, Spain.



Figure 3.2 – Set of additional measurement locations within UPC's Campus Nord in urban Barcelona, Spain.

In order to quantitatively analyse the spatial correlation of spectrum occupancy, various correlation metrics have been analysed in the context of this work. The first evaluated metric is the cross-correlation, which is computed based on the empirical measurements as:

$$R(\mathbf{U}, \mathbf{V}) = \frac{1}{N_s} \sum_{t=1}^{N_s} U_t \cdot V_t \quad (3.1)$$

where  $N_s$  is the number of samples,  $\mathbf{U}$  and  $\mathbf{V}$  are the vectors to be compared, and  $U_t$  and  $V_t$  are their components, respectively, i.e.  $\mathbf{U} = \{U_1, U_2, \dots, U_{N_s}\}$  and  $\mathbf{V} = \{V_1, V_2, \dots, V_{N_s}\}$ . In our case  $\mathbf{U}$  and  $\mathbf{V}$  correspond to the vectors previously defined, containing the average PSD of the pairs of points located at a certain distance  $h$ . The second evaluated metric is the covariance, which is obtained from the cross-correlation by subtracting from each vector its mean (average of the various mean powers):

$$\text{cov}(\mathbf{U}, \mathbf{V}) = \frac{1}{N_s} \sum_{t=1}^{N_s} (U_t - \bar{U}) \cdot (V_t - \bar{V}) \quad (3.2)$$

where  $\bar{U}$  and  $\bar{V}$  denote the average value of vectors  $\mathbf{U}$  and  $\mathbf{V}$ , respectively. The covariance is often extended by normalisation, thus leading to the normalised covariance, which is defined as:

$$\rho(\mathbf{U}, \mathbf{V}) = \frac{1}{N_s} \sum_{t=1}^{N_s} \frac{U_t - \bar{U}}{\sigma_U} \cdot \frac{V_t - \bar{V}}{\sigma_V} \quad (3.3)$$

where  $\sigma_U$  and  $\sigma_V$  are the standard deviation of vectors  $\mathbf{U}$  and  $\mathbf{V}$ , respectively. Finally, the last evaluated metric is the empirical semivariance, which is computed as:

$$\gamma(\mathbf{U}, \mathbf{V}) = \frac{1}{2|N(h)|} \sum_{t=1}^{N_s} (U_t - V_t)^2 \quad (3.4)$$

where  $|N(h)|$  denotes the cardinality of vector  $\mathbf{U}$  (or equivalently  $\mathbf{V}$ ). The representation of the semivariance as a function of the distance is known as semivariogram.

Figure 3.3 to Figure 3.6 show, respectively, the cross-correlation, covariance, normalised covariance and semivariance among the considered measurement locations as a function of their distance for the measurements performed in the DCS band, while Figure 3.7 to Figure 3.10 show the same metrics for the measurements performed in the UMTS band. In theory, as the distance between two considered locations increases, the spectrum occupancy observations of two CR nodes should be more unrelated and, as a result, their correlation should decrease. This means that the cross-correlation, covariance and normalised covariance are expected to decrease as the distance increases, while the semivariance is expected to increase with the distance. However, the results shown in Figure 3.3 to Figure 3.10 do not show a well-defined trend according to such expectations, but a rather random behaviour. This might be due to a few pairs of points having an abnormal behaviour, which might occur, for example, if during the measurements the equipments were affected by some external noise sources altering the measured PSD values. To verify this point, the individual values of every computed metric for every pair of locations were explored and compared to the resulting values observed in the obtained results. Since no pair of points was observed to lay far away from the average value, it was concluded that the apparently random behaviour of the computed metrics was not due to the presence of external noise sources interfering with the experiment, but rather to the fact that the underlying correlation process cannot be expressed as a function of the distance separating two given points. The more likely hypothesis explaining the random behaviour observed as a function of the distance is that different pairs of locations separated by the same distance may observe significantly dissimilar primary signals.



Effectively, the primary power level observed at each measurement location is the result of the constructive/destructive combination of all the primary signal components received through different propagation paths, which depend on the particular measured location and its surrounding propagation environment (buildings, walls, ground elevations, etc.). Therefore, different pairs of points separated by the same distance may observe dissimilar primary power levels depending on the particular location of each point and its surrounding environment. This can explain the random behaviour observed for the analysed correlation metrics as a function of the distance.

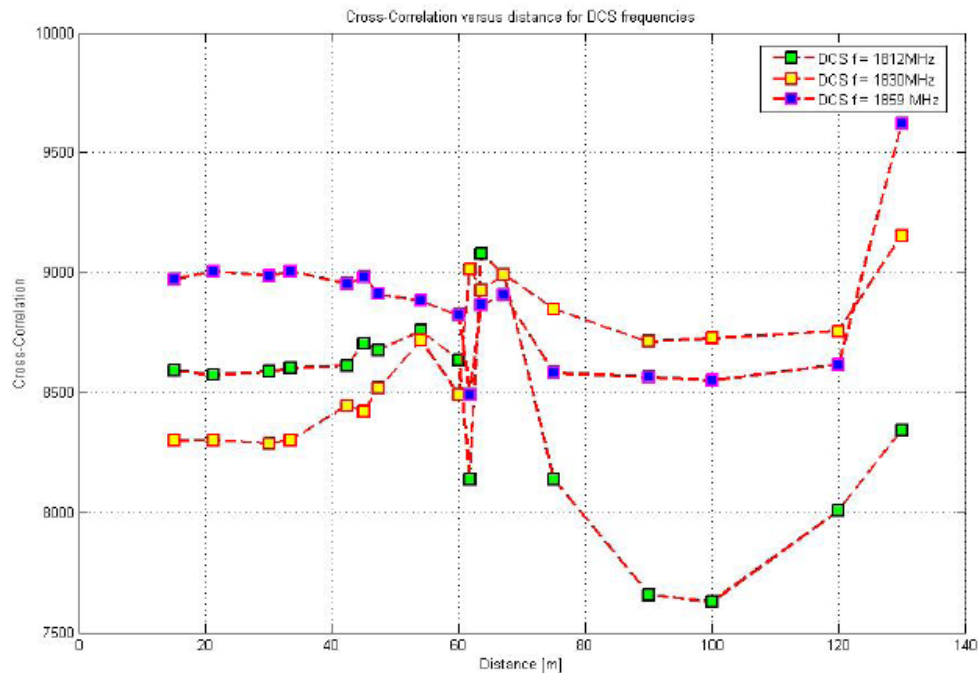


Figure 3.3 – Cross-correlation vs. distance for DCS.

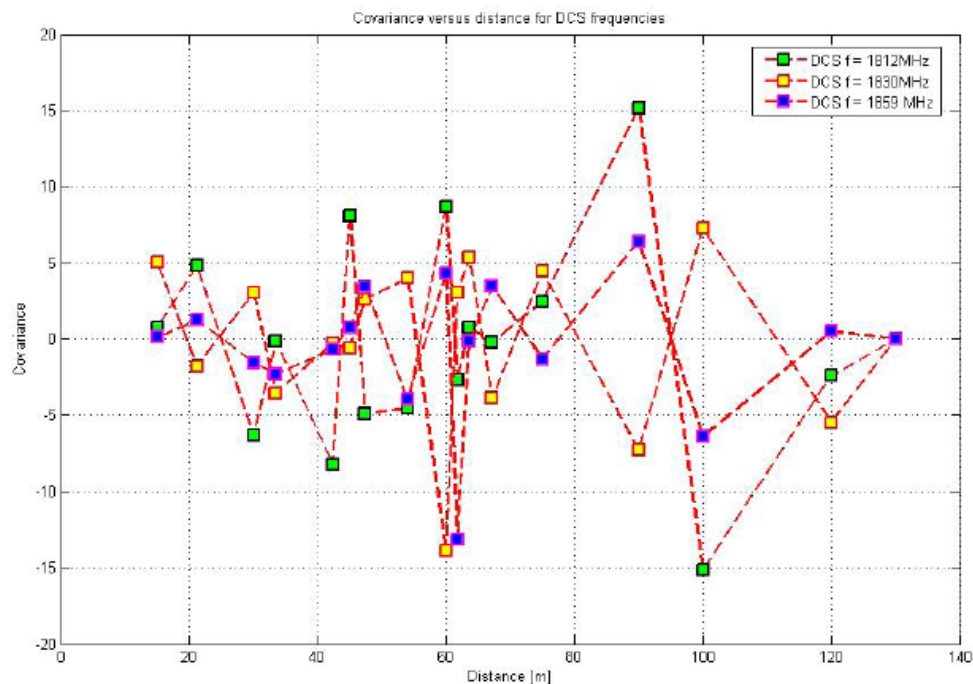


Figure 3.4 – Covariance vs. distance for DCS.

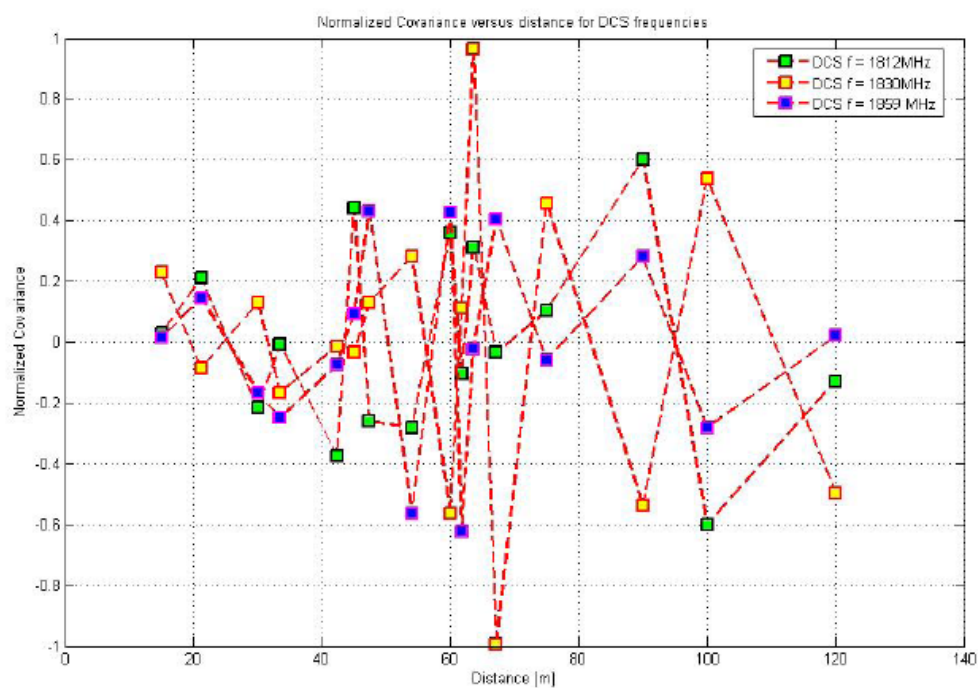


Figure 3.5 – Normalised covariance vs. distance for DCS.

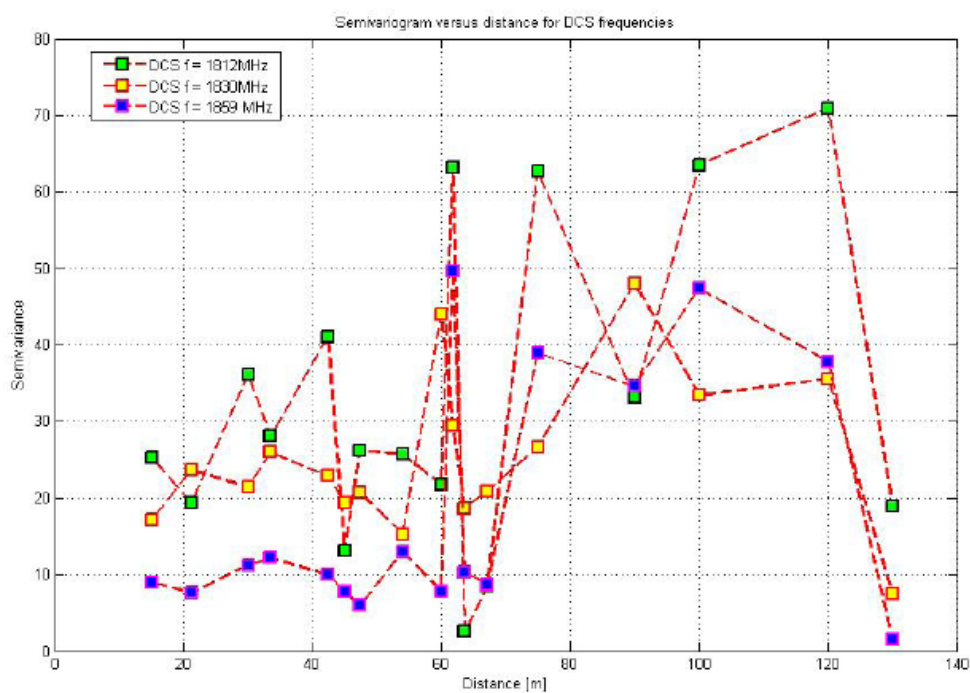


Figure 3.6 – Semivariance vs. distance for DCS.

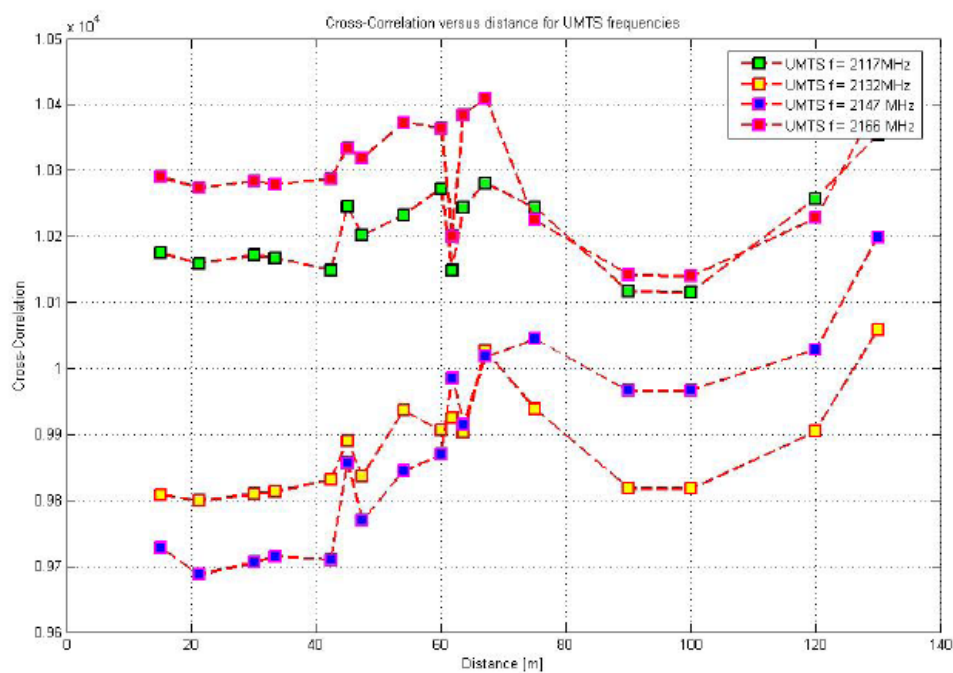


Figure 3.7 – Cross-correlation vs. distance for UMTS.

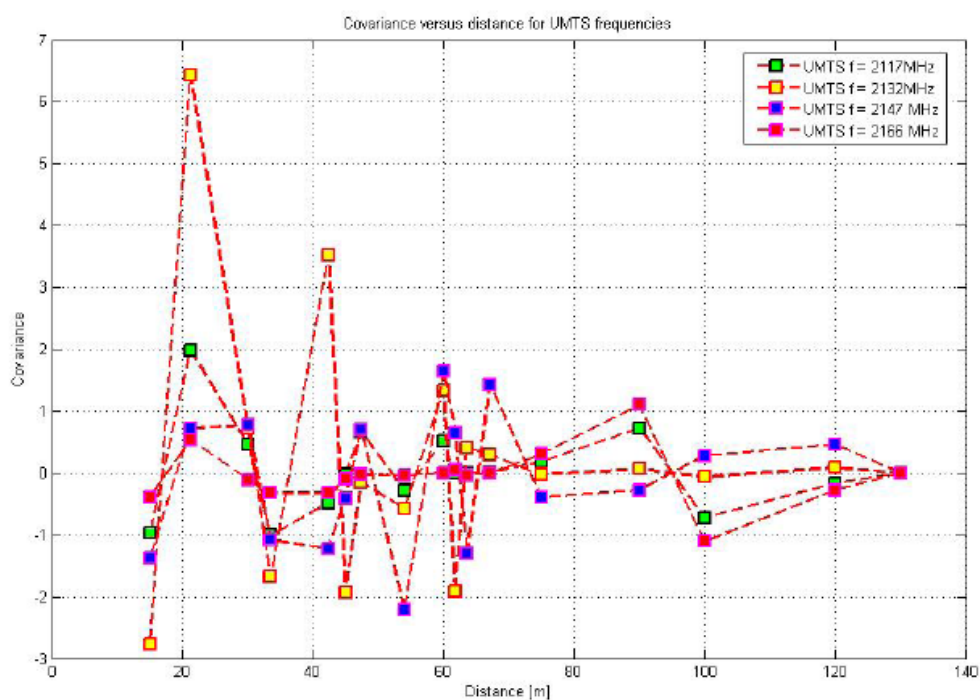


Figure 3.8 – Covariance vs. distance for UMTS.

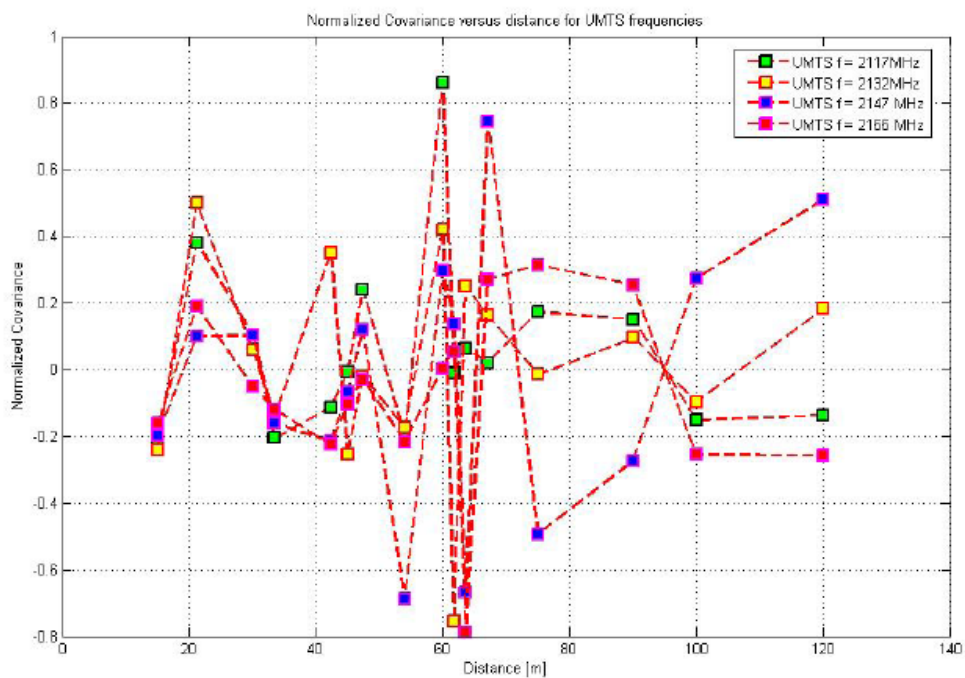


Figure 3.9 – Normalised covariance vs. distance for UMTS.

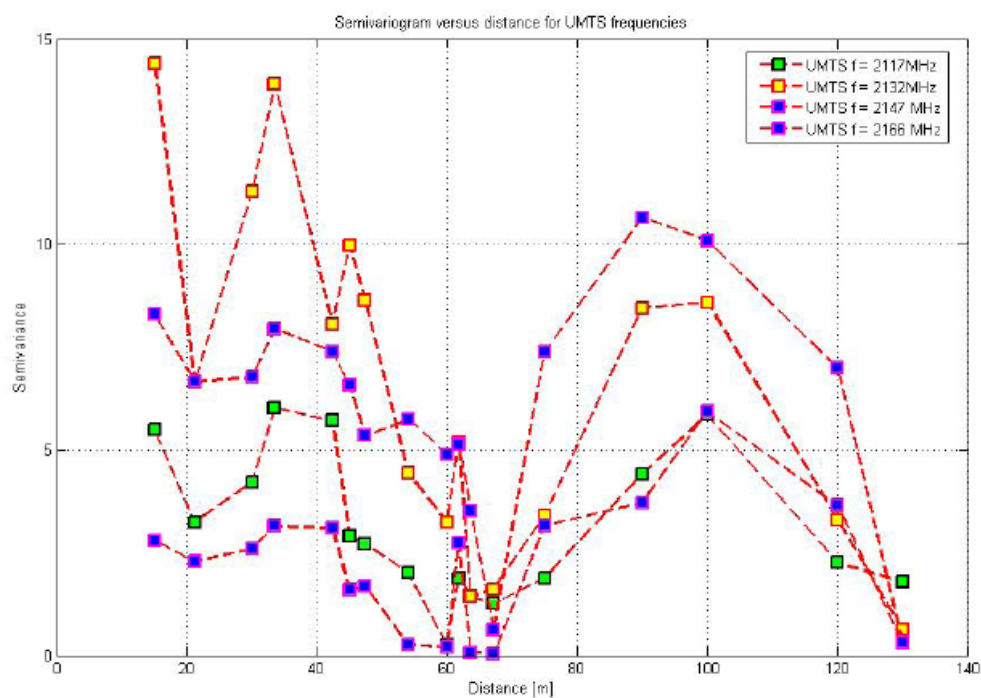


Figure 3.10 – Semivariance vs. distance for UMTS.

Based on the previous hypothesis, the considered correlation metrics were analysed as a function of the Signal-to-Noise Ratio (SNR) difference between the considered points, instead of the physical distance. The motivation of considering the SNR difference relies on the fact that the experienced SNR value is a more related parameter to the actual propagation conditions than the physical distance, since for the same distance very dissimilar SNR values may be experienced depending on the particular radio propagation conditions. The computation of the considered metrics as a function of the SNR difference required the pairs of points measured to be rearranged into new vectors  $\mathbf{U}$  and  $\mathbf{V}$ . In the previous analysis, pairs of measurement locations were grouped based on their physical distance. Now, the measured points are grouped by their SNR difference, which is equivalent to the difference between the average PSD measured in both locations, expressed in decibels (dBm). It is interesting to mention that this alternative classification criterion results in much more pairs of points. As in the previous case, a binning procedure is used such that two pairs of measurement locations  $x_i$  and  $x_j$  are considered to belong to the same set if  $k - \Omega \leq \|P_i - P_j\| \leq k + \Omega$ , where  $k$  denotes the SNR difference corresponding to the considered set,  $\|P_i - P_j\|$  is the actual difference between the average PSD values (in dBm) measured at locations  $x_i$  and  $x_j$ , which is equivalent to their SNR difference, and  $\Omega$  is an appropriate margin included in order to group points whose SNR difference is similar, but not exactly the same. This procedure was configured in order to guarantee a significant number of elements in each vector of SNR difference pairs. Therefore, for each set corresponding to a SNR difference  $k$ , it is possible to create two vectors  $\mathbf{U}(k)$  and  $\mathbf{V}(k)$ , which contain the average PSD, measured by the spectrum analyser, for all the pairs of locations associated to the SNR difference  $k$ .

Figure 3.11 to Figure 3.17 show the considered correlation metrics for DCS and UMTS as a function of the SNR difference, instead of the physical distance between points. It is interesting to observe, in this case, that the correlation parameters exhibit a well-defined trend according to their expected behaviours. In particular, the cross-correlation, the covariance and the normalised covariance tend to decrease as the SNR difference increases, while the semivariance appears to increase with the SNR difference. The different behaviours of the considered correlation metrics when analysed as a function of distance and SNR difference can be explained by the fact that for pairs of points separated by the same distance, the SNR difference may be significantly different depending on the particular radio propagation conditions at each measured location. The received primary power at a given location does not depend just on the distance from the primary transmitter (path loss component) but also on additional propagation phenomena such as multipath propagation (fast fading component) and shadowing (slow fading component). As a result, for the same distance, different and uncorrelated primary power (SNR) values may be experienced, which would explain the random behaviour of correlation parameters as a function of the distance. However, when the same correlation parameters are analysed as a function of the SNR difference, the impact of all the affecting propagation phenomena is implicitly taken into account in the SNR difference value, thus showing a well defined and logical trend as a function of the SNR difference. Based on this discussion, it can be concluded that the SNR difference between two arbitrary points can be considered as an appropriate parameter as a function of which spatial correlation metrics on spectrum occupancy can be adequately analysed and described, as opposed to the distance, which has commonly been employed in previous studies on spatial statistics in the context of CR.

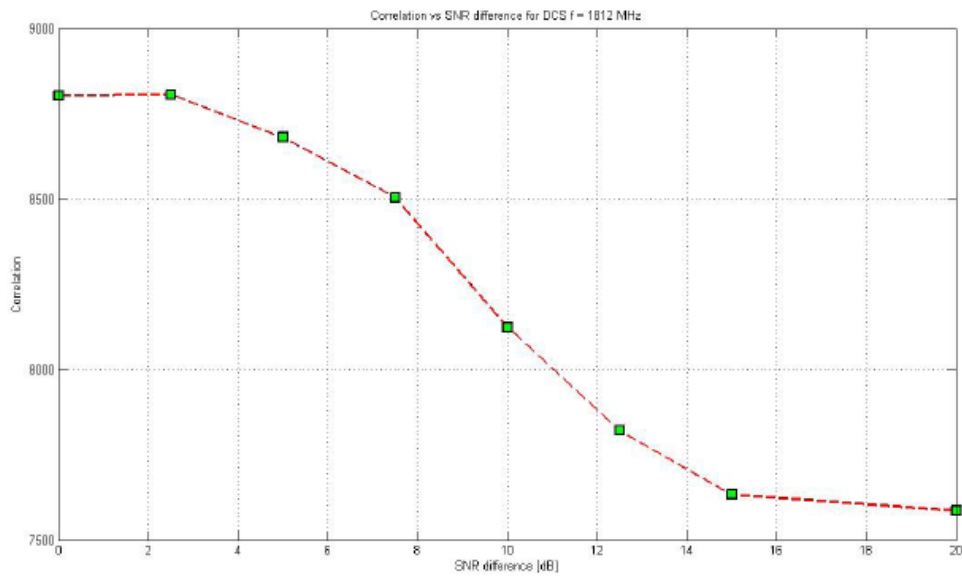


Figure 3.11 – Cross-correlation vs. SNR difference for DCS.

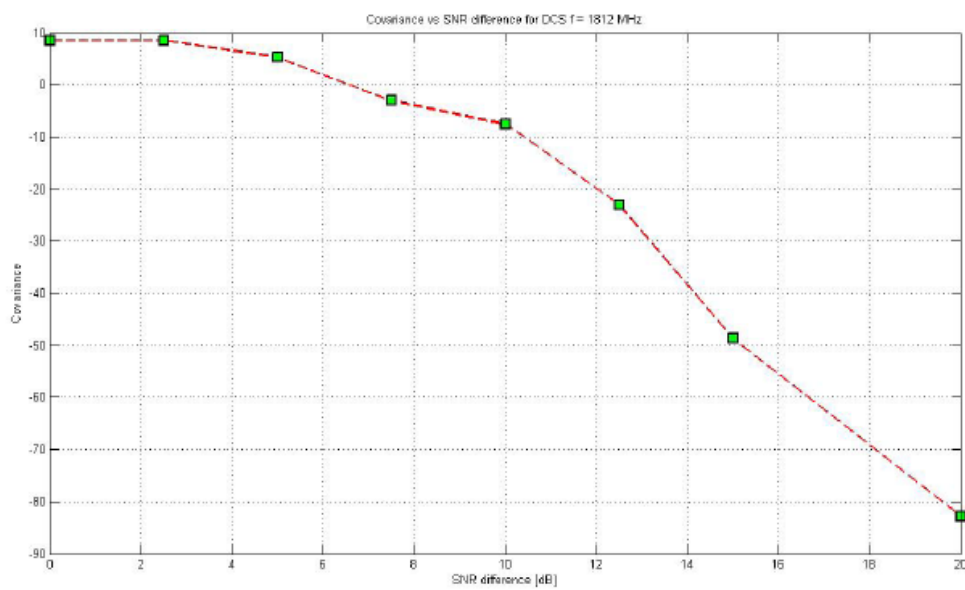


Figure 3.12 – Covariance vs. SNR difference for DCS.



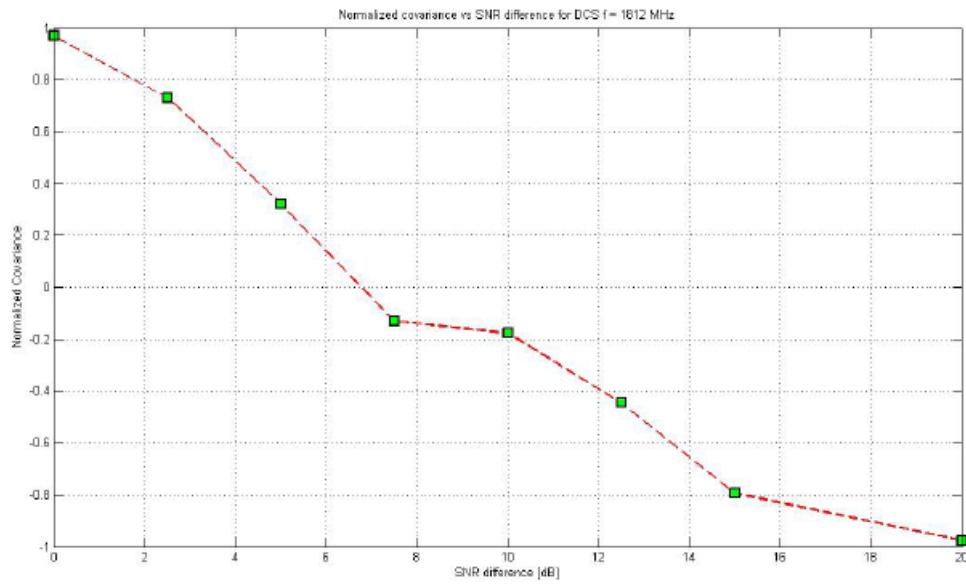


Figure 3.13 – Normalised covariance vs. SNR difference for DCS.

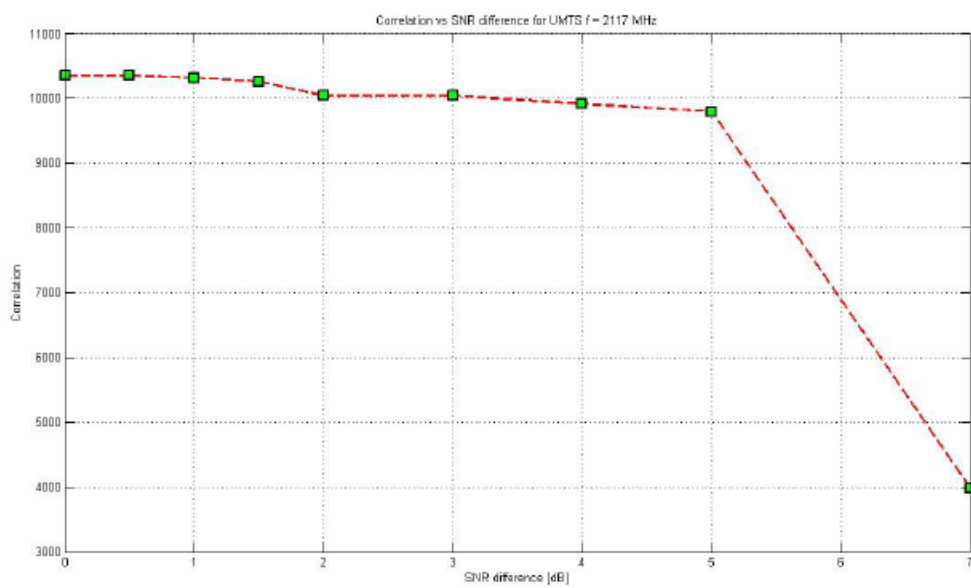


Figure 3.14 – Cross-correlation vs. SNR difference for UMTS.

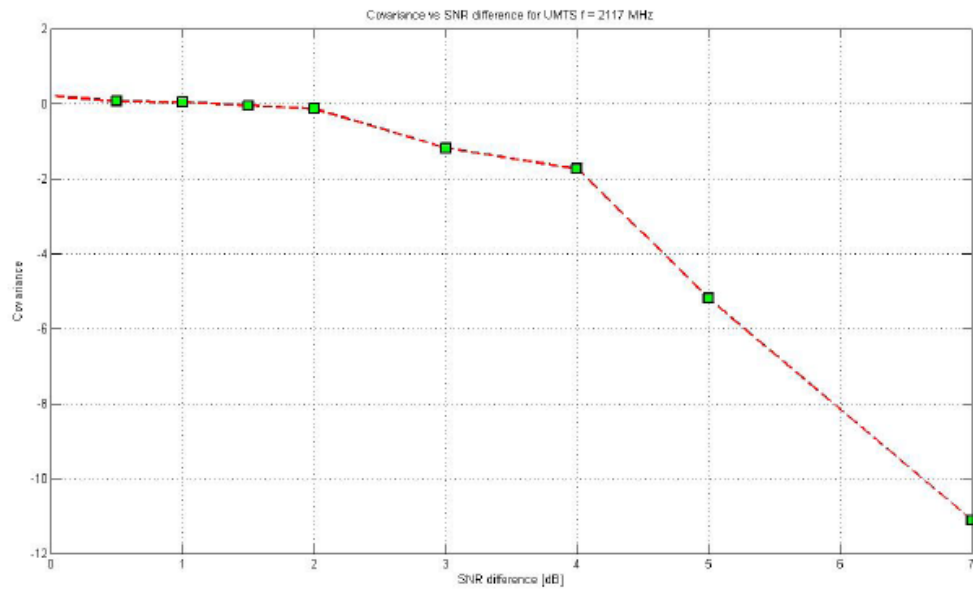


Figure 3.15 – Covariance vs. SNR difference for UMTS.

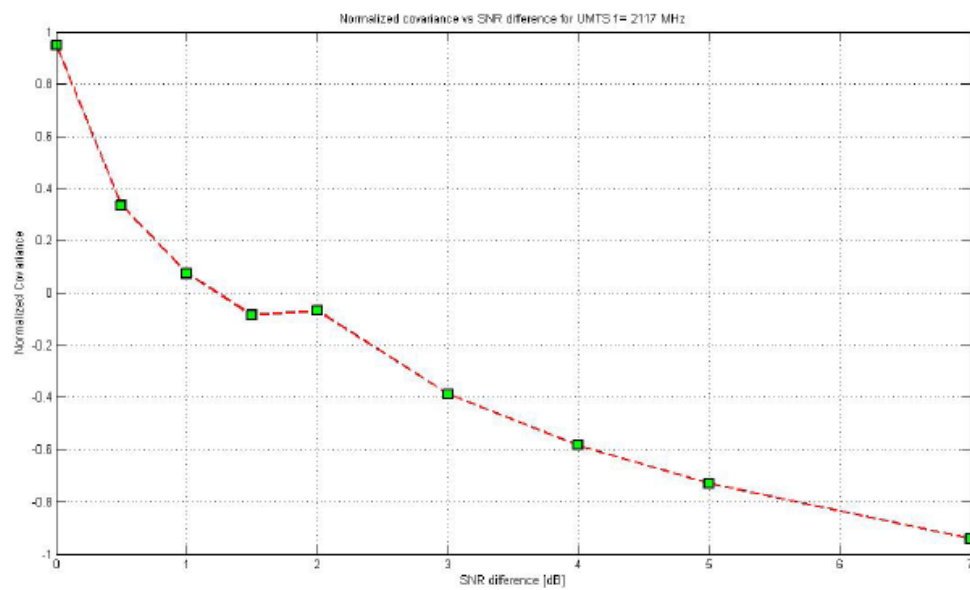


Figure 3.16 – Normalised covariance vs. SNR difference for UMTS.



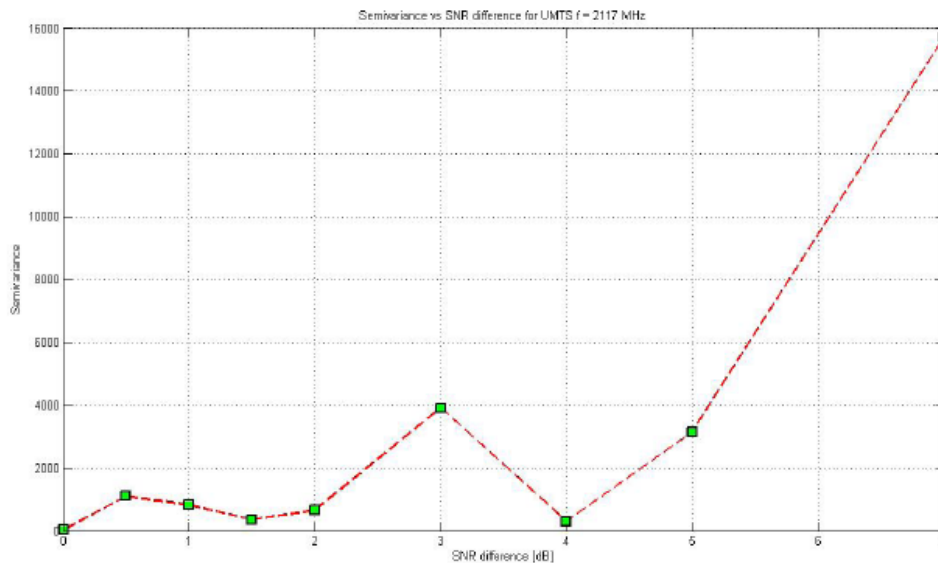


Figure 3.17 – Semivariance vs. SNR difference for UMTS.

### 3.2.3 Spectrum sensing studies

One of the first data post-processing steps in a measurement campaign, regardless of the particular use of the captured data is to determine which captured samples correspond to primary signals and which others to noise. To determine whether a frequency band is actually being occupied by a primary signal, different sensing methods have been proposed in the literature [105]. Depending on how much information is available about the primary signal, different performances can be reached. However, in the most generic case no prior information is available. If only power/amplitude measurements of the spectrum utilisation are available, the energy detection method is the only possibility left. Due to its simplicity and relevance to DSA/CR, energy detection has been a preferred approach for many past spectrum studies. Energy detection compares the received signal energy in a certain frequency band to a properly set predefined threshold. If the signal lies above the threshold the band is declared to be occupied by the primary network. Otherwise the band is supposed to be idle and could be accessed. Due to the simplicity and generality of this operating principle, energy detection can be applied regardless of the primary signal to be detected and, as such, its performance would be expected to be independent of the primary signal being detected. In this context, this section evaluates the performance of energy detection-based spectrum sensing for CR based on various real-world primary signals. The obtained results indicate that the detection performance of energy detection may actually vary with the primary radio technology being considered, but converges under certain conditions. The causes and consequences of the different detection performances for various primary signals are identified, analysed and discussed. The performance evaluation of energy detection for various radio technologies is important because it has an impact on the estimated spectrum occupancy levels for various allocated bands and therefore on any potential application of the captured data, including the development of spectrum occupancy models for DSA/CR. This section summarises the main features and results of the performed study. A detailed description of such study can be found in [106].

#### 3.2.3.1 Energy detection theoretical results

The performance of any spectrum sensing technique can be summarised by means of two probabilities: the probability of detection (i.e., the probability of declaring the sensed channel to be occupied when a primary signal is actually present) and the probability of false alarm (i.e., the probability of declaring the sensed channel to be occupied when it is actually free). For energy detection-based spectrum sensing, both probabilities are given by [106]:

$$P_d = Q\left(\frac{\lambda - N(\sigma_x^2 + \sigma_w^2)}{\sqrt{2N(\sigma_x^2 + \sigma_w^2)^2}}\right) \quad (3.5)$$

$$P_{fa} = Q\left(\frac{\lambda - N\sigma_w^2}{\sqrt{2N\sigma_w^4}}\right) \quad (3.6)$$

where  $Q(\cdot)$  is the standard Gaussian tail probability  $Q$ -function,  $\lambda$  is an energy decision threshold,  $N$  is the number of signal samples employed in the sensing process, and  $\sigma_x^2$  and  $\sigma_w^2$  are the signal and noise powers respectively. The decision threshold is normally set to obtain a target probability of false alarm. Solving equation (3.6) for  $\lambda$  yields:

$$\lambda = Q^{-1}(P_{fa})\sqrt{2N\sigma_w^4} + N\sigma_w^2 \quad (3.7)$$

and substituting into equation (3.5) yields the following expression for the theoretical performance of energy detection:

$$P_d(\gamma) = Q\left(\frac{Q^{-1}(P_{fa})\sqrt{2N} - N\gamma}{\sqrt{2N(1+\gamma)^2}}\right) \approx Q\left(Q^{-1}(P_{fa}) - \sqrt{\frac{N}{2}}\gamma\right) \quad (3.8)$$

Given a target performance in terms of  $P_d$  and  $P_{fa}$ , the required number of signal samples  $N$  to achieve such performance can be obtained from equations (3.5) and (3.6) as:

$$N = 2\left[\frac{Q^{-1}(P_{fa}) - Q^{-1}(P_d)(1+\gamma)}{\gamma}\right]^2 \quad (3.9)$$

which indicates that any arbitrary pair  $(P_d, P_{fa})$  can be achieved by simply increasing the sensing period  $N$ .

### 3.2.3.2 Measurement platform

The measurement platform employed in this study is based on the Universal Software Radio Peripheral (USRP) [107] and GNU Radio [108] architecture. USRP is an openly designed inexpensive Software Defined Radio (SDR) hardware platform that provides radio front-end functionalities, Analogical to Digital and Digital to Analogical Conversion (ADC/DAC), decimation/interpolation with filtering and a Universal Serial Bus 2 (USB2) interface to connect to an off-the-shell Personal Computer (PC). The PC runs the GNU Radio software, a free and open source toolkit that provides a library of signal processing blocks for building SDRs. In addition, it also provides blocks for communicating with the USRP. The general scheme of the measurement platform is illustrated in Figure 3.18.

The primary signal of interest is captured with an omni-directional discone-type antenna AOR DN753 that covers the frequency range 75–3000 MHz. The USRP Radio Frequency (RF) front-ends are provided in form of daughter boards that can be plugged to the USRP main board. In this study we have employed two receiver-only daughter boards: TVRX (50–860 MHz, 8 dB typical noise figure) and DBSRX (800–2400 MHz, 3–5 dB typical noise figure). The daughter boards are employed to tune to the carrier frequency of the desired primary signal and perform down-conversion to the Intermediate Frequency (IF) at which the USRP main board operates. The USRP main board includes 12-bit ADCs working at  $64 \cdot 10^6$  samples per second to digitise the received signal and a Field

Programmable Gate Array (FPGA) to perform filtering and digital down-conversion (decimation) from the IF band to the Base Band (BB). Decimation is required in order to adapt the incoming data rate to the USB2 and PC computing capabilities. A USB controller sends the digital signal samples to the PC in 16-bit I and 16-bit Q complex data format (4 bytes per complex sample), resulting in a maximum rate of  $8 \cdot 10^6$  complex samples per second. The maximum RF bandwidth that can be handled is therefore 8 MHz (narrower bandwidths can be selected by adjusting the decimation rate). The host PC runs the GNU Radio's `usrp_rx_cfile.py` script, which simply collects the digital signal samples sent by the USRP board through the USB2 interface and saves the received BB digital signal sequence to a file in the host PC's hard drive. After the on-line data capturing process, the set of files created by the script are processed off-line. To this end, the energy detection sensing scheme has been implemented in Matlab according the operating principles and theoretical relations abovementioned.

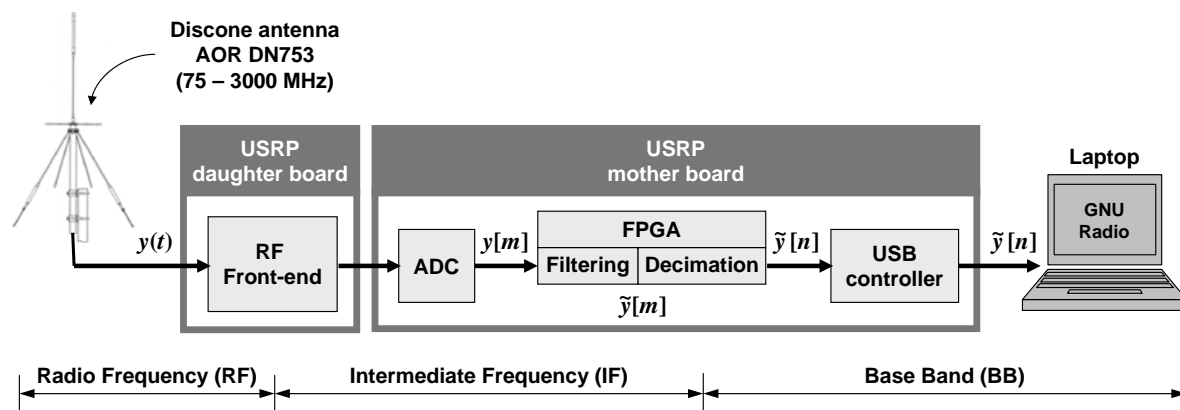


Figure 3.18 – General scheme of the measurement platform

### 3.2.3.3 Evaluation methodology

Since the aim of this work is to conduct a performance evaluation study of spectrum sensing based on real-world primary signals, signal captures are therefore required. To this end, the whole measurement platform was placed on a building roof in urban Barcelona (latitude:  $41^{\circ} 23' 20''$  north; longitude:  $2^{\circ} 6' 43''$  east; altitude: 175 meters) with direct line-of-sight to several transmitters located a few tens or hundreds of meters away from the antenna and without buildings blocking the radio propagation. This measurement scenario enabled us to reliably capture the desired signals under high SNR conditions.

With the aid of a spectrum analyser, various channels were selected for different radio technologies (see Table 3.1). Our criterion was to select those channels with the highest observed power levels (in order to maximise the receiving SNR) provided that the activity pattern was constant (i.e., the signal was always present in order to simplify some computations in the off-line data post-processing phase). For broadcast services (analogical TV, digital TV and DAB-T), the selection was straightforward since such kind of transmitters are always active and transmit at high power levels. For UMTS, the activity factor was not an issue (UMTS base stations transmit broadcast information in continuous mode), but the received signal level was carefully observed, selecting channels from the closest base stations (only a few tenths of meters apart). On the other hand, for TETRA, GSM and DCS, the most problematic aspect was the activity factor. In the case of TETRA we were able to identify transmissions from base stations in Downlink-Continuous Transmission (D-CT) mode. In the case of GSM and DCS, we selected various broadcast channels, which could readily be identified with a spectrum analyser by their high power level.

Table 3.1 – Channels measured in this study: Analogical/digital tv, TERrestrial Trunked RADio (TETRA), TERrestrial Digital Audio Broadcasting (DAB-T), Extended Global System for Mobile communications 900 downlink (E-GSM 900 DL), Digital Cellular System 1800 downlink (DCS 1800 DL) and Universal Mobile Telecommunications System Frequency-Division Duplex downlink (UMTS FDD DL).

System	Channel number	$f_{start}$ (MHz)	$f_{center}$ (MHz)	$f_{stop}$ (MHz)	Signal BW (MHz)	Decimation rate ( $M$ )	Sampled BW (MHz)	Gain (dB)	Cut-off frequency	Pass band (MHz)
Analogical TV	23	486	490	494	8	8	8	10	0.94	7.52
	29	534	538	542						
	34	574	578	582						
	38	606	610	614						
Digital TV	26	510	514	518	8	8	8	10	0.94	7.52
	48	686	690	694						
	61	790	794	798						
	67	838	842	846						
TETRA	37	420.8875	420.900	420.9125	0.025	256	0.25	70	0.1	0.03
	44	421.0625	421.075	421.0875						
	45	421.0875	421.100	421.1125						
	47	421.1375	421.150	421.1625						
	53	421.2875	421.300	421.3125						
DAB-T	08A	195.080	195.936	196.792	1.712	32	2	70	0.8	1.6
	10A	209.080	209.936	210.792						
	11B	217.784	218.640	219.496						
E-GSM 900 DL	60	946.8	947.0	947.2	0.2	64	1	70	0.3	0.3
	113	957.4	957.6	957.8						
	975	925.0	925.2	925.4						
DCS 1800 DL	546	1811.8	1812.0	1812.2	0.2	64	1	70	0.3	0.3
	771	1856.8	1857.0	1857.2						
	786	1859.8	1860.0	1860.2						
UMTS FDD DL	10588	2115.1	2117.6	2120.1	5	8	8	70	0.625	5
	10663	2130.1	2132.6	2135.1						
	10738	2145.1	2147.6	2150.1						

After having identified the channels to be measured, the required measurements were performed in the above-mentioned location, tuning the measurement platform to the centre frequency of each channel ( $f_{center}$  in Table 3.1) and employing the indicated decimation rates and RF gain factors. Decimation rates were selected so that the effectively sampled signal BandWidth (BW) was equal to or greater than the actual signal BW, whereas the gain factor was chosen so as to maximise the received signal level (and hence the receiving SNR) without incurring in saturation. For most of the channels the optimum gain value was 70 dB and in the particular case of TV (both analogical and digital) the gain was drastically reduced due to the proximity of the TV station ( $\approx 3$  km).

For each channel, a sequence of  $12 \cdot 10^6$  samples was captured and the first  $2 \cdot 10^6$  samples were discarded in order to remove any potential transient peaks that may appear during the first capturing instants of the USRP board. The resulting sequence was filtered in software with Matlab using a high order digital Butterworth filter with no more than 0.1 dB of losses in the pass band and at least 50 dB of attenuation in the stop band. The normalised cut-off frequencies for each channel are shown in Table 3.1, resulting in pass bands equal to or greater than the signal BW, except for TV channels where some BW was required to accommodate the filter's transient band (for DAB-T the RF bandwidth is 1.712 MHz but the signal information is confined within a BW of 1.54 MHz).

Before employing the signals obtained after the previous steps in our experimental study, we verified that they satisfied the two established requirements, namely high signal levels without saturation and activity factors equal to 100%. The fulfilment of the first requisite can be verified from Figure 3.19, where the average power spectrum of some captured signals is shown as an example. As it can be appreciated, the nearly perfect spectral shapes indicate a good SNR level without distortion by saturation. To verify the accomplishment of the second requirement, the employed antenna was replaced with a matched load and the measurements were repeated in order to measure the receiver system's noise. By comparing the instantaneous energy levels of both the signal and noise sequences, we verified that the energy levels present in the signal sequences were significantly higher than those measured for the noise sequences along the whole measurement period, thus indicating that a primary user signal was present with an activity factor of 100% in all the captured signal sequences.

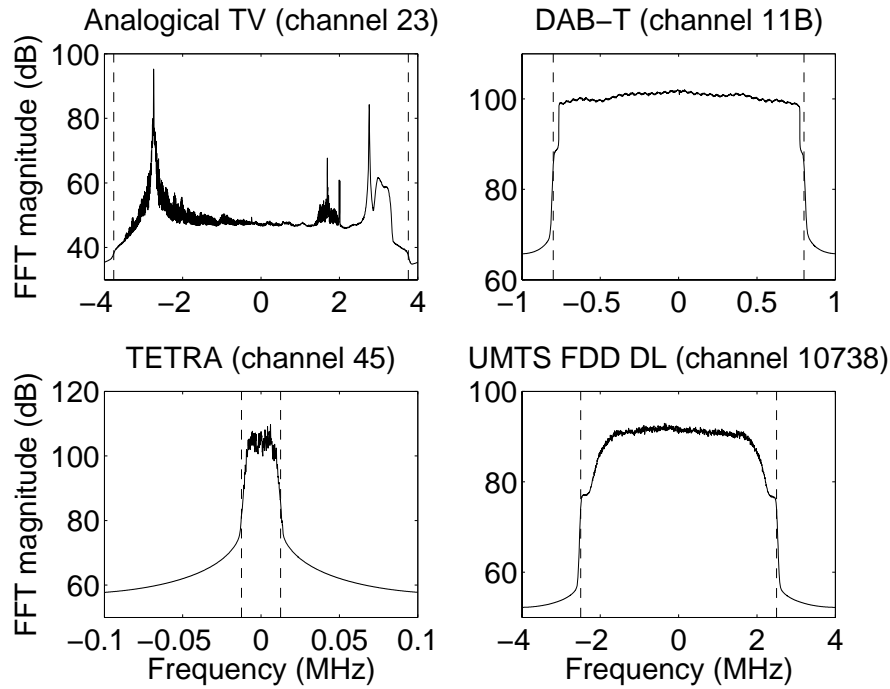


Figure 3.19 – Average power spectrum (averaged over more than 4800 2048-point FFTs) for some of the captured signals. Dashed lines represent the filter's cut-off frequencies.

To compute the performance metrics  $P_d$  and  $P_{fa}$ , input sequences are divided into blocks of  $N$  samples (sample length) and a sufficiently high number of such blocks is processed. For lower values of  $N$ , a higher number of blocks is processed in order to keep the statistical accuracy of the obtained results at an acceptable level. Assuming that the signal sequence is noise-free (which is a reasonable approximation for high SNR levels), the captured sequence's power is measured and the obtained value is considered as the actual signal power  $\sigma_x^2$ . Based on the desired SNR, an AWGN sequence with power level  $\sigma_w^2 = \sigma_x^2/\gamma$  is generated. Based on the values of  $N$  and  $\sigma_w^2$ , the energy decision threshold for a given target  $P_{fa}$  is set according to equation (3.7), and the energy of each  $N$ -sample input block is compared to the threshold. To compute the  $P_d$ , the sequence obtained by adding the signal and AWGN sequences is employed as input to the energy detector. The experimental  $P_d$  is then obtained as the proportion of blocks where the detection result is occupied channel (the primary signal is present in all the processed blocks since the activity factor for all channels is 100%). Similarly, the experimental  $P_{fa}$  is computed as the proportion of blocks where the detection result is occupied channel when the input signal is the AWGN sequence (no primary signal is present in any block).

### 3.2.3.4 Results

The performance of energy detection-based spectrum sensing has been evaluated for the 25 channels shown in Table 3.1. The obtained results indicated similarities among channels of the same radio technology. Since channels of the same system did not manifest significant differences among them in most of the cases, the set of channels corresponding to the same radio technology were averaged in order to obtain a single performance curve for each radio technology. This simplifies the study of the obtained results since only one performance curve needs to be analysed for each system (instead of one curve per individual channel). The obtained results are shown in Figure 3.20 and Figure 3.21 in terms of the  $P_d$  as a function of the SNR. Figure 3.20 shows the results for the case of perfectly calibrated noise, i.e. no noise uncertainty ( $\alpha = 0$  dB), while Figure 3.21 corresponds to the case where noise uncertainty is present ( $\alpha = 1$  dB and  $\alpha = 2$  dB).

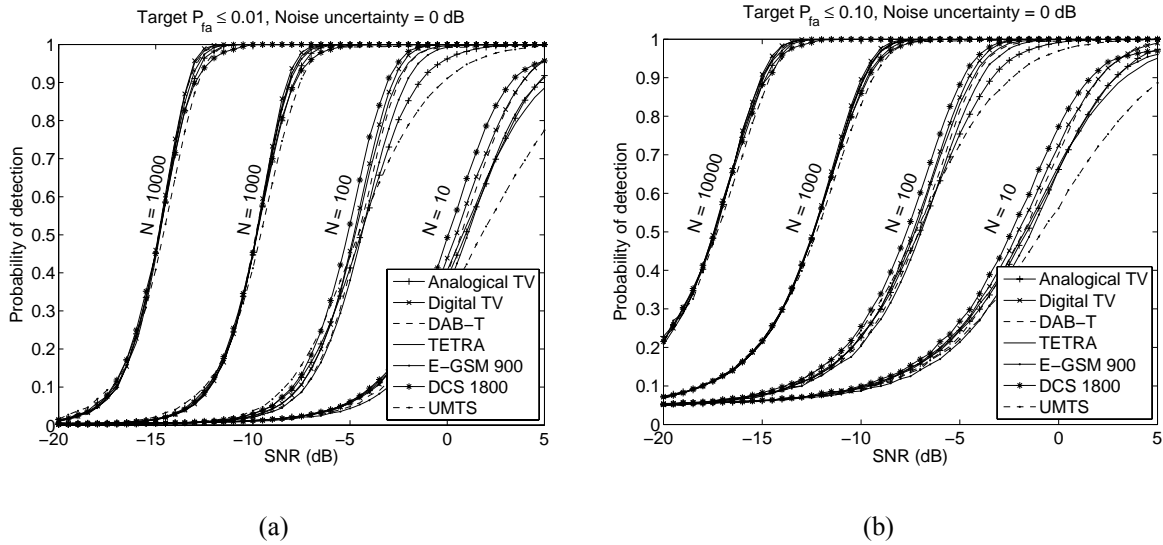


Figure 3.20 – Probability of detection versus SNR: (a)  $\alpha = 0$  dB ( $P_{fa} \leq 0.01$ ), (b)  $\alpha = 0$  dB ( $P_{fa} \leq 0.10$ ).

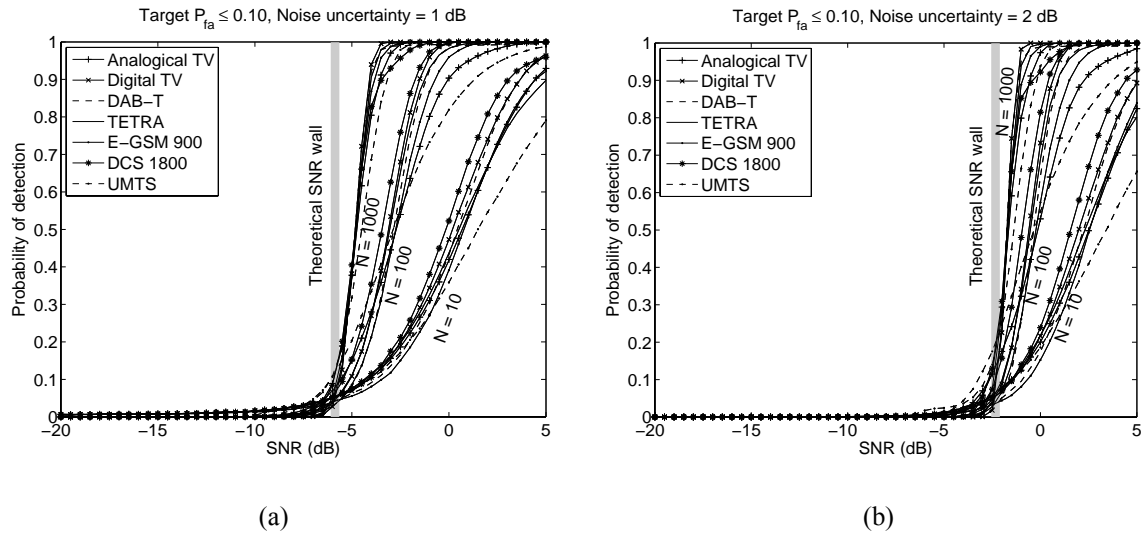


Figure 3.21 – Probability of detection versus SNR: (a)  $\alpha = 1$  dB ( $P_{fa} \leq 0.10$ ), (b)  $\alpha = 2$  dB ( $P_{fa} \leq 0.10$ ).

As it can be appreciated in Figure 3.20 and Figure 3.21, different performance curves are obtained for different systems although the same detection method (energy detection) is employed for all of them. One may think that this phenomenon might be due to the randomness of the experiments, which are based on measurements performed on a number of arbitrary channels during a short measurement period (from 1.25 to 40 seconds depending on the sampling rate, see Table 3.1). In fact, any empirical study suffers from a certain random component that cannot be avoided. Concerning this issue, it is worth noting that some experiments were performed with a lower number of iterations than the ones employed to obtain the results shown in this section. To determine the randomness of such curves and validate the obtained results, the number of iterations was doubled, leading to the curves shown in Figure 3.20 and Figure 3.21. Doubling the number of iterations resulted in slightly smoother curves, but it did not change the positions of the curves in the graph, thus guaranteeing the statistical reliability of the obtained results. Moreover, it is worth highlighting, as mentioned above, that the performance curves obtained for different channels of the same system do not manifest significant differences

among them. Therefore, the differences observed among the curves for different systems have to be ascribed to the particular features of each radio technology.

For the rest, the obtained results agree with the theoretical predictions. For example, the detection probability  $P_d$ , as expected, decreases with the SNR. On the other hand, increasing the target probability of false alarm  $P_{fa}$  implies reducing the energy decision threshold, which in turn results in an improved detection of weak signals and hence an enhanced  $P_d$ . The existing trade-off between  $P_d$  and  $P_{fa}$  can be clearly appreciated by comparing Figure 3.20 (a) and (b). Moreover, Figure 3.20 indicates that for perfectly calibrated noise the energy detector is a robust detection method, i.e. any arbitrary pair  $(P_d, P_{fa})$  can be met by simply increasing the sample length as indicated in (3.9). In the presence of noise uncertainty, however, there exists an SNR threshold (the SNR wall) below which the energy detector becomes non-robust, meaning that the probability of misdetection,  $P_{md} = 1 - P_d$  and the probability of false alarm,  $P_{fa}$ , cannot simultaneously be made to go to zero, no matter how long the observation interval  $N$  is. This trend is clearly appreciated in Figure 3.21, where increasing the observation interval  $N$  improves  $P_d$  only for SNR values above the SNR wall. Below the threshold imposed by the SNR wall, the probability of detection approaches zero regardless of the sensing interval  $N$ , making signal detection impossible. As observed in Figure 3.21, the existence of the SNR wall is experimentally verified with a very good agreement with the theoretical SNR wall [106].

The results shown in Figure 3.20 and Figure 3.21 indicate that the performance of the energy detector may strongly depend on the considered primary radio technology. This behaviour is not predicted by the classical theoretical result associated to the energy detection method, which is shown in equation (3.8). In fact, for a given set of target  $P_{fa}$ , sample length  $N$  and SNR  $\gamma = \sigma_x^2/\sigma_w^2$ , equation (3.8) suggests that resulting performance in terms of  $P_d$  is unique. However, Figure 3.20 and 3.21 clearly demonstrate that for constant  $P_{fa}$ ,  $N$  and  $\gamma$  values, the resulting  $P_d$  may strongly depend on the primary radio technology being detected. For example, for  $P_{fa} = 0.10$ ,  $N = 10$  and  $\gamma = 0$  dB, equation (3.8) provides a theoretical detection probability  $P_d = 0.68$ . However, for the same parameters, Figure 3.20 (b) indicates that the experimental detection probabilities for e.g. digital TV and UMTS are equal to 0.72 and 0.56, respectively. Moreover, it is interesting to note, as shown in Figure 3.20 and Figure 3.21, that the performance differences among various radio technologies are not constant, but increase as the sensing period  $N$  decreases. This indicates that the sensing period required for a given target performance  $(P_d, P_{fa})$  as predicted by equation (3.9), might be enough to detect some primary radio technologies but might actually result insufficient for some others, thus requiring longer sensing periods. If the maximum sensing period is constrained (by physical layer features or higher layer protocols), the resulting detection probability might be acceptable for some radio technologies but might result insufficient to reliably detect other primary signals, thus making some radio technologies more susceptible to interferences under the same conditions. As mentioned before, the performance differences observed among various radio technologies have to be ascribed to the particular features of each radio technology. The objective of this section is to identify and analyse the causes that originate the observed differences among various primary signals.

The performance of any spectrum sensing algorithm depends on the decisions made by such algorithm, which in turn depend on the algorithm's test statistic. Since the energy detector's test statistic is related to the received signal energy, it seems reasonable to look for the origins of the observed behaviour in the characteristics of the received signal energy or, alternatively, the received signal power. Since the signal power is related to the signal energy by a scaling factor  $N$ , the analysis of the power temporal evolution indicates how the energy detector's test statistic varies along time. Analysing the time evolution of the received signal power is expected to provide some insights into the divergences observed among various radio technologies in Figure 3.20 and Figure 3.21.

To evaluate the time evolution of the received signal power, and in order to enable a fair comparison among various signals under the same conditions, the captured signal sequences  $y[n]$  are normalised in order to obtain zero-mean, unit-variance (unit power) sequences  $Y[n]$  as follows:

$$Y[n] = (y[n] - \mu_y) / \sigma_y \quad (3.10)$$

where  $\mu_y$  and  $\sigma_y$  represent the sample mean and sample variance of sequence  $y[n]$ , respectively. This operation converts the originally captured sequences  $y[n]$  with different absolute signal powers into normalised sequences  $Y[n]$  with the same normalised signal power (which in the presence of the same noise power is equivalent to compare them under the same average SNR). The obtained sequences  $Y[n]$  are divided into blocks of  $N$  samples and the average power of each block is computed. The sequence of received power levels is smoothed by means of a moving average.

The resulting time evolution of the normalised received power is shown in Figure 3.22 for various channels when  $N = 100$ . Since such signals were captured under perfect line-of-sight and high SNR conditions, it is reasonable to assume that fading effects are negligible and the observed power variations are therefore mainly due to varying transmission power patterns. In fact, the observed patterns can be related to distinctive signal properties. For example, the highest peaks observed for analogical TV occur every 1600 blocks  $\times$  100 samples/block =  $1.6 \cdot 10^5$  samples, which for the employed sampling rate corresponds to the 50-Hz vertical frequency of the PAL system. The UMTS signal variations can be explained by the use of power control techniques that modify the transmitted power according to the system's load factor. On the other hand, the signals received in digital TV and DCS 1800 (broadcast) channels show a uniform power pattern, as expected.

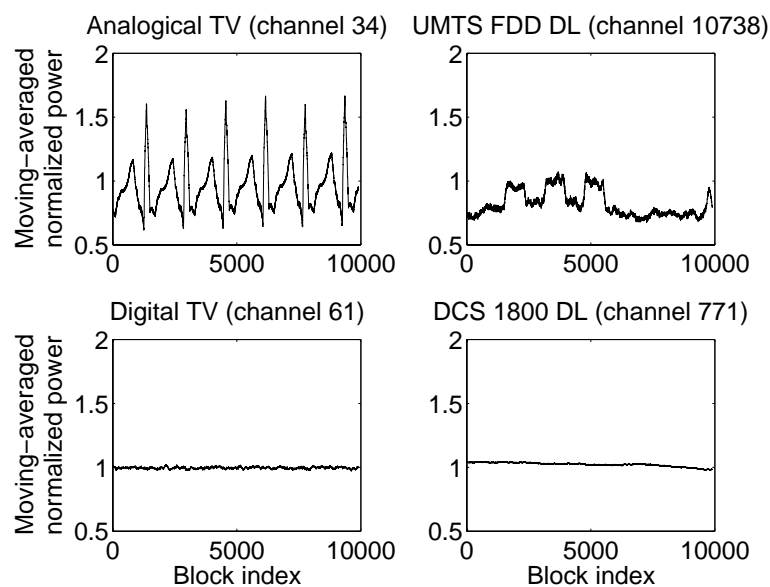


Figure 3.22 – Moving-averaged normalised power received for some captured signals (moving-averaging window of 100 samples).

From Figure 3.22 it is clear that for the selected short observation interval  $N = 100$ , the energy detector's test statistic follows the instantaneous variations of the received signal power. In such a case, if the instantaneous signal power falls below the energy decision threshold, the detection result will be a free channel, even if it should be an occupied one due to an average energy (power) actually greater than the decision threshold. Therefore, under the same average SNR conditions (i.e., signals with the same average power), this means that a higher power variability implies a higher probability that the instantaneous power level (and the energy detector's test statistic) falls below the decision threshold, which results in a lower detection probability. As a matter of fact, comparing the results shown in Figure 3.20 and Figure 3.21 for  $N = 100$  to the power patterns shown in Figure 3.22, it can be confirmed that the best detection performance is obtained for DCS 1800, followed by digital TV (the signals with the most uniform power patterns), while the worst detection performance corresponds to UMTS FDD, followed by analogical TV (the signals with the most alternating power patterns). This explains the different detection probabilities observed in Figure 3.20 and Figure 3.21 for various primary signals under the same average SNR conditions. As the number of samples  $N$  increases, the test statistic is computed over larger observation intervals, thus averaging any instantaneous power variations. In such a case, although the variability of the received power remains the same, the

Reference DR9.3



variability of the test statistic decreases and so does the probability of miss detection. For sufficiently long observation intervals, the test statistic ceases to follow the instantaneous signal power variations and its value closely resembles the true mean energy (power). When this occurs for all the considered signals, the obtained performance curves converge (i.e., the energy detector performance does not depend on the primary technology considered.) This explains the behaviour observed in Figure 3.20 and Figure 3.21 as the value of  $N$  increases.

The previous analysis indicates that the energy detector's test statistic may follow the instantaneous variations of the received signal power if short observation intervals are selected. When this occurs, the energy detector's performance strongly depends on the primary technology considered, being degraded for signals with higher power variability and affected to a lesser extent when detecting more uniform signal patterns. On the other hand, as the sensing time increases with respect to the primary signal dynamics, the peculiarities of each signal power variation pattern are averaged and the energy detectors's performance becomes therefore more independent of the primary signal being detected.

In spite of the general operating principle of the energy detection method, the results shown in the previous section highlight that certain technology-dependent inherent properties may result in different detection performances for various radio technologies. To quantitatively illustrate the impact of this phenomenon in practice, Figure 3.23 shows the detection probability as a function of the sample length for various primary signals. As it can be appreciated the performance for different signals follows a similar trend under the ideal case of no noise uncertainty (upper graph). For example, assuming an average SNR of  $-15$  dB, a target  $P_d = 0.9$  would require 9745 samples ( $\approx 1.22$  ms) in the best case (digital TV) and 14099 samples ( $\approx 1.76$  ms) in the worst case (UMTS). This difference is not very significant, but relies on the assumption that the noise power is perfectly known, which is never true in reality. In the more realistic case of noise uncertainty (lower graph), assuming an average SNR above the SNR wall of  $-5$  dB, a target  $P_d = 0.9$  would require 4532 samples ( $\approx 0.57$  ms) in the best case (digital TV), 38937 samples ( $\approx 4.87$  ms) in an average case (analogical TV), whereas in the worst case (UMTS) the desired  $P_d$  would never be achieved due to the presence of the SNR wall ( $P_d$  for UMTS does not increase beyond 0.8, no matter how long the observation interval is). These results exemplify the various detection performances that can be reached for different primary radio technologies in reality.

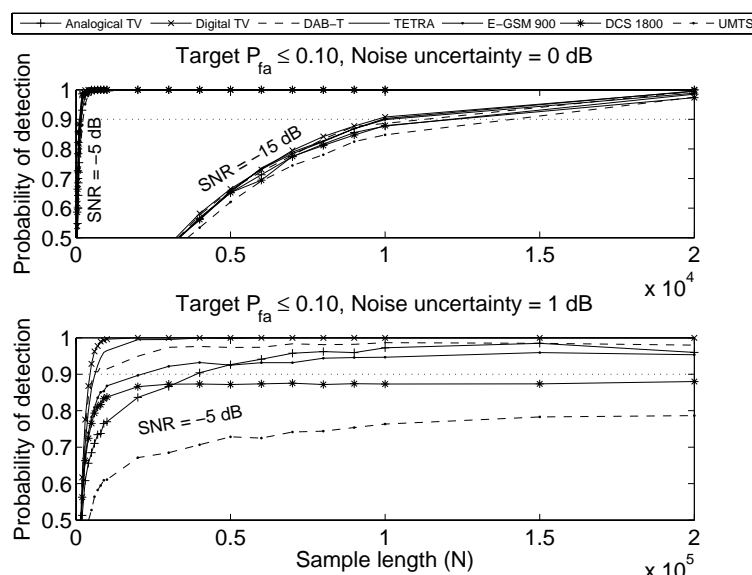


Figure 3.23 – Probability of detection versus sample length.

While previous section showed that different performances may be obtained with energy detection depending on the primary signal being detected, the results shown in this section indicate that, in practice, such differences can be so important that some primary signals might be reliably detected

while some others might not, no matter how long the sensing interval is, thus making some radio technologies more susceptible to interferences under the same conditions.

### 3.2.3.5 Conclusions

In spite of the general operating principle of the energy detection method, the results shown in this section have indicated that certain technology-dependent inherent properties may result in different detection performances for various primary radio technologies. The detection performance differences are more noticeable for short sensing intervals, where the energy detector's performance is more degraded for signals with higher power variability and affected to a lesser extent when detecting more uniform signal patterns. As the sensing interval increases, the energy detectors' performance becomes more similar for different radio technologies and thus more independent of the primary signal being detected. Although increasing the sensing interval improves the detection performance, the existing differences can be so important that, in practice, some primary signals might be reliably detected while some others might not, no matter how long the sensing interval is, thus making some radio technologies more susceptible to interferences under the same conditions. These results indicate that the energy detection principle in the real world may exhibit significantly divergent detection performances depending on the primary signal under detection. This observation is important since it has an impact on the estimated spectrum occupancy levels for various allocated bands when employing energy detection in order to determine its occupancy levels and patterns, and therefore on any potential application of the captured data, including the development of spectrum occupancy models for DSA/CR.

## **3.3 Dynamic Spectrum Access in Cognitive Radio Networks**

### **3.3.1 *Joint learning detection framework***

#### 3.3.1.1 Introduction and motivation

During the last century, most of the meaningful frequency bands were licensed to emerging wireless applications, where the static frequency allocation policy combined with a growing number of spectrum demanding services led to a spectrum scarcity. However, several measurements conducted in the United-States[113], first, and then in numerous other countries and/or contexts[83][85][86][96], showed a chronic underutilization of the frequency band resources revealing substantial communication opportunities in these licensed bands.

To alleviate the spectrum scarcity, the (Federal Communications Commission) FCC[113] suggested opening the licensed bands dedicated to primary users (PUs) to unlicensed users and services (usually referred to as secondary users, SUs), allowing them to exploit these bands if unoccupied at a particular time in a particular geographical area. Moreover, Cognitive Radio has been proposed as a promising technology to enable a harmless coexistence of PUs and SUs on a same frequency band.

In a nutshell, Cognitive Radio (CR) equipment is a communication device aware of its environment as well as of its operational abilities and capable of using them intelligently to fulfill its tasks. SUs based CR equipment are, thus characterized by their ability to gather information through their sensors and to use them to adapt their behavior to their nearby primary network [114]. In a generic scenario, a SU should first probe its environment to detect spectrum holes, and then access the available bands if needed.

In order to exploit as many opportunities as possible while ensuring minimum interference with PUs, spectrum sensing appears as a crucial step where SUs are required to perform quick and accurate detection of PUs while having minimum (or no) *a priori* information on PUs activity or the channels characteristics. To that purpose, extensive work has been provided by the Cognitive Radio community to design blind and efficient spectrum sensing tools[105].

In this study, we investigate a joint learning-detection framework to alleviate the lack of knowledge on the noise level. Section 3.3.1.2 introduces the usually considered theoretical model as well as the commonly used energy detector in case of a perfect knowledge on the noise level. Section 3.3.1.3 and Section 3.3.1.4 suggest using a learning algorithm to alleviate the absence of information on the noise level. Then, first experimental results on the performances of the introduced ratio detector are presented and discussed in Section 3.3.1.5.

### 3.3.1.2 System model

#### 3.3.1.2.1 Network assumptions

We consider a receiver willing to gather information on a pool of bands allocated to a primary network. For the sake of simplicity, we represent time as a discrete sequence of slots. In every slot, the CR can acquire a given number of samples depending on the characteristics of the receiver. Every time the CR collects samples on a specific band, only two observation outcomes are possible: the channel can be sensed either idle or busy. In the rest of the report, we will associate the numerical value 1 to a busy channel and 0 to an idle channel. We assume that the SU has no *a priori* knowledge on the characteristics of the bands (e.g., occupied or not).

Let  $r_t = [r_{t,0}, r_{t,1}, \dots, r_{t,M-1}]$  be  $M$  independent and identically distributed (i.i.d.) samples gathered by the CR receiver at the current slot  $t$ . The outcome of the sensing process can be modeled as a binary hypothesis test described as follows:

$$r_t = \begin{cases} n_t, & H_0 \\ x_t + n_t, & H_1 \end{cases} \quad (3.11)$$

where hypotheses  $H_0$  and  $H_1$  refer respectively to the case of an absent or a present signal on the sensed channel. On the one hand,  $x_t = [x_{t,0}, x_{t,1}, \dots, x_{t,M-1}]$  refers to the source signal where every sample  $x_{t,k}$  is perceived as an i.i.d. realization of a Gaussian stochastic distribution  $\mathcal{N}(0, \sigma_{x,t}^2)$ . On the other hand,  $n_t = [n_{t,0}, n_{t,1}, \dots, n_{t,M-1}]$  refers to i.i.d. additive white Gaussian noise (AWGN) samples  $\mathcal{N}(0, \sigma_{n,t}^2)$ . Moreover,  $x_t$  and  $n_t$  are assumed to be independent. Thus, we consider the following Gaussian received signals under either hypothesis  $\forall r_{t,i} \ i \in \{0, \dots, M-1\}$ :

$$\begin{cases} H_0 : r_{t,i} : \mathcal{N}(0, \sigma_{n,t}^2) \\ H_1 : r_{t,i} : \mathcal{N}(0, \sigma_{x,t}^2 + \sigma_{n,t}^2) \end{cases} \quad (3.12)$$

The previously introduced network considerations will be referred to as *Assumption 1*. Within this context, the detection outcome can be modeled as the output of a decision making policy  $\pi$  that maps the current samples  $r_t$  into a binary value  $d_t = \pi(r_t)$ ,  $d_t \in \{0, 1\}$ .

In the next subsection, we summarize the usually used criteria to evaluate the performance of a signal detection policy.

#### 3.3.1.2.2 Performance evaluation of a detection policy $\pi$

Under the previously considered binary hypothesis test, one can define two probabilities that characterize the performance of the detection policy  $\pi$  at the slot number  $t$ : The probability of false alarm ( $P_{fa,t}$ ) and the probability of detection ( $P_{d,t}$ ):

$$\begin{cases} \mathbf{P}_{fa,t} = \mathbf{P}(d_t = 1 | H_0) \\ \mathbf{P}_{d,t} = \mathbf{P}(d_t = 1 | H_1) \end{cases} \quad (3.13)$$

Usually, constraints impose to fix the  $\mathbf{P}_{fa,t}$  under a given level  $\alpha$ , such that  $\mathbf{P}_{fa,t} \leq \alpha$ . The most powerful decision policy is then defined as the one having the largest  $\mathbf{P}_{d,t}$  value for a given  $\mathbf{P}_{fa,t} = \alpha$ .

### 3.3.1.2.3 Neyman-Pearson energy detector

The Neyman-Pearson energy detector (NP-ED, also known as *radiometer*) is a commonly used spectrum sensor. It has been extensively analyzed for its proprieties as a semi-blind low complexity spectrum sensor, since it ignores the characteristics of the received signals and only relies on the perceived energy of the signal. It assumes known the noise level  $\sigma_{n,t}^2$  at every slot number  $t$ . As a first approximation, we consider in the rest of the report a constant noise level for all  $t$ ,  $\sigma_{n,t}^2 = \sigma_n^2$ . Under these assumption, the NP-ED is proven to be the most powerful test. Hence, NP-ED appears as an efficient approach when no information other than the noise level is available at the receiver side.

NP-ED relies on the computation of the received energy statistic  $\mathbf{T}_t$  at the slot number  $t$  defined such as:

$$\mathbf{T}_t = \sum_{i=0}^{M-1} |r_{t,i}|^2 \quad (3.14)$$

The decision policy  $\pi_{NP-ED}$  is a simple Heaviside function that depends only on the evaluation of the statistic  $\mathbf{T}_t$  on the current slot  $t$ :

$$d_t = \pi_{NP-ED}(r_t) \Leftrightarrow d_t = \mathbf{H}(\mathbf{T}_t - \xi_t(\alpha)) \quad (3.15)$$

where  $\xi_t(\alpha)$  is the selected threshold to guaranty  $\mathbf{P}_{fa} \leq \alpha$ . Such policies are usually described using the following notation:

$$\mathbf{T}_t \underset{>H_1}{<^{H_0}} \xi(\alpha) \quad (3.16)$$

The following two equations briefly remind the expressions of the  $\mathbf{P}_{fa,t}$  and the  $\mathbf{P}_{d,t}$  as well as their approximations for large  $M$ .

$$\begin{cases} \mathbf{P}_{fa,t} = 1 - F_{\chi_M^2} \left( \frac{\xi_t(\alpha)}{\sigma_n^2} \right) \approx Q \left( \sqrt{\frac{M}{2}} \left( \frac{\xi_t(\alpha)/M}{\sigma_n^2} - 1 \right) \right) \\ \mathbf{P}_{d,t} = 1 - F_{\chi_M^2} \left( \frac{\xi_t(\alpha)}{\sigma_n^2 + \sigma_{x,t}^2} \right) \approx Q \left( \sqrt{\frac{M}{2}} \left( \frac{\xi_t(\alpha)/M}{\sigma_n^2 + \sigma_{x,t}^2} - 1 \right) \right) \end{cases} \quad (3.17)$$

where  $F_{\chi_M^2}(\cdot)$  refers to the cumulative distribution function of a  $\chi^2$ -distribution with  $M$  degrees of freedom, and  $Q(\cdot)$  is the complementary cumulative distribution function of Gaussian random variable (also known as Marcum function), formally defined as:

Reference DR9.3

$$Q(x) = \frac{1}{\sqrt{2\pi}} \int_x^\infty \exp\left(-\frac{t^2}{2}\right) dt \quad (3.18)$$

NP-ED provides satisfactory behavior when  $\sigma_n$  is known (or accurately estimated). Unfortunately, when such knowledge is unavailable, its performances degrade very quickly.

### 3.3.1.3 Learning based ratio statistic

In this section, we aim at introducing general notations to define a statistic as a ratio of transformations of both the currently gathered samples and the past collected information. Mainly the ratio expression is introduced to alleviate the lack of knowledge on the noise level  $\sigma_n^2$ . We argue that the key enabling concept to guaranty given performances within an unknown environment is learning over past information. Thus, it is a joint learning-detection framework.

Let  $h_t = [h_{t,0}, h_{t,1}, \dots, h_{t,N-1}]$  denote a set of  $N$  samples collected in the past slots and memorized. We refer to  $h_t$  as the information or history vector. It is mainly introduced to enable the exploitation of past information on the environment to enhance the behavior of the Cognitive Radio decision making engine. Consequently, the detection outcome can be seen as the output of a decision making policy  $\pi$  that maps the current and past information, represented respectively, by the vectors  $r_t$  and  $h_t$  into a binary value  $d_t = \pi(r_t, h_t)$ ,  $d_t \in \{0,1\}$ .

Let us introduce the following statistic  $F_t$  and two real functions  $f(\cdot)$  and  $g(\cdot)$  such that:

$$F_t = \frac{f(r_t)}{g(h_t)} \quad (3.19)$$

Mainly, the function  $f(\cdot)$  represents a transformation of the currently received signals at the slot number  $t$ , while, the function  $g(\cdot)$  aims at extracting information on the noise of the sensed channel using past information. Since  $g(h_t)$  provides an estimation of the noise level, it is well known that the estimation uncertainty implies a less effective detection. Namely, there exist an *SNR wall* under which it is theoretically impossible to detect primary users' activity [109]. In the rest of this report, we consider the following well known form of the functions  $f(\cdot)$  :

$$f(r_t) = \frac{T_t}{M} \quad (3.20)$$

### 3.3.1.4 Learning model and tools

#### 3.3.1.4.1 History vector modeling

Let us consider the particular case of a history vector  $h_t$  containing all collected samples. Moreover let us assume that  $P(H_0) \neq \{0,1\}$ . In other words, the probed channel does not remain in the same state (busy or idle) indefinitely. In this case, a fair assumption would be to consider the vector  $h_t$  as a mixture of Gaussian distributions. Thus the history vector of observations is assumed to be drawn from a stochastic distribution  $\theta$  formalized as a Gaussian Mixture Model (GMM) with  $K$

components (to specify later on real data). Let  $\theta_{k \in \{0, \dots, K-1\}}$  denote the distribution of the  $k^{th}$  component of the distribution  $\theta$ , and  $p_{\theta_k}(\cdot)$  its associated probability density function (*pdf*):

$$p_{\theta_k}(h) = \frac{1}{\sqrt{2\pi V_k}} e^{-\frac{(h-\mu_k)^2}{2V_k}} \quad (3.21)$$

where  $\mu_k = \mathbb{E}[\theta_k]$  and  $V_k \Delta = \mathbb{V}[\theta_k]$ .  $\mathbb{E}$  and  $\mathbb{V}$  refer, respectively, to the expectation and the variance of the considered distribution.

Moreover, let us denote by  $a_{k \in \{0, \dots, K-1\}}$  the proportion of samples drawn from the  $k^{th}$  distribution and  $\mathbf{A}_k$  the set of samples drawn from the distribution  $\theta_k$ . Then we can define  $a_k$  such that:  $a_k = \frac{\#\{\mathbf{A}_k\}}{N}$ . Finally, the *pdf*,  $p_{\theta}(\cdot)$ , of the observed random data  $h$  can be written as:

$$p_{\theta}(h) = \sum_{k=0}^{K-1} a_k p_{\theta_k}(h) \quad (3.22)$$

Notice that depending on the spectrum sensing scenario, only a subset of these parameters might be of interest. As a matter of fact, on the one hand, in the case of extensive offline spectrum sensing, the decision maker, aims at evaluating the occupation pattern of the band. In this case, the parameters  $a_k$  appear crucial. On the other hand, in the case of online learning, evaluating the parameters related to the noise level and/or signal level would be prioritized.

The next subsection will briefly present different possible machine learning approaches to evaluate the parameters of Gaussian mixtures. Anticipating the empirical experiments on real observed data, we will only discuss algorithms that tackles two component ( $K = 2$ ) Gaussian mixtures.

#### 3.3.1.4.2 Learning algorithms

When dealing with a mixture of two Gaussian distributions, several alternative approaches can be suggested by the machine learning community. Among which the most famous and usually implemented: the *Expectation-Maximization* algorithm, the *K-means* algorithm and the *Moment Method*.

##### 3.3.1.4.2.1 Expectation-Maximization (EM)

The EM algorithm is an iterative algorithm that generalizes the maximum likelihood concept to GMMs [110][111]. It is known to be very efficient compared to other algorithms for a same training set. Unfortunately it can become computationally burdensome when the training set or the number of mixtures grow large. It mainly computes the *a posteriori* distribution of the evaluated parameters. This algorithm is usually presented as a soft clustering tool where all samples are used, with specific weights depending on the cluster, to evaluate the parameters of all clusters.

##### 3.3.1.4.2.2 K-means

The K-means algorithm is usually presented as a particular case of EM algorithms where every element of the training set is allocated to only one cluster (i.e., one Gaussian component).

##### 3.3.1.4.2.3 Moment-Method (MM)

The MM algorithm only relies on the empirical moments of the training set. It is a very low complexity algorithm compared to the EM algorithm. It is, unfortunately, also less efficient for a same number of training samples [112].

Reference DR9.3

Although, in general, learning algorithms have nice mathematical proprieties in theory (e.g., in terms of convergence), many practical difficulties can occur when implementing them. Briefly we can stress out, first, the usually high complexity of these algorithms to reach their solution (especially true for the EM algorithm). Moreover, if the stopping criteria are not carefully selected, they could lead to a non convergence of the algorithms. As a consequence, "wrong" estimations of the parameters' distributions could occur. Last but not least, if the algorithms rely on specific hypotheses on the data distributions (e.g., Gaussian mixtures in the case of EM and MM algorithms), not fulfilling these assumptions might significantly affect their behavior.

In the rest of this report, we chose to implement the EM algorithm and to present first results of its performances on real data collected during a spectrum measurement campaign. The goal being to characterize the distribution of the ratio statistic  $F_t$ . As a matter of fact, this would enable the design of a learning based detector where the probabilities of false alarm and miss detection could be evaluated and controlled.

### 3.3.1.5 Simulation performances and discussion

To evaluate the distribution of the statistic  $F_t$ , we conducted series of simulations on the measurements obtained using the USRP. The considered bands are the following: channels Ch08A, Ch10A and Ch11B of the DAB-T standard (described in Section 3.2.3.3). The data collected in these cases contain either noise or signal (i.e.,  $P(H_0) = i, i \in \{0,1\}$ ). For every band and each hypothesis ( $H_0, H_1$ ) we collected 10 million samples.

A quick evaluation of the used data shows that in both cases, whether the samples follow hypothesis  $H_0$  or  $H_1$ , and as a first approximation, we can indeed assume the samples as Gaussian as described in Section 3.3.1.2. However, the Gaussian assumption is not perfect. The Gaussianity of the samples becomes more satisfactory if the data is further down-sampled in software. Since we are limited in the amount of data used, in this study we chose to down-sample the data by a factor 2.

Thus, three training sets composed of a random mixtures ( $K=2$ ) of noise and signal collected from each of these bands are created. Then sequentially, the EM algorithm estimates the noise level (previously referred to as  $g(h_t)$ ) on 400 training sets of 25000 mixed samples of noise and signal. Thus, The learning process uses every time a set of 25000 samples (which could be considered, depending on the standards, as few slots:  $\leq 20$  slots).

We only consider, for the next results, the ratio statistic under hypothesis  $H_0$ . Evaluating this distribution would allow to develop a joint learning-detection framework, where the new detector could improve its detection capabilities while ensuring a given false alarm.

Figure 3.24, Figure 3.25 and Figure 3.26 show the learning results, respectively, for the channels Ch08A, Ch10A and Ch11B. In all figures, three curves appears: the empirical ratio distribution, the theoretical ratio distribution and Fisher-Snedecor distribution. First the empirical distribution represent, the ratio distribution where the function  $f(\cdot)$  is described in Section 3.3.1.3 with  $M = 100$  (however, different values for  $M$  were tested leading to equivalent results). The theoretical ratio distribution presents the simulated distribution of a ratio of independent scaled-Chi-square and scale-inverse Chi-square distributions with parameters respectively  $M = 100$  and  $N = 25000$ . This is due to the fact that the EM algorithm computes the posterior distribution of the variance, which is known to follow a scale-inverse Chi-square distribution. Finally, a Fisher-Snedecor distribution with parameters  $M = 100$  and  $N = 25000$  is also presented as possible approximation. This latter is usually employed in the analysis of variance. Since it only depends on known parameters, this approximation might be convenient to design a future detector.

Notice that in all cases, the empirical distribution can be fit, as a first approximation, by any of the other distributions. More specifically, in Figure 3.26 the empirical ratio distribution seems particularly well fitted. The biased observed can be explained by two factors: on the one hand, as noticed before, the samples are not perfectly Gaussian. On the other hand the EM algorithm stops sometimes before convergence which leads to a bad evaluation of the noise level. This results seems to suggest that is indeed possible to design a detector that relies on *a priori* known parameters  $M$  and  $N$ . Unfortunately although, these curves are interesting, they cannot be generalized yet. To confirm these results and to design an adapted joint learning-detector, a rigorous theoretical analysis supported by extensive measurements are needed.

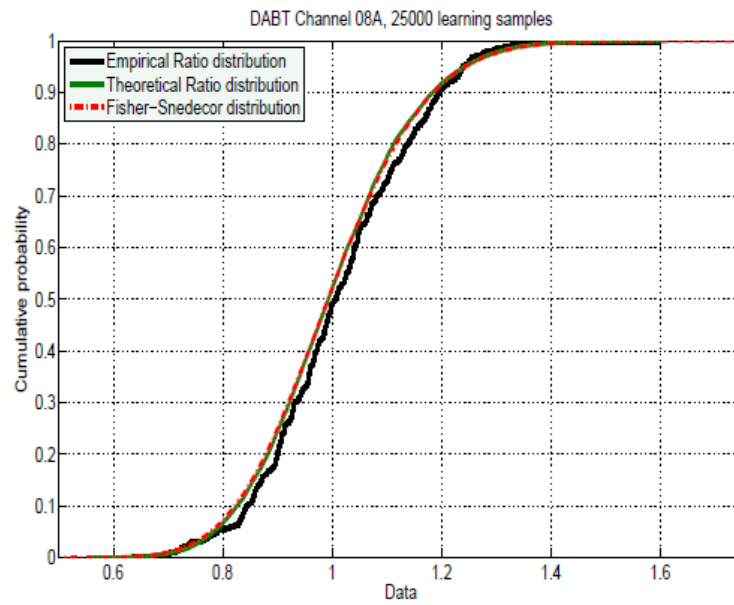


Figure 3.24 – Learning results tested on the channel 08A of the DAB-T standard. The curves compare the empirical ratio statistic to both the theoretical ratio distribution and Fisher-Snedecor distribution.

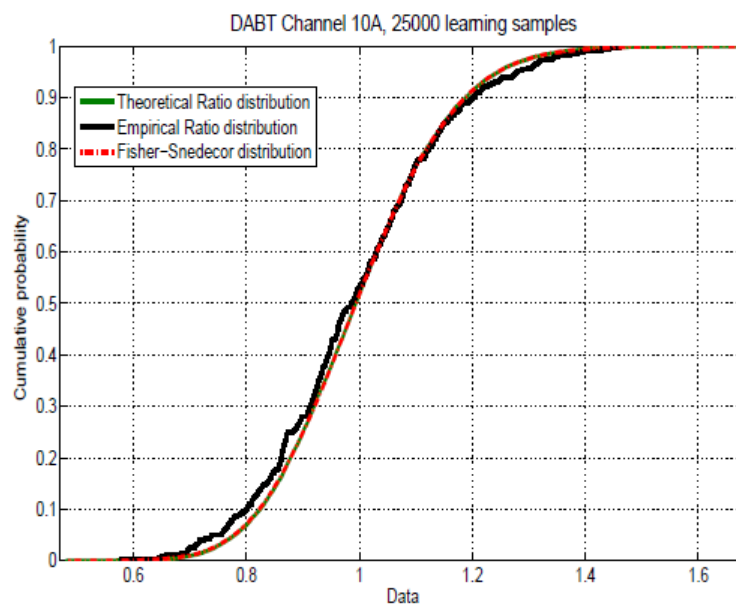


Figure 3.25 – Learning results tested on the channel 10A of the DAB-T standard. The curves compare the empirical ratio statistic to both the theoretical ratio distribution and Fisher-Snedecor distribution.



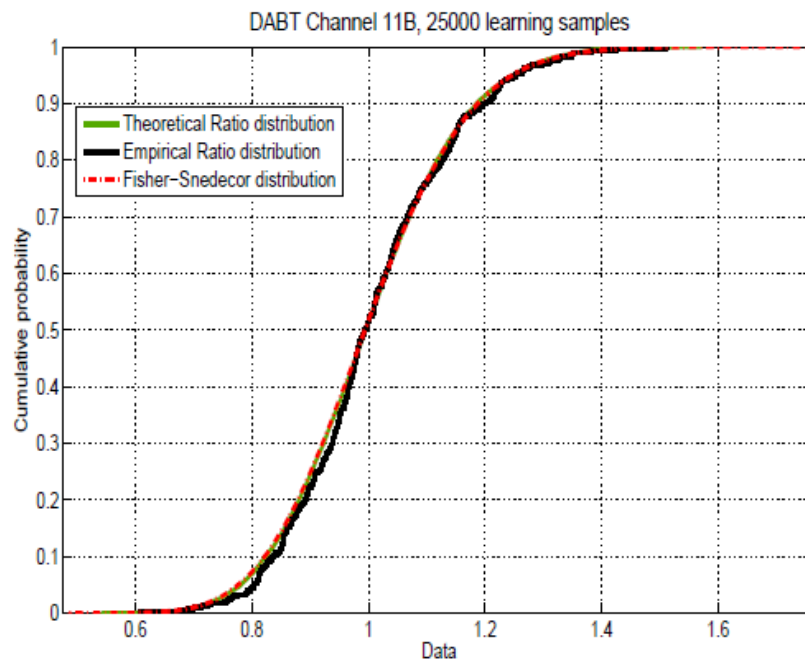


Figure 3.26 – Learning results tested on the channel 11B of the DAB-T standard. The curves compare the empirical ratio statistic to both the theoretical ratio distribution and Fisher-Snedecor distribution.

#### 3.3.1.6 Conclusion

We ventured, in this study, the analysis of an energy detector with no *a priori* information on the noise level. It relies on the computation of a statistic based on the ratio of a function of the currently collected samples and of some information provided by a learning algorithm that exploits past information on the environment. Thus a joint learning-detection framework was suggested. A first empirical analysis showed that it might be possible to design a detector that depends only on two known parameters: the number of samples in a slot and the number of samples used for the training set. Although this research show interesting results, it is still in its infancy and these results still need to be confirmed. To that purpose a theoretical analysis supported by extensive empirical measurements are currently, under investigation.

### 3.3.2 *Opportunistic Spectrum Access with sensing errors: evaluation of Upper Confidence Bound algorithms performances*

#### 3.3.2.1 Introduction

##### 3.3.2.1.1 Opportunistic Spectrum Access and Cognitive Radio

The concept of Opportunistic Spectrum Access (OSA) has been suggested as a promising approach to exploit frequency band resources efficiently, taking advantage of the various available opportunities. As a matter of fact, during the last century, most of the meaningful spectrum resources were licensed to emerging wireless applications, where the static frequency allocation policy combined with a growing number of spectrum demanding services led to a spectrum scarcity. However, several measurements conducted in the United-States [113], first, and then in numerous other countries, showed a chronic underutilization of the frequency band resources, revealing substantial communication opportunities.

The general concept of OSA defines two types of users: primary users (PUs) and secondary users (SUs). PUs access spectrum resources dedicated to the services provided to them, while SUs refer to a pool of users willing to exploit the spectrum resources unoccupied by PUs at a particular time in a particular geographical area. Since SUs need to access the spectrum while ensuring minimum interference with PUs and without *a priori* knowledge on the behavior of PUs, cognitive abilities (sensing its environment, processing the gathered information, and finally adapting its behavior depending on the environment constraints and users' expectations) are required to enable the coexistence of SUs and PUs. To fulfill these requirements, Cognitive Radio (CR) has been suggested as a promising technology to enable the OSA concept [113][114].

However several challenges arise to achieve an efficient spectrum use relying on CRs. On the one hand, an accurate and reliable detection of PUs activity, and on the other hand, a smart behavior enabling SUs' to adapt their channel selection and access policies to PUs' band occupation pattern. Proposing such algorithms to answer these challenges has been, in the last years, the center of a lot of attention [105][115].

### 3.3.2.1.2 Multi-Armed Bandit models for Opportunistic Spectrum Access

Recently, the Cognitive Radio community gave a particular attention to the Multi-Armed Bandit (MAB) paradigm. In a nutshell, based on the analogy with the one-armed bandit (also known as slot machine), it models a gambler sequentially pulling one of the several levers (multi-armed bandit) on the gambling machine. Every time a lever is pulled, it provides the gambler with a random income usually referred to as reward. Although we assume that the gambler has no *a priori* information on the rewards' stochastic distributions, he aims at maximizing his cumulated income through iterative pulls. In the OSA framework, the SU is modeled as the gambler while the frequency bands represent the levers. The gambler faces at each trial a tradeoff between pulling the lever with the highest estimated payoff (known as *exploitation* phase) and pulling another lever to acquire information about its expected payoff (known as *exploration* phase). We usually refer to this tradeoff as the *exploration-exploitation* dilemma.

Thus, several algorithms were borrowed from the machine learning community [116][117][118] and suggested as possible solutions to learn how to select and access the most available channels [119][120][121]. These algorithms, however assume perfect sensing. Namely, they assume that the SU can acquire an errorless knowledge on the state of the probed channel {idle, busy}. Under these assumptions, secondary users can maximize their cumulated income (channel access and/or throughput), in expectation, while completely avoiding harmful packet collisions with primary users.

The purpose of this study is to introduce a more realistic scenario. Thus we consider the OSA problem as a MAB problem with sensing errors. First, the network model is detailed in Section 3.3.2.2. Then we introduce the well known  $UCB_1$  algorithm in Section 3.3.2.3. In order to understand the behavior of this algorithm within this framework, Section 3.3.2.3.2 provides a theoretical analysis of its performances. Section 3.3.2.4 reports simulation results that illustrate the analysis conducted in Section 3.3.2.3 and, finally, Section 3.3.2.5 concludes.

### 3.3.2.2 Network model

#### 3.3.2.2.1 Framework

We consider the case of one secondary user willing to opportunistically exploit the available spectrum in its vicinity. The spectrum of interest is licensed to a primary network providing  $K$  independent but non-identical channels. We denote by  $k \in \{1, \dots, K\}$  the  $k^{th}$  most available channel. Every channel  $k$  can appear, when observed, in one of these two possible states {idle, busy}. In the rest of the report, we associate the numerical value 0 to a busy channel and 1 to an idle channel. The temporal

Reference DR9.3

occupancy pattern of every channel  $k$  is thus supposed to follow an unknown Bernoulli distribution  $\theta_k$ . Moreover, the distributions  $\Theta = \{\theta_1, \theta_2, \dots, \theta_K\}$  are assumed to be stationary.

In this section we tackle the particular case where PUs are assumed to be synchronous and the time  $t = 0, 1, 2, \dots$ , is divided into slots. We denote by  $\mathbf{S}_t$  the channels' state at the slot number  $t$ :  $\mathbf{S}_t = \{S_{1,t}, \dots, S_{K,t}\} \in \{0, 1\}^K$ . For all  $t \in \mathbb{N}$ , the numerical value  $S_{k,t}$  is assumed to be an independent random realization of the stationary distributions  $\theta_k \in \Theta$ . Moreover, the realizations  $\{S_{k,t}\}_{t \in \mathbb{N}}$  drawn from a given distribution  $\theta_k$  are assumed to be independent and identically distributed. The expected availability of a channel is characterized by its probability of being idle. Thus, we define the availability  $\mu_k$  of a channel  $k$ , for all  $t$  as:

$$\mu_k = \mathbb{E}[\theta_k] = \mathbb{P}(\text{channel } k \text{ is free}) = \mathbb{P}(S_{k,t} = 1) \quad (3.23)$$

where  $\mu_1 > \mu_2 \geq \dots \geq \mu_k \geq \dots \geq \mu_K$  without loss of generality.

Let us refer to the decision making engine of the CR equipment as Cognitive Agent (CA). The CA can be seen as the brain of the CR device. At every slot number  $t$ , the SU has to choose a channel to sense. To do so, the CA relies on the outcome of past trials. We denote by  $i_t$  the gathered information until the slot  $t$ . We assume that the SU can only sense one channel per slot. Thus selecting a channel can be seen as an action  $a_t \in \mathbf{A}$  where the set of possible actions  $\mathbf{A} = \{1, 2, \dots, K\}$  refers to the set of channels available.

Thus, we can model the CA as a policy  $\pi$  that maps for all  $t \in \mathbb{N}$ , the information  $i_t$  to an action  $a_t$ :

$$a_t = \pi(i_t) \quad (3.24)$$

The outcome of the sensing process is denoted by the binary random variable  $X_t \in \{0, 1\}$ . In the case of perfect sensing,  $X_t = S_{a_t,t}$ , where  $a_t$  refers to the channel selected at the slot number  $t$ . However since we assumed that sensing errors can occur, the value of  $X_t$  depends on the receiver operating characteristic (ROC). The ROC defines the accuracy and the reliability of a sensor through the measure of two types of errors: on the one hand, detecting a PU on the channel when it is free usually referred to as *false alarm*. On the other hand, assuming the channel free when a PU is occupying it usually referred to as *miss detection*. Let us denote by  $\varepsilon$  and  $\delta$ , respectively the probability of false alarm, and the probability of miss detection characterizing the CR equipment:

$$\begin{cases} \varepsilon = \mathbb{P}_{fa} = \mathbb{P}(X_t = 0 | S_{a_t,t} = 1) \\ \delta = \mathbb{P}_{md} = \mathbb{P}(X_t = 1 | S_{a_t,t} = 0) \end{cases} \quad (3.25)$$

Finally, the outcome of the sensing process can be seen as the output of a random policy  $\pi_s(\varepsilon, \delta, S_{k,t})$  such that:

$$X_t = \pi_s(\varepsilon, \delta, S_{k,t}) \quad (3.26)$$

The design of such policies [105] is however out of the scope of this study. Moreover  $\{\varepsilon, \delta\}$  are assumed to be unknown.

Depending on the sensing outcome  $X_t \in \{0, 1\}$ , the CA can choose to access the channel or not. We denote by  $\pi_a(X_t) \in \{0, 1\}$  the access decision, where 0 refers to *access denied* and 1 refers to *access granted*. The access policy  $\pi_a$  chosen in this section can be described as: *access the channel if*

*sensed available*", i.e.  $\pi_a(X_t) = 1_{\{X_t=1\}}$ . Notice that we assume the ROC to be designed such that the probability of miss detection  $\delta$  is smaller or equal to a given interference level allowed by the primary network. Moreover, we assume that if interference occurs, the transmission of the secondary user fails. When channel access is granted, the CA can receive a numerical acknowledgement. This feedback informs the CA of the state of the transmission {succeeded, failed}. Finally, we assume that for every transmission attempt, a packet  $D_t$  is sent. At the end of every slot  $t$ , the CA can use the different information available to compute a numerical value, usually referred to as reward  $r_t$  in the MAB literature. This reward informs the CA of its current performance. The form of the reward as well as the evaluation of the selection policy  $\pi$  are described and discussed in the next subsection.

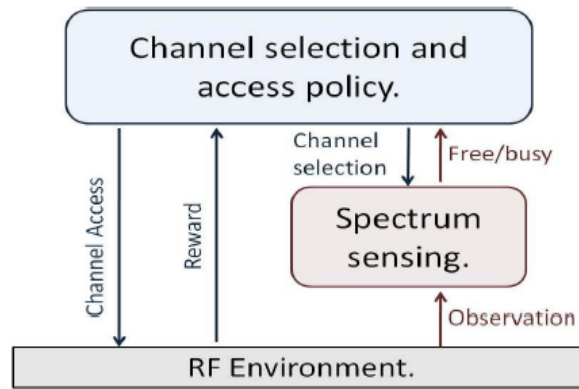


Figure 3.27 – Representation of a CA observing and accessing an RF environment.

Finally, the sequential steps described hereabove formalize the OSA framework we are dealing with as a MAB problem with sensing errors. A schematic representation of a CA observing and accessing an RF environment is illustrated in Figure 3.27.

#### 3.3.2.2.2 Performance evaluation

Thus, at the end of every slot  $t$ , the CA can compute a numerical value that evaluates its performance. In the case of OSA, we focus on the transmitted throughput. Relying on the previously introduced notations, the throughput achieved by the SU at the slot number  $t$  can be defined as:

$$r_t \Delta = D_t S_t \pi_a(X_t) \quad (3.27)$$

which is the reward considered in this particular framework. For the sake of simplicity we assume a normalized transmitted packet for all channels and all  $t$ ,  $D_t = 1$  bit. We can notice that the choices made on the access policy  $\pi_a$  and  $D_t$ , simplify the expression of the reward such that:

$$r_t = S_{a_t,t} X_t \quad (3.28)$$

where  $r_t$  equals 1 only if the channel is free and the CA senses it free. Consequently, the expected reward achievable using a channel  $a_t \in \mathbf{A}$  can be easily computed:

---

Indicator function:  $1_{\{\text{logical\_expression}\}} = \{1 \text{ if logical\_expression=true ; } 0 \text{ if logical\_expression=false}\}$ .

$$\mathbb{E}[r_t] = \mathbb{P}(X_t = 1 | S_{a_t,t} = 1) \mathbb{P}(S_{a_t,t} = 1) = (1 - \varepsilon) \mu_{a_t} \quad (3.29)$$

Thus, we refer to the channel  $\mu_1 = \max_k \mu_k$ , that maximizes the reward, as optimal whereas the other channels are said to be suboptimal. We usually evaluate the performance of a policy by its expected cumulated throughput after  $t$  slots defined as:

$$W_t^\pi = \mathbb{E} \left[ \sum_{m=0}^{t-1} r_m \right] \quad (3.30)$$

A good policy  $\pi$  is assumed to maximize the quantity  $W_t^\pi$ .

An alternative representation of the expected performance of a policy  $\pi$  until the slot number  $t$  is described through the notion of *regret*  $R_t^\pi$  (or expected regret). The regret is defined as the gap between the maximum achievable performance in expectation, if the most available channel were chosen, and the expected cumulated throughput achieved by the policy  $\pi$ :

$$R_t^\pi = \sum_{m=0}^{t-1} \max_{a_t \in \mathcal{A}} \mathbb{E}[r_t] - W_t^\pi \quad (3.31)$$

Hence, we define the regret of a channel selection policy  $\pi$  when sensing errors can occur as:

$$R_t^\pi = \sum_{m=0}^{t-1} (1 - \varepsilon) \mu_1 - W_t^\pi \quad (3.32)$$

The general idea behind the notion of *regret* can be explained as follows: if the CA knew *a priori* the values of  $\{\mu_k\}_{k \in \mathcal{A}}$ , the best choice would be to always select the optimal channel  $\mu_1$ . Unfortunately, since usually the CA lacks that information, it has to learn it. For that purpose, the CA explores the different channels to acquire better estimations of their expected availability. While exploring it should also exploit the already collected information to minimize the regret during the learning process. This leads to an exploration-exploitation tradeoff. Thus, the *regret* represents the loss due to suboptimal channel selections during the learning process.

Maximizing the expected throughput is equivalent to minimizing the cumulated expected regret. In the rest of the report, we will use the following equivalent formula of the regret:

$$R_t^\pi = (1 - \varepsilon) \sum_{k=1}^K \Delta_k \mathbb{E}[T_k(t)] \quad (3.33)$$

where  $\Delta_k = \mu_1 - \mu_k$  and  $T_k(t)$  refers to the number of times the channel  $k$  has been selected from instant 0 to instant  $t-1$ .

Finally we introduce a loss function  $\mathbb{L}^\pi(t)$  that evaluates the loss of performance due to sensing errors compared to the perfect sensing framework.

$$\mathbb{L}^\pi(t) = t \max_{a_t \in \mathcal{A}} \mu_{a_t} - W_t^\pi \quad (3.34)$$

The next section reminds, first, the form of the  $UCB_1$  algorithm. Then we prove that even if the characteristics of the receiver,  $\{\varepsilon, \delta\}$ , are unknown, this algorithm suffers a number of suboptimal channel selections upper bounded by a logarithmic function of the slot number  $t$ . Finally we conclude by an evaluation of both the regret  $R^\pi$  and the loss function  $\mathbb{L}^\pi$ .

### 3.3.2.3 Upper Confidence Bound index for OSA with sensing errors

#### 3.3.2.3.1 UCB<sub>1</sub> index

In a previous work [121] the authors suggested and discussed the use of Upper Confidence Bound (UCB) algorithms to build an efficient cognitive agent in order to tackle the OSA issue with perfect sensing. As a matter of fact, UCB based policies are known to offer a good solution to the exploration-exploitation tradeoff. The general approach suggested by the UCB algorithms aims at selecting actions based on indexes that provide an optimistic evaluation on the rewards associated to the channels the secondary user can potentially exploit.

A usual approach to evaluate the average reward provided by a resource  $k$  is to consider a confidence bound for its sample mean. Let  $\bar{X}_{k,T_k(t)}$  be the sample mean of the resource  $k \in \mathbf{A}$  after being selected  $T_k(t)$  times at the step  $t$ :

$$\bar{X}_{k,T_k(t)} = \frac{\sum_{m=0}^{t-1} r_m \cdot 1_{\{a_m=k\}}}{T_k(t)} \quad (3.35)$$

For every  $k \in \mathbf{A}$  and at every step  $t = 0, 1, 2, \dots$ , an upper bound confidence index (UCB index),  $B_{k,t,T_k(t)}$ , is a numerical value computed from  $i_t$ . For all  $k$ ,  $B_{k,t,T_k(t)}$  gives an over estimation of the expected reward obtained when the resource  $k$  is selected at a time  $t$  after being sensed  $T_k(t)$ .

The UCB indexes we use in this section have the following general expression:

$$B_{k,t,T_k(t)} = \bar{X}_{k,T_k(t)} + A_{k,t,T_k(t)} \quad (3.36)$$

where  $A_{k,t,T_k(t)}$  is an upper confidence bias added to the sample mean. In this section we consider the  $UCB_1$  index which has the upper confidence bias  $A_{k,t,T_k(t)}$  form:

$$A_{k,t,T_k(t)} = \sqrt{\frac{\alpha \cdot \ln(t)}{T_k(t)}} \quad (3.37)$$

An UCB policy  $\pi$  selects the next channel  $a_t$  based on the past information  $i_t$  such that:

$$a_t = \pi(i_t) = \underset{k}{\operatorname{argmax}}(B_{k,t,T_k(t)}) \quad (3.38)$$

A detailed version of the implementation of the algorithm  $UCB_1$  was described in a previous work [121].

#### 3.3.2.3.2 UCB<sub>1</sub> : channel selection with sensing errors

The following theorem shows that although the CA suffers imperfect sensing, it still can converge quickly to the most available channel.

**Theorem 1 (Logarithmic suboptimal channel selection)** *Let us consider a receiver with sensing characteristics  $\{\varepsilon, \delta\}$ , and an "access the channel if sensed available" policy. We consider the instantaneous normalized throughput as the CA's reward.*

Reference DR9.3

Then for all  $K \geq 2$ , if the receiver runs the  $UCB_1(\alpha > 1)$  policy on  $K$  channels having Bernoulli occupation pattern distributions  $\theta_1, \dots, \theta_K$  with support in  $[0, 1]$ , the expected number of selections  $\mathbb{E}[T_k(t)]$  for all suboptimal channels  $k \in \{1, 2, \dots, K\}$  after  $t$  slots is upper bounded by a logarithmic function such that:

$$\mathbb{E}[T_k(t)] \leq \frac{4\alpha \ln(t)}{((1-\varepsilon)\Delta_k)^2} \quad (3.39)$$

**Proof.** Due to space limitations and in order to make this report as self content as possible we provide an intuitive proof:

Let us consider Bernoulli occupation pattern distributions  $\Theta = \{\theta_1, \dots, \theta_K\}$  with support in  $[0, 1]$ . As noticed previously, CR equipment' sensors can be seen as functions  $\pi_s(\varepsilon, \delta, \cdot)$  with parameters  $\{\varepsilon, \delta\}$  that map a random realisation  $S_{k,t}$  drawn from the distribution  $\theta_k$ , at the slot number  $t \in \mathbb{N}$ , into a binary value  $X_t \in \{0, 1\}$  such that:

$$X_t = \pi_s(\varepsilon, \delta, S_{k,t}) \quad (3.40)$$

Let us define the set of reward distributions  $\tilde{\Theta} = \{\tilde{\theta}_1, \dots, \tilde{\theta}_K\}$  such that:  $\forall t \in \mathbb{N}$ , the reward  $r_t = S_{k,t}X_t$  computed when the channel  $k$  is selected follows the distribution  $\tilde{\theta}_k$ . Then the distributions  $\tilde{\Theta} = \{\tilde{\theta}_1, \dots, \tilde{\theta}_K\}$  are bounded distributions with support in  $[0, 1]$ .

Moreover let us define:

$$\forall k \in \{1, 2, \dots, K\}, \tilde{\mu}_k \Delta = \mathbb{E}[\tilde{\theta}_k] \quad (3.41)$$

Under the assumptions of this theorem, we can write for all  $k \in \{1, 2, \dots, K\}$ :

$$\begin{cases} \tilde{\mu}_k = (1-\varepsilon)\mu_k \\ \tilde{\Delta}_k = (1-\varepsilon)\Delta_k \end{cases} \quad (3.42)$$

Consequently we can apply the following theorem (Cf. [118] for proof):

For all  $K \geq 2$ , if policy  $UCB_1(\alpha > 1)$  is run on  $K$  channels having arbitrary reward distributions  $\theta_1, \dots, \theta_K$  with support in  $[0, 1]$ , then:

$$\mathbb{E}[T_k(t)] \leq \frac{4\alpha}{\Delta_k^2} \ln(t) \quad (3.43)$$

Finally, by substituting:  $\mu_k \Leftrightarrow (1-\varepsilon)\mu_k$  and  $\Delta_k \Leftrightarrow (1-\varepsilon)\Delta_k$  we obtain the stated result:

$$\mathbb{E}[T_k(t)] \leq \frac{4\alpha \ln(t)}{((1-\varepsilon)\Delta_k)^2} \quad (3.44)$$

The consequences of Theorem 1 are twofold: on the one hand, as in the case of perfect sensing,  $UCB_1$  based policies used in the case of OSA with sensing errors spend exponentially more time probing the optimal channel than suboptimal channels. On the other hand, we notice that the exploration phase, characterized by the time spent on suboptimal channels increases with a scale  $\frac{1}{(1-\varepsilon)^2}$  compared to

the perfect sensing framework. Thus, as expected the accuracy of the sensor is crucial in order to maximize SUs' profit.

**Corollary 1 (Regret and Loss function)** *Assuming that we verify the assumptions and conditions of Theorem 1, the regret and the loss function can be upper bounded as follows:*

$$\begin{cases} R_t^\pi \leq \sum_{k=1}^K \frac{4\alpha \ln(t)}{((1-\varepsilon)\Delta_k)} \\ L^\pi(t) \leq \varepsilon t + \sum_{k=1}^K \frac{4\alpha \ln(t)}{((1-\varepsilon)\Delta_k)} \end{cases} \quad (3.45)$$

**Proof.** First, we can notice that:

$$L^\pi(t) = \varepsilon t + R_t^\pi \quad (3.46)$$

The rest of the proof is an immediate application of the result of equation (3.39) of Theorem 1, to equations (3.33) and (3.34).

The first result of the corollary shows that the regret, as defined in machine learning, is still upper bounded by a logarithmic function of the slot number  $t$ . However, as for  $\mathbb{E}[T_k(t)]$ , due to sensing errors, the regret increases by a scaling factor equal to  $1/(1-\varepsilon)$ . The second result shows that compared to the perfect sensing framework, the SU suffers linear expected loss due to sensing errors.

#### 3.3.2.4 Simulations

In this section we present and comment simulation curves focusing on the regret and on the optimal channel selection. The curves compare the behavior of the  $UCB_1$  algorithm under various sensing characteristics.

We consider, in our simulations, one SU willing to exploit a pool of 10 channels. The parameters of the Bernoulli distributions are chosen as follows:  $[\mu_1, \mu_9, \dots, \mu_{10}] = [0.9, 0.8, 0.8, 0.7, 0.6, 0.5, 0.4, 0.3, 0.2, 0.1]$ . These distributions characterize the temporal occupancy of these channels. The sensing capabilities of the SU are fixed by the parameter  $\varepsilon$ . Since we only evaluate, in this section, the regret and the optimal channel selection, we purposely ignore the parameter  $\delta$  since it does not appear in the theoretical results. Notice however that in real scenarios,  $\varepsilon$  and  $\delta$  are related to one another. In order to evaluate the impact of these parameters on the CA's behavior, we chose to simulate the  $UCB_1$  algorithm with four different sensors:  $\varepsilon = [0, 0.1, 0.25, 0.4]$ . Moreover, in order to respect the conditions stated in Theorem 1,  $UCB_1$  was run with the parameter  $\alpha = 1.2$ . Every numerical result reported hereafter is the average of the values obtained over 100 experiments.



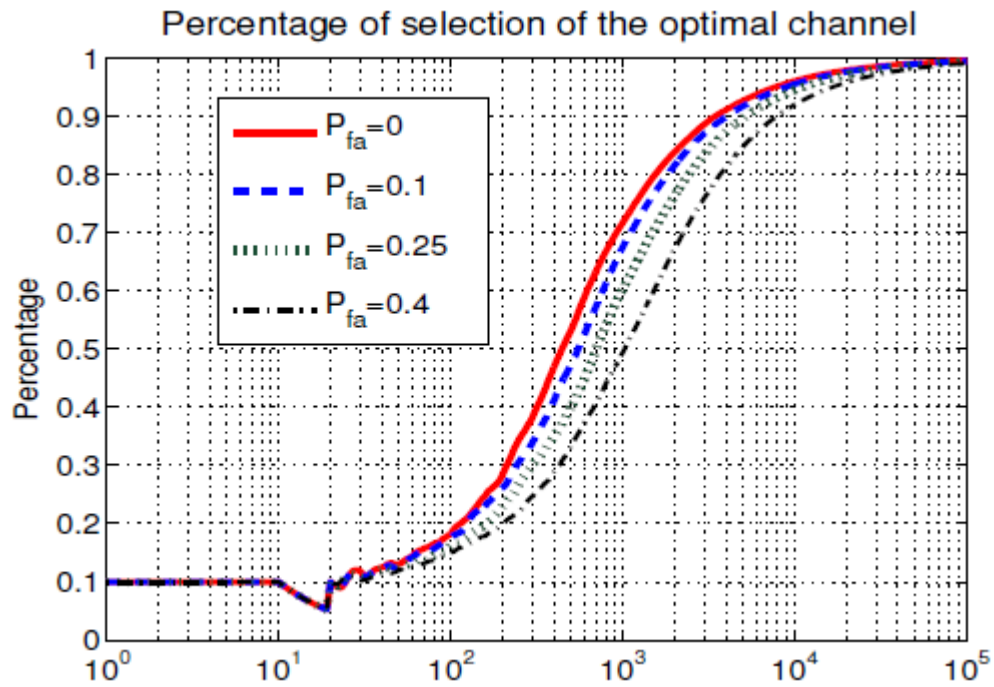


Figure 3.28 – Percentage of time the  $UCB_1$ -based CA selects the optimal channel under various sensing errors frameworks (over 10 available channels).

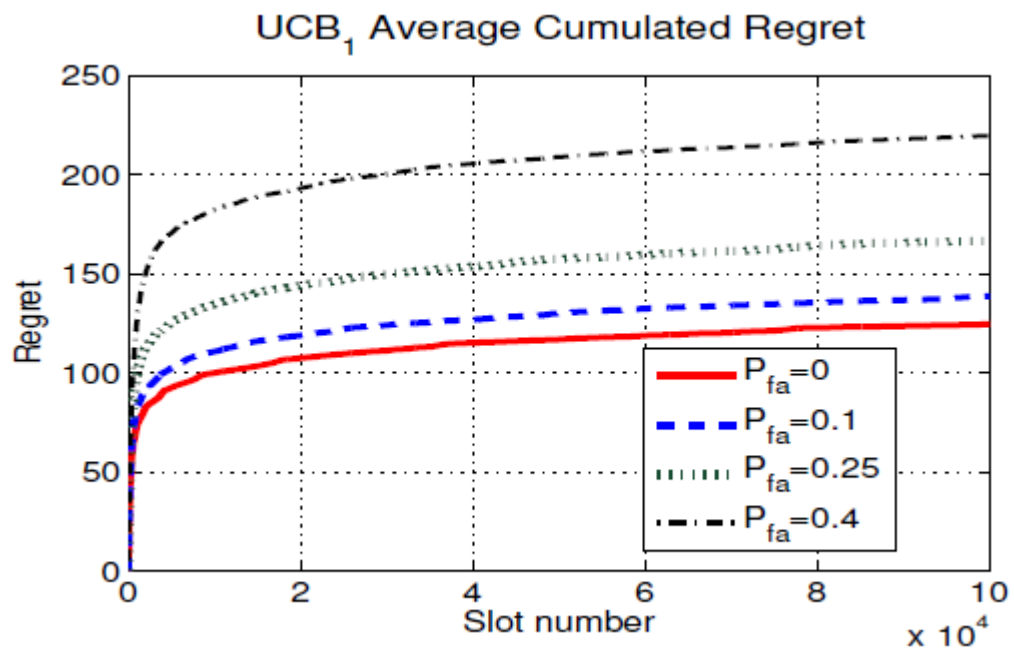


Figure 3.29 –  $UCB_1$  algorithm and Opportunistic Spectrum Access problem with sensing errors: regret simulation results.

Figure 3.29 shows the evolution of the average regret achieved by the  $UCB_1$  policy under various sensing characteristics. As expected (Cf. Corollary 1), we observe that the regret first increases rather rapidly with the slot number and then more and more slowly. We remind that the smaller the regret is, the better is the algorithm behaving. This shows that the UCB policy is able to process the past information in an appropriate way even if there are sensing errors such that most available resources are favored with time. Actually, one has the theoretical guarantee that it will converge to  $(1-\varepsilon)\mu_1$ , which is the largest probability of availability of the optimal channel within the herein modeled imperfect sensing framework. We however notice that the sensing errors increase the cumulated regret. The smallest regret is achieved as expected in the case of perfect sensing ( $\varepsilon = P_{fa} = 0$ ). Moreover, we can notice that the ratio of the regret in the case of perfect sensing and in the case of sensing errors characterized by  $\varepsilon \neq 0$  is approximately equal to  $1/(1-\varepsilon)$  which supports the theoretical results.

The optimal channel selection percentage  $p$  achieved by the  $UCB_1$  algorithm until the slot number  $t$  is illustrated in Figure 3.28, where  $p = 100 \cdot \frac{\sum_{m=0}^{t-1} 1_{\{a_m=1\}}}{t}$ . As one can observe the percentage of optimal channel selection increases progressively and tends to get closer and closer to 100% as the slot number increases.

As for the regret analysis, we observe that the performance of the  $UCB_1$  algorithm decreases when the  $P_{fa}$  increase. Thus, the  $UCB_1$  with perfect sensing performs best. The increasing rate of the other curves is slower depending on their sensing capabilities. As proven in the theoretical analysis provided hereabove, all  $UCB_1$  algorithms converge to the best channel, however the less accurate is their sensing outcome, the slower becomes their convergence rate.

### 3.3.2.5 Conclusion

We tackled in this study the OSA problem with sensing errors within a MAB framework. We argued that the  $UCB_1$  algorithm used as channel selection policy can still offer a good tradeoff to the exploration-exploitation dilemma faced by the SU. Thus, we showed that the time spent on suboptimal channels is upper-bounded by a logarithmic function of the slot number, ensuring a quick convergence to the optimal channel. Although these preliminary results are promising, many questions still need to be answered especially when several SUs compete to access the same resources.

## 3.4 Conclusions

This section has presented the different activities associated with the dynamic use of spectrum in wireless networks carried out in the context of WPR9. They have been tackled from both an empirical and a theoretical perspective, carrying out a measurement campaign used in the evaluation of sensing algorithms, and then developing spectrum selection mechanisms. The following outcomes have been obtained:

- After the previous results described in previous deliverable DR9.2 [5], the measurement campaign on spectrum occupancy has focused during the third year on the obtention of the spatial correlation from measurements in different positions. Spatial correlation has interest when devising cooperative spectrum sensing schemes since the process is more robust when samples from low correlated sensors are used. The spatial correlation study was conducted in the 1800–1880 MHz and 1880–2290 MHz band in a grid of different positions. The analysis has been carried out considering both the correlation as a function of the physical distance and of the SNR difference. Results have revealed that the SNR difference between two arbitrary

points can be considered as an appropriate parameter as a function of which spatial correlation metrics on spectrum occupancy can be adequately analysed and described.

- The energy detection method has been applied to different empirical measurements using a USRP platform. Obtained results indicate that certain technology-dependent inherent properties may result in different detection performances for various primary radio technologies. Differences are more noticeable for short sensing intervals and, as the sensing interval increases, the energy detectors' performance becomes more similar for different radio technologies and thus more independent of the primary signal being detected. As a result, the energy detection principle in the real world may exhibit significantly divergent detection performances depending on the primary signal under detection.
- A joint learning-detection framework has been developed for energy detection with no a priori information on the noise level. It relies on the computation of a statistic based on the ratio of a function of the currently collected samples and of some information provided by a learning algorithm that exploits past information on the environment. The framework has been empirically evaluated using results from the measurement campaign. First analysis has shown that it might be possible to design a detector that depends only on two known parameters: the number of samples in a slot and the number of samples used for the training set.
- Opportunistic Spectrum Access for secondary users based on the MAB framework has been studied in the presence of sensing errors. Decision making with respect to the channel to select for sensing and eventually transmitting is based on prior knowledge obtained from past trials through machine learning mechanisms. It has been obtained that the UCB<sub>1</sub> algorithm used as channel selection policy can still offer a good tradeoff to the exploration-exploitation dilemma faced by the SU, and that the time spent on suboptimal channels is upper-bounded by a logarithmic function of the slot number, ensuring a quick convergence to the optimal channel.

## 4 CONCLUSIONS

### 4.1 Overview of most significant outcomes

This deliverable has presented the research activities carried out in the context of the five working groups of WPR9, dealing with radio resource and spectrum management in heterogeneous scenarios. In the following the most significant outcomes of the different activities is summarised:

- Activities in WG1 have focused on the JRRM strategies in heterogeneous scenarios. In this framework, VHO performance policies in a scenario with coexisting low and high bit rate networks has been studied, using a new and simple model based on mobility, capable to combine multi-service traffic and heterogeneous networks capacity, and producing different performance metrics such as blocking or delay. Activities have also considered the radio resource management when virtual network operators share the network infrastructure, proposing a Cooperative Virtual Network RRM model that allows supporting the minimum bandwidth requirement in a wireless cluster, composed by several physical base stations from different RATs in a given coverage area. Finally, energy efficiency awareness in JRRM has been considered with the presentation of new metrics related with energy consumption in the radio interface and how they can be improved by the use of smart VHO strategies.
- Activities in WG2 have focused on the problem of spectrum allocation for OFDMA networks. The research on single-cell scenarios has investigated different algorithms elaborating trade-offs between different objective functions and quality-of-service indicators. New strategies have been proposed that allow achieving an efficient trade-off between resource efficiency and fairness. The research on multi-cell scenarios has addressed both the problems of distributed and coordinated resource allocation. In the first case, in order to counteract multiple access interference a loose cross layered architecture that integrates a packet scheduler with an adaptive resource allocator has been proposed. Each cell operates in a distributed way without any central controller, and dynamically adjusting the load to converge to a stable allocation. It has been obtained that the proposed architecture is able to guarantee both high spectral efficiency and throughput fairness among flows. In turn, in the coordinated resource allocation case, two algorithms have been proposed, derived from the utility theory. Comparison against other algorithms without any coordination or with fractional frequency reuse has revealed that significant gains in throughput and fairness can be achieved.
- Activities in WG3, dealing with game theory for RRM optimization have focused during the third year on the concept of crystallized rate regions, applying it to the MIMO and OFDM interference channels. It has been proposed to use the correlated equilibrium concept instead of the well-known Nash equilibrium. Also a new VCG auction utility function and the modified regret-matching algorithm have been derived for the generalized MIMO case. The approach has been verified in simulations of the 2-user 2-BS scenarios, showing that the proposed regret-matching algorithm provides rapid convergence to the correlated equilibrium. These activities have complemented prior ones carried out during the second year in which game theory was applied to the acquisition of resources in a cognitive radio system.
- Activities in WG4 have targeted a spectrum measurement campaign to identify the metrics of spectrum utilisation in the different bands, with the objective to apply the obtained knowledge to the cognitive radio design. During previous years, measurements in the whole band from 75 MHz to 7075 MHz aimed at obtaining the temporal usage patterns in the different bands, while during the last year, spatial correlation from measurements in different positions has been obtained in some specific bands. The outcomes from the measurement campaign have been used to empirically evaluate a joint learning-detection framework that has been proposed for energy detection with no a priori information on the noise level. It relies on the computation of a statistic based on the ratio of a function of the currently collected samples

and of some information provided by a learning algorithm that exploits past information on the environment.

- Activities in WG5 have focused on developing opportunistic spectrum access mechanisms for secondary users based on the Multi Armed Bandit framework. Decision making with respect to the channel to select for sensing and eventually transmitting is based on prior knowledge obtained from past trials through machine learning mechanisms. It has been obtained that even in the presence of sensing errors the proposed channel selection algorithm can still offer a good trade-off to the exploration-exploitation dilemma faced by the SU, while ensuring a quick convergence to the optimal channel. It is envisaged as future work to empirically test this algorithm making use of the measurements of the abovementioned campaign.

## 4.2 Integration activities

One of the main aims of the NEWCOM<sup>++</sup> project is the integration of the researchers and dissemination of the investigation results. Thus, several joint papers summarizing the outcomes of different WGs have been submitted to selected international conferences and workshops. These include:

- E. B. Rodrigues, Marco Moretti, Pawel Sroka, Giulio Dainelli, Fernando Casadevall, "Sub-carrier Allocation and Packet Scheduling in OFDMA-based Cellular Networks", NEWCOM<sup>++</sup> Acorn Workshop, Barcelona, 30th March – 1st April 2009. Joint paper UPC, PUT, CNIT.
- Emanuel B. Rodrigues, Fernando Casadevall, Pawel Sroka, Marco Moretti, Giulio Dainelli, "Resource Allocation and Packet Scheduling in OFDMA-Based Cellular Networks", Crowncom 2009, Hannover, 22nd – 24th June 2009. Joint paper UPC, PUT, CNIT.
- Emanuel B. Rodrigues, Michael L. Walker, and Fernando Casadevall "On the Influence of Packet Scheduling on the Trade-Off Between System Spectral Efficiency and User Fairness in OFDMA-Based Networks", EUNICE Conference 2009, Barcelona, September, 2009. Joint paper UPC, CNIT.
- S. Medina, M. Debbah, S. Lasaulce, H. Bogucka, "On the Benefits of Bandwidth Limiting in Decentralized Vector Multiple Access Channels", Crowncom 2009, Hannover, 22nd – 24th June 2009. This paper received the best student paper award at Crowncom 2009 conference. Joint paper CNRS, PUT.
- Miguel López-Benítez, Fernando Casadevall, Anna Umbert, Rachid Hachemani, Jacques Palicot, Christophe Moy "Spectral Occupancy Measurements in Urban Areas and their Applicability to the Blind Standard Recognition Sensor Concept", NEWCOM<sup>++</sup> Acorn Workshop, Barcelona, 30th March – 1st April 2009. Joint paper UPC, CNRS.
- M. López-Benítez, F. Casadevall, A. Umbert, J. Perez-Romero, R. Hachemani, J. Palicot, C. Moy, "Spectral Occupation Measurements and Blind Standard Recognition Sensor for Cognitive Radio Networks", Crowncom 2009, Hannover, 22nd – 24th June 2009. Joint paper UPC, CNRS.
- Miguel López-Benítez, Fernando Casadevall, Anna Umbert, Rachid Hachemani, Christophe Moy, Jacques Palicot "Blind Standard Recognition Sensor Validation with Data from Measurement Campaign", presentation at the workshop on Dynamic Spectrum Management in Cognitive Radio Networks held the day before the ICT Mobile Summit in Santander, 9th June 2009. Joint paper UPC, CNRS.
- M. López-Benítez, F. Casadevall, C. Martella, "Performance of spectrum sensing for cognitive radio based on field measurements of various radio technologies", in Proceedings of the 16th European Wireless Conference (EW 2010), Special session on Cognitive Radio, Lucca, Italy, April 12-15, 2010. Joint paper UPC, CNIT.

Reference DR9.3

- Adrian Kliks, Pawel Sroka, Merouane Debbah, "MIMO Crystallized Rate Regions", Proc. European Wireless 2010, Lucca, Italy, April 12-15, 2010. Joint paper PUT, CNRS.
- A. Serrador, A. Carniani, V. Corvino, L. M. Correia "Radio Access to Heterogeneous Wireless Networks through JRRM Strategies" Future Networks and Mobile Summit in Florence, 16-18th June, 2010. Joint paper IST-TUL, CNIT.
- M. López-Benítez, F. Casadevall, C. Martella "Empirical Study of Energy Detection-Based Spectrum Sensing for Different Radio Technologies", Poster presented at the NEWCOM<sup>++</sup> Dissemination day, Florence, June, 2010. Joint paper UPC, CNIT.
- Pawel Sroka, Adrian Kliks, Merouane Debbah, "MIMO-OFDM Crystallized Rate Regions", to be published at National Conference on Radiocommunications and Broadcasting (KKRRiT) 2010, Krakow, Poland, June, 2010. Joint paper PUT, CNRS.
- W. Jouini, A. Nafkha, M. López-Benítez, J. Pérez-Romero, "Joint Learning-Detection Framework: an Empirical Analysis", NEWCOM<sup>++</sup> WPR8/WPR9 workshop, Bologna, November, 25th, 2010. Joint paper CNRS, UPC.
- Giulio Dainelli, Marco Moretti, António Serrador, Luís M. Correia "Statistical Analysis of Power Distribution for Radio Resource Management in OFDMA Cellular Systems " NEWCOM<sup>++</sup> WPR8/WPR9 workshop, Bologna, November, 25th, 2010. Joint paper CNIT, IST-TUL.

Moreover, different demonstrations were given at different fora:

- "Spectral Occupancy Measurements in Urban Areas" ICT Mobile Summit in Santander, Spain, 10-12 June, 2009, by Miguel López-Benítez, Fernando Casadevall, Anna Umbert, Rachid Hachemani, Christophe Moy, Jacques Palicot
- "Spectral Occupancy Measurements in Urban Areas" NEWCOM<sup>++</sup> Dissemination day, Barcelona, Spain, April 2009, by Miguel López-Benítez, Fernando Casadevall, Anna Umbert, Rachid Hachemani, Christophe Moy, Jacques Palicot
- "Blind Standard Identification with Bandwidth Shape and GI Recognition using USRP Platforms and SDR4all Tools" by H. Wang, W. Jouini, A. Nafkha, J. Palicot, P. Leray, C. Moy, L. S. Cardoso, M. Debbah, NEWCOM<sup>++</sup> Dissemination day, Florence, June, 2010.

The partners involved in research within WPR9 were also active tutors. Three lectures were given at the NEWCOM<sup>++</sup> Winter School on Flexible Radio and related technologies, held in Aachen during the days 3rd to 6th of February 2009:

- H. Bogucka (PUT), "Game Theory Approach to Flexible RRM and Spectrum Sharing",
- R. Agustí (UPC), "Adaptive Radio Resource Management Techniques",
- J. Pérez-Romero (UPC), "Dynamic Spectrum Access: Advanced Topics and Case studies".

Another aspect of integration of researchers working in WPR9 has been the face-to face meetings, where aspects of collaboration between partners and common research topics were identified. In addition to six WPR9 plenary meetings and different on-line interactions through phone calls the following visits and exchanges of students and researchers took place:

- A visit of Mérouane Debbah from CNRS to PUT was carried out on 15th and 16th of June, 2009. He gave a talk on Mobile Flexible Networks and the use of game theoretic techniques to design the deployment of dense networks. Also different research issues were discussed.
- A visit of António Serrador from IST-TUL to CNIT-Pisa was carried out on June 22-24 2009 in order to coordinate activities on distributed radio resource allocation.

- A scientific visit of Wassim Jouini from CNRS-Supelec to UPC was carried out from 11th October to 2nd December 2010 in order to apply the results from the measurement campaign in a joint learning/detection framework.
- A scientific visit of H. Bogucka (PUT) to CNRS-Supelec in Rennes was carried out on 20th-22nd January 2010, where she also participated in the final judgement of an habilitation thesis.
- 4 students from CNIT were hosted at UPC, working on activities related with the measurement spectrum campaign, and on OFDMA studies.

Finally, several special sessions have been organised with the participation of WPR9 members:

- “Flexible and Opportunistic Wireless Access - the Newcom ++ vision”, Crowncom Conference, June 24th 2009.
- “Newcom++ Special Session on Cognitive Radio” in European Wireless 2010 conference, Lucca Italy, 12-15 April 2010.
- “Advances in Signal Processing for Cognitive Radios - Newcom++ Results” in 6th Karlsruhe Workshop on Software Radios (WSR), 3-4 March 2010.
- “Cognitive Radio: the NEWCOM++ vision” in Cognitive Information Processing (CIP 2010) conference, 14-16 June 2010, Elba Island, Italy.

With respect to cross-WP activities, the following ones should be mentioned:

- Joint NEWCOM++ WPR8&WPR9 workshop, in conjunction with the COST2100 & IC0902 Workshop, Bologna, 25th November, 2010.
- J. Pérez-Romero, D. Noguet, M. López-Benítez, F. Casadevall “Towards a more efficient spectrum usage: Spectrum Sensing and Cognitive Radio techniques”, URSI Radio Science Bulletin, December, 2010. This joint paper has been carried out in the context of a collaboration between WPR9 and WPRC. Joint paper UPC, CEA-LETI.
- M. Moretti, G. Dainelli, A. Pérez “Low-complexity efficient resource allocation for MIMO-OFDMA systems”, NEWCOM++ WPR8/WPR9 workshop, Bologna, November, 25th, 2010. Joint paper in the context of a collaboration between WPR8 and WPR9. Joint paper CNIT, UPC.

## REFERENCES

- [1] M. Liu, Z.C.Li, X.B.Guo, E.Dutkiewicz, D.K.Zhang, "Performance Evaluation of Vertical Handoff Decision Algorithms in Heterogeneous Wireless Networks," In *Proc. of GLOBECOM '06 - IEEE Global Telecommunications Conference*, San Francisco, CA, USA, Nov. 2006.
- [2] A.H. Zahran, B. Liang, "Performance Evaluation Framework for Vertical Handoff Algorithms in Heterogeneous Networks", In *Proc. of ICC'05 - IEEE International Conference on Communications*, Seoul, Korea, May 2005.
- [3] J.Hou, D.C. O'Brien, , "Vertical Handover-Decision-Making Algorithm Using Fuzzy Logic for the Integrated Radio-and-OW System", *IEEE Transactions Wireless Communications*, Vol. 5, No. 1, pp. 176-185, Jan. 2006.
- [4] M. Liu, Z.C. Li, X.B.Guo, E.Dutkiewicz, "Performance Analysis and Optimization of Handoff Algorithms in Heterogeneous Wireless Networks", *IEEE Transactions on Mobile Computing*, Vol. 7, No. 7, pp. 846-857, July 2008.
- [5] P. Sroka (ed.) et al., "Definition and evaluation of JRRM and ASM algorithms", NEWCOM<sup>++</sup> DR9.2 deliverable, EC-IST Office, Brussels, Belgium, Dec. 2009.
- [6] A.Serrador, L.M. Correia, "A Model to Evaluate Vertical Handovers on JRRM" in *Proc. of IEEE PIMRC 2010*, 21<sup>st</sup> Annual IEEE International Symposium on Personal, Indoor and Mobile Radio Communications, Istanbul, Turkey, Sep. 2010.
- [7] N.Feamster, L. Gao, and J. Rexford, "How to Lease the Internet in Your Spare Time", *ACM SIGCOMM Computer Communication Review*, Vol.37, No.1, Jan. 2007, pp.61-64.
- [8] A. Bavier, N. Feamster, M. Huang, L. Peterson, and J. Rexford, "In VINI Veritas: Realistic and controlled network experimentation", in *Proc. of ACM SIGCOMM*, Sep. 2006.
- [9] S.A.AlQahtani, A.S.Mahmoud, T.R.Sheltami, M. El-Tarhuni, "Adaptive Radio Resource Management for Multi-Operator WCDMA Based Cellular Wireless Networks with Heterogeneous Traffic", in *Proc. of PIMRC'06 - 17th Annual IEEE International Symposium on Personal, Indoor and Mobile Radio Communications*, Helsinki, Finland, Sep. 2006.
- [10] M.K. Johansson, "Radio Resource Management in Roaming Based Multi-Operator WCDMA Networks", in *Proc. VTC 2004 Spring - 59th IEEE Vehicular Technology Conference*, Milan, Italy, May 2004.
- [11] S. Hew, L.B.White, "Fair Resource Bargaining Solutions for Cooperative Multi-Operator Networks", in *Proc. of IZS - International Zurich Seminar on Communications*, Zurich, Switzerland, Feb. 2006.
- [12] J. Sachs, H. Wiemann, J. Lundsjo,, P. Magnusson, "Integration of multi-radio access in a beyond 3G network", in *Proc. of PIMRC 2004 - 15th IEEE International Symposium on Personal, Indoor and Mobile Radio Communications*, Barcelona, Spain, Sep. 2004.
- [13] J. Sachs, R. Aguero, M. Berg, J. Gebert, L. Jorgueski, I. Karla, P. Karlsson, G.P.. Koudouridis, J. Lundsjo, M. Prytz, O. Strandberg, "Migration of Existing Access Networks Towards Multi-Radio Access", in *Proc. of VTC'06 Fall - 64th IEEE Vehicular Technology Conference*, Montreal, Canada, Sep. 2006.
- [14] 3GPP, Improvement of RRM across RNS and RNS/BSS (Release 5), RAN, Technical Report TR 25.881 v5.0.0, Dec. 2001 (<http://www.3gpp.org>).
- [15] A. Serrador, L. M. Correia, "Policies for a Cost Function for Heterogeneous Networks Performance Evaluation", in *Proc. of PIMRC 2007 - 18th IEEE International Symposium on Personal, Indoor and Mobile Radio Communications*, Athens, Greece, Sep. 2007.
- [16] G. Nunzi, (ed.) et al., In-Network Management Concept, ICT-4WARD Project, Deliverable D4.2, EC-ICT Office, Brussels, Belgium, Mar. 2009.

Reference DR9.3



- [17] A. Serrador, (ed.) et al., “Simulation tools: final version capabilities and features”, IST-AROMA Project, Del. D13, EC-IST Office, Brussels, Belgium, May 2007. (<http://www.aroma-ist.upc.edu/>)
- [18] J. Jang and K. B. Lee, “Transmit power adaptation for multiuser OFDM systems,” *IEEE Journal on Selected Areas in Communications*, vol. 21, no. 2, pp. 171–178, 2003.
- [19] W. Rhee and J. M. Cioffi, “Increase in capacity of multiuser OFDM system using dynamic subchannel allocation,” in *Proc. IEEE 51st Vehicular Technology Conference - VTC Spring*, 2000, pp. 1085–1089.
- [20] Z. Shen, J. G. Andrews, and B. L. Evans, “Adaptive resource allocation in multiuser ofdm systems with proportional rate constraints,” *IEEE Transactions on Wireless Communications*, vol. 4, no. 6, pp. 2726–2737, 2005.
- [21] G. Song and Y. G. Li, “Cross-layer optimization for OFDM wireless networks - part I: Theoretical framework and part II: Algorithm development,” *IEEE Transactions on Wireless Communications*, vol. 4, no. 2, pp. 614–634, Mar. 2005.
- [22] 3GPP, “Technical Specification Group Radio Access Networks; Deployment aspects,” TR 25.943 v5.1.0, June, 2002.
- [23] F. Kelly, “Charging and Rate Control for Elastic Traffic,” *European Transactions on Communications*, vol. 8, pp. 33–37, 1997.
- [24] E. B. Rodrigues and F. Casadevall, “Adaptive Radio Resource Allocation Framework for Multi-User OFDM,” *IEEE 69th Vehicular Technology Conference - VTC Spring*, Barcelona, Spain, April, 2009.
- [25] H. Lei, L. Zhang, X. Zhang and D. Yang, “A Packet Scheduling Algorithm Using Utility Function for Mixed Services in the Downlink of OFDMA Systems,” in *Proc. IEEE 66th Vehicular Technology Conference VTC 2007-Fall*, pp. 1664-1668, September 2007.
- [26] R. Jain, D. Chiu, and W. Hawe, “A quantitative measure of fairness and discrimination for resource allocation in shared computer systems,” *DEC Research, Tech. Rep. TR-301*, September 1984.
- [27] I. C. Wong, Z. Shen, B. L. Evans, and J. G. Andrews, “A low complexity algorithm for proportional resource allocation in OFDMA systems,” in *Proc. IEEE Workshop on Signal Processing Systems*, 2004, pp. 1–6.
- [28] E. B. Rodrigues and F. Casadevall, “Fairness and Rate Adaptive Resource Allocation for OFDMA Networks”, submitted to *IEEE Transactions on Wireless Communications*, October 2010.
- [29] E. B. Rodrigues and F. Casadevall, “Rate Adaptive Resource Allocation and Utility-Based Packet Scheduling in Multicarrier Systems”, submitted to *Majlesi Journal of Electrical Engineering*, September 2010.
- [30] E. B. Rodrigues and F. Casadevall, “Control of the Trade-Off between Resource Efficiency and User Fairness in Wireless Networks Using Utility-Based Adaptive Resource Allocation”, submitted to *IEEE Communications Magazine*, September 2010.
- [31] P. J. G. Ameigeiras, *Packet Scheduling and Quality of Service in HSDPA*, Ph.D. dissertation, Aalborg University, Aalborg, Denmark, 2003.
- [32] WiMAX Forum, “WiMAX Forum Mobile System Profile,” May 2007.
- [33] K. I. Pedersen, T. E. Kolding, F. Frederiksen, I. Z. Kovács, D. Laselva, and P. E. Mogensen, “An Overview of Downlink Radio Resource Management for UTRAN Long-Term Evolution,” *IEEE Commun. Mag.*, vol. 47, no. 7, pp. 86–93, July 2009.

- [34] C. Wong, R. Cheng, K. Letaief, and R. Murch, "Multiuser OFDM with adaptive subcarrier, bit and power allocation," *IEEE J. Select. Areas Comm.*, vol. 17, no. 10, pp. 1747–1758, October 1999.
- [35] W. Yu and R. Lui, "Dual methods for nonconvex spectrum optimization of multicarrier systems," *IEEE Trans. Comm.*, vol. 54, no. 7, pp. 1310–1322, July 2006.
- [36] W. Yu, W. Rhee, S. Boyd, and J. Cioffi, "Iterative water-filling for gaussian vector multiple-access channels," *Information Theory, IEEE Transactions on*, vol. 50, no. 1, pp. 145–152, Jan. 2004.
- [37] A. Todini, M. Moretti, A. Valletta, and A. Baiocchi, "A modular cross-layer scheduling and resource allocation architecture for OFDMA systems," in *IEEE Globecom 2006*, November 2006.
- [38] I. Kim, I. Park, and Y. Lee, "Use of linear programming for dynamic subcarrier and bit allocation in multiuser OFDM," *IEEE Trans. Veh. Technol.*, vol. 55, no. 4, pp. 1195–1207, July 2006.
- [39] M. Moretti and A. Todini, "A reduced complexity cross-layer radio resource allocator for OFDMA systems," *IEEE Trans. Wireless Commun.*, vol. 6, pp. 2807–2812, 2007.
- [40] A. Abrardo, A. Alessio, P. Detti, and M. Moretti, "Centralized radio resource allocation for OFDMA cellular systems," in *Proc. IEEE ICC 2007*, 2007.
- [41] R. K. Ahuja, T. L. Magnanti, and J. B. Orlin, *Network Flows*. Prentice Hall, 1993.
- [42] D. Bertsimas and J. Tsitsiklis, *Introduction to Linear Optimization*. Athena Scientific, 1998.
- [43] TS 36.420, *Evolved Universal Terrestrial Radio Access Network (E-UTRAN): X2 general aspects and principles*, 3GPP-LTE Std., 2009.
- [44] B. Bensaou, D. Tsang, and K. T. Chan, "Credit-based fair queueing (CBFQ): a simple service-scheduling algorithm for packet-switched networks," *IEEE/ACM Trans. Netw.*, vol. 9, no. 5, pp. 591–604, Oct. 2001.
- [45] A. Abrardo, A. Alessio, P. Detti, and M. Moretti, "Radio resource allocation problems for OFDMA cellular systems," *Comput. Oper. Res.*, vol. 36, no. 5, pp. 1572–1581, 2009.
- [46] M. Pischella and J.-C. Belfiore, "Distributed resource allocation for rate-constrained users in multi-cell OFDMA networks," *IEEE Commun. Lett.*, vol. 12, no. 4, pp. 250–252, April 2008.
- [47] X. Z. H. Lei, L. Zhang, and D. Yang, "A novel multi-cell OFDMA system structure using fractional frequency reuse," in *IEEE 18th PIMRC*, 2007.
- [48] R. Y. Chang, Z. Tao, J. Zhang, and C.-C. J. Kuo, "A graph approach to dynamic fractional frequency reuse (FFR) in multi-cell OFDMA networks," in *Proc. IEEE Int. Conf. Communications ICC '09*, 2009, pp. 1–6.
- [49] 3GPP TS 36.300, "Evolved Universal Terrestrial Radio Access (E-UTRA) and Evolved Universal Terrestrial Radio Access Network (E-UTRAN); Overall description; Stage 2", V8.7.0, Dec. 2008.
- [50] Celtic Project CP5-026 WINNER+, "D1.4 Initial Report on Advanced Multiple Antenna Systems," Jan 2009.
- [51] 3GPP TR 36.814, "Further Advancements for E-UTRA Physical Layer Aspects", V9.0.0, Mar 2010.
- [52] M. Necker, "Interference Coordination in Cellular OFDMA Networks", *IEEE Network*, vol. 2, issue 6, pp. 12-19, November-December 2008.
- [53] Celtic Project CP5-026 WINNER+, "D2.2 Enabling Techniques for LTE-A and Beyond," Jun 2010.

- [54] Samsung Electronics, "Downlink MIMO for EUTRA," 3GPP TSG RANWG1 Meeting #44/R1-060335, February 2006
- [55] D. Piazza and U. Spagnolini, "Random beamforming for spatial multiplexing in downlink multiuser MIMO systems," in *Proc. IEEE PIMRC*, vol. 4, pp. 2161–2165, Berlin, Germany, September 2005.
- [56] Y. Linde, A. Buzo, and R. M. Gray, "An algorithm for vector quantizer design," *IEEE Transactions on Communications*, January 1980
- [57] Celtic Project CP5-026 WINNER+, "D1.5 Intermediate Report on System Aspect of Advanced RRM", Nov. 2009.
- [58] Report ITU-R M.2135 "Guidelines for evaluation of radio interface technologies for IMT-Advanced"
- [59] T. Yoo and A. Goldsmith, "On the optimality of multi-antenna broadcast scheduling using zero-forcing beamforming," *IEEE Journal Select. Areas Commun.*, vol. 24, no. 3, pp. 528 – 541, Mar. 2006
- [60] S. H. Won, H. J. Park, J. O. Neel, J. H. Reed, "Inter-Cell Interference Coordination/Avoidance for Frequency Reuse by Resource Scheduling in an OFDM-based Cellular System", *Proc. IEEE VTC'07-Fall*, pp. 1722-1725, 2007
- [61] M. Charafeddine, A. Sezgin, and A. Paulraj, " Rates region frontiers for n-user interference channel with interference as noise ", in *Proc. Annual Allerton Conference on Communications, Control and Computing*, Allerton, IL, September 2007
- [62] M. Charafeddine, Z. Han, A. Paulraj, and J. Cioffi, " Crystallized Rate Regions of the Interference Channel via Correlated Equilibrium with Interference as Noise " in *Proc. IEEE ICC 2009*, Dresden, Germany, June 14-18, 2009
- [63] R. Ahlswede, " The capacity region of a channel with two senders and two receivers" in *Annals of Probability*, vol. 2, pp. 805-814, October 1974
- [64] T. Han, K. Kobayashi " A new achievable rates region for the interference channel" in *IEEE Transactions on Information Theory*, vol. 27, issue 1, pp. 49-60, January 1981
- [65] G. Owen, *Game Theory*, 3rd ed., New York: Academic, 2001
- [66] R. J. Aumann, " Subjectivity and correlation in randomized strategy" , *Journal of Mathematical Economics*, vol. 1, no. 1, pp. 67-96, 1974
- [67] D. P. Bertsekas, A. Nedic, A. E. Ozdaglar " Convex Analysis and Optimization", Belmont, MA: Athena Scientific, 2003
- [68] S. Hart, A. Mas-Colell, " A simple adaptive procedure leading to correlated equilibrium" , *Econometrica*, vol. 68, no. 5, pp. 1127-1150, September 2000
- [69] A. Kliks, P. Sroka, M. Debbah, " MIMO Crystallized Rate Regions ", in *Proc. European Wireless 2010*, Lucca, Italy, 12-15 April 2010
- [70] A. Paulraj, R. Nabar, D. Gore, " Introduction to Space-Time Wireless Communications " , Cambridge University Press, 2003
- [71] G. Lebrun, J. Gao, M. Faulkner, " MIMO Transmission Over a Time-Varying Channel Using SVD ", *IEEE Transactions on Wireless Communications*, vol. 4, no. 2, pp. 757-764, March 2005
- [72] K. Huang, J. G. Andrews, R. W. Heath, Jr, " Performance of orthogonal beamforming for SDMA with limited feedback" , *IEEE Transactions on Vehicular Technology*, vol. 58, issue 1, pp. 152-164, January 2009

- [73] D. Piazza, U. Spagnolini, " Random beamforming for spatial multiplexing in downlink multiuser MIMO systems" , *Proc. IEEE PIMRC 2005*, vol. 4, pp. 2161-2165, Berlin, Germany, September 11-14, 2005
- [74] I. E. Telatar, " Capacity of multi-antenna Gaussian channels" , *European Transactions on Telecommunications*, vol. 10, no. 6, pp. 585-595, November-December 1999
- [75] R. S. Blum, " MIMO capacity with interference" , *IEEE Journal on Selected Areas in Communications*, vol. 25, issue 5, pp. 793- 801, June 2003
- [76] A. Goldsmith, S. A. Jafar, N. Jindal, S. Vishwanath, " Fundamental Capacity of MIMO Channels", *IEEE Journal on Selected Areas in Communications, Special Issue on MIMO systems*, vol. 21, 2002
- [77] H. Dai, A. Molisch, H.V.Poor, " Downlink Capacity of Interference-Limited MIMO Systems With Joint Detection " , *IEEE Transactions on Wireless Communications*, vol. 3, no. 2, pp. 442-453, March 2004
- [78] J. Choi, S.R. Kim, I-K. Choi, " Eigenbeamforming with Selection Diversity for MIMO-OFDM Downlink " , in *Proc. Vehicular Technology Conference 2004*, VTC04-Fall, vol. 3, pp. 1806-1810, Los Angeles, USA, 26-29 Sept. 2004
- [79] 3GPP TS 36.211, " 3rd Generation Partnership Project; Technical Specification Group Radio Access Network; Evolved Universal Terrestrial Radio Access (E-UTRA); Physical Channels and Modulation (Release 8) " , v. 8.4.0, September 2008
- [80] M. Sharif, B. Hassibi, " On the capacity of MIMO broadcast channels with partial side information" , *IEEE Transactions on Information Theory* , vol. 5, no. 2, pp. 506-522, 2005
- [81] E. G. Larsson, E. A. Jorswieck, J. Lindblom, R. Mochaourab, " Game theory and the flat-fading Gaussian interference channel" , *IEEE Signal Processing Magazine*, vol. 26, no. 5, pp. 18-27, September 2009
- [82] F. H. Sanders, "Broadband spectrum surveys in Denver, CO, San Diego, CA, and Los Angeles, CA: methodology, analysis, and comparative results," in *Proc. 1998 IEEE International Symposium on Electromagnetic Compatibility*, Aug 1998, vol. 2, pp. 988–993.
- [83] M. A. McHenry et al., "Spectrum occupancy measurements," Shared Spectrum Company, technical reports (Jan 2004 – Aug 2005). URL: <http://www.sharedspectrum.com/measurements>.
- [84] A. Petrin, P. G. Steffes, "Analysis and comparison of spectrum measurements performed in urban and rural areas to determine the total amount of spectrum usage," in *Proc. International Symposium on Advanced Radio Technologies (ISART 2005)*, Mar 2005, pp. 9–12.
- [85] R. I. C. Chiang, G. B. Rowe, K. W. Sowerby, "A quantitative analysis of spectral occupancy measurements for cognitive radio," in *Proc. IEEE 65th Vehicular Technology Conference (VTC 2007-Spring)*, Apr 2007, pp. 3016–3020.
- [86] M. Wellens, J. Wu, P. Mähönen, "Evaluation of spectrum occupancy in indoor and outdoor scenario in the context of cognitive radio," in *Proc. Second International Conference on Cognitive Radio Oriented Wireless Networks and Communications (CrowCom 2007)*, Aug 2007, pp. 1-8.
- [87] M. H. Islam et al., "Spectrum Survey in Singapore: Occupancy Measurements and Analyses," in *Proc. 3rd International Conference on Cognitive Radio Oriented Wireless Networks and Communications (CrownCom 2008)*, May 2008, pp. 1–7.
- [88] P. G. Steffes, A. J. Petrin, "Study of spectrum usage and potential interference to passive remote sensing activities in the 4.5 cm and 21 cm bands," in *Proc. IEEE International Geoscience and Remote Sensing Symposium (IGARSS 2004)*, Sep 2004, vol. 3, pp. 1679–1682.
- [89] J. Do, D. M. Akos, P. K. Enge, "L and S bands spectrum survey in the San Francisco bay area," in *Proc. Position Location and Navigation Symposium (PLANS 2004)*, Apr 2004, pp. 566–572.

- [90] M. Biggs, A. Henley, T. Clarkson, "Occupancy analysis of the 2.4 GHz ISM band," *IEE Proc. on Comms*, Oct 2004, vol. 151, n° 5, pp. 481–488.
- [91] S. W. Ellingson, "Spectral occupancy at VHF: implications for frequency-agile cognitive radios," in *Proc. IEEE 62nd Vehicular Technology Conference (VTC 2005-Fall)*, Sep 2008, vol. 2, pp. 1379–1382.
- [92] S. D. Jones, E. Jung, X. Liu, N. Merheb, I.-J. Wang, "Characterization of spectrum activities in the U.S. public safety band for opportunistic spectrum access," in *Proc. 2nd IEEE International Symposium on New Frontiers in Dynamic Spectrum Access Networks (DySPAN 2007)*, Apr 2007, pp. 137–146.
- [93] M. López-Benítez, F. Casadevall, "Methodological aspects of spectrum occupancy evaluation in the context of cognitive radio," To appear in *European Transactions on Telecommunications (Wiley)*, Special Issue on European Wireless Conference 2009.
- [94] M. López-Benítez, A. Umbert, F. Casadevall, "Evaluation of spectrum occupancy in Spain for cognitive radio applications", in *Proc. IEEE 69th Vehicular Technology Conference (VTC 2009 Spring)*, Apr 2009, pp. 1–5.
- [95] M. López-Benítez, F. Casadevall, A. Umbert, R. Hachemani, J. Palicot, C. Moy, "Spectral occupancy measurements in urban areas and their applicability to the blind standard recognition sensor concept," *Proceedings of the NEWCOM++/ACoRN Joint Workshop (NAW 2009)*, Barcelona, Spain, March 30-April 1, 2009, pp. 1-5.
- [96] M. López-Benítez, F. Casadevall, A. Umbert, J. Pérez-Romero, R. Hachemani, J. Palicot, and C. Moy, "Spectral occupation measurements and blind standard recognition sensor for cognitive radio networks," in *Proc. 4th International Conference on Cognitive Radio Oriented Wireless Networks and Communications (CrownCom 2009)*, June 2009, pp. 1–9.
- [97] M. López-Benítez, F. Casadevall, A. Umbert, R. Hachemani, C. Moy, J. Palicot, "Blind standard recognition sensor validation with data from measurement campaign," *18th ICT Mobile and Wireless Communications Summit (ICT-MobileSummit 2009)*, preconference workshop on Dynamic Spectrum Management in Cognitive Radio Networks, Santander, Spain, June 9, 2009.
- [98] M. López-Benítez, F. Casadevall, "On the spectrum occupancy perception of cognitive radio terminals in realistic scenarios," *Proceedings of the 2nd IAPR International Workshop on Cognitive Information Processing (CIP 2010)*, Special session on NEWCOM++, Elba Island, Italy, June 14-16, 2010, pp. 99-104.
- [99] M. López-Benítez, F. Casadevall, "Spectrum occupancy in realistic scenarios and duty cycle model for cognitive radio," *Advances in Electronics and Telecommunications*, Special Issue on Radio Communication Series: Recent Advances and Future Trends in Wireless Communication, vol. 1, no 1, pp. 26-34, April, 2010.
- [100] N. Hoven and A. Sahai, "Power scaling for cognitive radio," *Proceedings of the International Conference on Wireless Networks, Communications and Mobile Computing (WirelessComm 2005)*, vol. 1, Jun. 2005, pp. 250-255.
- [101] S. M. Mishra, A. Sahai, and R. W. Brodersen, "Cooperative sensing among cognitive radios," *Proceedings of the IEEE International Conference on Communications (ICC 2006)*, vol. 4, Jun. 2006, pp. 1658-1663.
- [102] A. Ghasemi and E. S. Sousa, "Collaborative spectrum sensing for opportunistic access in fading environments," in *Proceedings of the First IEEE International Symposium on New Frontiers in Dynamic Spectrum Access Networks (DySPAN 2005)*, Nov. 2005, pp. 131-136.
- [103] M. Wellens, J. Riihijärvi, M. Gordziel, and P. Mähönen, "Evaluation of cooperative spectrum sensing based on large scale measurements," *Proceedings of IEEE International Symposium on New Frontiers in Dynamic Spectrum Access Networks (DySPAN)*, October 2008.

- [104] M. Wellens, J. Riihijärvi, and P. Mähönen, “Spatial statistics and models of spectrum use,” Elsevier Computer Communications, Special Issue on Cognitive Radio and Dynamic Spectrum Sharing Systems, vol. 32, no. 18, pp. 1998-2011, December 2009.
- [105] Yucek, T. and Arslan, H. A Survey of Spectrum Sensing Algorithms for Cognitive Radio Applications. *In IEEE Communications Surveys and Tutorials*, 11, no.1, 2009.
- [106] M. López-Benítez, F. Casadevall, C. Martella, “Performance of spectrum sensing for cognitive radio based on field measurements of various radio technologies,” Proceedings of the 16th European Wireless Conference (EW 2010), Special session on Cognitive Radio, Lucca, Italy, April 12-15, 2010, pp. 969-977.
- [107] Ettus Research LLC, “Universal Software Radio Peripheral (USRP),” Available at: <http://www.ettus.com>.
- [108] E. Blossom, “Exploring GNU Radio,” Nov. 2004, Available at: <http://www.gnu.org/software/gnuradio/doc/exploringgnuradio.html>.
- [109] R. Tandra and A. Sahai. “SNR walls for signal detection”. *IEEE Journal of Selected Topics in Signal Processing*, 2(1):4-17, 2008.
- [110] A.P.Dempster, N.M.Laird, and D.B.Rubin, “Maximum Likelihood from Incomplete Data via the EM Algorithm.” *Journal of the Royal Statistical Society. Series B* 39(1), pages 1-38, 1977.
- [111] G.J.McLachlan, and T. Krishnan, “The EM Algorithm and its Extensions”. *Wiley*, 1997.
- [112] Cohen, A. Clifford. “Estimation in Mixtures of Two Normal Distributions”. *Technometrics*, Vol. 9, No.1, :15-28, 1967.
- [113] Federal Communications Commission. Spectrum Policy Task Force Report. 2002.
- [114] J. Mitola, and G.Q. Maguire, “Cognitive radio: making software radios more personal”. *Personal Communications, IEEE*, 6:13-18, 1999.
- [115] Q. Zhao, and B.M. Sadler, “A survey of dynamic spectrum access: signal processing, networking, and regulatory policy”. *in IEEE Signal Processing Magazine*, pages 79--89, 2007.
- [116] R.Agrawal, “Sample mean based index policies with  $O(\log(n))$  regret for the multi-armed bandit problem”. *Advances in Applied Probability*, 27:1054-1078, 1995.
- [117] P.Auer, N.Cesa-Bianchi, and P. Fischer, “Finite time analysis of multi-armed bandit problems”. *Machine learning*, 47(2/3):235-256, 2002.
- [118] J.-Y. Audibert, R. Munos, and C. Szepesvári, “Tuning bandit algorithms in stochastic environments”. *Proceedings of the 18th international conference on Algorithmic Learning Theory*, 2007.
- [119] L.Lai, H.E.Gamal, H.J. Jiang, and V. Poor “Cognitive Medium Access: Exploration, Exploitation and Competition.” [Online]. Available: <http://arxiv.org/abs/0710.1385>.
- [120] L. Keqin, Q. Zhao, “Distributed Learning in Cognitive Radio Networks: Multi-Armed Bandit with Distributed Multiple Players”. ICASSP Conference, June, 2010.
- [121] W. Jouini, D. Ernst, C. Moy, J. Palicot, “Upper confidence bound based decision making strategies and dynamic spectrum access”. *Proceedings of the 2010 IEEE International Conference on Communications (ICC)*, 2010.